Cranfield University

Manufacture of Novel Intermetallic Bond Coats from the Electroplating of Ionic Liquids

Mark Craig

School of Applied Sciences

Cranfield University

School of Applied Sciences

PhD Thesis

Academic Year 2009-2010

Mark Craig

Manufacture of Novel Intermetallic Bond Coats from the Electroplating of Ionic Liquids

Supervisors: Prof. J. R. Nicholls & Dr M. Robinson

This thesis is submitted to fulfil the requirements for the degree of Doctor of Philosophy

Acknowledgements

A PhD is meant to be your own work; however, this PhD and in fact this project would not have been possible without the help and assistance of the following people:

Prof. Nicholls and Dr Robinson have both been fantastic; they are both extremely knowledgeable, enthusiastic and provided expert guidance whenever it was needed. To have two supervisors of this calibre would give any student the confidence to pursue any PhD – as for me I am just extremely grateful.

All students and staff of the NHTSEC in Cranfield, however Mrs McGuire, Mr Rose Mr Prior, Mr Gray, Dr Kershaw and Mr Dyer need a special mention for their assistance during this project.

The project was funded by the European Union as part of the IOLISURF project. I would like to thank all the members of the group for making the project so enjoyable. Special thanks should go to Prof Bardi and Dr Caporali of INSTM, Italy, not only for Dr Caporalis help with ionic liquids and my questions about electroplating but for being such gracious hosts when I visited. Dr Pitner of Merck also deserves thanks, not only for supplying ionic liquids, but for also answering all questions posed. Miss Eugenio of IST, Portugal also deserves thanks for the help with the Cr plating. Finally, Miss Catena deserves a mention for her great management style and effectiveness in forming a great team.

I am also thankful to Prof Stiller and Miss Sonestedt of Chalmers University, Sweden, for all their help with TEM, atomic probe and the Dual Beam. Their knowledge and expertise was immense, however they were extremely gracious hosts and where kind enough to look after me during my two visits.

Additionally I would like to thank all my friends at Cranfield University – you have truly made my time here a great experience. James Fowler of Cambridge University also deserves a special mention, with all the help with getting electronic references. You have truly made my academic life easier!

My family have been great, throughout my travels and studies. So a big thanks to them, especially my Nan for looking after me in my slightly chaotic teenage years and my Mother for showing me that stubbornness is indeed a virtue.

Last but not least, danke ich Sandra von Herzen für all Ihre Unterstützung während meiner Doktorarbeit. Du bist einfach die Beste!

In Memory of my Mother - Pauline Ann Craig: 1957-2010

Abstract

Gas turbine engines for both aerospace and power generation are constantly being revised to improve running efficiency and performance. Gas turbine engines essentially consist of three distinct regions: compressor, combustion and turbine sections with the combustor and turbine sections required to experience higher and higher temperatures in pursuit of efficiency gains. Stage 1 high pressure turbine blades (buckets) are located closest to the combustion zone and experience extremely high temperatures. Further, turbine blades experience high centrifugal force whilst in operation and therefore engine designers must take into consideration both the mechanical effects of operation and the high temperatures associated with engine use. Environmental resistant coating systems are therefore employed to allow the design of the base material (nickel-based superalloys) to be biased towards mechanical properties (high creep resistance).

Nickel-platinum-aluminide coatings are the diffusion coating of choice for both aero- and industrial turbines with the platinum being typically deposited by electroplating on the nickel alloys, followed by heat treating to form a platinised enriched area which is then aluminised by insertion into a chemical vapour deposition (CVD) retort and reacting with an aluminium halide at elevated temperature. The CVD process is utilised as it is relatively easy to form desirable intermetallics though this route.

The electrodeposition of aluminium from aqueous media is not possible as water undergoes hydrolysis before the reduction potential of aluminium is reached. Ionic liquids are an alternative method of depositing aluminium via electroplating without the need of water as the electrolyte. Ionic liquids have numerous benefits including a wide electrochemical window and have low toxicity. In comparison to the CVD process, they are multiuse and can be easily recycled/reused as the ionic liquid itself is not consumed within the plating process.

Electroplating aluminium from ionic liquids to form a dense coating onto nickel-based superalloys is therefore proposed within this thesis as an alternative novel approach to achieving desirable nickel aluminide intermetallic coatings after post processing heat treatment. Furthermore, the post heat treatment may be done within

either a traditional CVD-type regime or with a new and novel low temperature heat treatment regime developed as part of this thesis – ICON. Both heat treatments form β-NiAl. The heat treatment using CVD-type parameters forms coatings akin to those produced using a CVD route, whereas the ICON coating shows improved chemical homogeneity and a smaller interdiffusion zone – both of which are shown to offer superior coating oxidation performance. Aluminium electrodeposited on CMSX4 heat treated with CVD-type parameters shows excellent cyclic oxidation data which is at least equal to, if not greater than those produced using traditional methods.

Table of Contents

List of Figures

Table of Abbreviations

Abbreviation	**Name**
Ionic Liquids	
ILs	Ionic Liquids
MeEtim Cl	1-methyl-3-ethylimidazolium chloride
DMPIC	1,2-dimethyl-3-propylimidazolium chloride
MEIC	1-methyl-3-ethylimidazolium chloride
TMHA-Tf_2N	Trimethyl-m-hexylammonium bis[(trifluromethyl)sulfonyl]amide
EMIM	1-ethyl-3-methylimidazoilum
BMIM	1-butyl-3-methylimidazoilum
$BMPTF_2N$	1-butyl-1-methyl pyrrolidinium bis(trifluromethylsulfonyl)imide
BPC	N-(nbutyl)pyridinium chloride
BTMAC	Benzyltrimthyl ammonium chloride
DMPIC	1,2-dimethy-3-propylimidazolium
EMIC	1-ethyl-3-methylimidazolium chloride
MEIC/ MeEtimCl	1-methyl-3-ethylimidazolium chloride
TMPAC	Trimethylphenylammonium chloride
BMPTFSI	1-N-butyl-1-methylpyrrolidinium
$Bu_3MeN^+TfN^-$	Tri-1-butylmethylammonium bis ((trifluoromethyl)sufonyl)imide
MDIM	1-methyl-3-[2,6-(S)-dimethylocten-2-yl]imidazolium
$EtNH_3NO_3$	Ethyl ammonium nitrate
General	
CVD	Chemical Vapour Deposition
EB-PVD	Electron Gun – Plasma Vapour Deposition
CMSX4	Type of nickel-based superalloy
GTD111	Type of nickel-based superalloy
Ni200	Commercially pure nickel
TBC	Thermal Barrier Coating
TGO	Thermally Grown Oxide
HTLA	High Temperature Low Activity CVD Process
LTHA	Low Temperature High Activity CVD Process
BCC	Body Centred Cubic Structure
FCC	Face Centred Cubic Structure
TCP	Topological Close Packed
SEM	Scanning Electron Microscope
TEM	Transmission Electron Microscope
BSD	Back Scatter Electron Detector
APM	Atomic Probe Microscopy
CS	Combustion Synthesis
SHS	Self-propagating high-temperature synthesis
RS	Reaction Synthesis
SPS	Self-propagating synthesis
K	Kelvin
A	Amps
kJ	Kilo Joules
Atm	Atmospheric pressure

1 Introduction

Since the first introduction of the gas turbine engine there has been a continual desire to improve its efficiency and generate more power. Therefore, components for these engines require materials which have exceptional mechanical properties at very high temperatures. Nickel-based superalloys, first used in the 1930's[1] have since become the material of choice for parts such as the high-temperature turbine blade, nozzle guide vanes etc. However, with higher temperatures being sought, to improve fuel and engine efficiency, alloy compositions have increased in refractory materials and been reduced in chromium so increasing the high temperature strength of the material at the expense of corrosion protection e.g. CMSX4[2-4]. For this reason surface engineering is used to improve both oxidation and corrosion resistance[5] of these single crystal superalloys.

High pressure turbine blades have progressed from wrought iron based materials to cast single crystal nickel-based superalloys, with numerous surface coatings employed to enable higher temperatures to be reached within the engine itself. A successful method of protecting these blades is to apply a platinum aluminide (PtAl) bond coat followed by a thermal barrier coating (TBC)[3,4,6]. Numerous types of PtAl coatings exist but all typically use a 5-10μm Pt layer, which is subsequently aluminised to form a platinum aluminide intermetallic coating. This permits growth of an Al_2O_3 surface oxide that acts as a diffusion barrier to the inward flux of oxygen, thus providing oxidation protection to the coating and substrate alloy.

Aqueous electrodeposition of Pt appears to be the production method of choice employed within industry to create these PtAl coatings. The electroplated platinum must be first diffused into the alloy using a thermal treatment then the aluminium is deposited using chemical vapour deposition (CVD). However, with the increasing interest in ionic liquids (ILs) as alternative solvents (compared to aqueous) for electroplating there is a real potential to transform current production techniques to encompass these ILs for both the electrodeposition of platinum and aluminium.

This study aims to advance the current understanding of manufacturing PtAl coatings, ionic liquids and electroplating of platinum. It will continue investigating the use of

ionic liquids to deposit aluminium and thus offer a new process route to manufacture high temperature aluminide coatings. This work was part of the IOLISURF consortium, whose aim was "to generate fundamental knowledge on ionic liquids as an electrochemical medium for cost effective and environmentally friendly processing methods for the electrodeposition of multi-functional materials operating in extreme conditions against corrosion and high temperature oxidation[7]. It was a European project supported within the sixth Framework programme for Research and Technological Development.

1.1 Superalloys

1.1.1 Introduction

Since Whittle's patent of the gas turbine engine in the 1930s, newer materials have been sought after and developed which allow for higher gas temperatures to be reached. Early components were produced using existing materials and technologies and austenitic stainless steels were the materials of choice[8]. Modern components are now produced using nickel-based superalloys which have a γ/γ' structure, however, this is not such a novel step as in 1929 it was noted that 80/20 NiCr when doped with Al and Ti showed improvements in creep strength – a γ' phase in a γ matrix[9,10]. However, these continual improvements now allow turbine blades to be made from cast single crystal alloys with large volume fractions of γ' in a γ matrix (Figure 1-1).

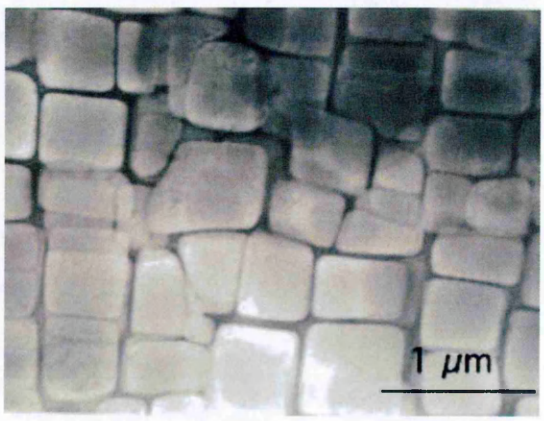

Figure 1-1: Transmission Electron Micrograph Showing a Large Volume Fraction of Cuboidal γ' particles in a γ matrix[11]

1.1.2 γ matrix

As stated above, most current high temperature components used within turbine engines are made of nickel-based superalloys, mainly due to nickel's higher temperature stability over iron and nickel phase stability when alloyed. Solid solution strengthening by the use of elements such as Al, Co, Cr, Mo, Re, Ta, Ti and W results because these atoms 'sit' within the matrix and prevent dislocation movement due to different atomic size and the associated lattice mismatch.

1.1.3 Precipitation hardeners

The major precipitation hardening phase in these nickel-based alloys is γ′. γ′ exists in the form X_3Y (e.g. Ni_3Al) where X is the major alloying element (Ni) and Y can be either Al, Nb, Ta or Ti. In the case of γ′ the precipitates aimed for within the aerospace and power generation industry are typically cuboidal for creep resistance (as cuboidal systems are resistant to dislocation movement every 90°, it is a coherent precipitate with similar lattice parameters to γ). Similarly to solid solution strengthening, the precipitates hinder dislocation movement by forcing it to loop, cut through or climb the precipitates. Ideally, fine precipitates which are evenly distributed give the greatest resistance to dislocation movement. The strength of the alloy is dependent on 4 major factors[12]:

- Volume fraction of γ′
- Radius of γ′
- Solid solution strengthening of both γ and γ′
- Presence of hyperfine γ′ precipitates

Table 1-1 and Table 1-2 show how elemental additions affect strengthening mechanisms within nickel-based superalloys.

Table 1-1: Elements used in Ni-Superalloys [12]

	Ni	Co	Fe	Cr	Mo, W	Nb, Ta, Ti	Re	Al	C, B, Zr, Hf
Matrix	X	X	X	X	X		X		
γ′				X		X		X	
Grain Boundary									X
Carbide Formers				X	X	X			
Oxide Scale Formers				X				X	

Table 1-2: Elements Showing Partition Preferences against Atomic Diameter from Nickel (% Difference) [12]

IIIA		IVB													
B	-21	C	-27												
Al	+6	IVA		VA		VIA		VIIA		VIIIA					
		Ti	+9	V	+5	Cr	+3			Fe	+3	Co	+1	Ni	0
Y	+45	Zr	+28	Nb	+18	Mo	+12								
		Hf	+27	Ta	+18	W	+13	Re	+10						

	Element partitions to γ
	Element partitions to grain boundaries
	Element partitions to γ′

1.1.4 Carbides and TCP Phases

Carbides tend to form at the grain boundary to act as grain boundary strengtheners (B, Zr and Hf also strengthen grain boundaries as refractory metal carbides and borides) in nickel-based alloys. However, in single crystal superalloys (like CMSX4), such grain boundary carbides are no longer needed; these single crystal alloys are cast with low carbon content. Topological Close Packed (TCP) phases may also form and are normally detrimental in both polycrystalline and single crystal superalloys. They form at the grain boundaries in a 'basket weave' where the atoms form in closely packed layers separated by relatively large interatomic distances. In single crystal alloys they tend to form on preferred low energy planes. They are detrimental within superalloys as their brittle nature provides excellent sites for fracture initiation. They are of particular interest within newer 3rd and 4th generation of superalloys, as Re is known to induce TCP formation. Therefore, some authors have looked at superalloys devoid of Re[13] to reduce the likelihood of TCP formation.

1.2 Intermetallics

This project is concerned with the formation of intermetallic coatings on various superalloys including CMSX4 and GTD111. An intermetallic may be defined as a compound comprising two or more metallic elements (including silicon) which, when bonded, typically show long-range crystallinity. Intermetallics tend to form compounds based on simple stoichiometric ratios. Thus γ′, mentioned previously, is

probably the best known intermetallic, through its wide use to strengthen nickel-based superalloys[14].

1.2.1 Nickel Aluminides

Nickel aluminides have been historically produced by pack cementation (aluminizing) where very fine particles of aluminium (as a cement type mixture with a halide activator) provides the source of aluminium halide vapour required to transport Al to the nickel-based superalloy. It then diffuses within the alloy to form an aluminide coating. The amount of aluminium added to the cement mixture varies depending on the required composition but it should be noted that not all the aluminium is incorporated within the new alloy or coating that is formed[3,4].

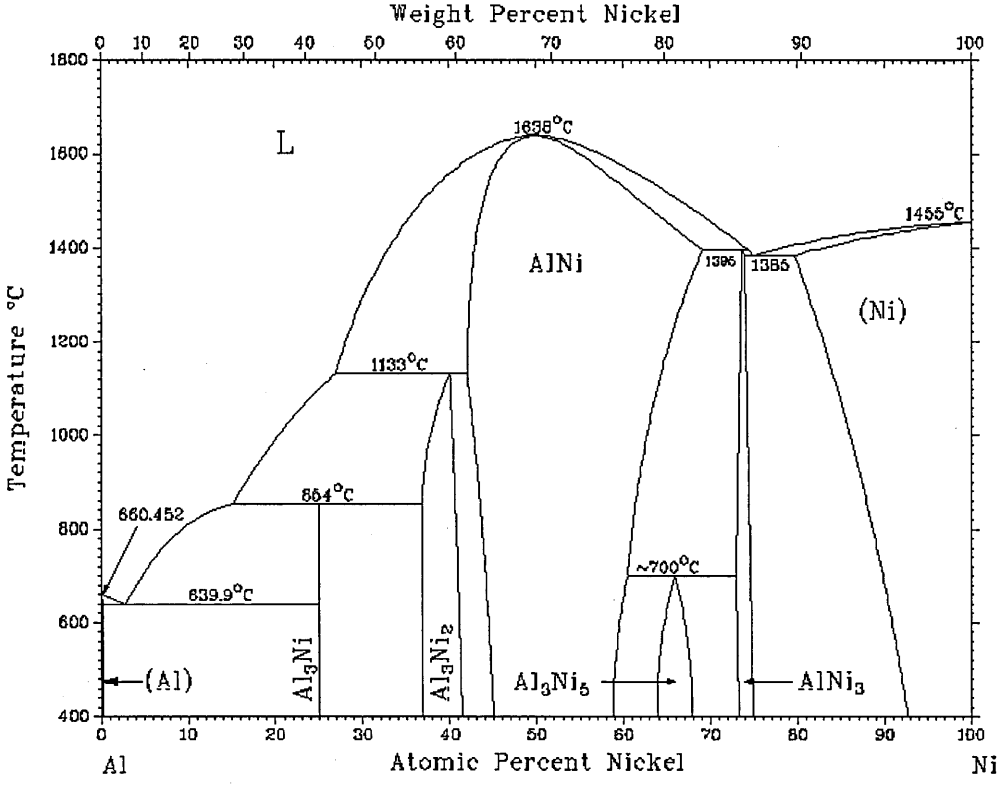

Figure 1-2: NiAl Phase Diagram[15]

The Nickel/Aluminium phase diagram is illustrated as Figure 1-2 and shows the presence of five discreet $Ni_{(x)}Al_{(y)}$ intermetallic phases: $NiAl_3$, Ni_2Al_3, NiAl (β), Ni_5Al_3 and Ni_3Al (γ′) which vary in composition from 25% to approximately 75% nickel (atomic fraction). It should be noted that this diagram shows characteristics

which are present in many intermetallic phase diagrams: line intermetallics. One line intermetallic ($NiAl_3$) within NiAl phase diagram is formed below 854°C and with a nickel composition of approximately 25at%. The phase diagram also demonstrates why the compound NiAl has become so interesting for high temperature coatings; nickel and aluminium have melting points of 1455°C and 660°C respectively, whereas, when alloyed in an atomic ratio 1:1, the melting point increases to 1638°C.

Thus nickel aluminide, in a 1:1 atomic ratio, as shown above, improves the melting point considerably over a pure nickel component. This is of particular interest in the aerospace industry where nickel is used in turbine blades and other high temperature applications. This intermetallic alloy does not share the same high temperature mechanical properties as Ni_3Al; it is ordered body centred cubic structure, and exhibits good ductility at high temperatures, high creep rates but low ductility at low temperatures. Creep resistance may be improved with the introduction of elements such as tantalum, niobium and hafnium[16].

There are many beneficial reasons for the β-NiAl coating. These include:

- Large aluminium reservoir allowing formation of a thermally grown oxide (TGO), consisting of Al_2O_3
- Oxidation of β-NiAl coatings forms a metastable alumina phase (θ and γ) when oxidised below 1000°C, which later transforms into an alpha phase. Above 1000°C, α-Al_2O_3 phase forms directly[17-20]
- The α-Al_2O_3 is advantageous in high temperature applications as it slows oxygen ingress and thus oxidation degradation of base metals through the formation of less protective oxides i.e. spinels, NiO, Cr_2O_3 etc.[21]
- The rate limiting step of TGO formation is the diffusion of oxygen through the alumina scale, although aluminium does play a small part in this scale growth[17]
- Additions of Pt[22-24], Hf[22,25], Pd[26], Zr[27] and various other elements improve oxidation resistance
- Additions of Hf will reduce creep of the TGO on NiAl[28]

1.2.2 Intermetallic Coatings

The aluminium is of particular use within coatings as it develops a thermally grown oxide, preferably α-alumina, which acts as an excellent oxidation barrier[3] as stated above. Intermetallic coatings may be deposited by a combination of processes including: electroplating, pack cementation, physical vapour deposition (PVD) and thermal spraying[3,4]. For example, the intermetallic PtAl may be applied using the PVD/electroplating process followed by aluminising[3,4]. Such intermetallics can be deposited as an alloy or as discreet layers[29,30] which are then subsequently heat-treated to form a single intermetallic structure. Bi-layer structures have been deposited commercially and are the standard practice to produce platinum aluminides following some heat treatment. It should be noted that this multilayered approach, to date, has only be demonstrated using the PVD method[31].

1.3 Traditional Methods of forming Diffusion Aluminide Coatings

The predominant method of depositing aluminide coatings within both industry and academia is Chemical Vapour Deposition or CVD. The CVD process, as the figure below depicts (Figure 1-3) shows that aluminium in the form of a pack is transformed into an aluminium halide with the use of an activator (typically a halogen) which in turn reacts with the base metal to form nickel aluminides. A review of traditional diffusion coating methods and the coating structures produced was conducted by Nicholls, Long and Simms which is due to be published in 2010[32].

Traditionally, diffusion aluminide coatings have been produced by CVD. The aluminising process using pack cementation was patented as long ago as 1911 by Van Aller[33] and was incorporated into the aerospace industry on nickel-based alloys in 1952[34]and cobalt-based airfoils in 1957[35]. Work by Goward and Boone in 1971[36] demonstrated that there were two possible diffusion mechanisms: inward diffusion of Al or outward diffusion of Ni (for nickel-based alloys), with the coating formed being an intermetallic compound based on NiAl.

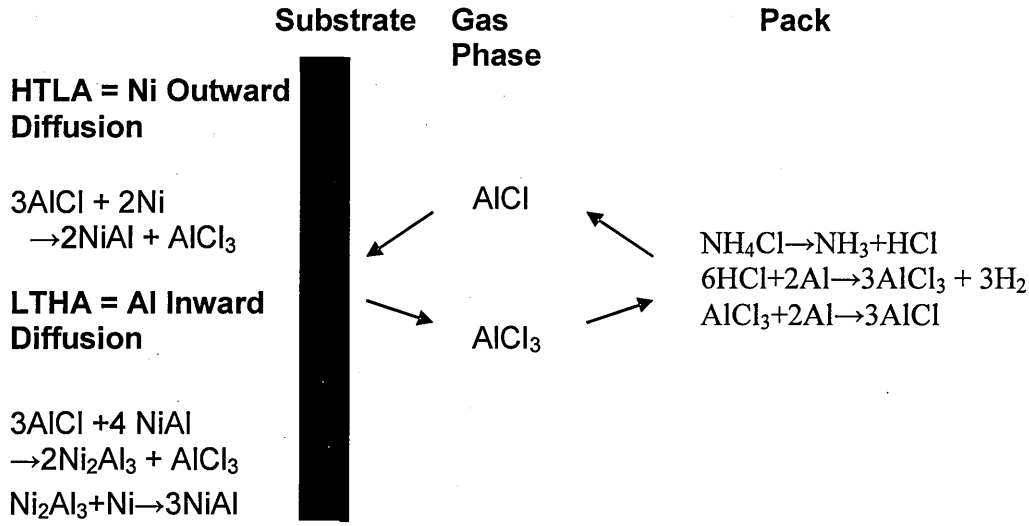

Figure 1-3: Schematic of CVD Processes[37]

Such chemical vapour deposition (CVD) techniques can be further classified into two different categories: In-pack and above-pack aluminising with in-pack aluminising, being the most popular.

In-pack aluminising requires that samples or components are placed into a retort and then covered by the 'pack' which is a mixture of aluminium oxide (approx. 98% and is a bulking agent), aluminium source (approx 1%) and an 'activator' (0.5-1%). The retort is then sealed and backfilled with argon to remove oxygen from the chamber and prevent oxidation reactions occurring during the process. The chamber is then heated to a preset temperature and soaked where the activator reacts with the source to form aluminium halides in a gaseous phase.

The aluminium source may be pure aluminium (in the form of flake, powder etc.) or a combination of aluminium and an element such as silicon to improve the melting point and therefore reduce aluminium activity. Pratt and Whitney use aluminium with 12% silicon, whereas other authors have used aluminium nitride[36]. The amount of aluminium added to the cement mixture varies depending on the required composition but it should be noted that not all the aluminium is incorporated within the new alloy formed[3,4].

1.3.1 Mechanisms of Aluminide Coating Formation – Work of Goward and Boone[36]

Goward and Boone published the first work that showed that two different processes can occur during aluminising: inward and outward diffusion mechanisms (low temperature with high activity (LTHA) and high temperature and low activity (HTLA) respectively.)

1.3.1.1 LTHA coatings

LTHA coatings are formed due to inward movement of aluminium due to a high activity transport mechanisms, which form the Ni_2Al_3 aluminide. This aluminide (Ni_2Al_3) must be post heat treated to form the desirable β-NiAl (1975°F (1075°C) in their work)

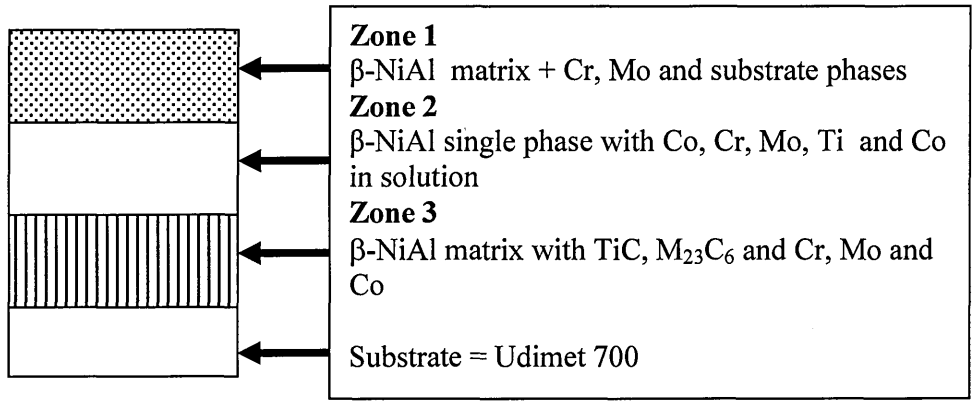

Figure 1-4: Schematic of LTHA Coating on Udimet 700

As Figure 1-4 illustrates, the coating is made of three distinct zones, the outer zone (zone 1) consisted of a β-NiAl matrix with substrate secondary phases present as precipitates, zone 2 was essentially a single phase of β-NiAl with all other constituents remaining in solution and zone 3, the interdiffusion zone consisting of a β-NiAl matrix plus phases from the substrate, especially carbides. The interdiffusion zone is created by the movement of Ni out from the substrate, rather than Al into it.

It should be noted that in the final coatings and within the Ni_2Al_3 stage, Goward and Boone observed that carbides were frequently found within zone 1. They also noted that the aluminium rich β-NiAl has a defective BCC structure with vacancies on the Ni sites (cube corners). The Ni_2Al_3 structure is very similar, but with vacancies sometimes found at the cube centres. Furthermore, the secondary phases found in the

zone 1 are metastable phase precipitates, due to the 'high rate and low temperature growth of the coating layers'.

1.3.1.2 HTLA Coatings

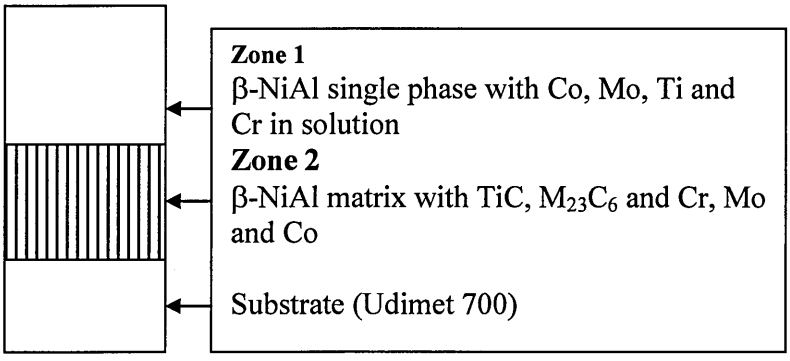

Figure 1-5: Schematic of HTLA coating on Udimet 700

As Figure 1-5 illustrates[36], HTLA coating consists of 2 different zones rather than the three characterising LTHA coatings. Zone 1, the outermost part of the coatings, was a single phase β-NiAl coating with other elements (Co, Cr etc) remaining in solution. Carbides are found within zone 2 up to and including the boundary layer with zone 1, but not within the upper layer.

Janssen and Rieck[38] observed that the formation of $NiAl_3$ and Ni_2Al_3 was via aluminium diffusion though these phases and it was further noted that the diffusion rates of Al in Ni_2Al_3 were extremely high. Levine and Caves[39] further noted that the CVD process was dominated by diffusion mechanisms, either solid state or gaseous.

It has been reported by numerous authors, including Angenete[40], that the cleaner structure of outward grown aluminide coating offers greater oxidation resistance, primarily due to fewer tramp elements being present in the outermost zone of an outwardly grown coating.

1.3.2 Platinum Aluminide Coatings

Platinum aluminide coatings are used throughout both industry and academia and are the predominant and preferred method of protecting high temperature components. Das *et al.*[41] were able to demonstrate that the addition of platinum to aluminised CM

247 improved the oxidation resistance by a factor of 10 at 1200°C (the difference becoming more pronounced as the temperature increased), before TBC spallation. These results were also confirmed by Angente[42] and Krisha[6]. Krisha *et al*[6] also noted that the addition of platinum improved the overall uptake of aluminium in the high-activity aluminizing process, provided that at least 2.5μm of Pt was deposited. Purvis and Warnes[43] reviewed the effect of varying the thickness of Pt deposited with low activity aluminising and showed that increasing the Pt thickness improved oxidation resistance, for a given aluminide coating thickness.

Platinum has been noted in platinum nickel aluminides to[44]:

- Increase both high and low temperature hot corrosion resistance[45 46]
- Eliminate Cr rich precipitates and prevent refractory elements diffusing into the outmost layers. It also enhanced coating stability [47,48]
- Improve oxide scale adherence[48-52] through the formation of oxide 'pegs'[51] or by eliminating sulphur segregation at the TGO and thus increases fracture toughness at the interface [53]
- Reduce formation of voids at the interface between the metal and oxide [52,54]
- Improve stability[47,48] of β-NiAl[45] and also prevent the formation of $\gamma' Ni_3Al$[50] within the β-NiPtAl layers
- Improve Al uptake during the CVD process[6] although a minimum of 2.5um was required[50]
- Reduce the diffusion rates of tramp elements from the substrate[45]
- Increase bulk modulus but decrease sheer modulus of β-NiAl[55]

Chen and Little[5] found that upon heating to 1100°C, several phases of Pt-Al on CMSX4 were evident due to interdiffusion of coating and substrate elements. The 'as coated' phase (β-(Ni,Pt)Al) transformed to β+ γ′ after 75 hours and finally to γ′/γ after 150 hours. Furthermore the aluminium content decreased from 25-26 atomic % in the γ′ phase to 14-15% in the γ phase.

1.3.3 Different Types of Platinum Aluminide Coatings

There are essentially 4 different types of Pt-modified aluminide coatings which are generally referred to by their commercial names:

- LDC-2: single phase of $PtAl_2$ which is homogenous (Figure 1-6)
- RT22: biphasic layer of β(Ni,Pt)Al and $PtAl_2$ (Figure 1-7)
- CN91: β(Ni,Pt)Al as a single phase (Figure 1-8)
- JML-1 & JML-2: A 2 layered coating consisting of an outer layer of Pt_2Al_3 and a complex triphase layer ($[Pt(Ni)]_2Al_3$ + PtAl, PtAl + β(Ni,Pt)Al and β(Ni,Pt)Al) (Figure 1-9)

1.3.3.1 LDC-2 Coating[56]

A 6-10μm platinum layer is deposited via electroplating followed by a high temperature aluminising process (HTLA). LDC-2 coatings (figure 1-6) is reputed to have improved cyclic oxidation and high temperature hot corrosion resistance by 4 and 2 times respectively when compared to aluminide coatings[57].

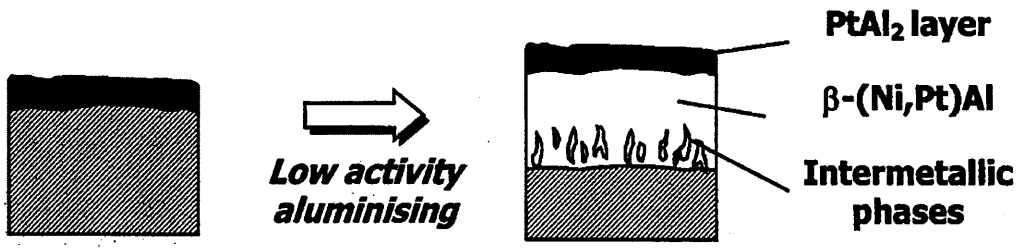

Figure 1-6: LDC-2-Type[58]

1.3.3.2 RT22 Coating[56]

This is a variation of the LDC-2 type coating produced by Rolls Royce/Chromalloy. A 5-10μm layer of platinum is electrodeposited onto a nickel-based superalloy which is then heat-treated and LTHA (low temperature high activity) aluminised. As it can be seen in Figure 1-7 this gives a two phase structure which is beneficial over the LDC-2 type (single phase) due to improved mechanical properties (particularly crack resistance), increased oxidation resistance and improved coating stability[43].

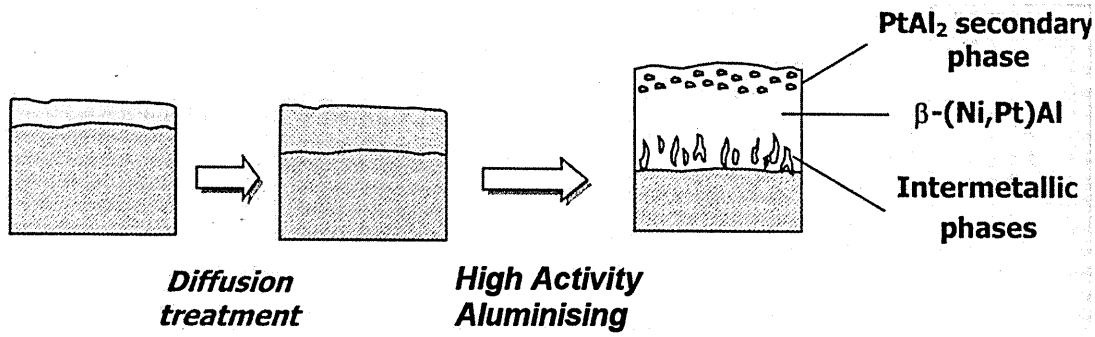

Figure 1-7: RT22-Type Coating (modified from [58])

1.3.3.3 CN91 Coating[59]

CN91 (figure 1-8) is a variant on the RT22-type coating but, instead of high activity aluminising, low activity aluminising is performed. This results in outward diffusion of Ni into the aluminium layer, rather than the inward diffusion of Al which occurs in the RT22 type coatings[40]. It should also be noted that CN91 is the trade name used by Chromalloy, it is also referred to as RT69 (Rolls Royce) and a similar coating is produced by Howmet, MDC-150L.

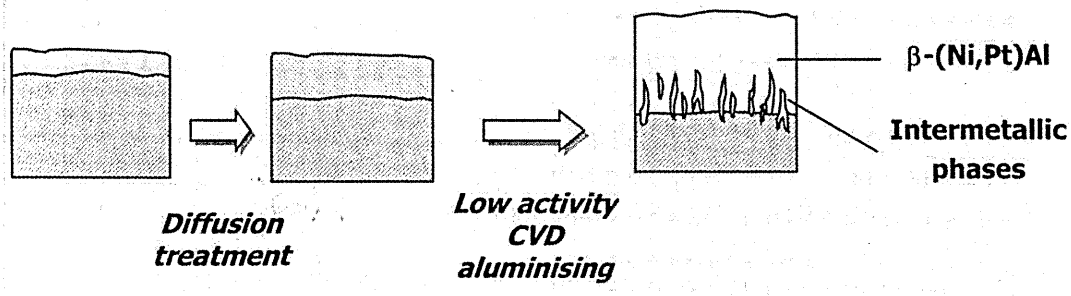

Figure 1-8: CN91-Type Coating[58]

1.3.3.4 JML-1 and JML-2 Coatings

JML 1 and JML 2 coatings (figure 1-9) were developed as a collaboration between Rolls Royce and Johnson Matthey[56] to make PtAl coatings more consistent. The Pt is deposited by fused salt deposition followed by a high temperature heat-treatment. Then low temperature aluminising is used to form a 50μm Al-rich layer. The coating has a complex multiphase microstructure.

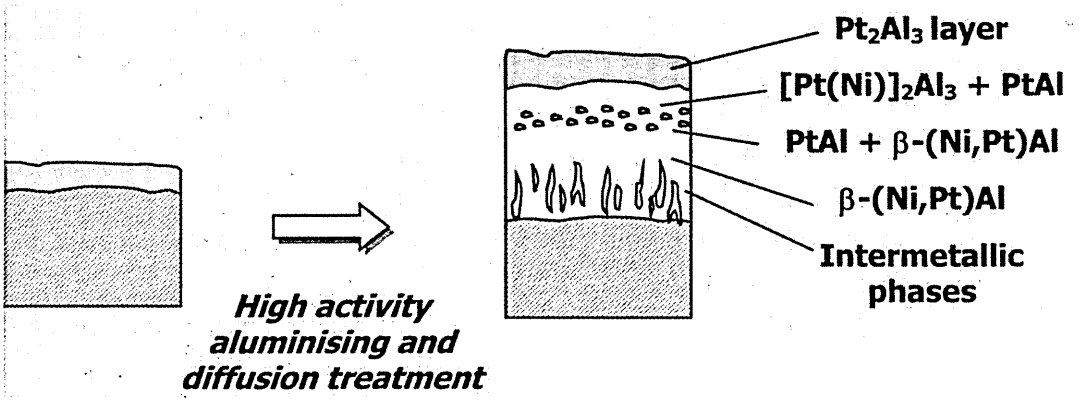

Figure 1-9: JML-1-Type Coating[58]

1.4 Oxidation Mechanisms of β-NiAl Coatings

Coatings designed for high temperature applications will undoubtedly undergo some degree of degradation, typically oxidation. Therefore an oxide scale forms which adheres to the coating, to limit the further ingress of oxygen, through acting as an oxygen diffusion barrier. However, initially oxygen reacts by bonding directly with the coating to form oxide nuclei, which expand laterally to form a very thin continuous layer. Diffusion through this layer must then only occur through solid state diffusion via defects in the crystal structure (point, line and surface defects) to permit short circuit diffusion paths.

However, the laws of thermodynamics and kinetics must be adhered to for its formation. Typically, metals react directly with oxygen to form a metal oxide as shown in the equation below:

$$M_{(s)} + \tfrac{1}{2} O_{2(g)} = MO_{(s)}$$

However, for this oxide to be formed, the reaction must be thermodynamically viable and therefore must have a negative ΔG value or Gibbs free energy.

$$\Delta G = \Delta H - T\Delta S$$

Where:

ΔG is the standard free energy change, ΔH is the standard change in enthalpy, ΔS is the standard change in entropy and T is temperature in Kelvin.

As reported in 1944 by Ellingham[60] and since termed Ellingham Diagrams, Figure 1-10 shows a plot of ΔG against temperature for oxide formation with various metals. As it can be seen from the figure, all oxide reactions shown are energetically favourably. Aluminium is a constituent part of most bond coat systems for high temperature applications and readily forms an oxide at room temperature when the partial pressure of oxygen exceeds 3.38×10^{-84} atm.

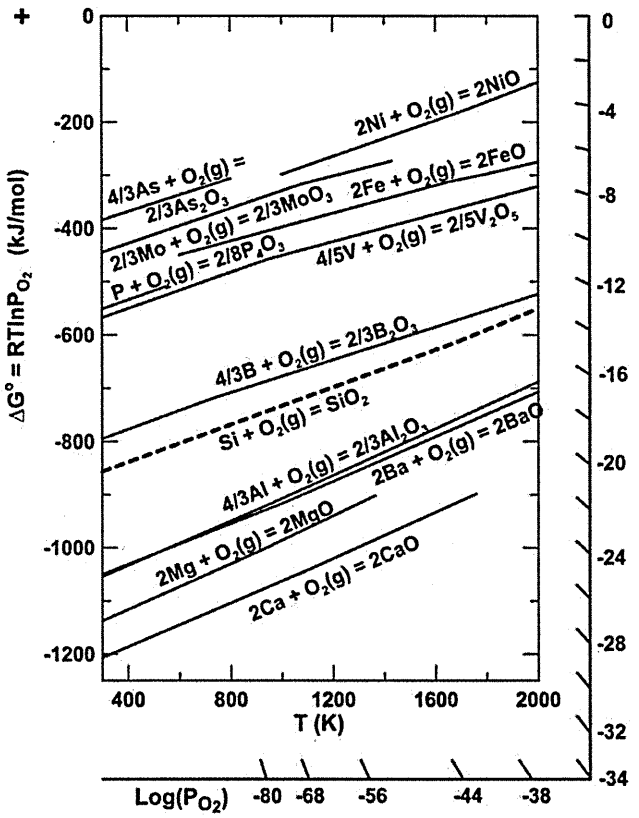

Figure 1-10: Ellingham Diagram[61]

Wagner noted that oxidation typically follows parabolic growth and is the main mechanism of oxidation of coatings and metals in high temperature applications. Immersing a coating in a high temperature environment for a given time (t) results in an oxide film of a given thickness (x). Therefore, the oxide film thickness grows in a parabolic manner (rather than linearly when oxide thickness grows proportionally to

time at temperature) at a rate governed by the parabolic rate constant (k_p) for a given amount of time.

$$x^2=k_p t$$

The oxidation mechanism of alloys and/or intermetallics is very complex and will not be discussed here in any further detail. For further reference see Smialek and Meier[62]

1.4.1 Oxidation of NiAl Coatings

Oxygen is initially adsorbed onto the coating surface, which forms nucleation sites for the oxide (various oxides of Ni, Co, Al or spinels). The most stable of these nuclei then grow laterally until a continuous layer is formed (termed the transient phase). Once the continuous layer is formed, the oxidation rate is controlled by transport through and growth of the most stable oxide (selective oxidation)[63]. Initially, at lower temperatures transient aluminas are observed (δ, γ, (both cubic structures) and θ (monoclinic structure)) which transform at higher temperatures to the most stable α-alumina[64].

Angenete[65] noted that early stage oxidation (20 hours) showed the onset of whisker shaped alumina phases (either metastable γ or θ) suggesting that this phase is formed by outward cation movement during alumina formation. When the oxidation was extended, the metastable alumina transformed to the more stable α-Al_2O_3. Furthermore, the addition of Pt was found to retard spinel formation and enhances formation of α-Al_2O_3. Finally, as the alumina scale continues to grow with the bulk movement of Al (phase transformation of β-NiAl to γ'Ni_3Al) the diffusion kinetics alter: Al depleted β-NiAl favours Ni diffusion whereas Al-rich β-NiAl favours Al diffusion[66].

Kim and Walter[67] (Figure 1-11) notes that microstructure of the NiAl bondcoat is dependent on the type of thermal oxidation as two distinct microstructures were present after 80 hours of iso-thermal and cyclic oxidation at 1200°C.

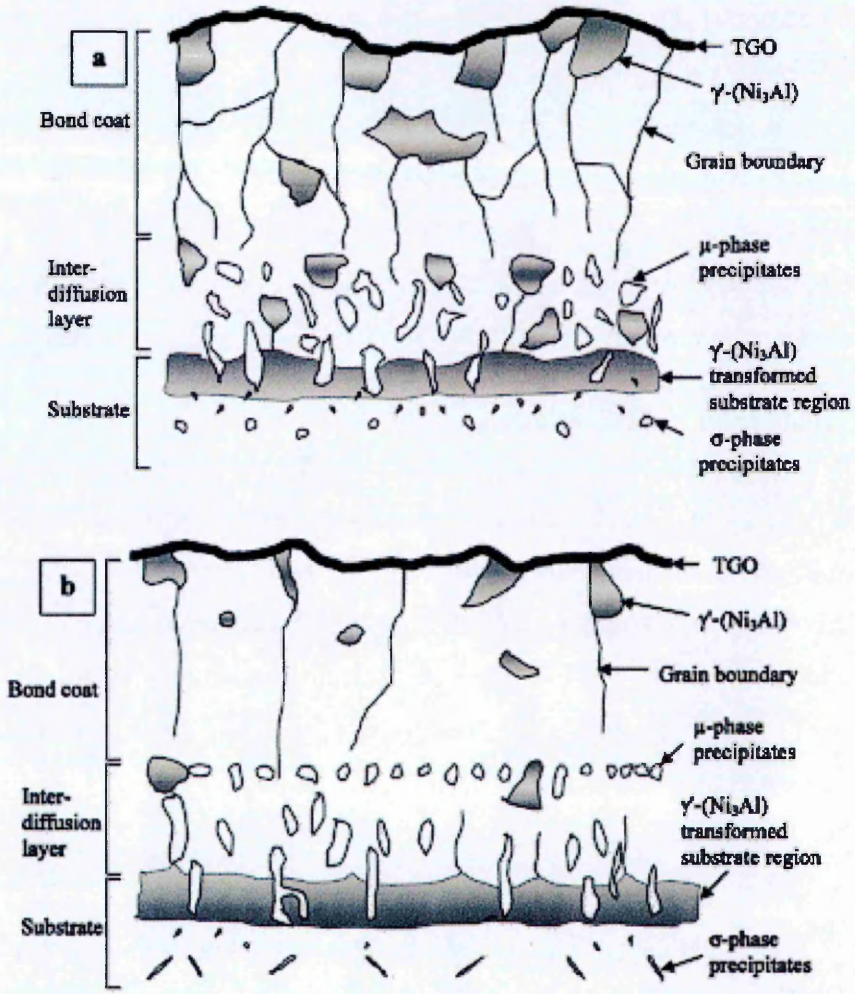

Figure 1-11: Microstructure of NiPtAl Coating after 80hours of Heating at 1200°C (a=cyclic oxidation, b=isothermal oxidation) [67]

1.4.2 Mechanisms for the Oxidation and Failure for NiPtAl/NiAl/TBC Systems

Numerous different failure mechanisms have been reported. They include:

- Continual growth of the TGO layer results in spallation and failure of the ceramic coating[19](typically 5-6μm[68]).
- With increasing thickness of the TGO as oxidation continues, the elastic strain will also increase[19] leading to failure when the interfacial fracture energy is reached
- Long term oxidation shows that the β-NiAl transforms to γ'-Ni_3Al.[3,19,26]
- Formation of γ' leads to 'short circuit corrosion paths' leading to premature failure of the coating[3,34]

- Phase changes from γ to α-Al_2O_3 account for a 14% reduction in volume which may be exhibited as cracks or voids in the TGO layer[19]. However, this would only occur with low temperature oxidation
- Any sulphur present moves to the TGO /alloy interface where it has deleterious effects especially on interfacial strength[69] (2% of interfacial coverage is enough to cause this[53]).
- During rapid cooling, there is a phase transformation from the β-NiAl (B2 to $L1_0$ (BCC to FCT) which is reversible[70]) to a martensitic phase due to Al depletion from within the coating
- The volume change (2%[70]) from transforming between BCC and FCT resulted in a 'rumpling' effect of the TGO[71]
- Martensitic formation occurred before significant formation of Ni_3Al during thermal cycling between 773-1373K[72] and is stable below 620°C[70] and occurs more readily in platinum rich NiPtAl alloys[73]

1.5 Electroplating

Electroplating is credited to Luigi Brugnatelli, an Italian chemist, who was able to deposit gold using a Voltaic Pile (named after Allesandro Volta) in 1805. He published in the Belgian Journal of Physics and Chemistry stating that:

> *"I have lately gilt in a complete manner two large silver medals by bringing them into communication by means of a steel wire, with a negative pole of voltaic pile, and keeping them one after the other immersed in ammoniuret of gold newly made and well saturated"*[74]

No other work was published on electroplating until John Wright, an English engineer, noted that potassium cyanide was a suitable electrolyte for both gold and silver electroplating. Wright's work, combined with the work of the Elkington cousins and independently by Barratt, resulted in a number of patents being filed in the 1840's for the plating of silver and gold[75]. Independently, Russian and British scientists were able to deposit nickel, tin, brass and zinc and make it into an industrial process[75] in the mid to late 19th century. Between the 1850's and 1940's technological improvements for the electroplating industry remained rather static. However, since the 1940's, a great deal of improvement in the bath solution chemistry (less noxious) and depth of understanding has allowed the industry to progress significantly.

1.6 Principles of Electroplating [76 77]

Faraday stated 2 laws which are now the basis for electroplating:

- The amount of chemical change produced by an electric current is proportional to the quantity of electricity that passes.
- The amounts of different substances liberated by a given quantity of electricity are proportional to their chemical equivalent weights.

A coulomb (C) is defined as the amount of electrical charge transported by a steady flow of current (amps) per unit time (seconds).

However, generally speaking 96,500C is referred to as a Faraday (F). Combining the two Faradays laws it is possible to derive the equation:

$$w = \frac{Iet}{96500}$$

Where: w = amount of material reacting, I = current (Amps), e = chemical equivalent weight, and t = time in seconds. Furthermore, if the voltage is known then the energy consumed may be calculated by: volts x ampere-hours = watt-hours (W.h).

1.7 Electrode Potentials

The values shown in Table 1-3 give an indication of how easily elements are able to be oxidised or reduced when immersed in solutions of their own salt. Furthermore, this table gives an indication whether a metal is noble or active. Therefore those ionic solutions with a high ΔG value for ion reduction or ones with a high negative E^O value (Li, Mg, K etc.) form stable ions. Contrary to this, those with a negative ΔG or positive E^0 values with respect to ion reduction show that they are more stable in the reduced form.

Once a metal electrode is placed into a solution containing ions an equilibrium is set up:

$M = M^{n+} + ne^-$ where e^- = 1 electron

Table 1-3: Electrochemical Series[78]

Equilibrium	E° (volts)
$Li^{+}_{(aq)} + e^{-} \rightleftharpoons Li_{(s)}$	-3.03
$Ca^{2+}_{(aq)} + 2e^{-} \rightleftharpoons Ca_{(s)}$	-2.87
$Na^{+}_{(aq)} + e^{-} \rightleftharpoons Na_{(s)}$	-2.71
$Mg^{2+}_{(aq)} + 2e^{-} \rightleftharpoons Mg_{(s)}$	-2.37
$Al^{3+}_{(aq)} + 3e^{-} \rightleftharpoons Al_{(s)}$	-1.66
$Zn^{2+}_{(aq)} + 2e^{-} \rightleftharpoons Zn_{(s)}$	-0.76
$Fe^{2+}_{(aq)} + 2e^{-} \rightleftharpoons Fe_{(s)}$	-0.44
$Pb^{2+}_{(aq)} + 2e^{-} \rightleftharpoons Pb_{(s)}$	-0.13
$2H^{+}_{(aq)} + 2e^{-} \rightleftharpoons H_{2(g)}$	0
$Cu^{2+}_{(aq)} + 2e^{-} \rightleftharpoons Cu_{(s)}$	+0.34
$Ag^{+}_{(aq)} + e^{-} \rightleftharpoons Ag_{(s)}$	+0.80
$Au^{3+}_{(aq)} + 3e^{-} \rightleftharpoons Au_{(s)}$	+1.50

The magnitude of the potential difference between a metal and a solution of its ions is given by the Nernst equation.

$$E = E^{0} + \frac{RT}{zF} \ln\left[\frac{Oxidized}{Reduced}\right]$$

Where:

E = potential in volts, E^{o} = Electrode potential referred to that of hydrogen, z = valency, T = temperature in Kelvin, F = Faraday constant, R = gas constant (8.314 $Jmol^{-1}K^{-1}$),

Finally, it should be noted that 2 distinct reactions occur at the anode and cathode surface within aqueous solutions[77]:

Cathode:

Metal deposition ($M^{2+} + 2e = M_0$)

Hydrogen evolution ($2H^+ + 2e = H_2$)

Metal reduction ($M^{3+} + e = M^{2+}$)

Anode

Metal dissolution ($M^0 = M^{2+} + 2e^-$

Oxygen evolution ($2H_2O = O_2 + 4H^+ + 4e^-$)

Oxidation ($M^{2+} = M^{3+} + e^-$)

For a more comprehensive review see Gabes book titled 'Principles of Metal Surface Treatment and Protection[77].

1.8 Electrodeposition of Platinum

Elkington in 1837[79] and Böttger[80] in 1878 are the first to be credited with plating techniques for platinum; however it should be noted that both used molten salts for the electrolyte and that the solution was unstable. The use of molten salts continued until 1910 when McMillian and Cooper[81] stated that 'electroplating platinum is hard' even though nine different process routes had been reported by this time. Today, platinum plating may be defined into 3 different categories: divalent aqueous platinum salts, tetravalent aqueous platinum salts and other ionic forms of platinum salts.

1.8.1 Divalent Aqueous - Chloride Based Solutions

These salts have no real significance in current work. However, these salts were the first to be technically beneficial. The basis for this is the platinum chlorides ($PtCl_4 \cdot H_2O$ and $H_2PtCl_6 \cdot H_2O$) and form the basis of methods proposed by Böttger[80]. The solution is operated at 90°C, with a current efficiency of approximately 70% which produced coatings which were fine, but irregular grained.

Further work was conducted by Grube and Reinhart[82], followed by Atkinson[83], on chlorinated baths and they were able to produce crack-free coatings of up to 20μm thick. In addition to this, Atkinson went on further to say that baths using the $H_2PtCl_6 \cdot H_2O$ salt must be kept within a tight pH range (2-2.2) in order to prevent hydrolysis. It should be noted that during the plating process that discolouration of the coating normally occurs due to the increased concentration of chloride ions. If more acidic solutions are used along with low current densities the platinum anode dissolves (preventing the need to replenish the concentration of the salt in the bath). Conversely, if low concentrations of HCl are used, an insulting layer of $(NH_4)_2PtCl_6$ is formed at the anode.

1.8.1.1 Dinitrodiammine based solutions

These salts are used primarily to stabilize the Pt at the divalent state (i.e. prevent oxidation to the Pt(IV) state) by complexing the Pt with amino compounds. Keitel and Zschiegner[84] in 1931 created the dinitrodiammine salt (cis-dinitrodiamine platinum – $Pt(NH_3)_2(NO_2)_2$) which is now called the Pt-P-salt. During the early stages of electroplating, the majority of impurities (non metallic) are released in gaseous form. A variation of this was invented by Lacroix and Beclier[85]and patented in 1967 which involved the use of fluoroboric acid and an insoluble platinum anode to produce deposits up to 7μm thick. However, some authors suggest that this solution will only give a good quality coating when the platinum is only present in the divalent state[86]. Furthermore, it should be noted that the use of fluroborate allows current densities of up to 5A/dm^2 to be used (the highest rate of all Pt electroplating routes).

1.8.1.2 Dinitrosulphatoplatinous Acid Based Solutions

These baths are typically based on the $H_2Pt(NO_2)_2SO_4$ complex and are free from both ammonia and amines. This solution allows the deposition of platinum coatings onto materials such as copper, silver, nickel lead and titanium; however, zinc, cadmium, and iron substrates require a bond-coat of nickel or silver[87]. Coatings of up to 25μm are easily produced which are bright in appearance, using a relatively high current density of 2.5A/dm^2. The pH needs to be kept low (approx. pH 2 typically using dinitrosulphatoplatinous acid (DNS) with sulphuric acid). The bath is very stable and does not typically degrade over time, however, it should be noted that thicknesses above 25μm tend to lead to cracked coatings when using this solution.

1.8.2 Tetravalent Complexes

1.8.2.1 Alkaline

These solutions produce dense and brightly coloured coatings and are based on the hexahydroxyplatinic salt i.e. $Na_2Pt(OH)_6$ or $K_2Pt(OH)_6$[88] maintained at a pH of 13. If the solution is allowed to stand for a period of time the deposits become less brightly coloured and 'spongy'. It should be noted that if the salt concentration falls below 3g/l then the current efficiency drops to a couple of percent. However, at high concentrations (12g/l) then current densities up to $2A/dm^2$ may be employed.

Johnson Matthey has recently developed a plating solution ('Q' Salt) which is able to deposit thick platinum coatings (>5μm) at high deposit rates[89]. Le Penven[90] showed that when operating at bath temperatures above 363K the platinum salt complex was reduced in a pH of 10.4. Basirun *et al.*[91]noted that on starting electroplating the voltage increased as the initial Pt nuclei were formed, and then returned to a steady state once a continuous layer was formed. In another study, Basirun[92] also noted that if the processing temperature was below that recommended, in this case 358K, the deposition rate was lower. However, the current efficiency remained the same independent of temperature.

1.8.2.2 Phosphate-based electrolytes

These solutions are based on platinum (IV) chloride or hexachloroplatinic acid[79]. However, current densities are low ($0.3\text{-}1A/dm^2$) and thicknesses up to 0.5μm only may only be deposited.

1.8.3 Electroless Deposition

This form of deposition has been termed due to the absence of an external source of an electric current. Depositions are due to the introduction of a reducing agent (such as hydrazine) within the plating bath. Numerous plating solutions have been suggested, since Osters early work in 1969[93]. However, these routes tend not to be favoured for industrial uses and will not be reviewed further.

1.9 Ionic Liquids

The term "Ionic Liquids" is becoming increasingly used throughout both academia and industry. This niche area is expected to become even more popular as the understanding behind 'Green Chemistry' applications improves and legislation against traditional solvents becomes increasingly more stringent. Ionic Liquids (ILs) have been traditionally defined as salts which have a boiling point below that of water[94]. However, they are now thought of as salts which are liquid at room temperature (RTIL (room temperature ionic liquids))[92]. ILs have been incorporated into the 'Green Chemistry' field due to the fact that these liquids have been termed the 'ultimate non-volatile organic solvent'[95], furthermore, they have negligible vapour pressure, a wide electrochemical window (up to 5.5V)[96] (the electrochemical window for ILs may be thought of as the ability to resist either the oxidation or reduction of cation and anion respectively), are stable up to 400°C[97], have a density greater than that of water (1-1.6gcm^{-3}) and dissolve substances which are both inorganic or organic at the same time[92,98]. However, some authors have criticised the term 'green-chemistry' as the thermal stability of ILs is dependent on the nature of both ions[99].

It has been noted in the past that ILs tend to have a large temperature range between the liquidus and solidus range[95]. However, chemically, ILs shows remarkable similarity; the majority possess both an organic cation and a polyatomic inorganic anion. As these cations and anions can differ immensely, the sheer number of potential variations of ILs is huge – thus to find a new IL is theoretically a relatively simple process. However, to find a functional use of ILs is more difficult due to the time and technology needed to determine its chemical and physical properties[92,95]. To highlight the continued importance of ILs, Holbrey *et al.*[95]calculated that approximately 10^{18} ionic liquids could be available.

Within the literature there is some debate about the history of ILs. However, ethylammonium nitrate [$EtNH_3$][NO_3] was found to be in a liquid state at room temperature in the early 20th century[100]. Other ILs were proposed based on this salt; however, in 1963 the American Air Force under the direction of Major Dr Lowell researched alternatives to the electrolyte LiCl/KCl for thermal batteries which led to the formulation of the $NaCl/AlCl_3$ electrolyte[92,94,95]. It should be noted, however, that

this mixture has a melting point of 107°C so it is not technically an IL based on the definition that it should be a liquid at room temperature. However, this is considered the birth of modern ILs.

Hussey[101], also of the American Air Force, looked into methods of predicting the reduction of cations after alkylpyridinium cations were noted to reduce with relative ease. The dialkylimidazolium salts with particular reference to 1-ethyl-3-methylimidazolium (EMIM) chloride were of prime interest, as when mixed with $AlCl_3$ the resulting compounds were liquid at room temperature. This new salt acted well as a new type of electrolyte, and worked as both a catalyst and a solvent[102].

Ionic liquids have not been limited to electroplating. ILs have been used for conducting polymers, synthesis of colloidal nanoparticles, carbon nanotubes, batteries, catalysts etc. For a review of the wider use of ionic liquids see Endres and Zein El Abedin[103].

1.9.1 Ionic Liquids and Electrochemistry

The majority of metals can be deposited using aqueous solutions. However, for certain metals hydrogen evolution causes embrittlement of the deposit[97,104]. Furthermore, metals with a reduction potential greater than that of water (i.e. Al) are problematic for electroplating when water is used as a solvent as the water decomposes before the metal deposits. Hurley *et al.*[105] were the first to note the importance of ILs and their electrochemical properties especially in their ability to deposit aluminium using electroplating routes. ILs are deemed favourable for electroplating due to their wide electrochemical potential window, good solvent transportation, wide liquidus phase, good electrical conductivity and ability to solvate a range of organic and inorganic molecules[92].

1.9.2 Ionic Liquids and Water

Many authors have noted that impurities can influence the effectiveness of ILs (especially those of halides and water in non-haloaluminate ILs[106]). Schroder *et al.*[107] and Abbott[108] noted that anhydrous versions of 1-butyl-3-methylimidazolium tetrafluroborate [BMIM][BF_4] (a model of BMIM is illustrated in Figure 1-12) gave an electrochemical window of 4.1V compared to studies with additions of 3% w/w water which reduced the usable potential to 1.95V. In practical terms the use of cyclic

voltammetry is employed where three electrodes (typically glassy carbon, tungsten and platinum) where an increasing and decreasing current passed through the electrodes until the oxidation and reduction limits are met. Furthermore, the addition of water, chlorides and organic solvents to the system can form impurities (normally oxides) which are active within the window and therefore reducing the ILs efficiency[101,106,109]. It has been proposed that phosgene may be employed to remove these oxides[109].

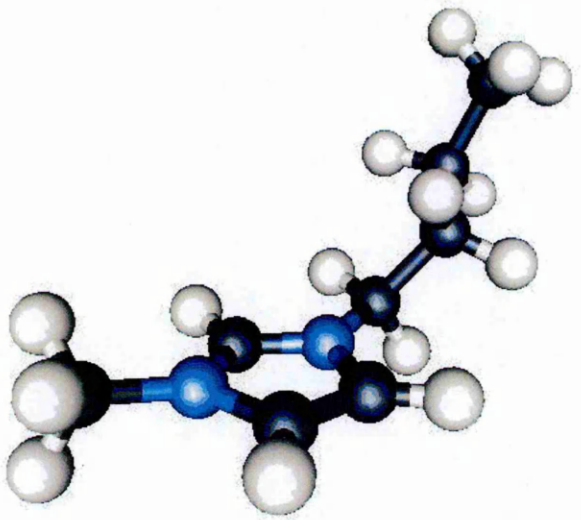

Figure 1-12: Model of 1-butyl-3-methylimidazoilum [BMIM][110] (blue atoms = Nitrogen, Black atoms = carbon and white atoms = hydrogen)

The solubility of the IL for water depends on both the anion and cation, as Schroder[107] stated, for example that [BMIM]PF_6 could have a water/IL equilibrium of 12.1% water, whereas [BMIM]BF_4 and [MDIM]BF_4 had values of 25.2 and 15.8 wt% water respectively.

1.9.3 Properties of Ionic Liquids

It can be observed from above; the potential of different electrolytes based on ionic liquids is very large. Galinksi[111] reviewed this extensively in 2006 and named over 60 different electrolytes used in the past quoting molar weight, densities, conductivities and viscosity. The paper highlights that the conductivities of ILs are greatly reduced compared to those of classically used electrolytes. ([EtMeIm] and sulphuric acid in water are 10 and 730 mS/cm respectively). However, this is influenced by the viscosity of the liquids. Some physical properties of some ionic liquids is shown in table 1-4.

Table 1-4: Physical Properties of Some Ionic Electrolytes

Ionic Liquid		Measured at 25°C				
Generic Grouping	**Formula**	**M (g/mol)**	**Density g/cm^{-3})**	**σ (mS/cm)**	**η (cP=0.1Ns/m^2)**	**Ref**
Imidazolium	$[MeMeIm]^+ [N(CF_3SO_2)_2]^-$	391.0	1.559	8.40	44	112
	$[EtMeIm]^+[BF_4]^-$	197.8	1.24	14	25.7	113
	$[EtMeIm]^+[CF_3SO_3]^-$	260	1.39	8.6	45	112
	$[EtMeIm]^+[N(CF_3SO_2)_2]^-$	391	1.52	8.8	34	99
	$[EtEtIm]^+ [N(CF_3SO_2)_2]^-$	405	1.42	8.5	35	99
	$[1\text{-Et-}2,3Me_2Im]^+$ $[N(CF_3SO_2)_2]^-$	405	1.495	3.2	88	112
	$[BuMeIm]+[BF_4]^-$	225.8	1.21	3.53	180	114
	$[PrMeIm]+[BF_4]^-$	211	1.24	5.9	103	114
Pyrrolidinum	$[nPrMePy]^+[N(CF_3SO_2)_2]^-$	408	1.45	1.4	63	96,115
	$[nBuMePy]^+[N(CF_3SO_2)_2]^-$	422	1.41	2.2	85	115
Tetraalkyammonium	$[Me_3BuN]^+[N(CF_3SO_2)_2]^-$	386	141	1.4	116	115
	$[Bu3HexN]+[N(CF_3SO_2)_2]^-$	550	1.15	0.16	595	116
	$[nHexEt3N]+ N(CF_3SO_2)_2]^-$	466	1.7	0.67	167	115,116
Pyridinium	$[BuPi]^+[BF4]^-$	223	1.22	1.9		117
Piperidinium	$[MePrPp]^+[N(CF_3SO_2)_2]^-$	422		1.51	117	118

Where: M = Molar weight, σ = conductivity and η = viscosity

Numerous metals have been deposited from ionic liquids using electroplating. These include: indium ([DMPIC])[119], tellurium ([MEIC])[120], palladium ([BMPTFSI])[121], tantalum ([BMPTf_2N])[122], caesium (B_3MNTf_2N)[123], aluminium ([EMImCl]/$AlCl_3$)[124] [BMIm]Al_2Cl_7)[125]([TMPAC]$AlCl_3^-$)[126]([MEIC]$AlCl_3^-$)[127] ([MeEtimCl]$AlCl_3$][128], silver ([BuMeIm]BF_4) [129], platinum ([BMIm]$BF_4$and [BMIm]PF_6)[130], cobalt ([MeEtimCl)[131], copper ([MEIM])[128], zinc ([EMIm])[132], sodium ([MEIC])[133], Gallium ([EMIm])[134], tin ([TMHA-Tf_2N])[135] etc.

1.9.4 Electrodeposition of Aluminium Coatings from Ionic Liquids

The majority of aluminide coatings are made by co-depositing with aluminium, therefore, a brief overview will be presented here.

Numerous ILs have been used to deposit aluminium but most use either aluminium heptachoride ($Al_2Cl_7^-$) or $AlCl_3$. $Al_2Cl_7^-$ reacts at the cathode:

$$4Al_2Cl_7^- + 3e^- \rightarrow Al + 7AlCl_4^- \quad [92]$$

Which can be re-oxidised at the anode 2.7V[127] to form:

$$4AlCl_4^- \rightarrow 2Al_2Cl_7^- + Cl_2 \uparrow + 2e^- \quad [136]$$

Giving the overall equation:

$$8Al_2Cl_7^- + 12AlCl_4^- \rightarrow 2Al + 14AlCl_4^- + 6Al_2Cl_7^- + 3Cl_2$$

However in the presence of water $AlCl_4^-$ reacts to form HCl and Al(Cl)x(OH)y where x can be either 0,1 or 2 and y = 3-x. The HCl is present within ILs as HCl_2^- or complexes with $AlCl_4^-$.

Jiang *et al.*[137] used TMPAC $AlCl_3^-$ to study nucleation of Al onto W and Al substrates. They noted that Al exhibited instantaneous nucleation. However, using cyclic voltammetry, the deposition/stripping of Al was noted to be quasi-reversible. Carlin *et al.*[127] used MEIC to obtain Al coatings and noted that nucleation sites were less than 0.5μm when an overpotential of less than -0.2V was employed which lead to very smooth coatings (Jiang[9] obtained almost identical results with [TMPAC]$AlCl_3$). Nucleation size increased when higher concentrations of $Al_2Cl_7^-$ were used.

The majority of ionic liquids used for the plating of Al are water, and air-intolerant (type 1). However, $BMPTF_2N$ (1-butyl-1-methyl pyrrolidinium bis (trifluromethylsulfonyl)imide - a water and air stable IL) with $AlCl_3$ has been used to produce nanocrystalline Al coatings at both room temperature and at 60°C[104].

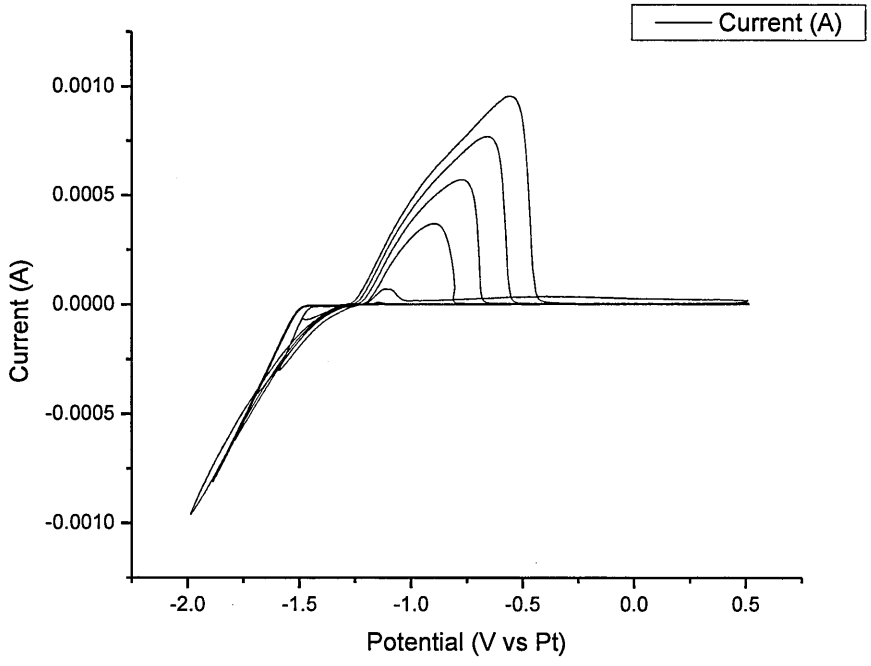

Figure 1-13: Cyclic Voltammetry Plot of [BMIM] Al_2Cl_7[138]

Figure 1-13 shows a cyclic voltammetry plot of [BMIM] Al_2Cl_7 which clearly shows reduction and oxidation peaks associated with the stripping and depositing of aluminium i.e. the those peaks with a negative current show where Al is reduced from Al^{3+} to Al, whereas those with a positive value show where Al metal is oxidised to Al^{3+}.

1.9.5 Ionic Liquids and Deposition of Aluminide Coatings

$Ni_{85}Al_{15}$ was deposited by Pitner *et al.* using [MeEtimCl][139] and a NiCl salt, however the resulting coating had a disordered FCC lattice. According to the NiAl phase diagram[15] this coating should exist as a $\gamma+\gamma'$ matrix under equilibrium conditions, and could have a potential for future aerospace alloys. Further work done by Pitner and Hussy[140] using the same ionic liquid showed that the content of aluminium in nickel aluminide deposits was linear with respect to nickel concentration but non-linear with respect to current density.

The nickel aluminides Ni_3Al and NiAl have both been deposited by Moffat in 1994[141]. However, it should be noted that the electrolyte was $2AlCl_3$-NaCl with addition of Ni^{2+} ions. Depositions were conducted at 150°C, and so were not particularly practical for productionising. Using a potentiostatic set-up, voltages of above 0.7V gave Ni

deposits and below 0.6V gave NiAl alloys where the alloy composition was a function of potential. Moffat[141] was also able to record open circuit potentials of 0.8V for Ni, 0.770-0.799 for Ni_3Al, 0.736 for NiAl and 0.0 for Al.

Mitchell et al.[131] in 1996 were able to co-deposit CoAl alloys from $AlCl_3$ MeEtimCl (with the Co being dissolved into solution) and noted that the Co concentration of the resulting alloy was particular to the potential applied and the concentration of the Al in the electrolyte. The potential also had an effect on the nucleation mechanism, as at 0.2V the nodules produced were dense and finely grained, whereas at 0V these nodules appeared to be a loosely adherent black powder. In addition to this, Ali et al.[142] were able to deposit various colbalt aluminides (Co reaching up to 60 atomic%) using [BPC] at a current efficiency of approximately 98%.

Chromium aluminides[143] ($Al_{100-x}Cr_x$ where x=11,14,25 and 41) have been co-deposited in $2AlCl_3$-TMPAC and $CrCl_2$ to form numerous intermetallics. Ali et al.[144] were also able to deposit a number of chromium aluminides using the BPC electrolyte and varying the Cr concentration from 0-94 atomic % (depending on the potential, current density and Cr^{2+} electrolyte composition). They also noted that Cr-Al alloys which contained between 20-50 atomic % Cr exhibited excellent high temperature oxidation resistance (600-800°C).

Abbott *et al.*[145] were able to co-deposit a Pt/Al coating (using [BTMAC] $AlCl_3$ with PtCl in solution) , but the Pt content was variable and microstructure was very nodular and inhomogeneous. It should also be noted that the nucleation mechanism varied depending on the Pt-complexes added to the IL by altering the solubility of the complex.

Tierney *et al.*[128] deposited copper aluminide alloys using $AlCl_3$-MeEtimCl. The copper was introduced into the electrolyte by applying a potential of 0.85V to a copper wire anode causing electrodissolution. The weight loss of the anode allowed confirmation of the copper concentration in the electrolyte. Similarly to the above aluminides, the chemical composition and morphology of the resulting alloy varied depending on the potential applied.

Carlin *et al.*[146] also have been able to deposit numerous aluminides including Co, Fe, Ni, Cu and Ag all from EMIC based ILs. Varying the potential in each case resulted in different alloying element compositions.

1.10 Conclusions from the Review of Ionic Liquids

Significant improvement and understanding of ILs has occurred since their conception almost 100 years ago. The formation of intermetallic coatings from ionic liquids is relatively new. However, the co-deposition of aluminium with other metals has been shown in the past to be feasible. In fact, with time, it would appear possible to pre-define alloy composition and produce said coating by modifying certain deposition parameters. Therefore, the sheer potential of intermetallics coatings that can be produced with ionic liquids is immense.

1.10.1 Other non aqueous deposition methods of Depositing Aluminium

Hurley in 1951[147] reported that by using toluene he and his group were able to deposit Al at room temperature with values of 81%, 92% and 91.8% cathode efficiency for 0.21A/dm^2, 1A/dm^2 and 1.75A/dm^2 respectively. Aluminium-copper alloys were similarly deposited by Capuano et al.[148] who used toluene, produced bright well adhered coatings that can undergo anodising. Table 1-5 shows a number of alternatives to electroplating aluminium rather than using ionic liquids.

Alumiplate[149], an engineering company in the US, are one of the few commercial entities electrodepositing aluminium from toluene-based systems. It is advertised as giving a 100% current efficiency but is completely enclosed preventing air and human contact with the plating bath. Toluene offers significant fire and health hazards.

Alternative electrolytes to deposit aluminium are shown in table 1-5.

Table 1-5: Ionic Liquid Alternatives to Plating Aluminium[150]

Electrolyte	A/m^2	CE (%)	Comments
$AlBr_3$, Ethyl Bromide, Na Br, KBr	200	60-70	Thin Al films with good adhesion
$AlBr_3$, Dimethyl Aniline		95	Smooth, bright and ductile coatings
NaF, $Al(C_2H_5)_3$, Toluene	60-80		Aluminium coatings with high corrosion resistance
LiH or $LiAlH_4$, $AlCl_3$ in Diethyl Ether	500	-100	Thickness can be up to 2mm with addition of methyl borate.
$AlBr_3$, Xylene or other Aromatic Solvents (Alkyl Benzene, Toluene)		50-80	Can be plating in small concentrations of water even in atmosphere.

1.11 Exothermic Reaction Synthesis: Forming Nickel Aluminides

Previous work done in Cranfield and in other institutions has shown that the formation of all nickel aluminide compounds is exothermic. The work done in Cranfield by Carlin[31] and by Silva[58] and externally, especially by Kleppa and Meschel[151,152,153]noted that aluminide reactions are predominately exothermic ranging from -13.7kJ/g-atom ($NbAl_3$)[153]to -185 kJ/g-atom (IrAl)[154]. Many authors have stated that nickel aluminides have a negative Gibbs enthalpy of formation value. However, work by Nash and Kleppa showed that by varying the composition of NiAl the enthalpy of formation varied betwee[1]n -51.3 kJ/g-atom($Al_{0.39}Ni_{0.61}$) and -61.2kJ/g-atom($Al_{0.495}Ni_{0.505}$). A table showing the properties of the nickel aluminides can be seen in Table 1-6 , enthalpy of formation of various aluminides in Figure 1-14 and a comparison of aluminides to germinides enthalpy of formation in Figure 1-15.

Table 1-6: Nickel Aluminide Composition, Melting Point and Enthalpy of Formation[58]

Phase	Melting Point (°C)	Enthalpy of formation (kJ/g-atom)	Composition (%at Ni)		Composition (%at Al)	
			Upper	Lower	Lower	Upper
Al	660.45	-	0	3.3	96.7	100
$NiAl_3$	854	-38	25	25	75	75
Ni_2Al_3	1133	-56	36.8	41.5	58.5	62.8
NiAl	1638	-60	41.5	65	35	58.5
Ni_5Al_3	700	-56	63	68	32	37
Ni_3Al	1400	-40	73.8	76.6	23.4	26.2
Ni	1455	-	80	100	0	20

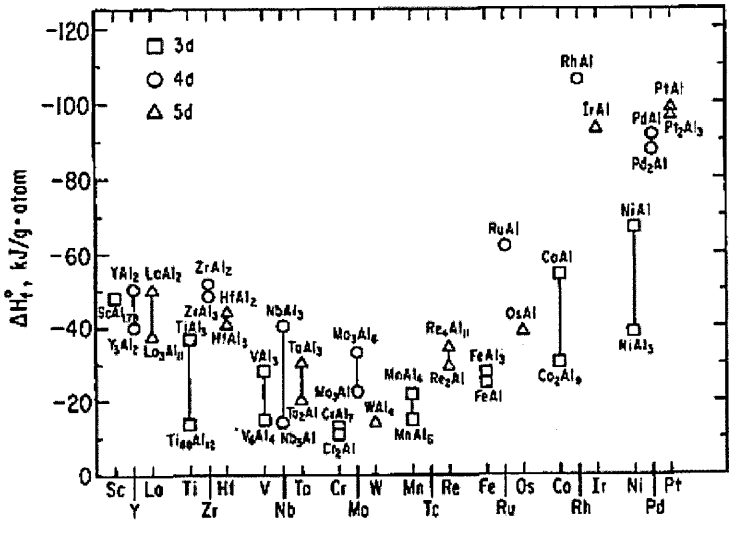

Figure 1-14: Comparison of Enthalpies of Formation for 3d, 4d, and 5d Aluminides[152]

[1] Note: Enthalpy of formation values are quoted directly from literature. g/mole and g/atom, although theoretically different are used interchangeably throughout this chapter.

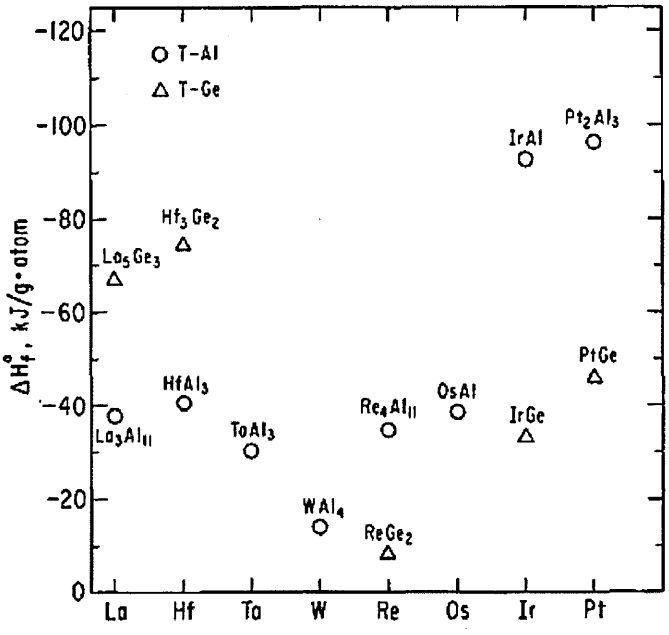

Figure 1-15: Comparison of Selected Aluminides against Germanides[152]

Gibbs free energy (Gibbs function) is a measurement of the thermodynamic potential of a given reaction and is stated in the equation below.

$$G = H - TS$$

Where H, T and S equals the enthalpy, temperature and entropy in the system.

The enthalpy of formation is the main driving force for intermetallic formation as entropy values and change in T are thought to have a minimal effect on the formation of an ordered compound. Therefore, free energy change ΔG may equate to enthalpy change (ΔH) which may be described as:

$$\Delta H_{reaction} = \Delta H_{products} - \Delta H_{reactants}$$

It should be noted that there is some ambiguity of final enthalpies of formation as different methods have been used to deduce the result from ball milling, vapour pressure, calorimetry etc. However, Miedema[155] formulated a model for predicting enthalpies of formation which was extended by Goncalves and Almeida[156] to include more than two elements.

Miedema original equation:

$$\Delta H = \frac{f(c)P(C_A V_A^{2/3} + C_B V_B^{2/3})}{(nw_{ws}^{-1/3})_{average}}\left[-(\Delta\partial^*)^2 + \frac{Q}{P}(\Delta n_{ws}^{1/3})^2 - \frac{R}{P}\right] + C_B \Delta H_{Btrans}$$

Where P, Q and R = constants from the phase diagram, C_M = Atomic concentration, V_M = molar volume of metal (M). ΔH_{Btrans} = energy needed to convert B into metallic

state from non metallic state, $(n_{ws}^{-1/3})_{average}$ = average electrostatic screening length, f(c)= concentration function

Modified Equation:

$$\Delta H_{fME} \frac{P(F_{MET}V_M^{2/3} + f_{EMT}V_E^{2/3})}{2(n_{ws}^{-1/3})_{average}} \left[-(\Delta\partial^*)^2 + \frac{Q}{P}(\Delta n_{ws}^{1/3})^2 - \frac{R}{P} \right] + c\Delta H_{trans}$$

Where:
C =concentration of element (M or E), H_{fME}= enthalpy as a function of elements M and E, MET = distance between M element (central atom) and E element (central atom)

1.11.1.1 Previous Cranfield Work: Silva[58]

Silva in his MSc thesis title "The Manufacture and Characteristics of NiAl Intermetallic Coatings by Exothermic Reaction Synthesis" formed intermetallic coatings by depositing alternate layers of Ni and Al by sputtering and then heat treating to form nickel aluminides.

Table 1-7: Summation of Silvas' Work

System	Approx Coating Thickness (um)	After Heat Treatment (700°C 2 hours)
3 layers	7	Ni_2Al_3
5 layers	7	Ni_2Al_3
9 layers	9	Ni_2Al_3 ($NiAl_3$)
5 layers (+0.5 Al)	8	Ni_2Al_3 (NiAl)
9 layers (+0.5 Al)	9	NiAl

With a thickness ratio of 1.51: 1 (Al:Ni) it was possible to form the desirable NiAl intermetallic. It should be noted that it was thought that the ½ Al layer thickness on top enabled Al_2O_3 to form and therefore entrap heat and induce complete transformation. Although the thesis title mentions 'Exothermic Reaction Synthesis' very little theory or mechanism of action for the diffusion process is stated. The reaction enthalpies noted by Silva are given in Table 1-6 and a summary of his work is shown in Table 1-7.

1.11.1.2 Previous Cranfield Work: Carlin[31]

Carlins thesis looked at sputtering Ni, Pt and Al to make very thin bond coats of up to 25 layers producing a coating thickness of no more than 5um. Carlin noted that adherence was an issue and was due to volume shrinkage during formation (500

minutes at 700 and at 900°C). At no time during the project was β-NiPtAl formed (the subject of this thesis), but an alternative low cost α-NiPtAl bond coating was manufactured and although an exothermic reaction was noted, no mechanism of action was proposed. A heat ramp of 2°C/ min was used and the enthalpy of formation was measured at -38kJ/g-atom.

1.12 Summary on the Free Energy of Formation of NiAl

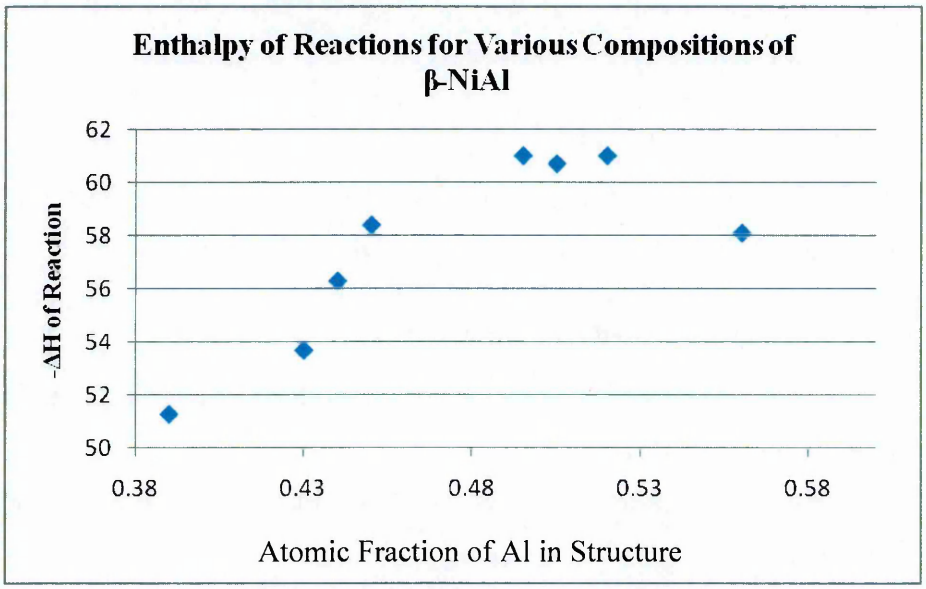

Figure 1-16: Enthalpy of Formation for Various Composition of β-NiAl

The free energy of formation of NiAl varied between -51.3 to -61.2 kJ/g.atom which varied with composition. For $Ni_{0.61}Al_{0.39}$, ΔH = -51.3 kJ/g atom at $Ni_{0.5}Al_{0.5}$, ΔH = 61.2kJ/g.atom as shown in Figure 1-16. The difference may be accounted for by changes to the defect structure in β-NiAl (when Ni rich β-NiAl tends, according to the Bradley/Taylor model, to contain Ni atoms sitting on Al sites of the Al sub lattice (anti-site point defect) and conversely vacancies sitting on the nickel site in Al rich β-NiAl alloys). Therefore, in Al rich β-NiAl where Ni vacancies exist it is thought that the crystal structure has distorted towards a more hexagonal structure (as observed in Al_3Ni_2 (hP5)) although retaining the basic constructs of a cubic structure as seen in β-NiAl. It is also suggested that Ni rich βNiAl, where Ni sits on the Al sub lattice, contorts into an almost orthorhombic structure whilst retaining the cubic structure. Therefore, the reduced enthalpies of formation for the Ni and Al rich β-NiAl may be due to this rearrangement of the atoms from the near orthorhombic/hexagonal to cubic therefore absorbing some of the energy generated.

2 Thesis Aims

2.1 Platinum plating:

1. Develop the use of the '5Q' platinum salt for the use in high temperature bond coat applications.
2. Assess whether 5Q produced bond coats offer improvements over the current Platinum P salt produced bond coats

2.2 Electroplating From Ionic Liquids:

3. Assess the ability to deposit Al from ionic liquids on a laboratory and industrial scale

2.3 Heat Treating Deposited Aluminium:

4. Assess the possibility of using Al from ionic liquids as an alternative bond coat production method.
5. Characterise concentration gradients of electroplate formed intermetallic bond coats compared to those using the CVD process.
6. Examine the possibility of forming bond coats on a pilot plant scale
7. Assess the feasibility of using a low temperature heat treatment regime.

2.4 Reasoning:

2.4.1 Platinum plating:

- The '5Q' salt is thought to offer an exciting prospect within the aerospace industry as it is claimed that this salt can deposit good quality thick deposits quickly. This thesis will review the effectiveness of this salt for the deposition of platinum using electroplating compared to the deposition of platinum using electroplated P salt sputtering techniques. The feasibility of using this salt in a semi-production capacity will also be evaluated.

2.4.2 Electroplating from Ionic Liquids:

- It is not possible to deposit Al from aqueous solutions due to the decomposition of water before the reduction of aluminium. Furthermore, it is

interesting to see if it is possible to deposit Al on turbine blades with a view to industrialise the process.

2.4.3 Heat Treating Al Deposits

- Typically, bond coats for high temperature turbine blades consist of a nickel-platinum aluminide coating which during processing form a thin alumina (Al_2O_3) top layer or thermally grown oxide (TGO). This TGO acts as primarily as a barrier for oxidation. With continual use at high temperatures this barrier increases in thickness using the bond coat as an aluminium reservoir. The accepted method of producing this aluminium rich layer is via chemical vapour deposition as aqueous electroplating of this metal is not possible. The use of CVD aluminising results in interdiffusion and the incorporation of refractory elements from the base metal into the coating. Furthermore, contaminants from the CVD process may also ingress into the coating, further reducing the coating's effectiveness. The use of ionic liquids as an electroplating medium has been achievable in the past, but to date, no-one has used aluminium from ionic liquids to create an aluminide coating on top of a nickel-based superalloy.
- Review the feasibility of heat treating deposited Al on nickel-based superalloys to form desirable bond coats: If it is possible to produce these coatings, can they be overcoated with thermal barrier coatings and is it possible to scale up from the laboratory to industry?

2.5 Overall:

- This project was funded within a European Framework Programme 6 proposal as part of the IOLISURF consortium, which had several industrial sponsors. Therefore the aims are strongly biased towards industrial goals. It is hoped that those aims which are directly linked to industrialisation, if successful, can be incorporated directly with minimal further development into production.

3 Experimental

3.1 Introduction:

This chapter will endeavour to explain how the practical side of this thesis was carried out from fabrication to analysis of coatings.

3.1.1 Samples

CMSX4 and GTD111 samples were supplied as 160mm feeder rods, which were turned down to a diameter of approx. 14.5mm and then sectioned using wire EDM to create 3mm thick coupons. Other samples of Ni200 and IN738 were also studied.

3.1.2 Cleaning of Substrates

One of the major issues of depositing any coating is the cleanliness of the substrate, as a contaminated coating will lead to a poorly adhered coating. At the start of the project, column cleaning in heated IPA was the method of choice within Cranfield with the samples undergoing at least 3 cleaning cycles before use. However, this was felt not to be suitable for the industrialisation aspect of this project (time taken was approximately two hours and was difficult for large parts). Therefore, grit blasting (Al_2O_3) followed by 30 minutes at 30°C in an ultrasonic IPA bath was used as the cleaning regime.

3.2 Coating Production

3.2.1 Platinum Plating

CMSX4 samples were spot welded to a stainless steel welding rod which acted as a cathode holder. The anode used was pure (99.99%) platinum gauze (Johnson Matthey) and was inserted into the Johnson and Matthey 5Q salt solution (adjusted for pH). Both the anode and cathode were attached to a simple power source for purely galvanic plating and to a potentiostat with a KCl reference for potentiostatic electroplating. The solution was heated to 91°C and then adjusted to a pH of 10.5 using 10% NaOH. Various current densities were used ranging from $0.02A/m^2$ to $3A/m^2$.

3.2.2 Platinum Sputtering

A platinum target (10''x 4'', approximately 250x100mm)) was loaded into a Nordico 2500 machine. The samples were placed into tooling, which itself was placed into the vacuum chamber of the machine. The system was then pumped down to a pressure of at least $8x10^{-6}$ torr before sputtering commenced. A 30 second target clean was used prior to all depositions. All samples were sputtered for a period of 52 minutes at 0.7A and approximately 350W (a rate run showed this to give 7μm), allowed to cool for one hour in vacuum and then the chamber was vented to atmosphere and samples removed.

3.3 Heat Treatment of Platinum

Platinum was heat treated in the Cranfield University vacuum furnace (table 3-1). A base pressure of at least $1x10^{-6}$ mbar was achieved before the heat cycle started.

Table 3-1: Initial Heat Treatment Start Parameters

Ramp Rate °C/min	Target Temperature (°C)	Time at Temperature (mins)
10	40	1
10	200	10
10	450	10

Ramp Rate °C/min	Target Temperature (°C)	Time at Temperature (mins)
40	1100	60
40	0	1

3.4 Aluminium Plating

3.4.1 Glove Box for Aluminium Plating

The glove box was filled with argon gas which was set at a positive pressure between 1mbar and 20mbar. The gas recycling unit within the glove box was set between 70 and 100% to minimise water content within the gas. Additionally sodium pentoxide was also used to reduce water within the glove box. From an electrical perspective, a 240V electrical supply was installed which was connected to a 4 way extension allowing for ancillary electrical devices to be utilised within the glove box. Furthermore, 2 off 5A rated electrical connections were installed into a protective junction box within the glove box. The glove box always operated within an argon atmosphere and water content less than 2ppm, usually at 0.8ppm.

3.4.1.1 Preparation of Samples and Plating Bath for Electroplating

The samples were grit blasted with Al_2O_3 grit at a pressure of approximately 1bar. The samples were then placed in a beaker containing isopropanol (IPA) which was then placed in an ultrasonic cleaner for 30 minutes at 30°C. Following this, aluminium wire was wrapped around each test piece to act as a cathode holder and then placed within the anti-chambers of the glove box (supplied by Innovative Technologies). The anti-chambers were pumped down to -30 inches Hg (<0.03bar) and then back-filled using the gas from the main chamber of the glove box. This last step was repeated at least 3 times to minimise the water content entering the main chamber. The sample/cathode holder were then attached to crocodile clips and then inserted into a beaker containing the ionic liquid (1:1 molar ratio of 1-butyl-3methyl-imidazolium and Al_2Cl_7 (supplied by MERCK)) – thus creating the circuit to commence electroplating.

3.5 Vacuum Furnace and Heat Treatment

All samples were washed in IPA prior to all heat treatment trials. Once the vacuum furnace was opened, the samples were placed on top of a clean aluminium oxide support plate. 20mm support tubes, also made of alumina, were placed on the support plate allowing for another support plate to be placed on top so 'sandwiching' the samples and preventing any contamination occurring during the heat treatment. A graphite 'hat' is placed on top to maintain insulation and then the furnace is sealed. The furnace is then pumped down to approximately $5x10^{-6}$ mbar before the heat treatment commences. The initial heat up sequence remained constant

Following this initial set up the following vacuum heat treatments were used for the various coating alloy systems in this study

3.5.1 Aluminium Diffusion Treatments

ICON Heat Treatment

Ramp Rate °C/min	Target Temperature (°C)	Time at Temperature (mins)
10	620	60
10	820	60
40	0	END

NP Heat Treatment

Ramp Rate °C/min	Target Temperature (°C)	Time at Temperature (mins)
40	1120	120
40	845	480
40	0	END

3.6 Fabrication of CVD Diffusion Coatings

Samples are grit blasted and cleaned with IPA as with the electroplated samples. The samples are placed within a tray entirely covered by pack aluminising powder. The tray is then placed into the CVD retort and the vessel is evacuated until a chamber pressure of -0.9bar and then back-filled with Ar until atmospheric pressure is reached. There is no fixed ramp rate within the chamber and a temperature is set on the controller. Any post-aluminising heat treatment is done within the vacuum chamber.

3.7 Thermal Barrier Coating (TBC) Deposition

Once the bond coat had been applied and heat treated (as reported in sections 3.4 and 3.6), a TBC was applied using the small custom EB-evaporator in the National High Temperature Surface Engineering Centre (680 Ion Plater). The samples were inserted within the chamber which was then pumped down to $2x10^{-5}$ mbar. Once the desired pressure was reached within the chamber it was heated to 1000°C whereupon gas (90% O_2 and 10%Ar) was admitted into the working chamber until the base pressure stabilised at $1x10^{-2}$ mbar. The electron beam gun was then turned on using an accelerating voltage of 10kV, and the current set to 5.5-6A. The electron beam was rastered across a zirconia-8%wt yttria source rod which melted the tip of the ingot. The gun ran for 80 minutes at which point approximately 200μm of ceramic was deposited.

3.8 Metallographic Preparation

3.8.1 Sectioning of Samples

The coated samples were sectioned using the ATA Brilliant 200 precision saw located within the metallographic laboratory at a disc speed of approximately 3000RPM and a feed rate of 0.8mm/min. Water cooling was used throughout.

3.8.2 Mounting of Samples

All samples were mounted using conductive Bakelite in a hot mount press at 170°C and at 200bar. The heating and cooling times were 7 and 3 minutes respectively.

3.8.3 Grinding and Polishing of Samples

All metallographic polishing was conducted using a semi-automatic Beuhler Metaserv Motopol 12 polisher. The load applied during polishing equated to 4 lbs/sample (1.8kg/sample) and the holder always turned in the same rotation direction as the grinding plate. The following procedure was used as shown in Table 3-2:

Table 3-2: Metallographic Process Route Used

Grit/Diamond Size	RPM	Time (approx)
#220	300	Until ground
#800	300	1 min
#1200	300	1 min
#2500	300	1 min
#4000	300	1 min
0.4μm colloidal silica	150	50 seconds and 10 seconds flush with water

3.9 Surface Analysis

3.9.1 Focused Ion Beam

The FIB used was the FEI 200 machine with FEI software. The chamber was evacuated to 5 $x10^{-6}$mbar with milling currents of between 6600pA and 11pA. Typically, the viewing current was 70pA.

3.9.2 Dual Beam

A dual beam FIB at Chalmers Technical University in Sweden was used. It was an FEI Strata 235. The dual beam is a combination of an SEM and a FIB and is especially useful in the preparation of samples for the TEM.

3.9.3 Scanning Electron Microscope[157]

The scanning electron microscope (SEM) used was the XL300 SFEG with the INCA analysis software. It is a versatile analytical tool used for surface characterisation especially with surface coatings. A brief overview will be given here but a more

comprehensive guide was written by Charles Evans *et al.*[157]. The SEM uses electrons generated from an electron gun fired (with a tungsten cathode) into a vacuum (to increase the mean free path). The electrons are focused using magnets onto the sample where they bombard and excite the atoms (typically in a tear-drop shape) to such an extent that electrons are released from the surface, which are collected by a detector. Scanning the beam produces a varying electron signal from the surface, which is relayed to a computer screen as an image. Within this thesis the majority of the samples viewed under the SEM were electrically conductive and therefore needed no special treatment for SEM analysis. However, in some instances the resin used was non-conductive and then a carbon or gold/palladium coating was sputtered to ensure electrical conductivity. Analysis may be done by either using secondary or back scatter electrons (much higher energies), with the latter aiding composition analysis as higher atomic number elements emit back scatter electrons more strongly than low atomic numbers.

3.9.4 Transmission Electron Microscopy[157]

The Transmission Electron Microscopes that were used at Chalmers Technical University, Sweden, were the Philips CM200 and a FEI Tecnai T20 TEM. Whereas, the samples for SEM need very little prior preparation, samples for transmission electron microscopy (TEM) need considerable work as electrons must be able to pass through the sample (less than 100nm thick). Like the SEM, the TEM relies on an electron gun to fire electrons into a vacuum, which are focused onto the sample using magnets. The electrons pass through the sample and are focused onto a fluorescent screen or photographic plate/decoder. Within 'brightfield' mode, heavier elements absorb more electrons and therefore appear darker on the screen and therefore when no sample is present a bright field is observed.

A schematic showing the comparison between optical, SEM and TEM is shown in Figure 3-1.

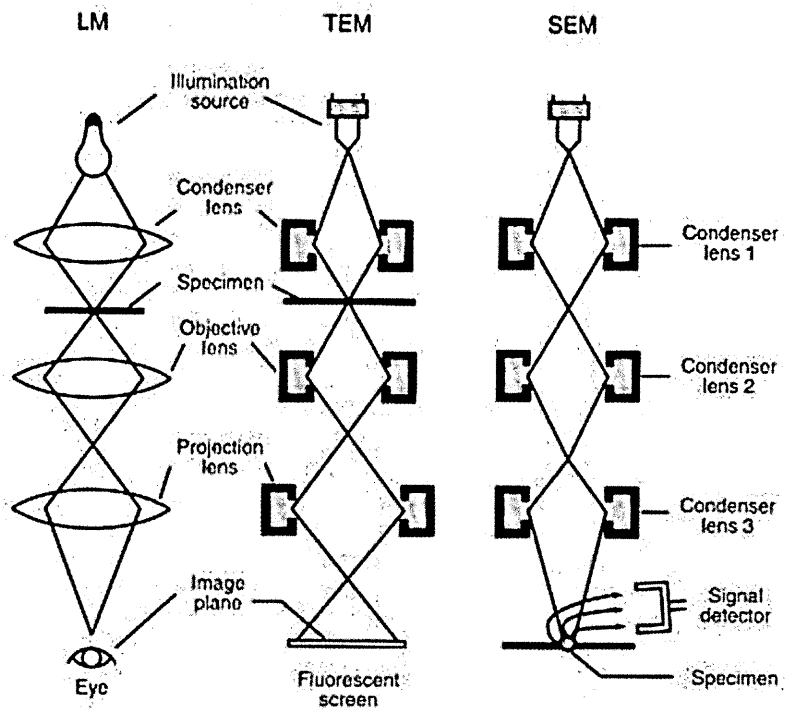

Figure 3-1: Comparison of lenses for Optical, Scanning Electron and Transmission Electron Microscopy[158]

The main problem with the TEM work, as mentioned before, was sample preparation. Within Cranfield it is possible to use a Focused Ion Beam (FIB) to section and thin a sample, which is then transferred to a copper 'grid' ready for analysis. Alternatively, in Chalmers University, the 'Dual-Beam' FIB (which encompass a FIB and an SEM) allows sample thinning, removal from bulk, attachment to a grid and continued thinning within one instrument.

3.9.5 X-ray Diffraction[157]

A Siemens D5005 X-ray Diffraction (XRD) machine was used throughout this project. XRD is a non-destructive method of analysing the crystal structure on the surface of any sample (schematic shown in Figure 3-2). The X-rays penetrate the sample and diffract off various atom planes allowing the measurement of interatomic distance (d)(Figure 3-3). Within crystallographic constraints, the interatomic distance depends on the lattice orientation which (Figure 3-4) can be described in Miller Indices.

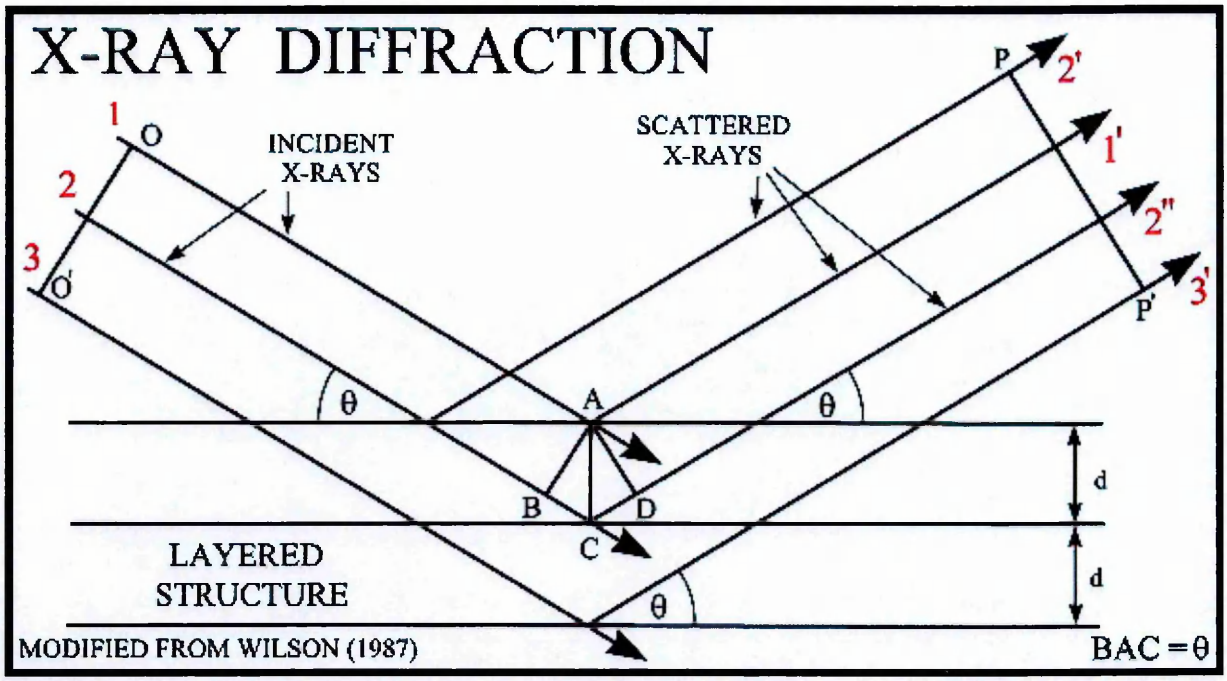

Figure 3-2: Graphical Representation of XRD[159]

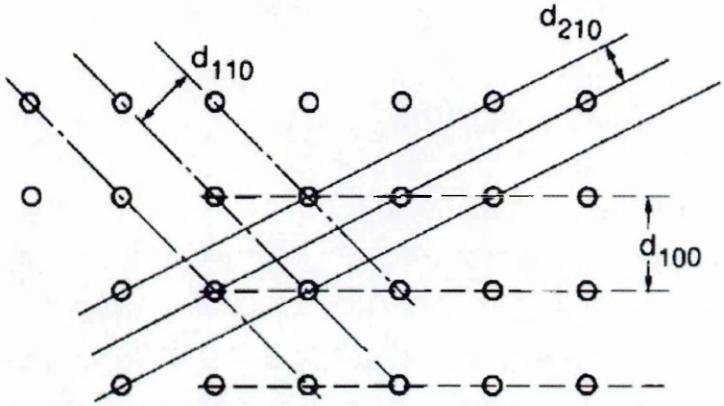

Figure 3-3: Graphical Representation of XRD (with D Spacing) [157]

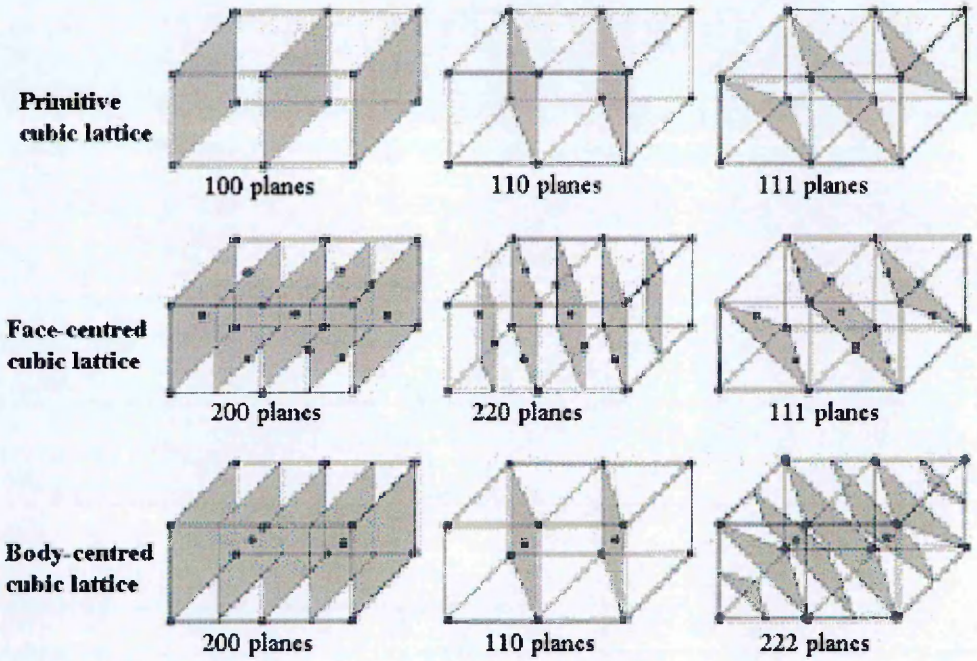

Figure 3-4: Graphical Representation of Different Miller Indices[160]

3.10 Analysis of Thermal-Chemical Properties

3.10.1 Differential Scanning Calorimetry

Differential Scanning Calorimetry (DSC) is a thermoanalytical technique, which enables measurement of the heat flow from exothermic or endothermic reactions compared to a standard. The DSC at Cranfield is a SETSYS Evolution 16 system produced by Setaram and is calibrated regularly with Pb, Zn Al, Ag, Au, Ni and Pd standards which have melting points and enthalpy of fusion (J/g) of 327.5°C & 23, 419 °C and 107.4, 660.4 °C & 104.8, 1064.2 °C & 64.5, 1455 °C & 300 and 1554 °C & 162 respectively. During endothermic reactions (as shown in Figure 3-5), the heat flow is negative and can be calculated by integrating the peak and creating tangents along the slope of each peak. For exothermic reactions a positive displacement of the peak would be observed.

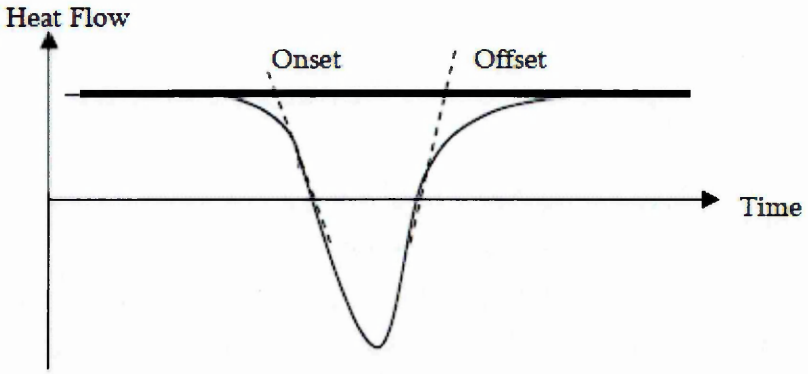

Figure 3-5: DSC Plot of an Endothermic Reaction and Calculation of Enthalpy of Reaction

The enthalpy of fusion is calculated by $\Delta H = H/K \times M$ where H is the total heat flow taken by integrating the peak (done by the software)), K is the calibration constant and M is the MW of the compound.

4 Results: Electroplating

4.1 Platinum from Aqueous Media (5Q salt)

RT22 type coatings appear to be the PtAl coating of choice within European aerospace industries, and as such have formed the basis of coatings produced within this thesis. Commercially this form of PtAl coating is manufactured using electroplating from the P salt and thus much research is reported as to the performance of coating made with this deposition process. The 'Q' salt produced by Johnson Matthey is seen as an alternative, new method of industrially plating platinum, hence the reason for using this salt. To date no literature exists for the formation of platinum aluminide coatings using this electroplating salt, except that presented by the author[161] and the results are given below as part of this thesis study.

4.1.1 Electroplating using 5Q Salt

Three different coatings were produced: highly reflective metallic, matt metallic and matt black coatings (as shown in figures Figure 4-1 to Figure 4-3 respectively) irrespective of the current densities used (the 5Q salt was pH adjusted to 10.5 using NaOH and various low current densities (0.05-1A/dm^2 with a temperature of 91°C)). These coatings were sectioned with the FIB with micrographs below:

Highly Reflective

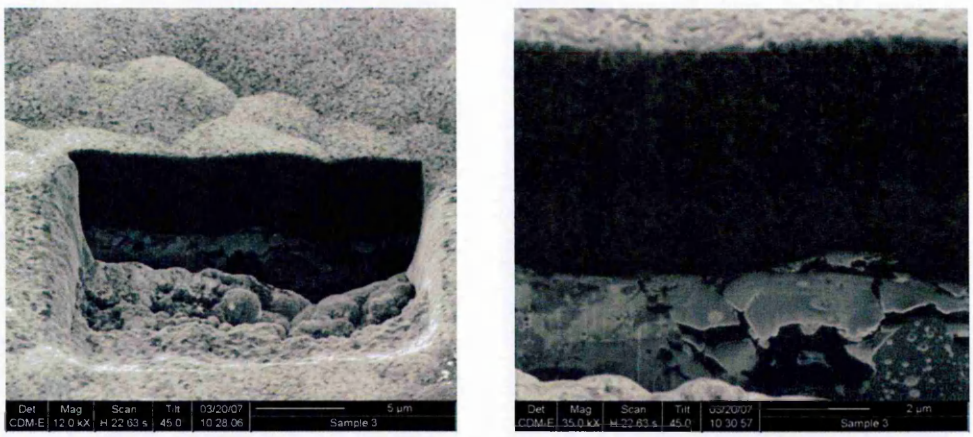

Figure 4-1: FIB Sections of 'Highly Reflective' Electrodeposited Platinum

Matt Metallic

Figure 4-2: FIB Sections of 'Matt Metallic' Electrodeposited Platinum

Black Metallic

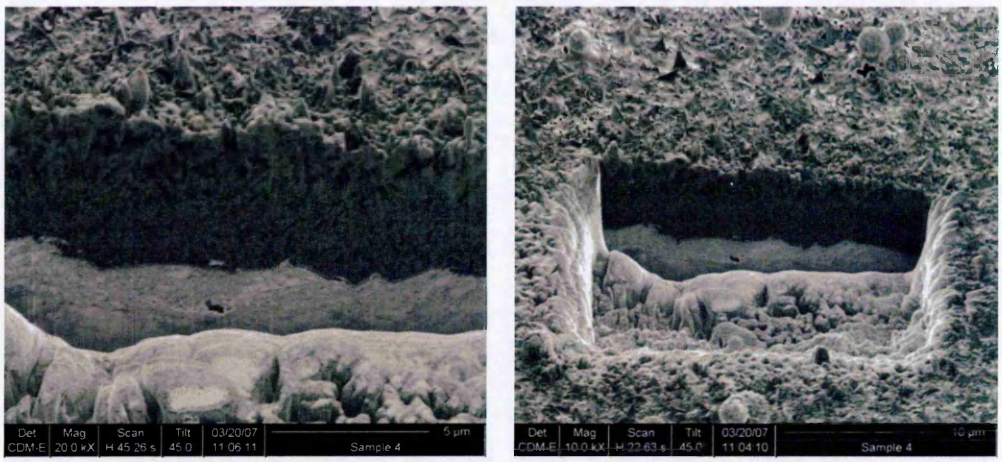

Figure 4-3: FIB Sections of Black Metallic Electrodeposited Platinum

As one would expect, the rougher the surface finish of the coating, the less reflective the coating becomes. Initially, it was thought that the highly reflective coating was the most desirable. However, this deposit is highly stressed and subsequently has poor adhesion. After heat-treatment the deposit blisters which results in an undesirable coating microstructure, therefore the matt-metallic finish was decided to be the coating finish of choice and the black finish would be used for comparison.

4.1.2 Sputter Deposition

Cranfield University typically uses sputter deposition for platinum layer deposition, rather than electroplating, to form RT22 type coatings. Thus, sputter deposited platinum will be used as a reference; therefore, this thesis will compare sputtered and electroplated RT22 type coatings. All samples for the first part of this study were prepared on the superalloy CMSX4. All have been treated identically: swab degrease

in IPA, followed by grit blasting with Al_2O_3, clean in IPA at 30°C for 30 minutes in an ultrasonic bath and cleaned in deionised water.

Three runs of sputter deposition were conducted to deposit approximately 7μm of Pt. (0.7A, 300W at 5mtorr). These were then heat treated (1100°C for 1 hour), aluminised and a TBC deposited (EB-PVD) (micrograph shown in Figure 4-4).

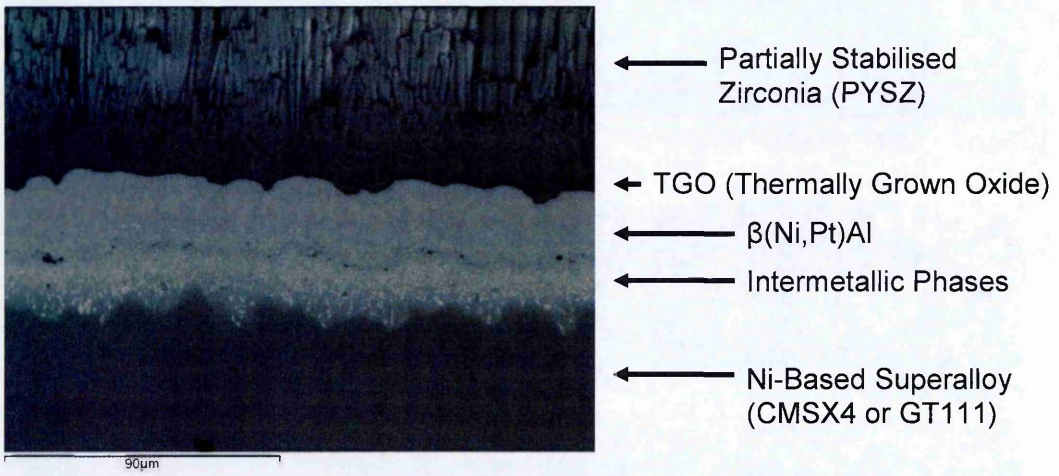

Figure 4-4: Photomicrograph of Sputtered NiPtAl Coating

4.2 Heat treatment and Aluminising of Sputtered and Electroplated Samples

The deposits were heat treated at 1100°C for 1 hour to diffuse the platinum into the nickel alloy surface, followed by aluminising using standard CVD techniques (1050°C, yellow pack, 20 minutes followed by 1120°C for 2 hours in a vacuum furnace). A photomicrograph of the sputtered deposit are shown in Figure 4-5 whereas the microstructure of the electroplated platinum samples are shown in figures Figure 4-6 and Figure 4-7 (black electroplated and matt metallic electroplated platinum deposit respectively). It should be noted that it was not possible to heat treat the highly reflective platinum deposit due the stresses within the coating which blistered during processing.

4.2.1 Sputtered Platinum Followed by CVD Aluminising

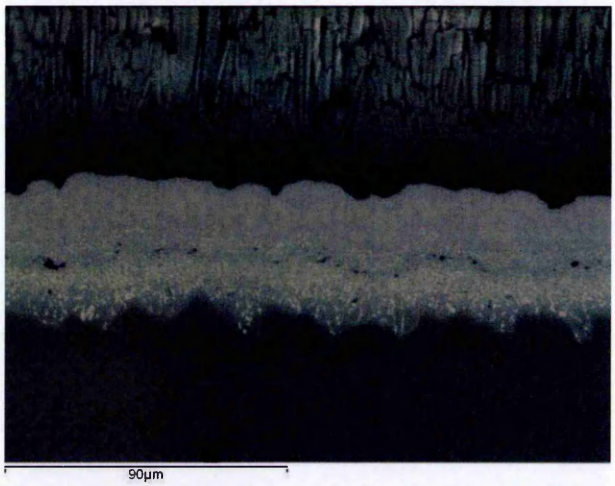

Figure 4-5: SEM Micrograph of RT22-type Coating Produced by Sputtering Platinum

4.2.2 Black Electroplated Platinum Deposit Followed by CVD Aluminising

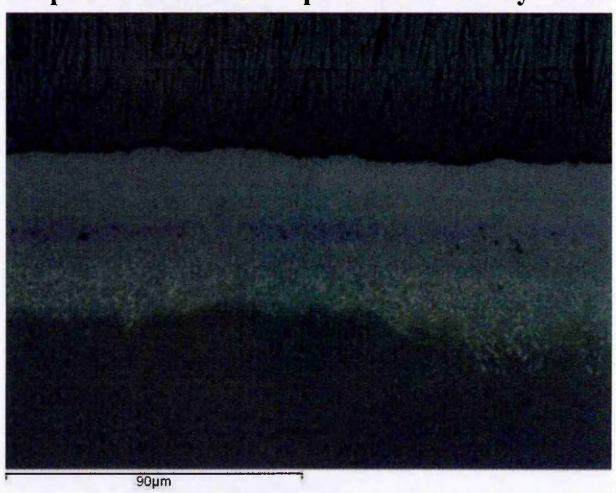

Figure 4-6: SEM Micrograph of RT22-type Coating Produced by Electrodeposition of 'Black' Platinum

4.2.3 Matt Metallic Platinum Deposited Followed by CVD Aluminising

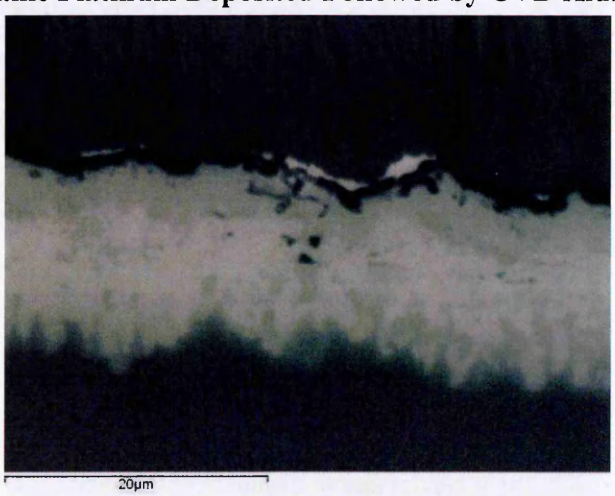

Figure 4-7: SEM Micrograph of RT22-type Coating Produced by Electrodeposition of 'Matt Metallic' Platinum

As can be seen from Figure 4-5 to Figure 4-7 electroplated black and matt metallic Pt coatings produce different microstructures when processed with similar procedures; whereas the sputtered platinum is akin to that to the black metallic coating. The matt metallic coating (Figure 4-7) produced coatings that appear to limit aluminium diffusion into the alloy and thus act as a diffusion barrier to the aluminising process. Unfortunately no chemical profiles were produced for any of the three coating types although aluminising runs were conducted at the same time and the same thickness of platinum was deposited in each case.

4.2.4 Conclusions for PtAl Coatings

- Sputtered and Black electroplated Pt gave similar microstructures.
- Matt Pt gave a completely different microstructure (Pt acting as a diffusion barrier with this deposited structure).
- Pt nucleation directly affects post heat treatment diffusion

The biggest challenge with the plating with the 5Q salt was the reproducibility of the deposit with the three distinct variations (bright, matt and black coatings) occurring irrespective of current density or bath temperature used. This work was presented at the ICMCTF[161] in San Diego in 2009 and it was noted that industry has also experienced extreme difficulties in the reproducibility of these coatings due to a 'very narrow operational window'[162].

Differing coating morphologies also had been noted by Basirun and Pletcher[163]. However, these different morphologies formed depending on the electropotential within the cell (-650mV for highly reflective, -750mV for a matt metallic like finish and -850mV for the black deposit (all against Ag/AgCl). The work of Basirun was repeated within this study but it was found not to be reproducible even when identical cell potentials were achieved. It is also thought that Basirun's work, based on potentiostatic plating, is not practical within an industrial setting, due to difficulty of maintaining constant potentials for large, complex-shape parts (especially turbine blades).

Finally, due to the difficulty associated with the electroplating of platinum from the 'Q' salt it was decided to use sputtered platinum in the manufacture of any platinum

aluminide samples within this thesis as comparisons to coatings produced by plating from ionic liquids

4.3 Results: Electroplating of Aluminium from Ionic Liquids

As stated earlier within the literature review, electrodeposition of aluminium from aqueous solutions is not possible. Therefore an alternative method needs to be used. Ionic liquids (ILs) have been shown to be suitable solvents to deposit aluminium and therefore this method was adopted for this study. Before any depositions could be undertaken, an environmental chamber, which could maintain a low water vapour pressure, was needed. This was purchased, installed and commissioned (Figure 4-8) to undertake this study.

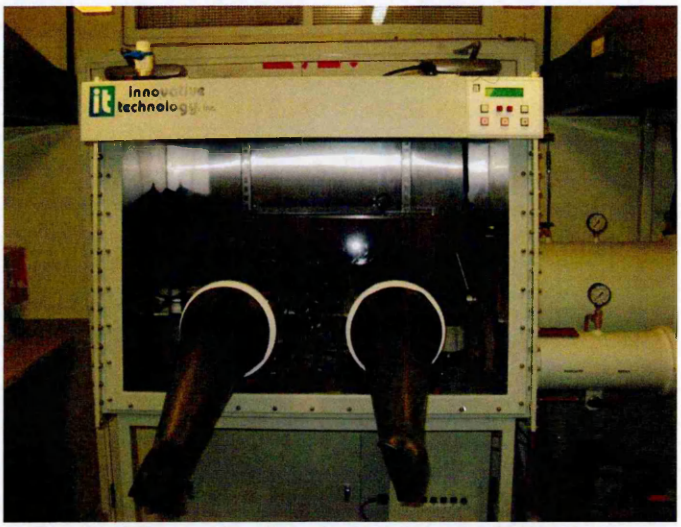

Figure 4-8: Glove box used in Cranfield

Schematically the glove box comprises of four separate units, main chamber, gas regeneration plant, vacuum pump and antechambers (figure 4-9).

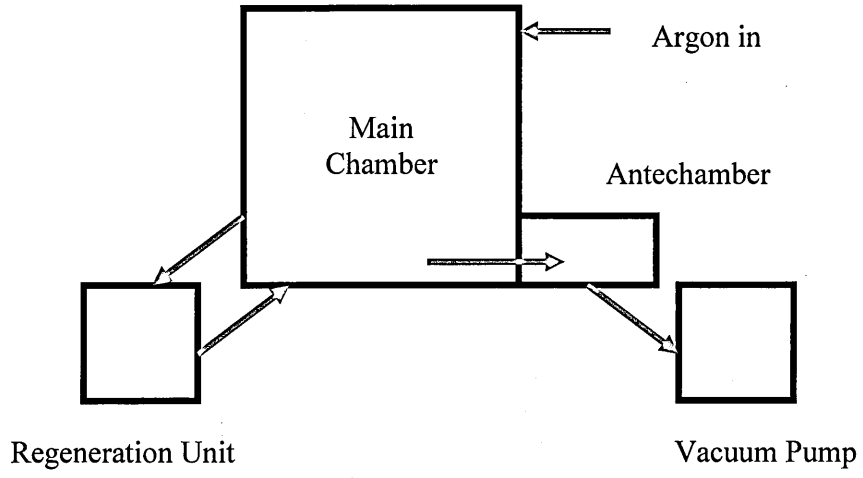

Figure 4-9: Schematic of Environmental Chamber Setup

Main Chamber: This is the largest element of the system and allows the electroplating to be undertaken. It is air-tight with 2 glove ports for manual handling experiments and test set-up within the chamber.

Gas Regeneration: Within these studies, high purity Argon was used for most of the deposition work (99.9999% pure). However, some water vapour would be present within the gas and ingress through the antechambers during sample loading. Therefore the gas was regenerated to remove excess water (typically below 0.7ppm).

Vacuum Pump and antechambers: The vacuum pump was used to eliminate water and air from the antechambers during sample loading. Gas from the main chamber was then backfilled to equalise pressure.

4.4 Results: Depositing Al from BMIM Al_2Cl_7

4.4.1 Depositing Al at $1A/dm^2$

$1A/dm^2$ was the current density used for the plating of aluminium as this has been shown previously to be the optimum current density[138] for dense adherent coatings.

As seen in Figure 4-10; the coating is dense, homogenous and adherent with no sign of delamination. Furthermore, the XRD trace (Figure 4-11) shows that pure aluminium is deposited, as the red lines on the 2θ axis indicate where the synthetic

aluminium peaks would be expected. The peaks are shifted slightly to the left from the theoretical peak positions indicating a small degree of tensile stress within the film.

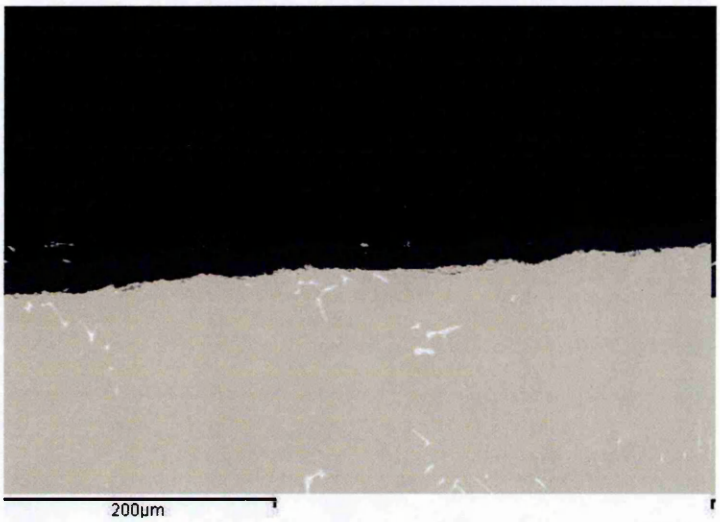

Figure 4-10: Aluminium plated using 1A/dm2 with <1ppm Water

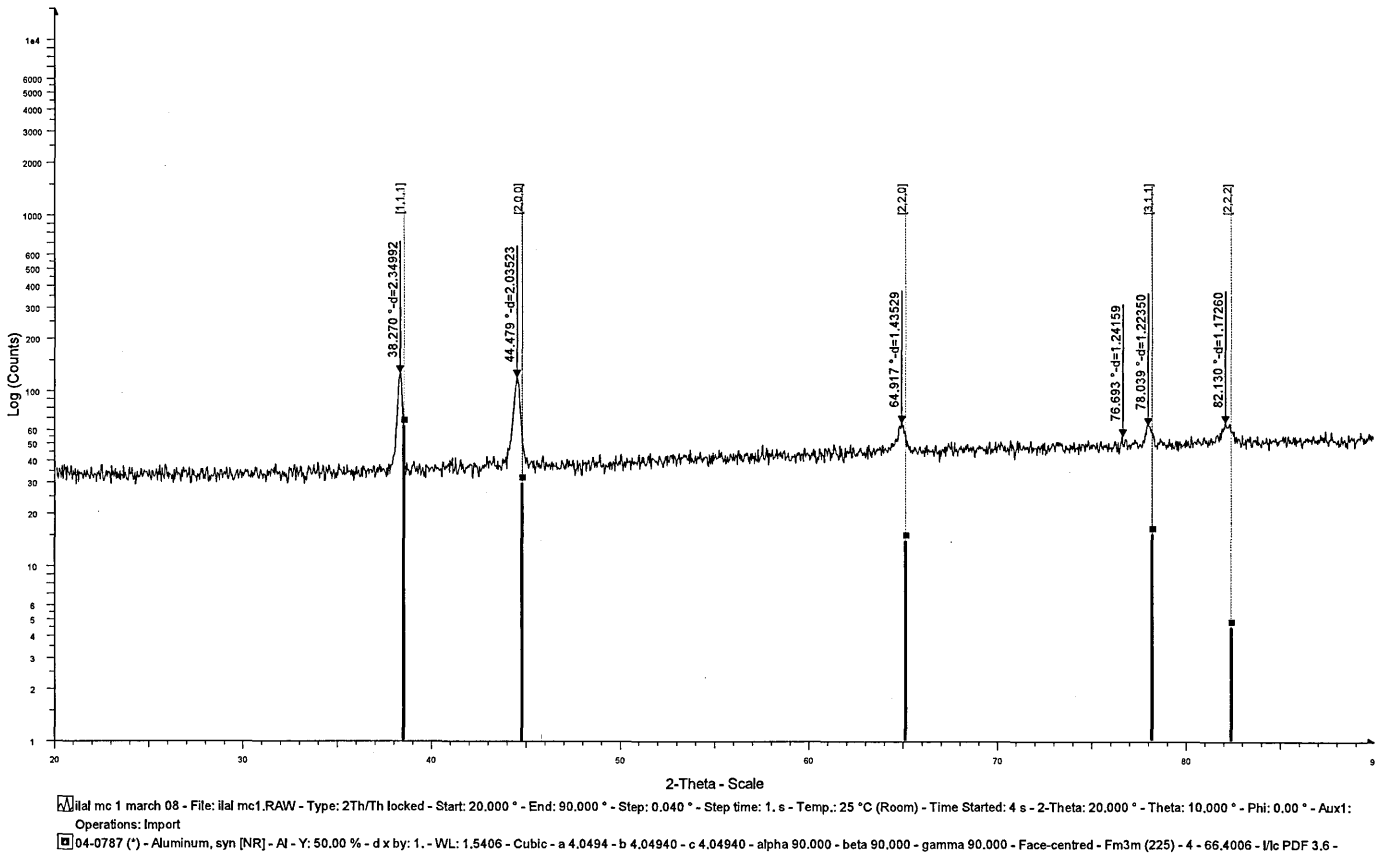

Figure 4-11: XRD Trace of Electroplated Aluminium at 1A/dm^2 and <1ppm Water

4.5 Depositing Al at higher current densities

It has been shown possible to increase the current density. This thesis is looking at industrialising the process. Increasing current density will reduce plating times and thus reduces production time. Thus this thesis has examined varying the current densities between 1-3A/dm^2. Viewing the samples optically prior to imaging under the SEM reveals that there are some differences between the deposits (figure 4-12). These visual differences are probably due to the surface roughness of the deposit as well as, in the case of the 3A/dm^2, the thickness of the coating.

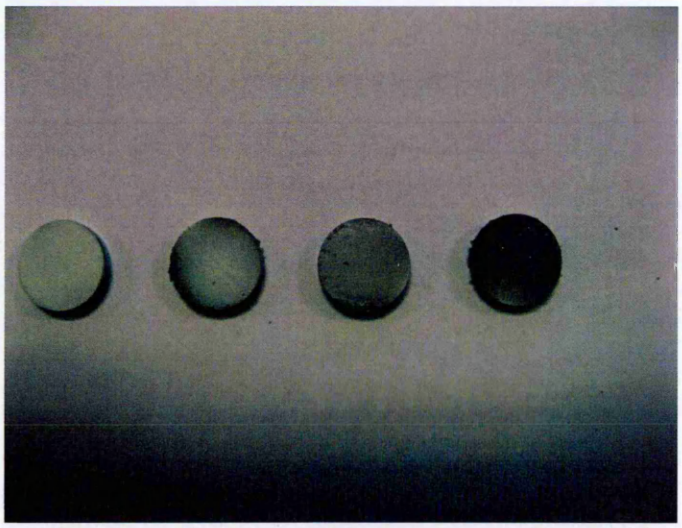

Figure 4-12: Photo of Test Pieces Shown with Increasing Current Densities (from left to right: 1, 2, 2.5 and 3A/dm^2))

Microstructurally there is very little difference between the deposits except when the current density reaches 3A/dm^2. In this study, the deposition times were varied with the aim of depositing similar coating thicknesses. Micrographs of the coatings at the four coating densities are reproduced in Figure 4-13 to Figure 4-16.

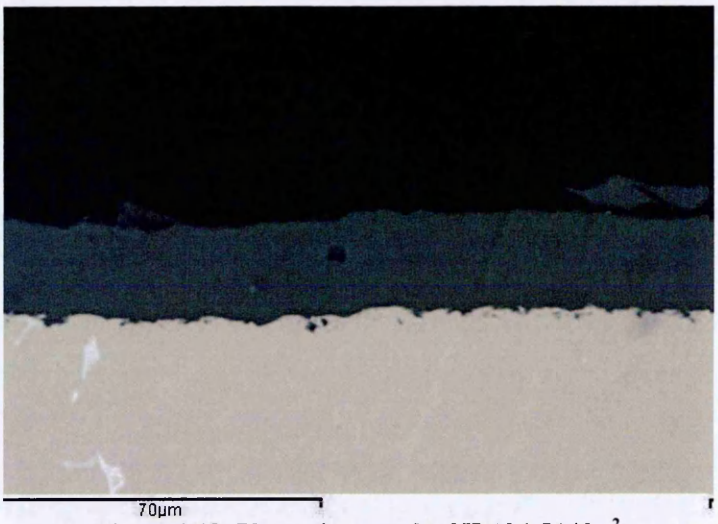

Figure 4-13: Photomicrograph of ILAl 1.5A/dm^2

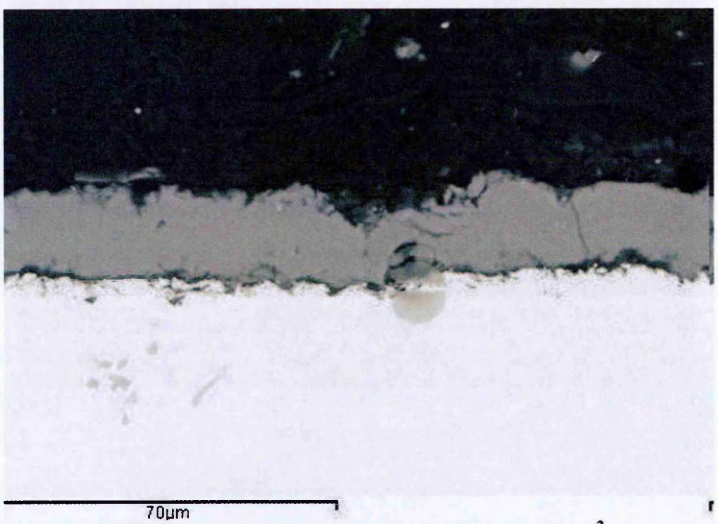

Figure 4-14: Photomicrograph of ILAl A/dm^2

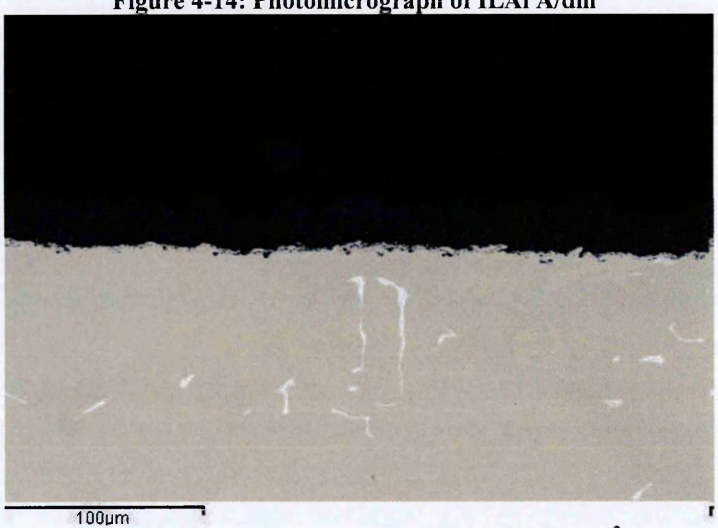

Figure 4-15: Photomicrograph of ILAl 2.5A/dm^2

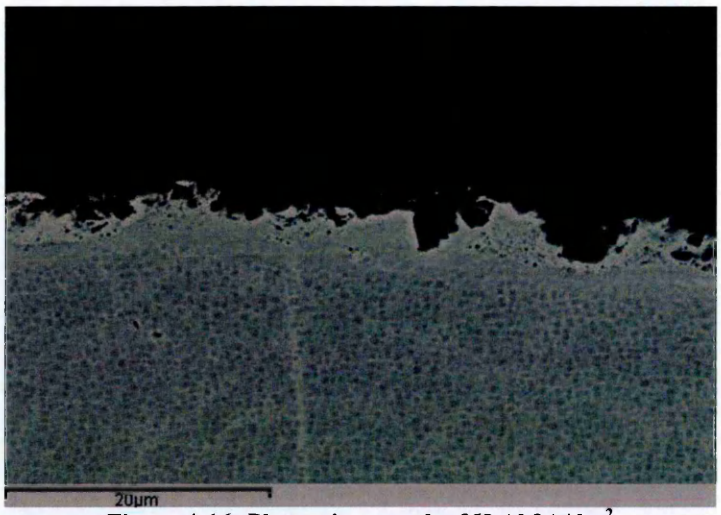

Figure 4-16: Photomicrograph of ILAl 3A/dm^2

It can be seen from Figure 4-13 to Figure 4-16 that that current density affects the final microstructure. When current densities exceed 2A/dm^2, nucleation and film growth starts to become columnar rather than dense. Current densities of 3A/dm^2 have a detrimental effect on the coating itself. Now, instead of columnar coatings being deposited, a varied, pitted, coating resulted. This is consistent with observations of Jianga *et al.*[137] who noted that when using the IL TMPAC (trimethylphenylammonium chloride with $AlCl_3$) with galvanic deposition and current densities of between 50-200mA/cm^2 (5-200A/dm^2) black, powdery coatings resulted. Mitchell et al.[131] also noted that the potential directly affected the nucleation mechanism as the deposit varied from dense and finely grained to loosely adherent black powder depending on the potential at the cathode. Hence it is postulated that a change in nucleation may occur at higher densities because the limit of mass transportation has been met in the IL or more probable the nucleation mechanism changed due to a change in potential at the cathode. The limit of mass transport theory is observed in industry during the plating of zinc or nickel when the current is increased excessively. The limit of mass transport theory hypothesis could be tested in follow up studies by either:

- Increasing the concentration of Al^{3+} salt within the bath,
- Agitation of the electrolyte,
- Cathode movement,
- Increasing bath temperature.

Furthermore, during experimentation it was noted that at higher current density regions (6A/dm^2 for the EMIM, lower for BMIM) Al was loosely deposited on the sample and especially on the cathode holder in agglomerations. These agglomerations became detached either when the sample was removed from the bath (the deposits are found within the beaker) or are removed after post-plating washing.

4.6 Current Efficiencies Vs Cell Potential Studies

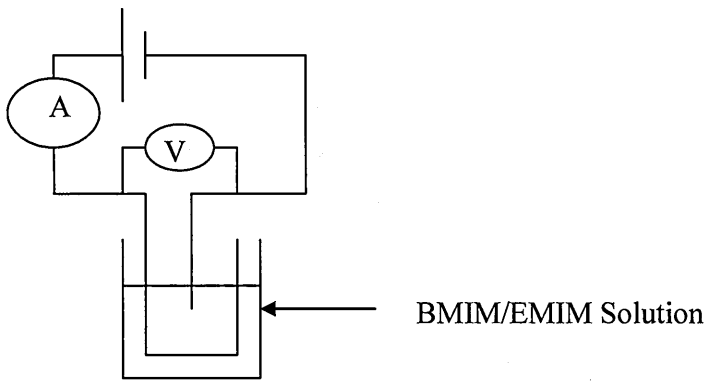

Figure 4-17: Electrical Diagram of Measurement of EMIM/BMIM Current Density/Cell Potential

Current efficiencies against cell potential studies were undertaken as shown in figure 4-17.Plotting the log of the current densities against the cell voltage produces a plot that is shown below (Figure 4-18). The plot from 1-10A/dm^2 and 1-5A/dm^2 for EMIM and BMIM respectively are very linear, however, above this maximum current density of EMIM a distinct change in slope of the plot is observed. It is thought that this change corresponds to the distinct agglomeration of Al on the coating holder. It would be expected that on increasing the current density of the BMIM (both virgin and used) it too would show a movement away from linearity. However, the nobler EMIM plot does show that this IL is more conductive and hence the potential is reduced.

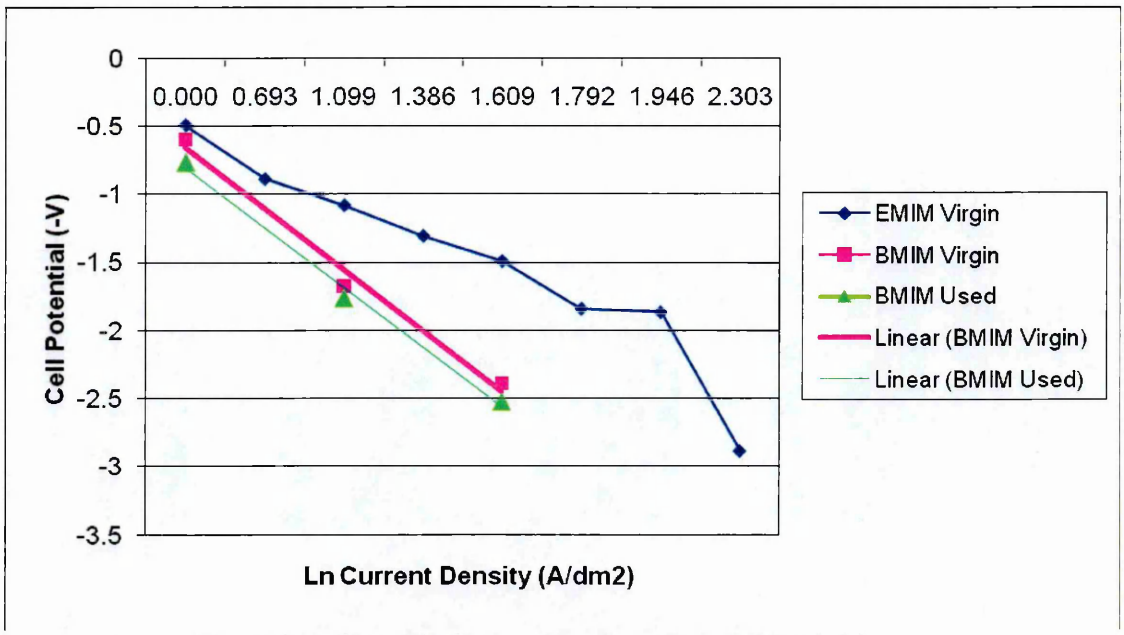

Figure 4-18: Plot of Ln Current Density against Cell Potential

Therefore, it can be concluded that an increase in current density leads to a reduction of current efficiency: a more active cell voltage. The movement away from a noble cell potential at room temperature and at the chosen Al_2Cl_7 salt concentration, suggests that side reactions would occur. However, within the current system this would be highly unlikely (EMIM/BMIM is incredibly stable). Therefore, side reactions are more likely to lead to agglomeration of the deposited Al metal at the cathode/cathode holder. These deposits are readily seen and are loosely adhered. At $6A/dm^2$ very large deposits were visible for EMIM, therefore it can be assumed that at lower current densities smaller deposits may form and are removed upon removal from the liquid/cleaning of the sample.

4.7 Current Efficiencies

A number of current densities were examined, with both used and virgin BMIM, furthermore, another IL (EMIM Al_2Cl_7) was studied. EMIM has a much lower viscosity than BMIM and as specific conductivity is inversely related to viscosity, then EMIM should be more conductive than BMIM; however, it should be noted that EMIM is more expensive that BMIM to produce.

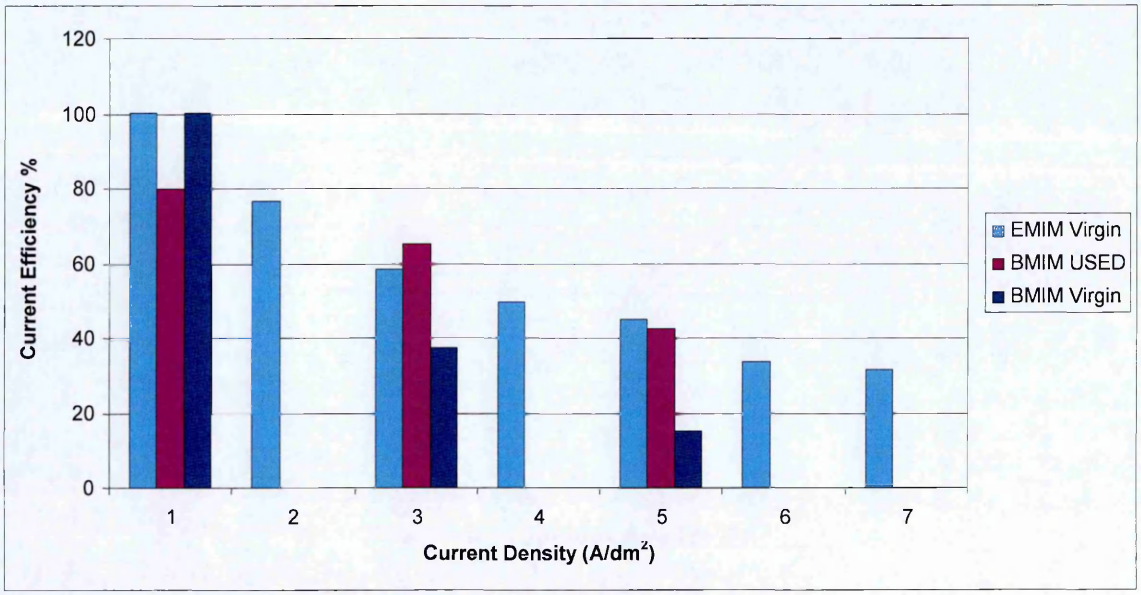

Figure 4-19: Current Densities of ILs

As it can be seen from Figure 4-19 both virgin EMIM and BMIM gave current efficiencies of 100% at $1A/dm^2$ but this decreased when the current density was increased. Conversely, 'used' (approximately 3 months old) BMIM had reduced current efficiencies at $1A/dm^2$. Furthermore, used BMIM and virgin EMIM gave similar results for both 3 and $5A/dm^2$, whereas the virgin BMIM gave lower efficiency results. The viscosity of the EMIM is lower than BMIM, so possibly the used BMIM has reduced in viscosity compared to virginal BMIM. The reduction in cathode efficiency agrees with hypothesis stated previously that above $1A/dm^2$ the limit of mass transport has been met for both used and virginal BMIM as well as EMIM. Marsh has reported that 'aged' [BMIm][PF_6] increased in density by 3% [98].

4.8 Water Content and Electrodeposition of Aluminium from Ionic Liquids

Working in collaboration with INSTM in Italy, deposition of aluminium in environments with increased water vapour was analysed. The figures above (Figure 4-10 and Figure 4-13 to Figure 4-16 were achieved with water concentrations below 1ppm (typically 0.7ppm); whereas the INSTM group have worked with water concentrations below 100ppm.

.

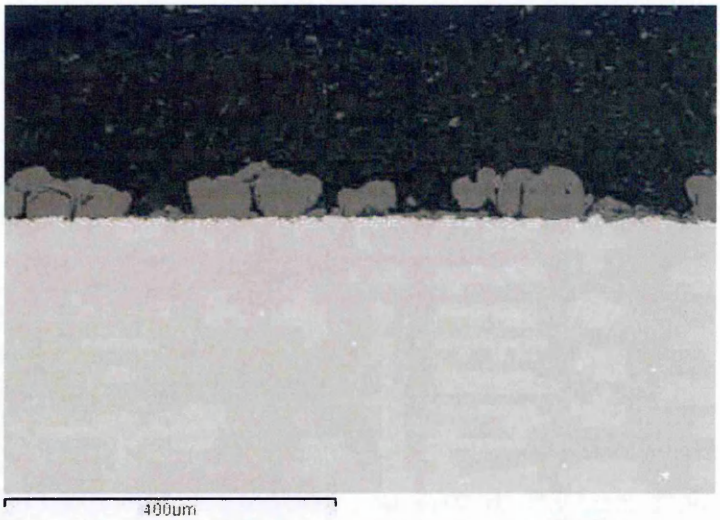

Figure 4-20: Photomicrograph of Plated Al in a Water Contaminated Environment (1A/dm^2)

As the micrograph (Figure 4-20) above suggests, water does indeed directly affect the nucleation mechanism where increased water content within the environmental chambers lead to more columnar and less dense coatings (evident by comparing the figures above with those previously shown for increasing current density (Figure 4-13 to Figure 4-17). INTSM did note that with the water contamination of up to 100ppm coating deposition changed from smooth to columnar in just a few days of operation, clearly showing that water vapour is incorporated into the ionic liquid and that used ionic liquid may contain unknown levels of water vapour in solution.

Water affects the IL by oxidising the solution (transparent to brown tinge) and with the hydrogen ions (from decomposing water) reacting with the Cl^- ions to form $HCl_{(g)}$[164]. Additionally, the affinity of aluminium for oxygen is very high, therefore formation of Al-O complexes[109] probably account for the change in colour of the IL. It has been reported by Sneddon *et al.*[106] that increasing water content increases the density of the IL and would therefore restrict transport of the $AlCl_3^-$ ions towards the cathode. Schroder *et al.*[107] published that water reduced the diffusion of ionic liquids therefore affecting mobility of the liquid and thus reducing the efficiency of the plating process.

Hydrogen has been shown to affect the topography of Ni deposits from aqueous electrolytes[165]. It may be possible that any hydrogen not accounted for by the formation of HCl may be absorbed into the IL. During the plating process H_2 is

evolved preventing dense coatings from being deposited. This could be reversed by 'drying' out the IL in a drier environment with the addition of $EtAlCl_2$ to act as a proton acceptor as described by Zawodzinski[166] where the $EtAlCl_2$ reacts with the HCl present forming $C_2H_6 + AlCl_3$.

Simulation studies conducted by Hanke and Lynden-Bell[167] suggest that water molecules will, in small quantities in ILs, exist as independent clusters and in larger concentrations as a 'continuous network'. Schroder *et al.*[107] suggests that 'wet' ILs should not be considered as homogenous liquids, rather as 'nano-structured' with polar and non polar elements. It could be possible that water present near the cathode forms as small islands, therefore only allowing the Al^{3+} to be reduced in small areas and therefore forming columnar/nodular structures rather than the dense coatings which are observed in environments with <1ppm water.

5 Results: Production of High Temperature Coatings from Ionic Liquids

5.1 Introduction

The manufacture of intermetallics from ionic liquids is not a totally new concept as they have previously been produced as part of experiments on co-deposition[31]. However, the fabrication of high temperature intermetallic coatings is new. Co-deposition as a manufacturing method for coatings is very difficult to do and control on an industrial scale using electroplating and one of the aims of this project was to look at potential industrialisation of any of the processes developed. This thesis is the first to show that high temperature protective intermetallic coatings can be formed by the heat treatment of electroplated aluminium from ionic liquids.

The nickel aluminide intermetallic family are sought after by the aerospace and power-generation industries as the β phase (NiAl), shown in Figure 1-2, has a high melting point, is very stable and can, in very hot environments, act as an aluminium reservoir for the formation and repair of a protective α-alumina scale, limiting high temperature oxidation problems.

Traditionally, nickel aluminide coatings are produced using chemical vapour deposition (CVD). Two different mechanisms or temperature profiles are used: a low temperature high activity (LTHA) and a high temperature low activity (HTLA) process which are characterised by either the net inward movement of Al or the net movement of Ni outwards from the substrate for LTHA and HTLA respectively. As previously described in the literature survey (1.3 page 7), these two alternative process routes for CVD deposition can be schematically summarised as in Figure 1-3.

5.2 Results: Heat Treatments to form Aluminide Coatings

Three ways were researched of heat treating electroplated deposits of aluminium, deposited onto nickel. These were either using temperatures similar to that used in the production of CVD type HTLA or LTHA coatings, which will later be shown to produce a composition gradient coating very similar to a high temperature CVD produced microstructure. Alternatively, as developed in this study, a new low temperature heat treatment regime was proposed. The ICON (**I**OLISURF **C**oatings **o**f **N**ickel alloys) process, as it has been termed, utilises temperatures below that

typically used for CVD processes, creates coatings which show little variation in chemical composition compared to the CVD type coatings. Ensuring a superior reservoir of aluminium, yet develops a β-NiAl based coating.

5.2.1 Ionic Liquid plated Aluminium (ILAl) with Traditional Heat Treatment Techniques[2]

Jointly with an industrial partner (Niouvo Pinoni – (NP)) and a partner university (INSTM) using NP standard CVD heat treatment (1120°C 2 hours and 845°C for 4 hours) it was shown possible to heat treat nickel-based superalloys coated with electroplated Al to form a NiAl coating. Figure 5-1 and Figure 5-2 illustrates a NiAl bond coat from ILAl coating heat treated using NP standard CVD process conditions on GTD111. Figure 5-1 shows the heat treated ILAl coating used as a bondcoat to EB-PVD TBC coated system produced using facilities at Cranfield.

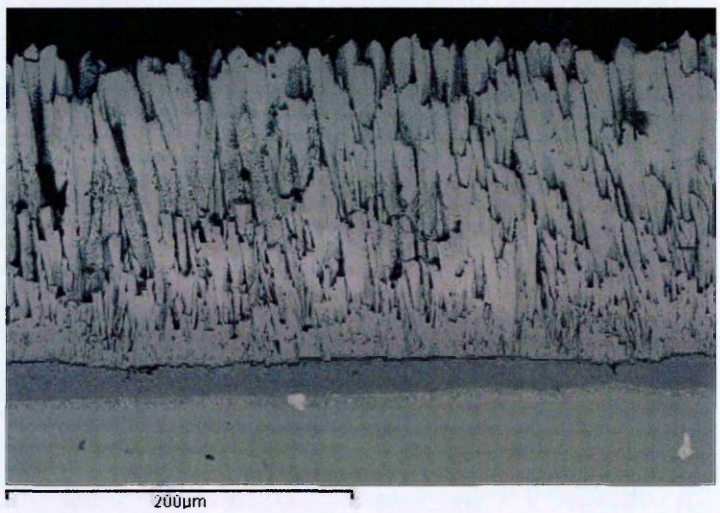

Figure 5-1: Back Scattered Electron Image of an ILAl Heat Treatment Using NP Parameters with TBC

Details of the coating microstructure can be seen in Figure 5-2, by magnifying an ILAl diffused coating heat treated at 1120°C at 2 hours and 845°C for 4 hours.

[2] A joint patent has been applied for the heat treating of ILAl using standard regimes to form desirable nickel aluminide intermetallics with INSTM.

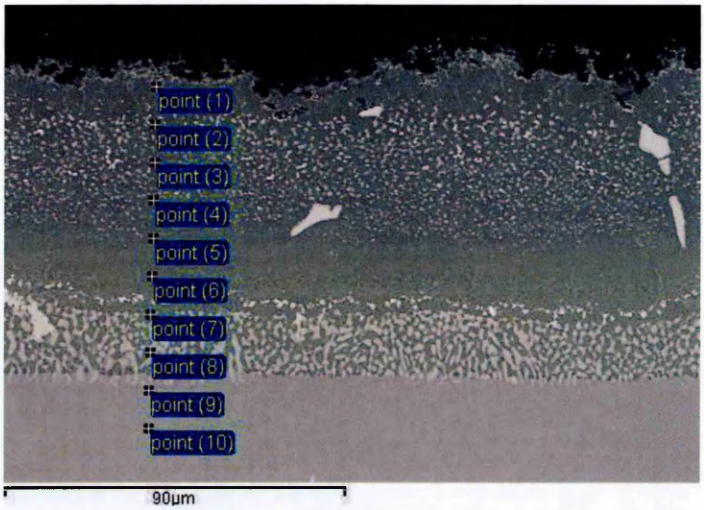

Figure 5-2: NiAl Bondcoat formed from ILAl Heat Treatment Using NP Parameters (BSE Image)

The chemical profile through the above microstructure is shown in Figure 5-3. It shows a clear composition gradient between the Al and Ni. Assigning partition coefficients (Table 5-1) it can be seen that points 1-4 (Figure 5-3) are β-NiAl (moving from slightly Al rich to Ni rich). However, it should be noted that this coating is much thicker than would normally be expected for a typical CVD type coatings (40-70µm). Furthermore, point 1 may not be representative of the outer coating composition as its position is very close to the oxide formed on the coating, which is alumina. It should be noted that within the microstructure shown as Figure 5-3, 4 distinct regions can be identified: the light grey area with points 9 and 10 is the substrate (GTD111), points 7 and 8 represent the interdiffusion zone where refractory elements precipitate out of solution, points 5 and 6 represent single phase β-NiAl, points 2 to 4 represent β-NiAl with secondary phases precipitated out (typically refractory metals) shown as the white speckles or dots and the large white phases shown within the microstructures are carbides.

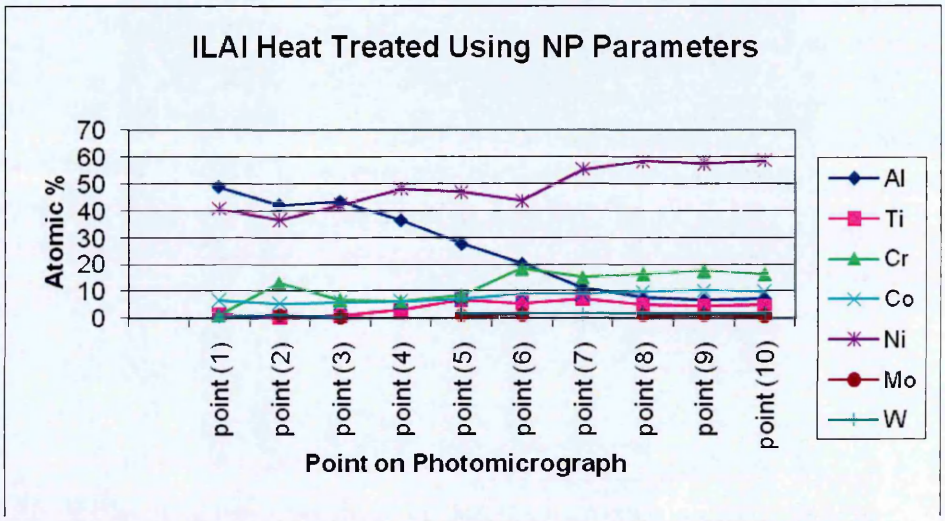

Figure 5-3: Composition Profile of ILAI Heat Treated using NP Parameters

Table 5-1: Partition Coefficients for ILAI Heat Treated using NP Parameters (atomic %) (Partitioning of Effective Nickel and Aluminium Content Assuming Co, Mo and W substitute for Ni; Ti substitutes for Al and Cr Substitutes 50%Ni and 50% Al)

	Al	Ni
point (1)	51	49
point (2)	51	49
point (3)	48	52
point (4)	43	57
point (5)	40	60
point (6)	35	61
point (7)	26	72
point (8)	20	76
point (9)	20	76
point (10)	20	76

5.2.2 The ICON Process[3]

The ICON process utilises a two-step heat treatment regime, just below and above the melting point of aluminium and aims to capitalise on the exothermic heat of forming β-NiAl to drive the reaction and therefore forming process from the ionic liquid deposited aluminium. The ICON process comprises of a heat treatment of 620°C for 1 hour followed by second step of 820°C for further hour then allowed to cool. A typical coating produced with the ICON process when used as a bond coat for a TBC is illustrated in (Figure 5-4).

[3] The ICON process will be patented once the application of heat treating ILAI with standard regimes to form desirable intermetallics has been approved and granted.

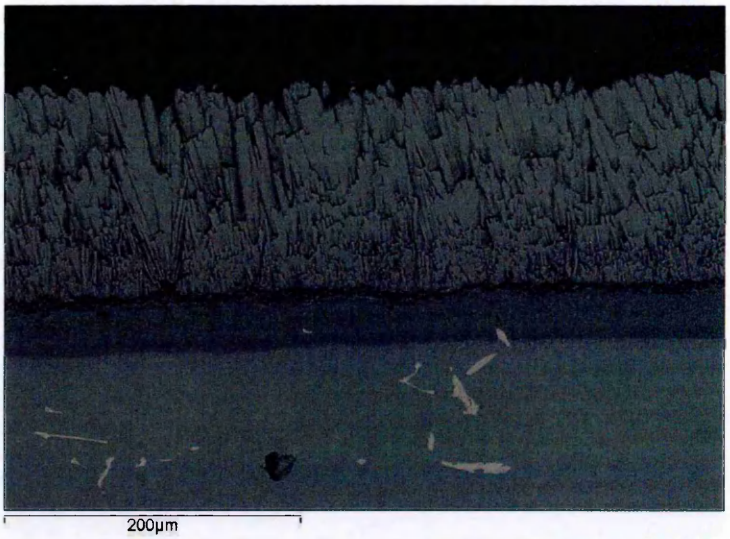

Figure 5-4: Photomicrograph of ILAl Heat Treated with ICON followed by Application of TBC (BSE Image)

Figure 5-5 is a magnification of the bondcoat produced and illustrates the location of the SEM-EDX analytical positions. The analysis is given in Figure 5-6.

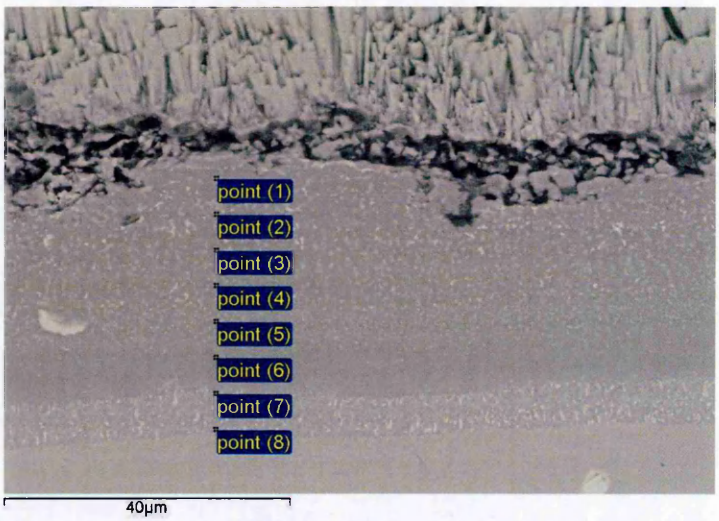

Figure 5-5: Magnified Photomicrograph of ILAl Heat Treated using ICON with Applied TBC (BSE Image)

It should be noted that the TGO shown above is much thicker than typically expected for a CVD aluminide coating. However, one must realise that the above coating was heat treated (ICON) and a TBC applied - all within a single step. This prevented any possibility to remove the oxide layer by grit blasting between heat treating and applying the ceramic coating. However, it does show the versatility of this method by showing a potential industrialisation of the process and thereby negating both the CVD retort and separate vacuum furnace treatments necessary for conventional CVD processing. The points highlighted in Figure 5-5 give rise to Table 5-2 and Figure 5-6:

Table 5-2: Chemical Composition of ILAl Heat Treated using the ICON Process (atomic %)

	Al	Ti	Cr	Co	Ni	Ta	W
point (1)	48.79	1.28	5.10	5.27	37.55	1.28	0.73
point (2)	45.95	1.85	11.44	5.06	34.76	0.00	0.95
point (3)	48.34	3.51	5.97	5.24	36.54	0.00	0.40
point (4)	46.32	5.35	7.33	5.53	35.10	0.00	0.37
point (5)	44.06	1.36	5.86	5.45	41.90	0.78	0.58
point (6)	45.13	1.55	2.39	5.15	45.77	0.00	0.00
point (7)	35.63	5.15	5.42	7.71	46.09	0.00	0.00
point (8)	20.13	11.92	17.46	9.23	38.50	1.42	1.35

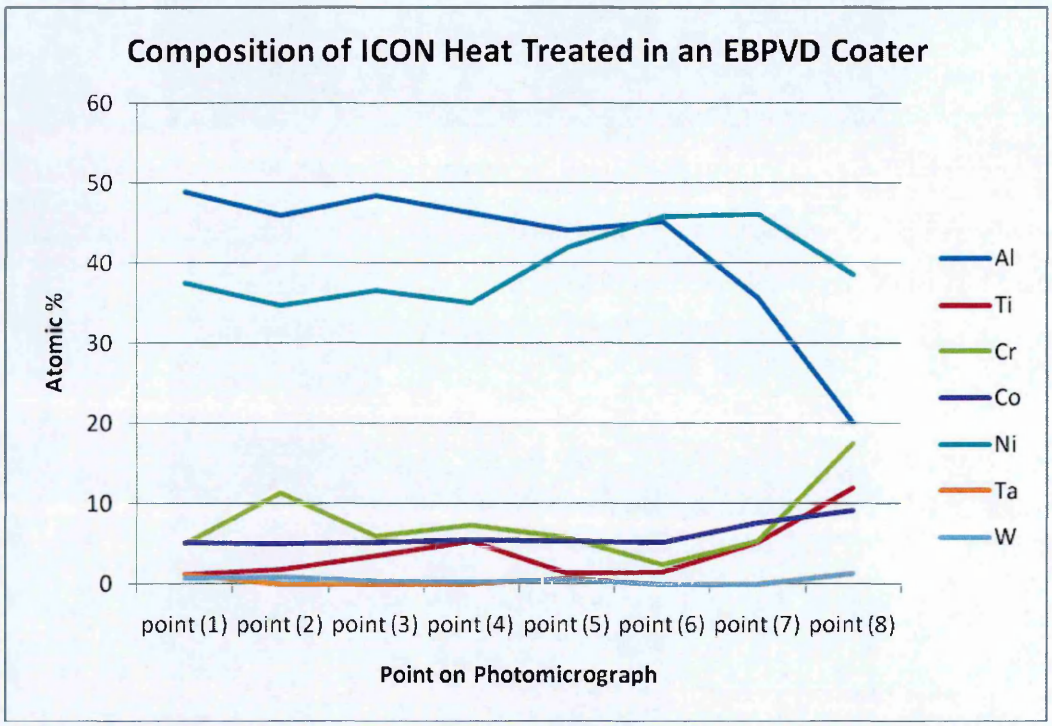

Figure 5-6: Chemical Composition of ILAl Coating Produced within an EBPVD Coater using ICON Parameters

Additionally, an elemental map of the ICON coating was produced to visually study the differing concentrations of aluminium and nickel throughout the coating. The elemental map (Figure 5-7) below highlights the aluminium rich areas (red) against the nickel rich areas (green). It should be noted that the red, if pure, aluminium would be scarlet red rather than the orange/yellow colour that is shown in the figure, this shows very elegantly that no free aluminium is present within the post heat treated coating and that the aluminium has indeed reacted with the Ni to form various nickel aluminides

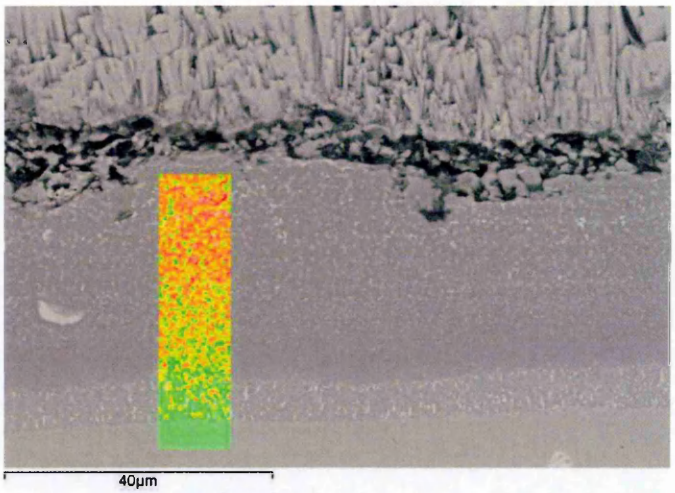

Figure 5-7: Elemental Map of ICON Produced Coating with TBC Applied (BSE Image)

Assigning partitioning coefficients to the various elements in the coating the effective nickel and aluminium composition ratios can be calculated (Table 5-3). It can be seen that the coating is very uniform with regards to chemical composition and all points (excluding the interdiffusion zone (IDZ) and the base metal) form β-NiAl albeit aluminium rich β-NiAl to the outer part of the coating. Interestingly the four most outermost points of the coating are aluminium rich. This suggests that this coating would excel in oxidation trials due to a larger reservoir of Al ready to form a protective alumina scale especially compared to ILAl heat treated with standard CVD parameters, or a commercial CVD deposited NiAl coating.

Table 5-3: Effective Ni and Al Composition Profile of ICON Coating (atomic %)

	Al	Ni
point (1)	52.62	45.37
point (2)	53.52	45.53
point (3)	54.84	44.77
point (4)	55.34	44.29
point (5)	48.36	50.28
point (6)	47.88	52.12
point (7)	43.49	56.51
point (8)	40.78	56.45

Highlighting the IDZ, it is evident that this zone is incredibly thin (<10um and in some instances <3um) in comparison to traditional CVD coatings. This has numerous advantages, especially with the bulk of the coating retaining a β-NiAl phase. The smaller IDZ limits the build-up of refractory elements in the IDZ, or in the aluminide coating for that matter, and therefore promotes stability within the substrate; hence, the mechanical properties, which the substrate is designed for, will not be compromised to the same degree to that expected with CVD coatings and a thicker

IDZ. From the literature it has been calculated that the ductile to brittle transition temperature of aluminium rich β-NiAl could be expected to be approximately 800°C[168]. Such values are not dissimilar to high activity NiAl coatings produced by CVD. Furthermore, Wang et al[169] has studied the expansion coefficients of various nickel aluminides when compared to nickel.

As it can be seen from Figure 5-8 Figure 5-10 the thermal expansion of γ, β and γ′ are very similar, therefore suggesting that the mechanical properties are not dissimilar enough to promote mechanical failure (providing the coating thickness is not excessive). In addition to this, the brittle to ductile transition temperature for β-NiAl quoted in the literature varies between 550 to 868°C[168], however, Darolia has noted that crystal orientation can have significant impact on the DBTT[170]. Furthermore, Vogel *et al.*[171] noted that HTLA coatings had lower DBTT than LTHA coatings and high Al content NiAl increased the DBTT[40].

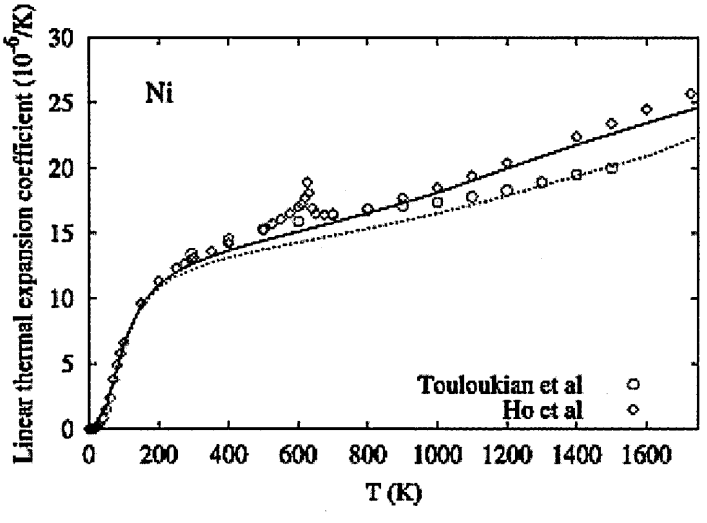

Figure 5-8: Calculated Thermal Expansion Co-efficient for Ni[169]

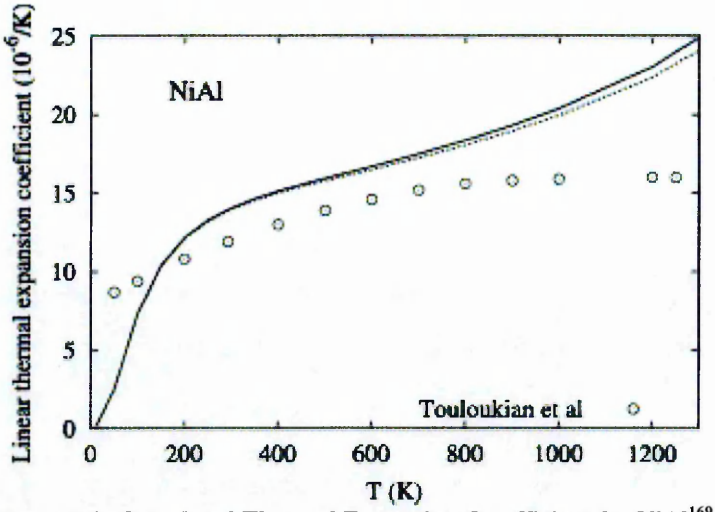

Figure 5-9: Calculated Thermal Expansion Co-efficient for NiAl[169]

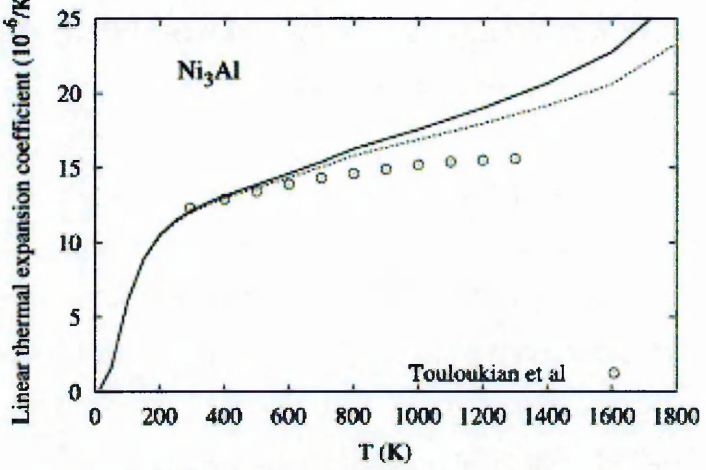

Figure 5-10: Calculated Thermal Expansion Co-efficient for Ni_3Al[169]

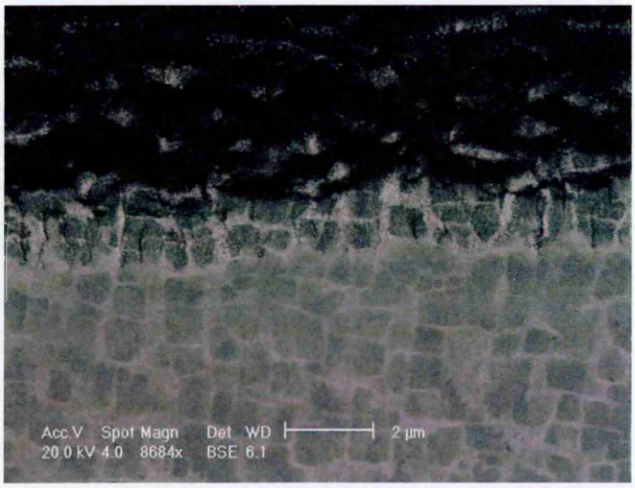

Figure 5-11: BSE Image if ICON Coating on GTD11 showing IDZ , Coating and Substrate (γ/ γ′)

The image in Figure 5-11 shows the microstructure of the small IDZ which appears to maintain the γ/ γ′ structure but with an increase in heavier elements within the γ phase

(hence the lighter areas between the cuboidal γ′ precipitates). The structure is completely different to that produced by conventional CVD and diffusion heat treatment routes.

XRD analysis shows that after the initial heat treatment the intermetallic $NiAl_3$ is formed without any free Al being present which is then transformed to β-NiAl upon the second heat treatment and these steps in the process are examined more closely below.

5.2.3 The ICON Process: The Steps and Coatings as Analysed by XRD

The ICON process is essentially a 3 step process:

1. Electrodeposit Al from an ionic liquid (mostly BMIM Al_2Cl_7 in this study) onto a Ni-based superalloy (XRD plot shown in Figure 5-12)

Figure 5-12 shows that the lattice spacing of the a plane of the FCC structure has changed from 4.049 to 4.056Å indicating that there is a slight tensile strain within the deposit. This also agrees with the peaks lying slightly to the left of where they are expected in accordance to Braggs law ($n\lambda=2d\sin\theta$). The 2θ on the bottom of the graph is twice the angle of the diffractometer. Furthermore, this trace shows that only pure Al is deposited during electroplating from BMIM.

2. Place into a vacuum furnace (bespoke or one incorporated within an EBPVD coater) and heat to 620°C for 1 hour (Figure 5-13) to form the intermetallic $NiAl_3$ with no free Al present.

It can be observed in Figure 5-13 that the deposit exhibits some tensile stresses as the peaks are slightly to the left of where they are expected. The lattice spacing moves from a = 6.598, b=7.352 and c=4.802Å to a=6.646, b= 7.880 and c= 4.796 suggesting that whereas planes a and b are in tension, c is in compression so therefore the unit cell is elongating in just two directions.

1. Electrodeposit Al from an ionic liquid (mostly BMIM Al_2Cl_7 in this study) onto a Ni-based superalloy

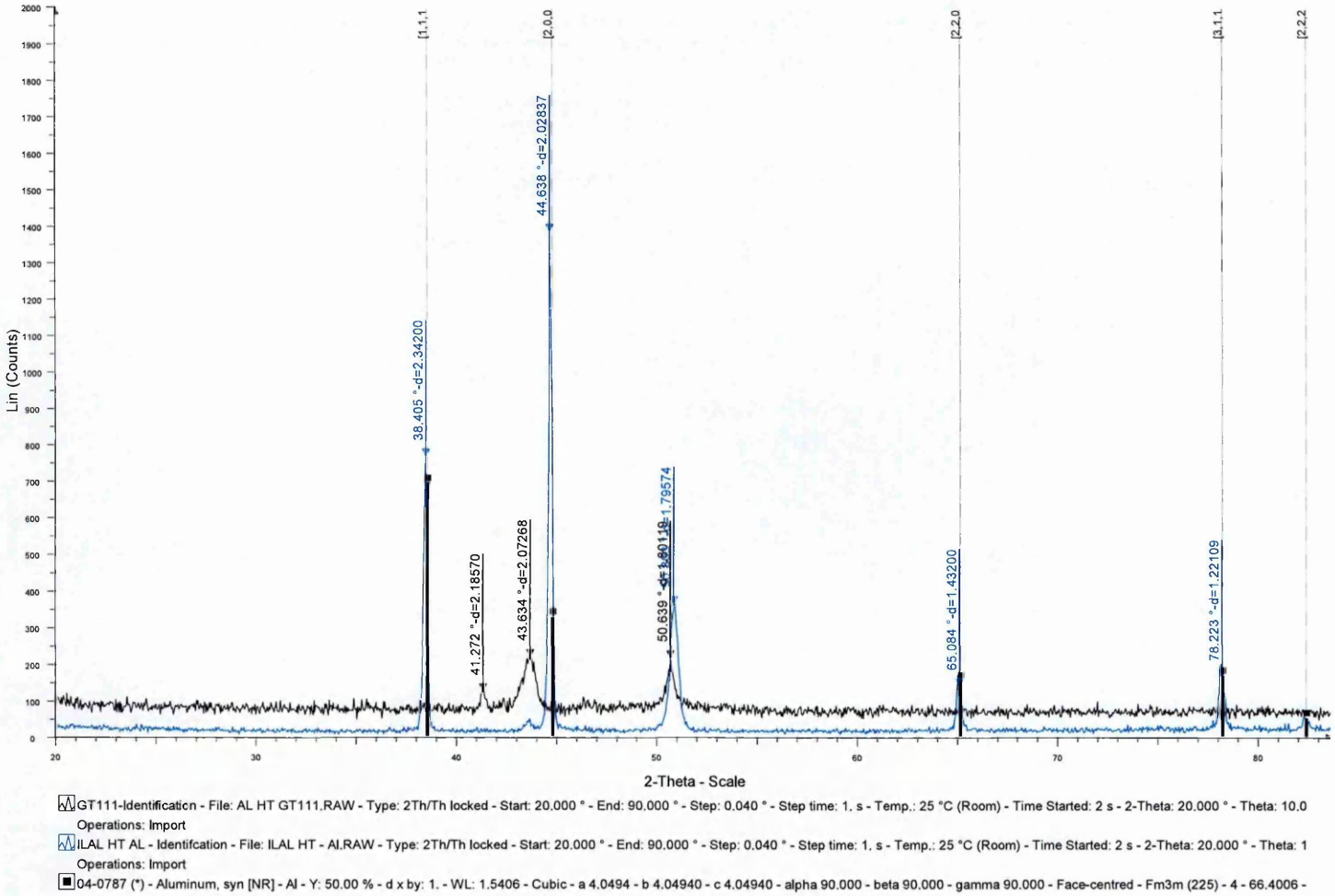

Blue trace = ILAl
Black trace = GT111
Black Lines = Al Present

Figure 5-12: XRD Trace for ILAl Coating

2. Place into a vacuum furnace (bespoke or one incorporated within an EBPVD coater) and heat to 620°C for 1 hour

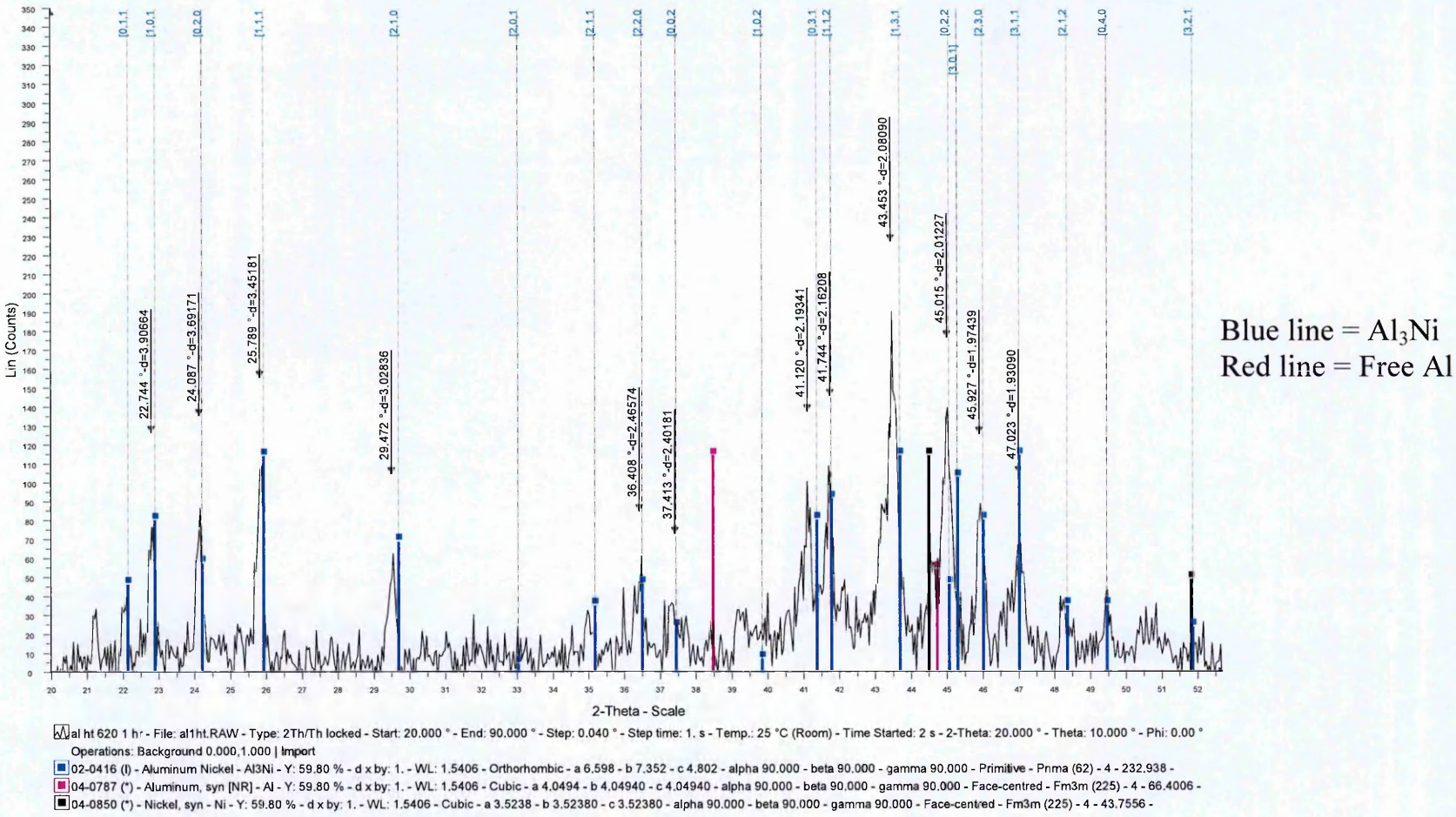

Blue line = Al_3Ni
Red line = Free Al

Figure 5-13: XRD Trace for ILAl Heat Treated 1 Hour at 620°C

3. Continue heating for a further hour at 820°C to transform the $NiAl_3$ ro β-NiAl

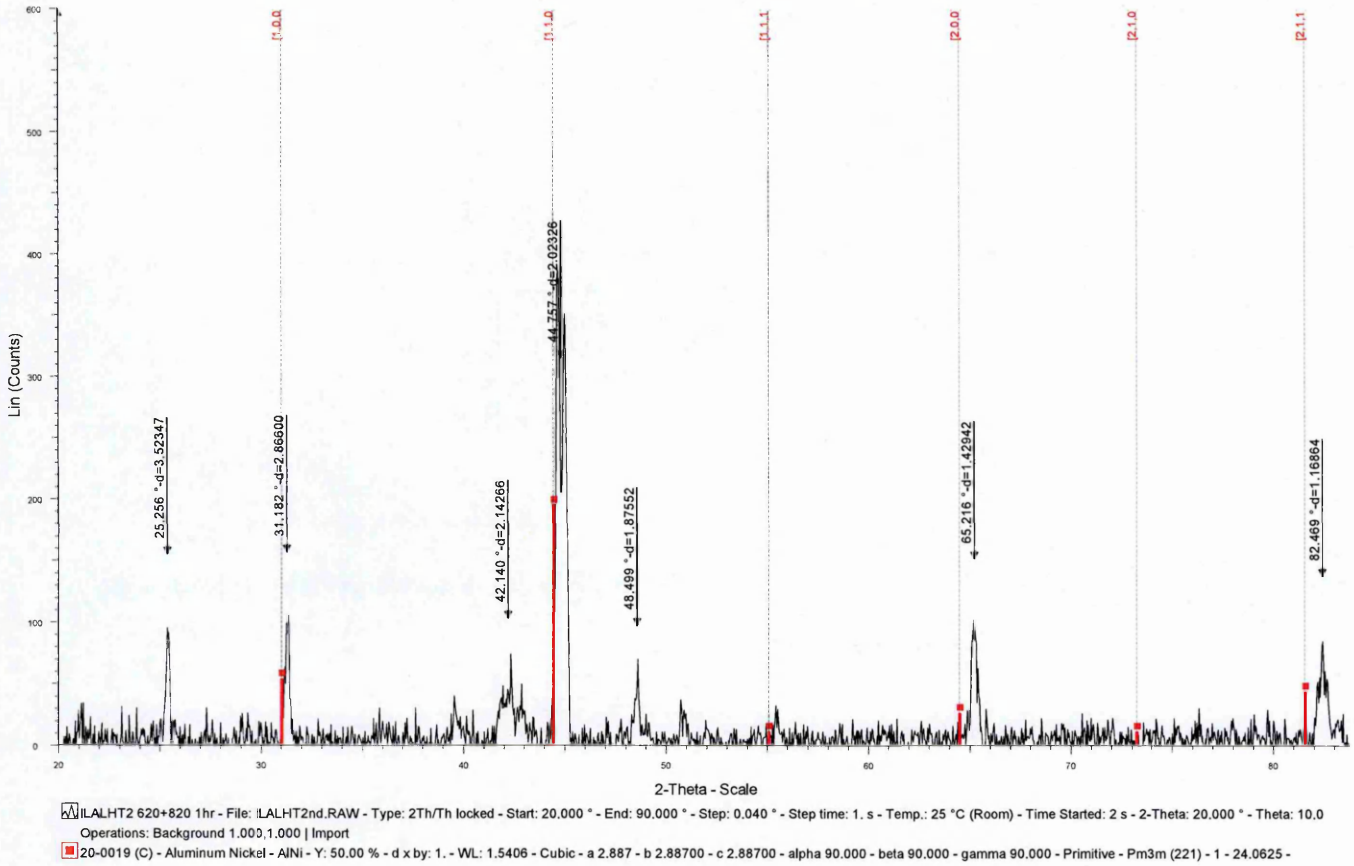

Red lines = NiAl

Figure 5-14: XRD Trace for ILAL Heat Treatment for 1 Hour at 620°C, then 1 Hour at 820°C

3. Continue heating for a further hour at 820°C to transform the $NiAl_3$ ro β-NiAl

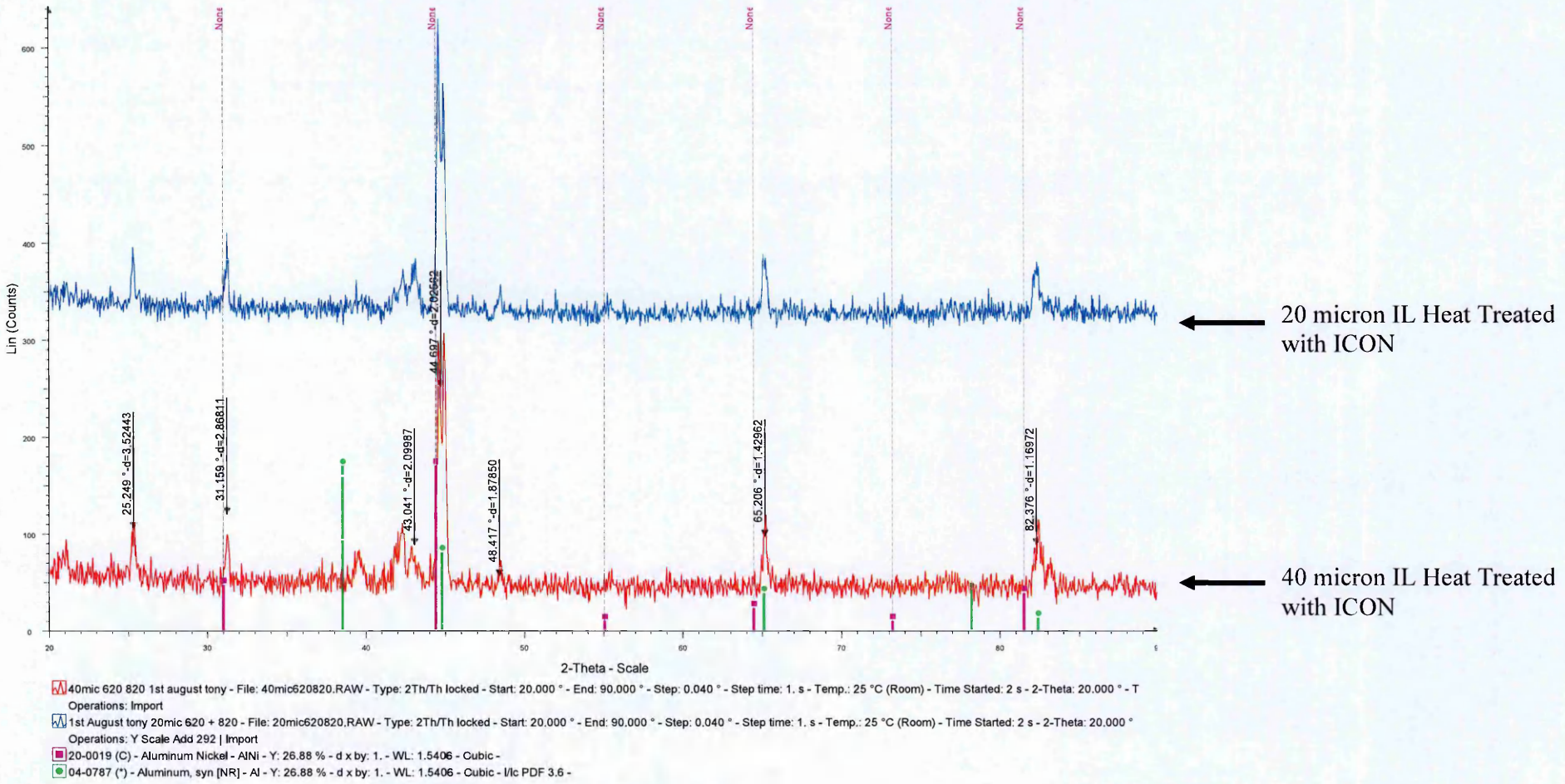

Figure 5-15: XRD of 2 ILAl Coatings

3. Continue heating for a further hour at 820°C to transform the $NiAl_3$ or β-NiAl (Figure 5-14)

Within Figure 5-14 there appears to be a shift in the coating stresses from tensile to compressive. The lattice spacing has moved from the expected 2,887Å to 2.860Å the change is most likely due to influx of nickel atoms into the coating from the substrate and the heat treatment being stopped before equilibrium of stresses can be achieved.

4. Differing thicknesses of ILAl Heat Treated with ICON form β-NiAl (Figure 5-15)

Within the final XRD plot (Figure 5-15) there appears to be no difference between the final composition and the compressive stress of the coating regardless of the thickness of the original coating, prior to heat treatment.

5.3 Influence of Alloy Composition on the Reproducibility of ICON

The ICON process depends on the alloy. Thus the ICON process does not produce the same β-NiAl coatings on different superalloys or substrates. The post heat treatment of the Al coating/substrate shows that the coating produced is dependent on the substrate composition when heat treated according to the ICON process. Figure 5-16 and Figure 5-17 illustrate and compare the coatings produced on GTD111 and CMSX4 nickel-based superalloys respectively. Ascertaining the reasoning behind this behaviour will assist in the understanding of how the ICON process works and assist in proposing a mechanism of action.

5.3.1 Problems associated with ICON Coating Manufacturing

As shown in Figure 5-16, the coating morphology expected with the ICON process is typically dense, single phase (but with some small precipitates) and with an even composition gradient, especially on substrates such as Ni200, N75, GTD111 and IN738. However, on the single crystal alloy CMSX4 this proved not to be the case. Instead, a distinct bi-phase intermetallic coating was formed with an obvious 'line' of second phase particles formed at the original substrate surface during the ICON process (Figure 5-17), resulting in a less- desirable coating chemistry.

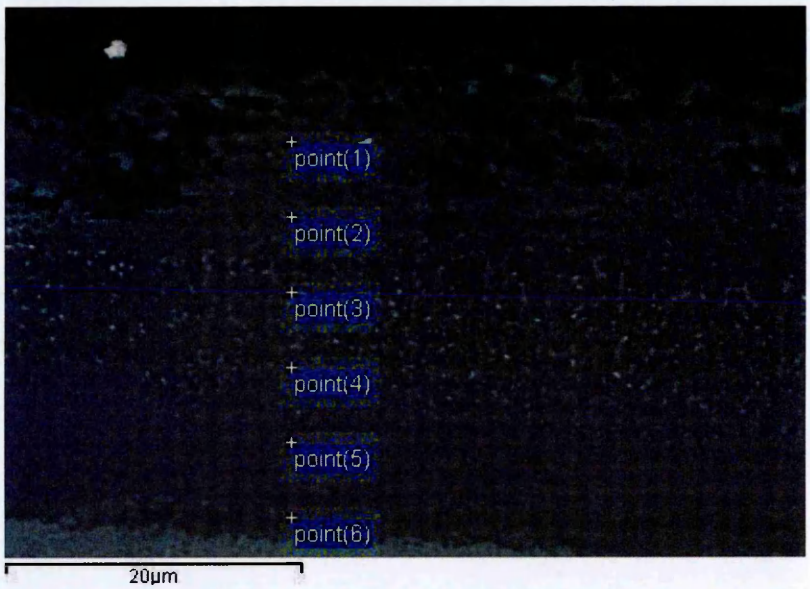

Figure 5-16: ICON on GTD111 (BSE Image)

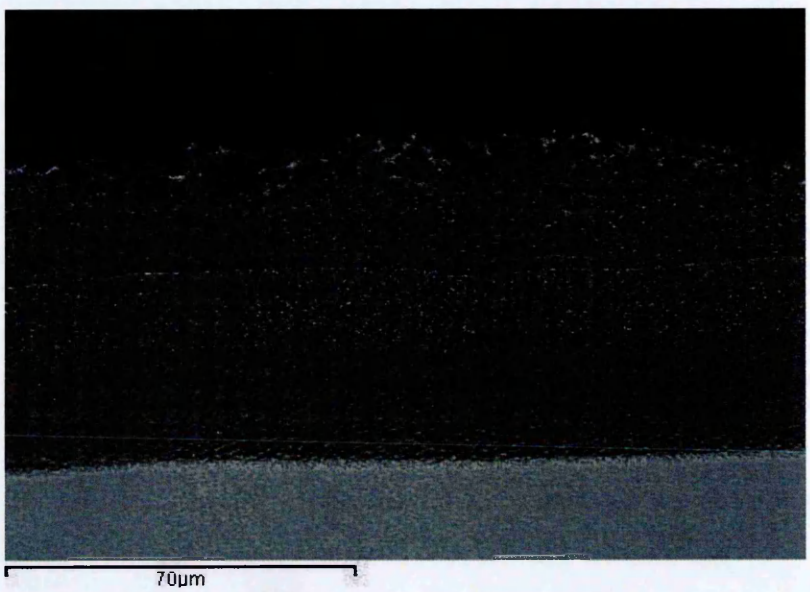

Figure 5-17: ICON on CMSX4 (contrast/brightness modified to emphasis line)

Figure 5-18 shows an ICON coating on CMSX4 after being FIBed and viewed under the Back Scattered Electron image in an SEM at 45°, this shows that the 'line artefact' is not just an artefact induced by polishing etc. but does in fact pervade through the coating, as a plane of precipitates at what was believed to be the original coating/substrate interface, prior to aluminium plating.

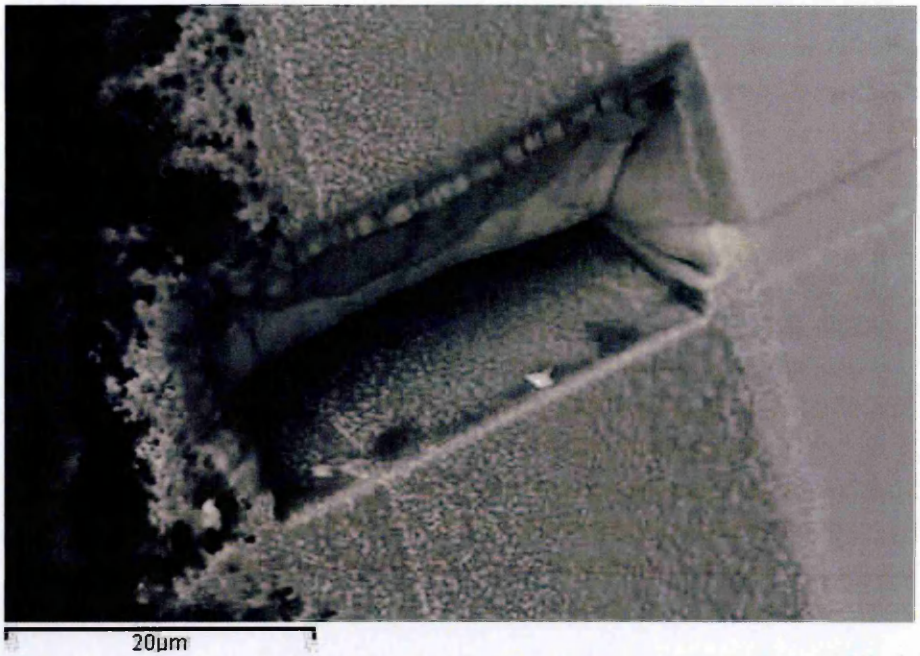

Figure 5-18: ICON Coating on CMSX4 after FIB and mounted at 45° (BSE Image)

By magnifying and rotating the FIBed coating shown in Figure 5-18 it is possible to highlight the line region and emphasis the regions above and below this area (Figure 5-19).

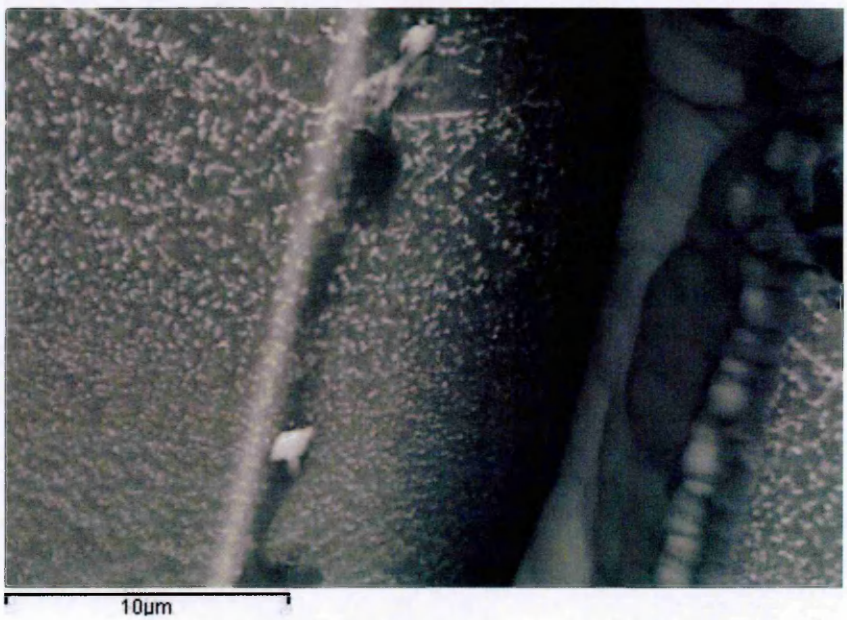

Figure 5-19: Magnified Image of ICON on CMSX4 after FIB and mounted at 45° (BSE Image)

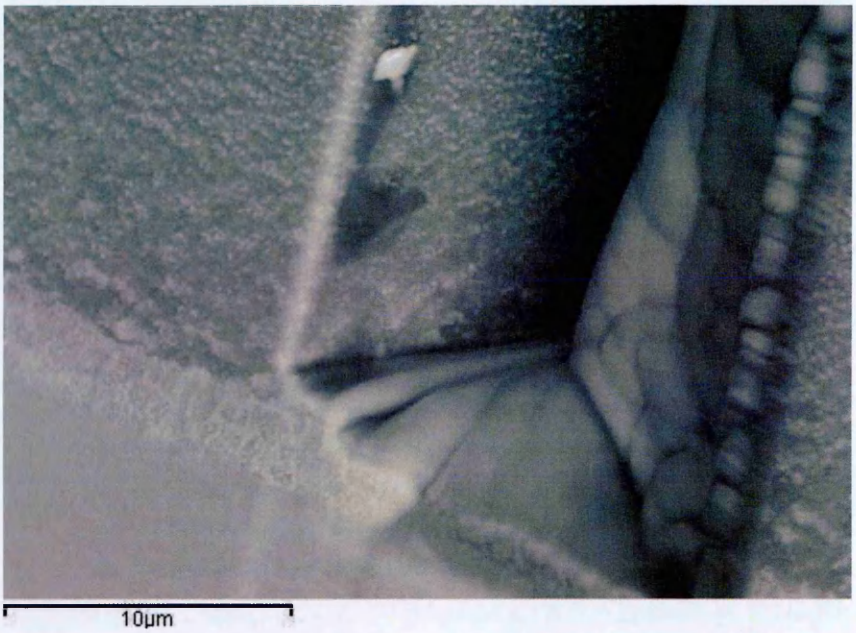

Figure 5-20: Magnified Image of ICON (lower portion) on CMSX4 after FIB and mounted at 45° (BSE Image)

Understanding that this is not a surface anomaly and exists within three dimensions means that it is possible to examine the area more closely to understand why and how this 'planar artefact' is produced. It should be also noted that from the micrograph Figure 5-20 it can be seen that the IDZ is relatively thin and maintains some of the cuboidal γ/γ' structure of the substrate, as previously reported for GTD111.

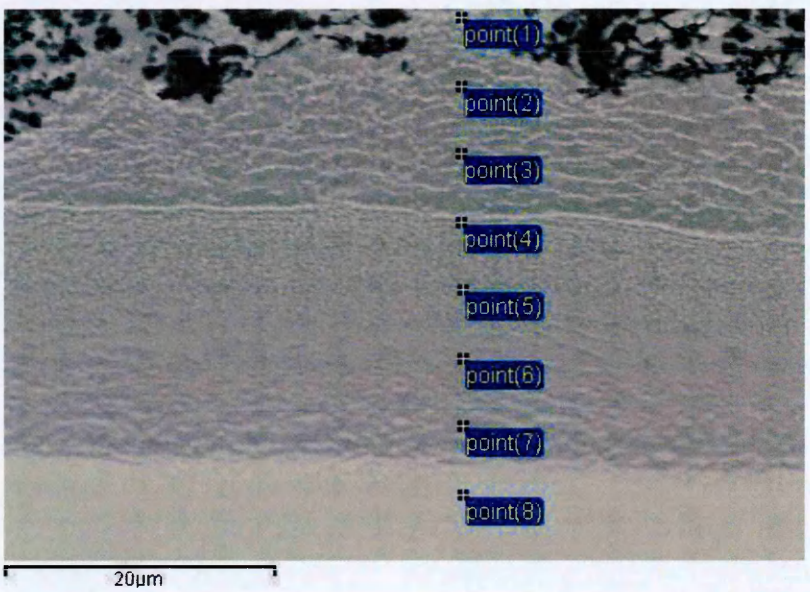

Figure 5-21: Magnified ICON Coating on CMSX4 Indicating Analysis Points (BSE Image)

The chemical analysis of the line scan (figure 5-21) is illustrated in tabular form (Table 5-4) and graphically as in Figure 5-22.

Table 5-4: Chemical Analysis of Coating Composition of ICON on CMSX4 (atomic %)

Spectrum	Al	Ti	Cr	Co	Ni	Ta	W	Re
point(1)	58	1	3	4	31	1	1	
point(2)	58	1	2	4	31	3	1	
point(3)	59	1	2	4	34			
point(4)	58	1	3	5	33			
point(5)	55	3	3	5	32	2	1	
point(6)	54	1	3	5	34	2	1	
point(7)	52	0	2	5	40	1		
point(8)	11	1	13	13	59		2	1

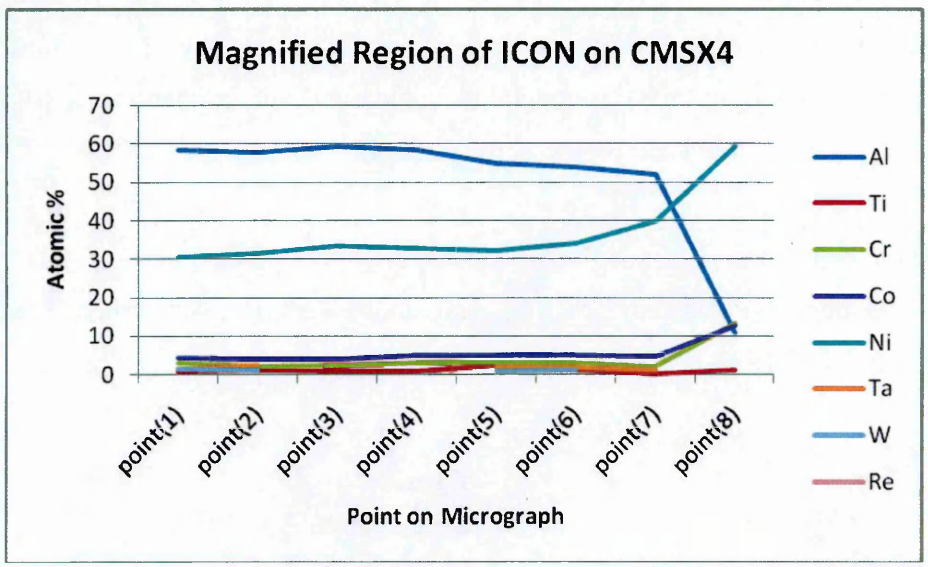

Figure 5-22: Chemical Composition of ICON Coating on CMSX4

Again, assigning partition coefficients (as explained in Table 5-1) the effective nickel to aluminium ratios are given in Table 5-5:

Table 5-5: Ni and Al Ratios for ICON on CMSX4 (atomic %)

	Al	Ni
1	Ni	Al
2	61	39
3	60	40
4	61	39
5	61	39
6	59	41
7	57	43
8	53	47

Table 5-5 illustrates that the ICON heat treatment of Al on CMSX4 results in a coating which is between the β-NiAl and the δ-Al_3Ni_2 phases, with, the Al_3Ni_2 phase predominately in the outermost section of the coating (points 1-4). Furthermore, after point 4 (where the secondary phase planar artefact is found) the Al composition decreases steadily in concentration. Assuming that $NiAl_3$ is formed initially during the initial heat treatment phase then reaction with the CMSX4 substrate or something on the surface of the CMSX4 must be acting as a diffusion barrier (inhibitor of diffusion) so preventing any further inward flux of aluminium and the formation of β-NiAl. However, nothing unique in terms of composition can be seen at position 4, other than the onset of the Ni and Al gradient. It should be noted that point 7 on the micrograph (Figure 5-21) is actually the β-NiAl composition, suggesting that Ni migrates from the substrate into this coating area during the ICON process. This also suggests that there is some mechanism inhibiting Ni diffusion, as if more Ni is allowed to diffuse outward (possibly increasing time or temperature could achieve this) then more NiAl phase would result within the inner region of the coating.

Al_3Ni_2 is formed when the Ni composition lies between approximately 37-41.5% (at) at 820°C. It has an hP5 (Pearson symbol) structure and is very complex compared to the BCC structure of NiAl. The structures of both Ni_2Al_3 and NiAl are shown in figure 5-23.

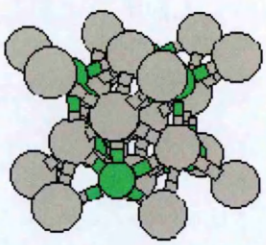

Al_3Ni_2

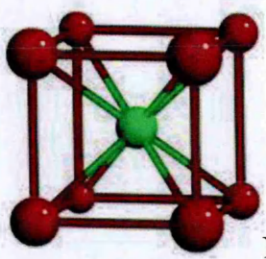

NiAl

Figure 5-23: Structures of Al_3Ni_2 and NiAl[172]

Magnifying the coating further makes it possible to see the distinct phases (Figure 5-24), a brighter precipitate and a darker matrix whilst viewing under the BSE imaging in the SEM. The secondary phase intermetallic precipitates appear to form in 3 distinct regions and three morphologies: broad towards the outermost sections of the coating; small but continuous forming the planar surface layer (the 'line' in the micrograph) which divides a finely dispersed precipitate to a plate-like precipitate.

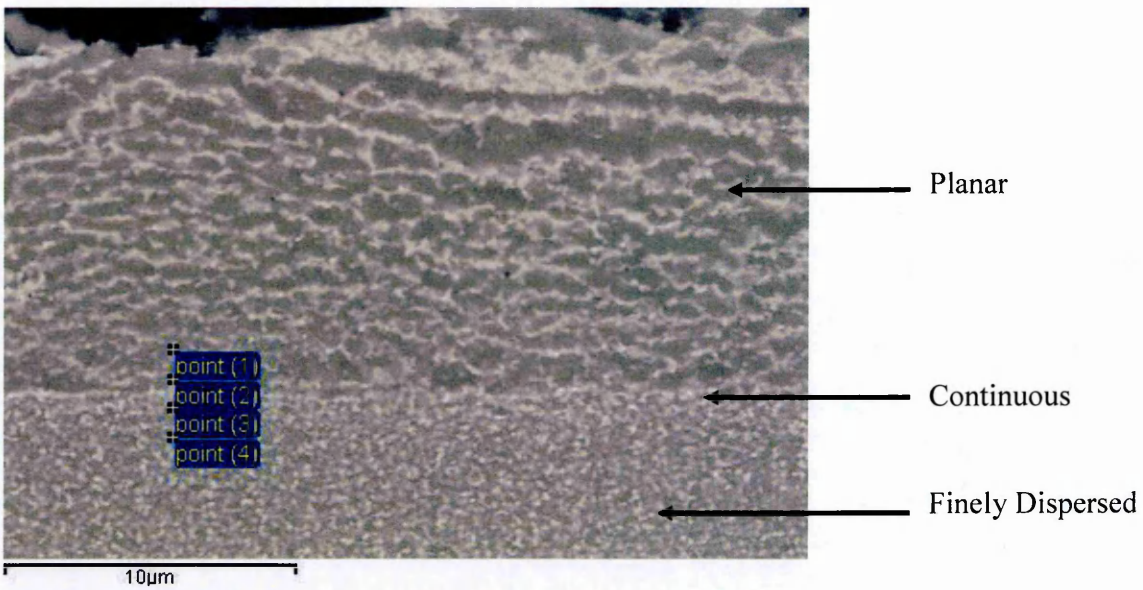

Figure 5-24: Further Magnification of ICON on CMSX4 (BSE Image)

Table 5-6: Atomic Composition of Points Shown in Figure 5-24 (%)

Spectrum	Al	Ti	Cr	Co	Ni	Ta	W	Re
point (1)	58	0.4	3.5	4.9	31.4		0.6	0.1
point (2)	57	0.7	4.2	4.9	30.0	0.9	1.1	0.4
point (3)	57	0.8	3.7	5.0	30.1	0.9	1.1	0.5
point (4)	57	0.7	3.0	5.2	31.3	0.9	1.2	

The above table (table 5-6) shows no apparent difference between the two phases; however, this may be due to the depth of coating generating the x-rays used for chemical composition analysis. Analysing the uppermost phase of the coating and comparing the darker matrix with the lighter linear precipitates it is possible to explain the variation in colour whilst looking at the coating in back scatter mode. It should be noted that both the heavy elements W and Re are found both above and below the secondary phase line as shown in Table 5-7.

Figure 5-25 shows the same coating as figure 5-24 but with different sites of anylysis which were also tested for chemical compostion.

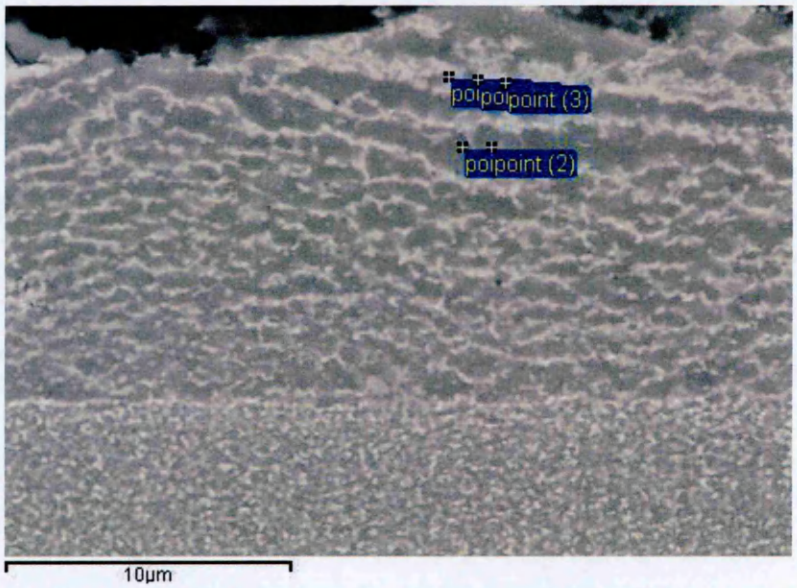

Figure 5-25: Micrograph of Different Phases of ICON Coating on CMSX4 (BSE Image)

Table 5-7: Atomic Composition of Different Phases within the ICON Coating on CMSX4 (%)

Spectrum	Al	Ti	Cr	Co	Ni	Ta	W	Re
point (1)	58.9	1.0	9.3	4.9	20.7	1.6	2.3	1.2
point (2)	59.1	1.4	10.6	3.9	17.8	2.3	3.5	1.4
point (3)	59.8	1.2	6.5	5.2	22.1	2.2	2.2	0.8
point (1)	58.3	0.5	2.7	4.0	31.5	1.8	1.3	
point (2)	58.5	0.3	2.5	4.4	33.8		0.5	

Table 5-7 shows that there are some differences between the matrix and the precipitate, with the lighter area containing the heavier element Re and a higher concentration of Ta, W, Cr and Ti: Re, Ta and W will be depicted as lighter regions when analysed under the back scatter detector of an SEM. The darker matrix does show an increase in Ni concentration even though the Co like the Al, are found in almost equi-concentrations throughout the matrix and precipitate. This does suggest that the finely dispersed precipitates below the secondary phase surface layer (this secondary phase intermetallic line) are comprised of Re, Ti, Ta, Cr and Co containing aluminides. It is thought that continuous phase line represents where the initial coating/substrate interface was found (due to coating composition pre and post this line) suggesting that significant energy is present to transport relatively large atoms (Re and W) outward from the substrate into the outer part of the coating. A number of papers produced by Narita *et al.*[173] and Josso *et al.*[174] have shown that Ni-Co-Re-Cr and Ni-W compositions can act as a diffusion barrier. It is therefore thought that Re

and W intermetallic phases act as a diffusion barrier during the ICON process on CMSX4.

5.4 Results: Modifying Substrate Surface Chemistry

To date the ICON process has proved 'successful' i.e. formed a dense NiAl coating on GTD111, IN738 and Ni200 and 'unsuccessful' with only the superalloy CMSX4. It is therefore worth comparing the compositions of the multicomponent commercial turbine alloys, as these differences between the resulting coatings are thought to be due to substrate alloy composition and microstructure differences. Selectively modifying the substrate chemistry may allow the elimination of some of the alloying additions, permitting the identification of those alloying additions that have the greatest bearing on the formation of undesirable secondary phases.

Table 5-8: Composition of Alloys Used with this Study (Wt%)

Alloy	Ni	Cr	Co	Al	W	Ti	Mo	Ta	Re	Nb	Fe	Hf	C
CMSX-4	60.7	6.5	9.6	5.6	6.4	1.0	0.6	6.5	3.0	0.0		0.1	
GTD 111	60.6	13.5	9.5	3.3	3.8	4.8	1.5	2.7			0.2		0.1
IN 738	61.0	16.0	8.5	3.5	2.5	3.5	1.8	1.8		0.8	0.5		0.2
IN 738 LC	69.0	11.6		5.8	2.6	3.4	4.1	1.8		1.8			0.1

From the table above (Table 5-8) the only variation from CMSX4 is a slight increase in Al, a larger increase in W and Ta, and Re: it is the only alloy to include the heavy element Re. CMSX4 has lower quantities of Cr and Ti and is without C (due to its single crystal nature), therefore modifying CMSX4 with both Cr and Ti may help elucidate if these two elements influence the diffusion mechanism in ICON.

5.4.1 Sputtered Cr and Ti Surface Enrichment

As can be seen from the table above (Table 5-8) the alloys used all share similar alloying additions albeit in varying concentrations (with the exception of CMSX4 which also contains Re, Hf and is without C). The roles of Cr and Ti were further investigated. The elements of Ta and Re also vary between these substrates but these are less easy to investigate using available coating target materials at Cranfield, especially with the cost associated with Re as a sputtering target. In these studies, CMSX4 was modified by sputter deposition of Cr or Ti layers, which were diffused for 1 hour at 1100°C before plating with aluminium and heat treating according to the ICON process. Neither Cr nor Ti (Figure 5-26 and 5-27) enrichment could account for the difference in microstructure observed between CMSX4 and GTD111.

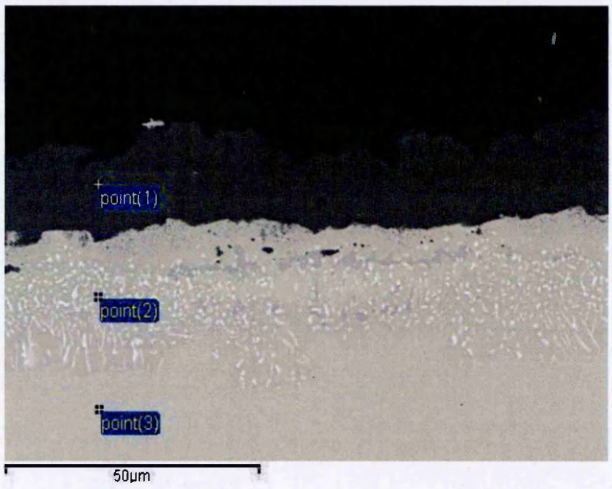

Figure 5-26: Titanised CMSX4 with Electroplated Al Prior to ICON Heat Treatment

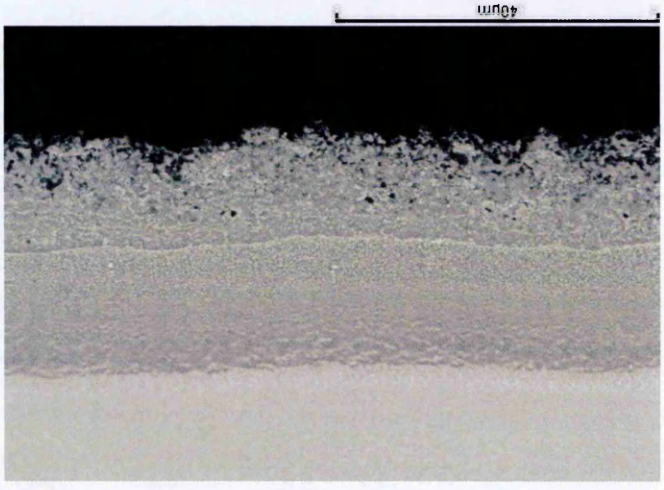

Figure 5-27: Titanised CMSX4, Aluminium Plated and Heat Treated (ICON) to Produce Ni(Al,Ti) Coating

5.4.2 Electroplating of Cr from Ionic Liquids

Chromium was also deposited via electroplating from ionic liquids ([BMIm][BF_4] 10 wt% $CrCl_3.6H_2O$) in collaboration between Cranfield and IST based in Lisbon, Portugal[4].

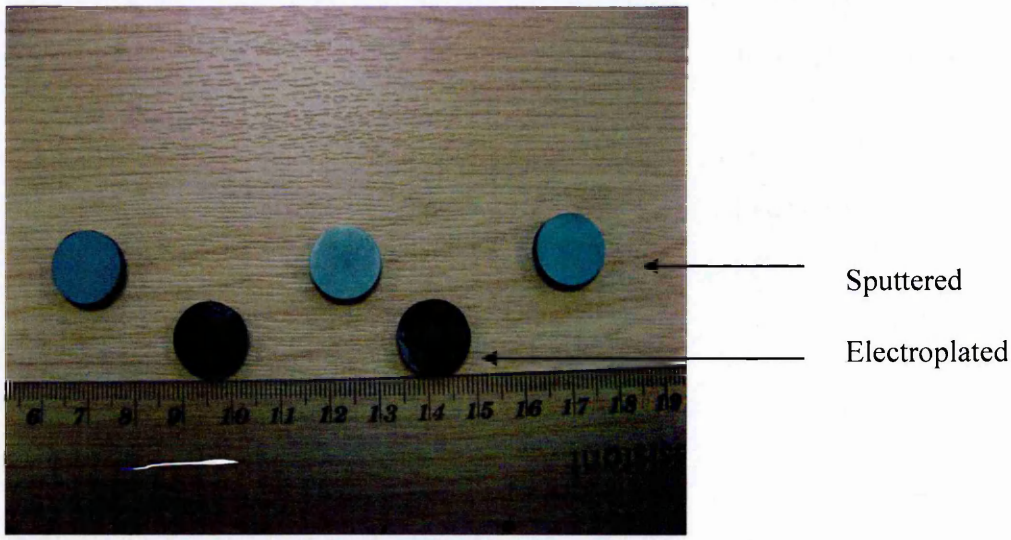

Figure 5-28: Comparison of Sputtered and Electroplated Cr Samples on CMSX4

Unlike the sputtered samples, the electroplated samples were black in appearance (Figure 5-28). However, both received the same heat treatment regime. The electroplated Cr produced a similar coating to that of the sputtered Cr. One should note that Cr plating from ionic liquids is not a standard process and it is believed that this post processing with IL to 'Chromise' the surface has never been attempted or reported before. However, the resulting coating was similar to the sputtered coatings (both Ti and Cr) and therefore it can be assumed that the formation of Ti and or Cr modified aluminides is not critical in the formation of the ICON coating although both are exothermic (Table 9-1). The outcome of this study would imply that it is either the Re or Ta (or a combination of both) that interacts and modifies the ICON process on CMSX4.

---

[4] The conditions were: Electrolyte used: 1-butyl-3-methylimidazolium tetrafluoroborate [BMIm][BF_4] + 10 wt% $CrCl_3.6H_2O$ (with agitation), Temperature set at 85°C, Counter-electrode used was platinised titanium plate and electrodeposition under potentiostatic conditions (Applied potential: -1.8V (vs Pt wire QRE)).

5.4.3 Pt Enrichment of CMSX4 and GTD111

Platinum enrichment not only conveys benefits for oxidation resistance etc. as described within the literature review, but also, it was thought that due to the large atomic size, platinum could act in a similar way to Re in CMSX4. Therefore, Pt was sputtered onto both CMSX4 and GTD111 to investigate the role of large precious metal element additions.

Pt enrichment of CMSX4 was done by depositing 7um of platinum by sputtering, heat treated and then aluminium plated, followed by the ICON heat treatment (Figure 5-29 and 5-30 and Tables 5-9 and 5-10).

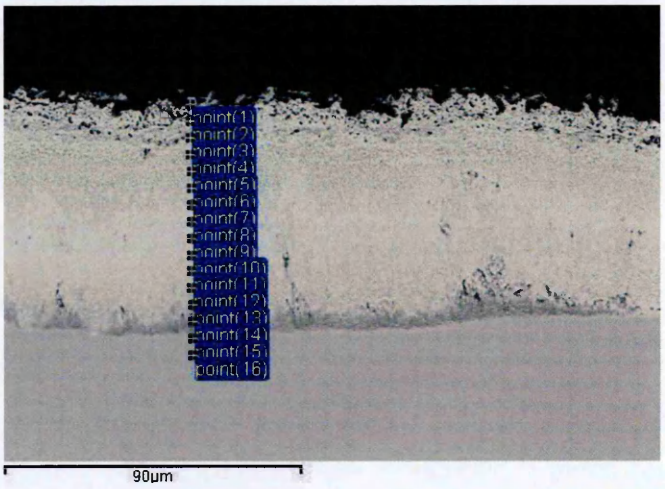

Figure 5-29: Photomicrograph of Pt Enriched CMSX4 with Analysis Points Depicted

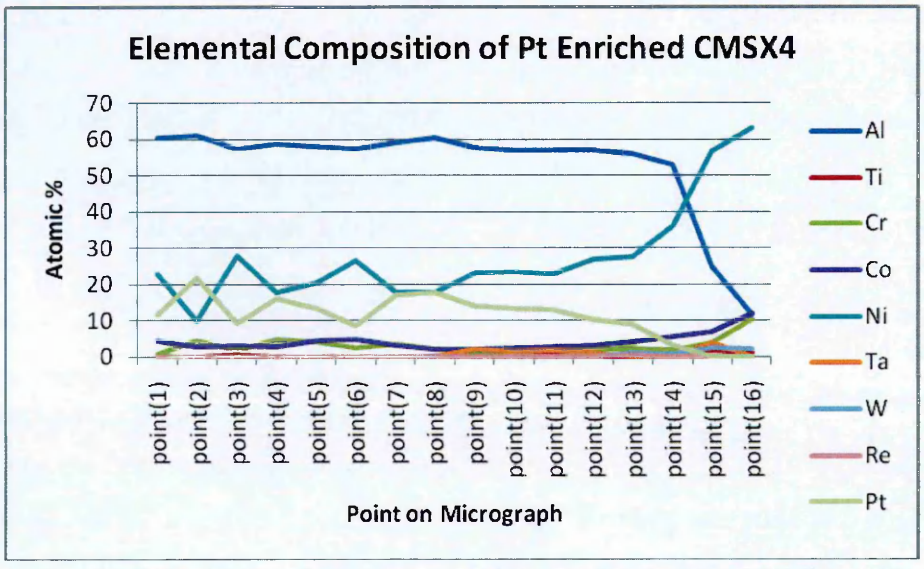

Figure 5-30: Elemental Composition of Pt Enriched CMSX4

Table 5-9: Elemental Composition of Points Depicted in Figure 5-5(atomic %)

	Al	Ti	Cr	Co	Ni	Ta	W	Re	Pt
point(1)	60.5	0.0	0.8	4.5	22.6	0.0	0.0	0.0	11.6
point(2)	61.1	0.0	4.6	2.7	10.0	0.0	0.0	0.0	21.7
point(3)	57.2	0.6	1.9	3.2	27.7	0.0	0.0	0.0	9.3
point(4)	58.8	0.0	4.6	2.7	17.8	0.0	0.0	0.0	16.1
point(5)	57.8	0.0	4.1	4.5	20.4	0.0	0.0	0.0	13.2
point(6)	57.5	0.0	2.4	4.8	26.6	0.0	0.0	0.0	8.7
point(7)	58.9	0.0	3.4	3.2	17.6	0.0	0.0	0.0	17.0
point(8)	60.4	0.0	2.1	2.1	17.6	0.0	0.0	0.0	17.7
point(9)	57.6	0.0	1.2	2.1	23.1	2.1	0.0	0.0	13.8
point(10)	57.1	0.7	1.5	2.5	23.5	1.5	0.0	0.0	13.2
point(11)	57.0	0.8	1.9	2.8	22.9	1.8	0.0	0.0	12.8
point(12)	56.8	0.0	2.0	3.2	26.8	1.1	0.0	0.0	10.1
point(13)	55.9	0.0	2.3	4.1	27.4	0.0	1.2	0.4	8.8
point(14)	53.0	0.0	1.7	5.5	36.0	0.0	0.7	0.0	3.1
point(15)	24.9	1.6	3.9	6.8	56.6	3.8	2.4	0.0	0.0
point(16)	11.5	1.2	10.3	11.8	63.0	0.0	2.2	0.0	0.0

Table 5-10: Atomic Ratios for Pt Enriched CMSX4 followed by ICON (atomic %)

	Al	Ni	Pt
point(1)	60.9	27.1	11.6
point(2)	63.4	12.7	21.7
point(3)	58.8	30.9	9.3
point(4)	61.1	20.4	16.1
point(5)	59.9	24.9	13.2
point(6)	58.7	31.4	8.7
point(7)	60.6	20.8	17.0
point(8)	61.5	19.7	17.7
point(9)	58.2	27.4	13.8
point(10)	58.6	27.5	13.2
point(11)	58.8	27.5	12.8
point(12)	57.8	31.1	10.1
point(13)	57.0	33.1	8.8
point(14)	53.9	42.1	3.1
point(15)	28.4	69.6	0.0
point(16)	17.8	77.1	0.0

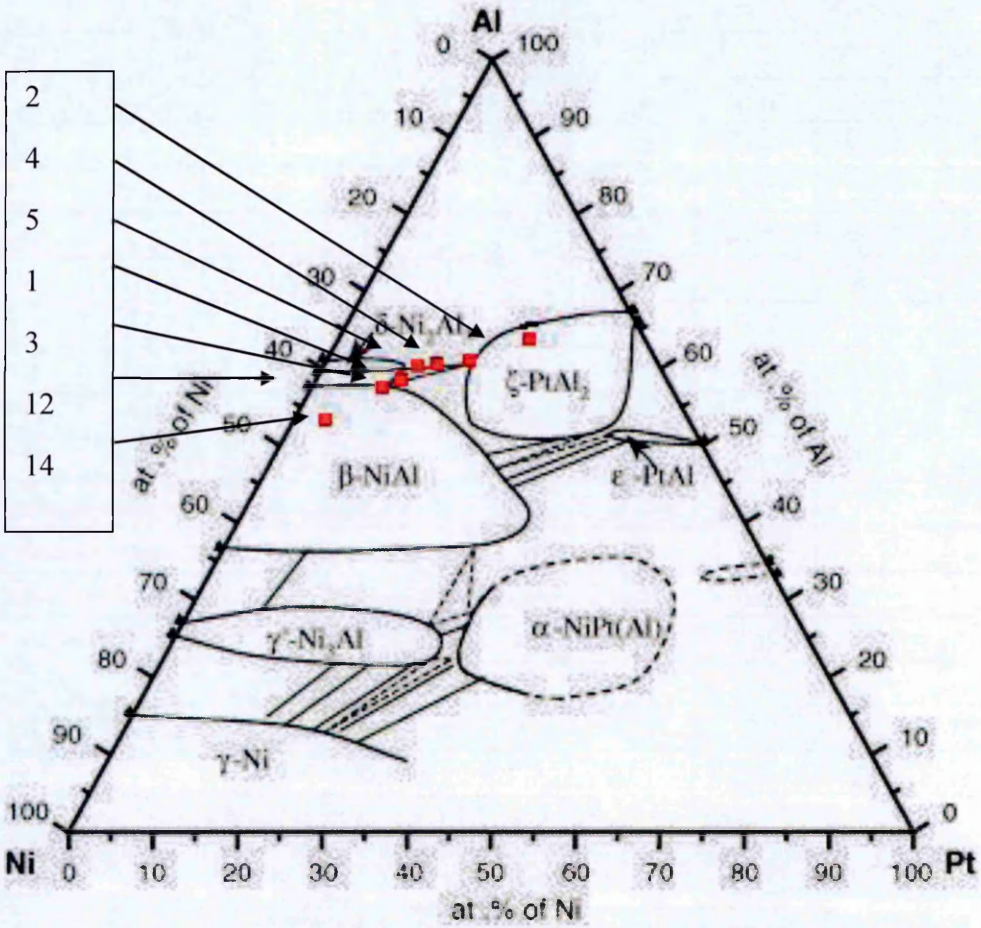

Figure 5-31: Ternary Phase Diagram Showing Phases Highlighted in Table 5-10

Figure 5-31: Ternary Phase Diagram Showing Phases Highlighted in Table 5-10

shows that assigning partitioning coefficients as per the ternary diagram (as reported by Gleeson[175]) and further assuming that Pt and Ni substitute on the nickel sub lattice[176] shows that the coating comprises of platinum-enriched compound similar to the delta Ni_2Al_3 phase. However, within the striated region there is some $PtAl_2$ phase.

This suggests that large atoms such as Pt and Re may act either as a diffusion barrier directly or more likely act to form diffusion barriers through the formation of rhenium- or platinum-modified aluminides most probably based on $PtAl_2$. The Al-Re phase diagram (Figure 5-32) illustrates that a number of different Al/Re intermetallics are possible and most are aluminium rich.

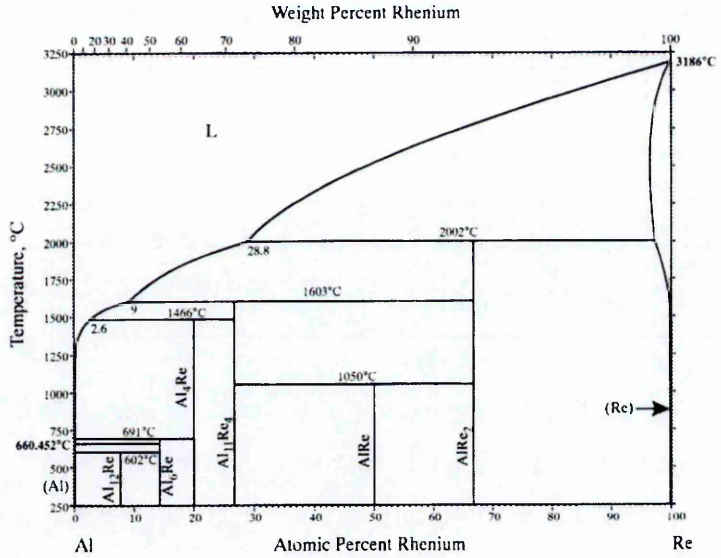

Figure 5-32: Al-Re Phase Diagram[177]

5.4.4 Platinum Enrichment of GTD111

As with CMSX4, GTD111 was enriched with platinum, heat treated, aluminium plated and heat treated according to the ICON heat treatment. Figure 5-33 illustrates the micrograph of the coating produced using this platinum diffusion treatment, prior to aluminium plating and ICON heat treatment as a bond coat under a TBC. Adhesion of the EB-PVD TBC to the bond coat is excellent. The composition for each point shown in table 5-11.

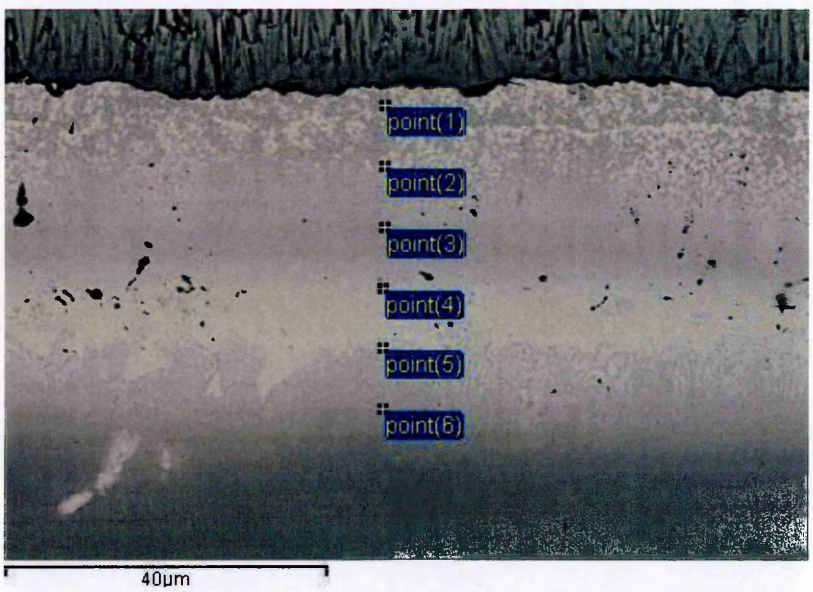

Figure 5-33: Pt Enriched GTD111 followed by ICON Heat Treatment

Table 5-11: Chemical Composition of Pt Enriched GTD111 followed by ICON (atomic%)

Spectrum	Al	Ti	Cr	Co	Ni	W	Pt
point(1)	44.6	3.7	3.7	4.7	32.5		10.9
point(2)	47.3	2.3	4.1	3.5	26.2		16.7
point(3)	44.8	2.9	2.0	3.5	34.1		12.8
point(4)	33.8	8.0	5.5	6.0	31.3		15.3
point(5)	20.0	8.7	17.6	7.4	30.3	1.7	14.3
point(6)	4.8	3.3	17.3	10.5	56.0	2.5	5.8

As for CMSX4, the Ni/Pt/Al compositions of the coated GTD111 were mapped onto the Ni-Pt-Al ternary diagram. This is reproduced in Figure 5-34. As figure 5-33 shows, this combined treatment forms a layered coating, containing a series of discreet second phase particles. It is known that this can occur for very high aluminium activities[42] when manufacturing platinum aluminide coatings, RT22 compared to CN91 (both made by Chromalloy).

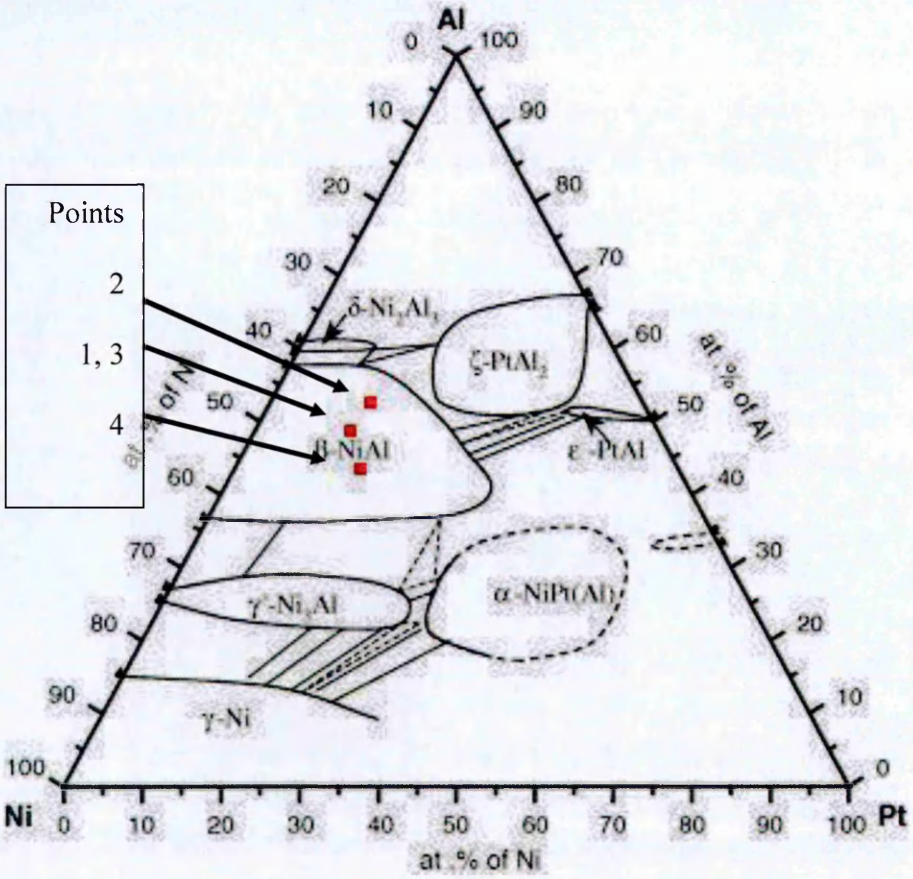

Figure 5-34: Ternary Phase Diagram Showing Phases from Table 5-11

Transferring the data into the NiPtAl ternary diagram it is possible to see that although the coating appears to be biphasal with the lighter striated region on top and

a darker matrix beneath, it is in fact entirely β-phase. This suggests that the large Pt atom does not act as a diffusion barrier and neither does the formation of Pt_xAl_x act to hinder β-formation. Therefore, Re is the more likely candidate to account for the two phase microstructure produced on CMSX4 alloy either by the large atom acting as a direct diffusion barrier (in a similar way to tungsten as proposed by Josso *et al.* but it is unlikely, due to the data in Table 5-7) or that the Re is competing with Ni to form intermetallics (possible as Re forms highly stable line compounds with aluminium). One issue is how representative is the 1100°C ternary phase diagram produced by Gleeson[175] for processing at 820°C.

By combining this ternary diagram with the three component binary system it is possible to estimate the shape of the phase fields as a function of temperature.

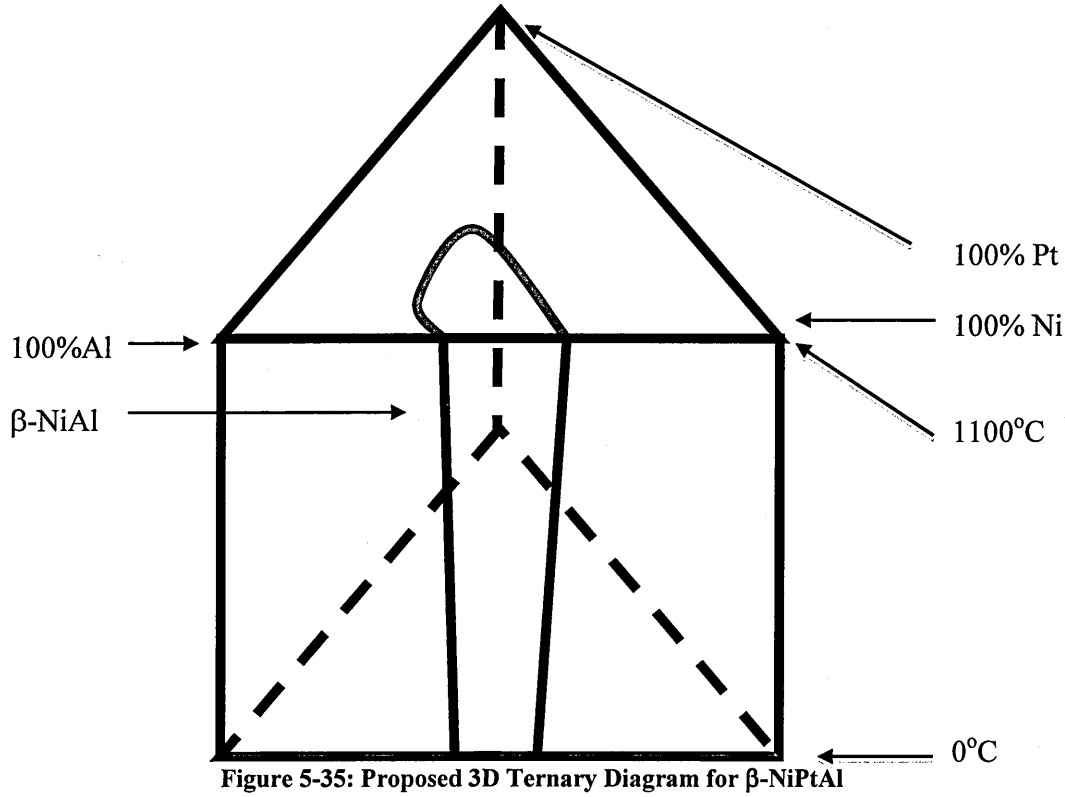

Figure 5-35: Proposed 3D Ternary Diagram for β-NiPtAl

Figure 5-35 represents the proposed 3D phase diagram with upper 'triangle' segment showing Gleesons ternary phase diagram which converges with a standard binary Ni-Al phase diagram. In practice Pt does not segregate out in the majority of most β-phase coatings when they are at room temperature. Therefore it is assumed that Pt containing β-phase will be almost identical at 620 and 820°C.

This coating on GTD111 also shows evidence of forming a layered structure suggesting that precious metals such as Pt (and Re) may act as elemental selective diffusion barriers, resulting in the formation of intermetallic second phases within the coating. The Al-Re phase diagram (Figure 5-32) does show that the Al-Re intermetallics are all line intermetallics suggesting that they will only form when specific stoichiometries are present. Furthermore, it is interesting to note that Re has migrated to the outermost part of the coating as shown in Figure 5-25. This could only happen in the second stage of the ICON process once the temperature has exceeded 691°C, and would imply that a Re containing molten Al alloy must be present, even with small fractions of Re present. This is possible for temperatures above 690°C, where Re is less than 20%At.

As a result of this surface modification study, one may conclude that the second phase intermetallic formation is most likely due to the presence of Re and possibly also Ta (although Ta could not be directly studied but the Al-Ta phase diagram shows a similar liquid + β ($TaAl_2$) field above 668°C in CMSX4). It is likely that such layers may spontaneously form when large precious metal atoms are present. During the exothermic reaction, they have high heats of formation as shown in Figure 1-14. Heats of formation of TiAl and CrAl are also exothermic, but these seem to be insufficient, with regards to the present ICON treatment to result in the formation of discrete Ti or Cr intermetallic phases. Alternatively, the Ta and Re compete for Al against Ni and therefore prevent formation of the favourable NiAl phase.

6 Is the ICON Process a High or Low Activity Aluminising Process?

As reviewed within the literature and mentioned before, CVD aluminising can either be categorised as LTHA or HTLA with either inward or outward movement of aluminium or outward movement of nickel respectively. To identify which mechanism was rate controlling within the ICON process a review of the microstructures was needed. In Figure 6-1, carbides can be seen to be present within the coating, however, it is not possible to form these carbides at the pressures and temperatures used when fabricating the ICON based coating. Therefore it is thought that these phases must have been present in the original substrate (GTD111). These large and immobile phases may be thought of as Kirkendal markers as the energy needed[38,178] to move these large stable phases will not be present at the temperatures used in the ICON heat treatment. Figure 6-1 illustrates that the carbides can be observed in the outmost region of the coating. Therefore this implies that the ICON process is a high activity process with a net inward movement of Al.

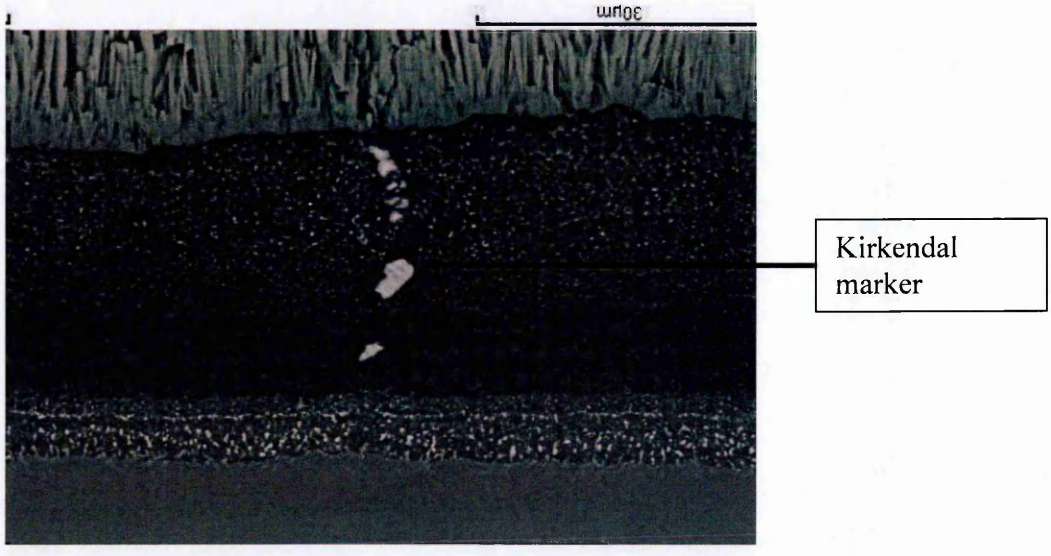

Figure 6-1: Microstructure of Carbides Entrapped in NiAl Coating Produced using ICON

6.1.1 CVD Inward Diffusion

According to the data above, the ICON process should be similar to that of a traditional CVD LTHA coating with inward diffusion of Al accounting for the formation of NiAl. According to Boon and Goward[36] inward diffusion (LTHA) requires a 2 stage reaction mechanism. First, the AlCl generated from the aluminising powder reacts with nickel to produce a δNi_2Al_3 phase, which is then transformed to β-NiAl upon further heat treatment.

Initial CVD coating studies to develop reference coatings used an 'in-pack' system at 1050°C for 20 minutes. This method produced a β-NiAl directly and was therefore a HTLA process. To produce an inward diffused coating, therefore a different heat treatment regime was employed which used a much lower deposition temperature (860°C) for 6 hours. This second processing route enabled δNi_2Al_3 to be formed as shown in the trace below.

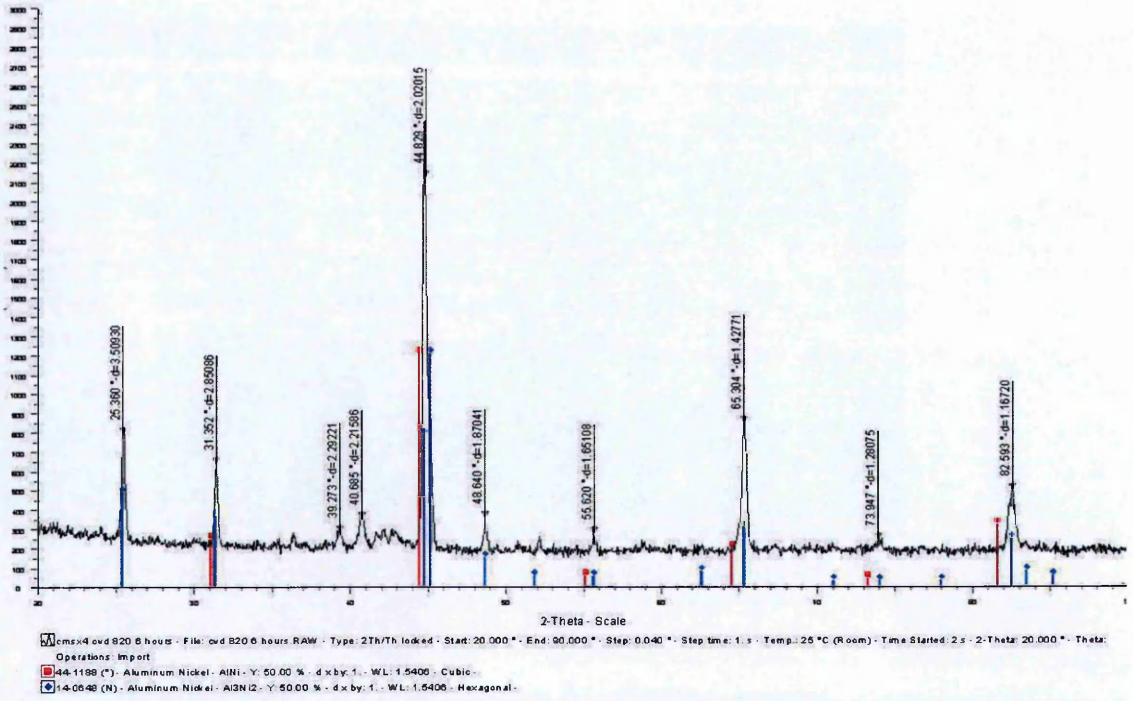

Figure 6-2: XRD Trace of CVD Aluminized CMSX4 after 860°C for 6 hours

From the XRD trace above (Figure 6-2), the red peaks equate to where NiAl would be found, whereas the blue lines represent the peak lines for Ni_2Al_3, shows that Ni_2Al_3

had been formed in this low temperature CVD process with the possible presence of β-NiAl.

This sample was then sectioned, mounted and polished to enable analysis using EDX and SEM techniques (Figure 6-3, Figure 6-4 and Table 6-1). The coating contained Al and Ni with additions of Co, Cr, W and Ti (Table 6-1).

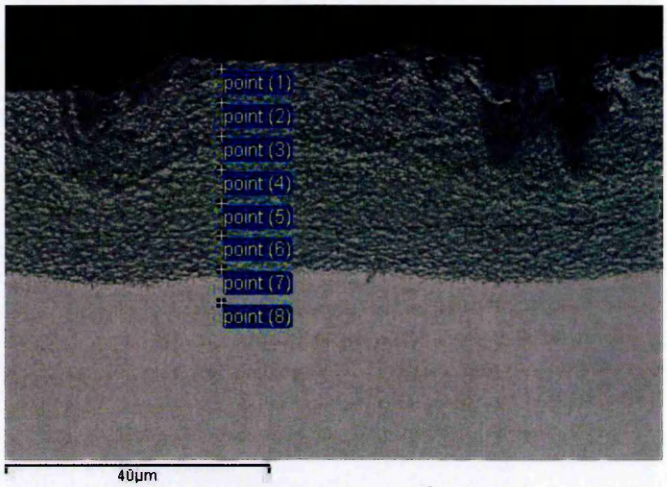

Figure 6-3: CVD Produced Ni_2Al_3 after 860°C for 6 Hours on CMSX4

Table 6-1: Chemical Profile of CVD Produced Intermetallic after 860°C for 6 Hours

Spectrum	Al	Ti	Cr	Co	Ni	W
point (1)	38.0		4.0	7.0	45.1	6.0
point (2)	37.6		4.6	7.1	45.7	5.0
point (3)	36.3		4.5	8.6	44.5	6.0
point (4)	34.4		6.0	7.8	40.6	11.3
point (5)	32.8	0.4	5.3	7.4	42.5	11.5
point (6)	32.0	0.5	5.7	8.0	45.5	8.4
point (7)	7.8	1.0	9.0	11.3	58.8	12.1
point (8)	4.4	0.5	10.0	14.0	58.9	12.2

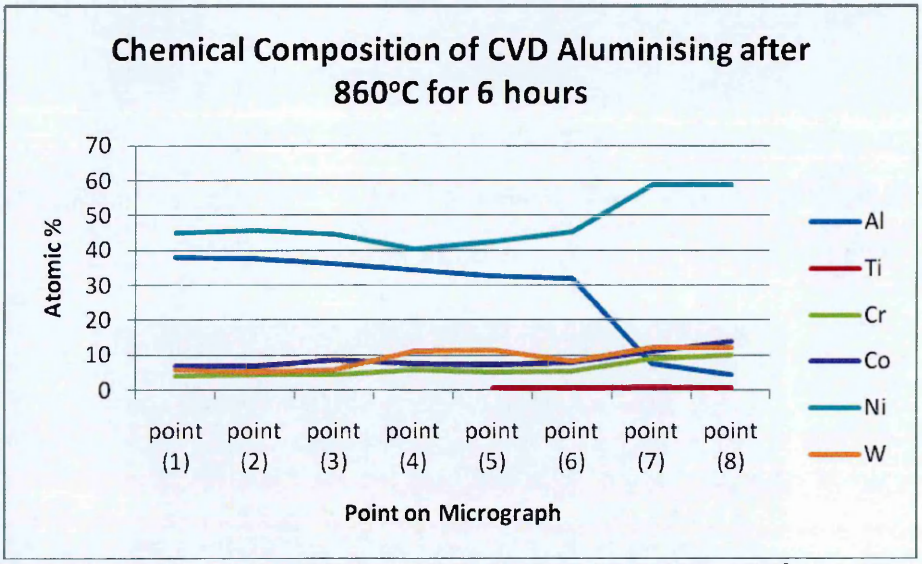

Figure 6-4: Diffusion Profile of CVD CMSX4 after Heat Treatment at 860°C for 6 Hours

Assuming that Cr adopts both Al and Ni lattice sites and Co and W adopts Ni sites and Ti adopts Al sites it can be said that the ratio of Ni to Al is as follows (table 6-2).

Table 6-2: Calculation of Ni and Al lattice Site Occupation

Point	Ni Sites	Al Sites
1	40.0	60.0
2	39.9	60.1
3	38.6	61.4
4	37.4	62.6
5	35.9	64.1
6	35.3	64.7
7	13.3	86.7
8	9.9	90.1

Which, in accordance with the NiAl phase diagram (Figure 1-2) shows that the phase equilibrium is within the delta phase with the exception of point 4 where the refractory element W accumulates. This suggests that point 4, or possibly point 3 is where the edge of the substrate previously sat, implying both inward and outward diffusion is occurring to account for the level of W in the outer coating.

Heat treating the samples at 1050°C for 1 hour transformed the residual δNi_2Al_3 to β-NiAl which produced the following XRD trace (figure 6-5), microstructure (figure 6-6) and chemical profile (table 6-3 and figure 6-7).

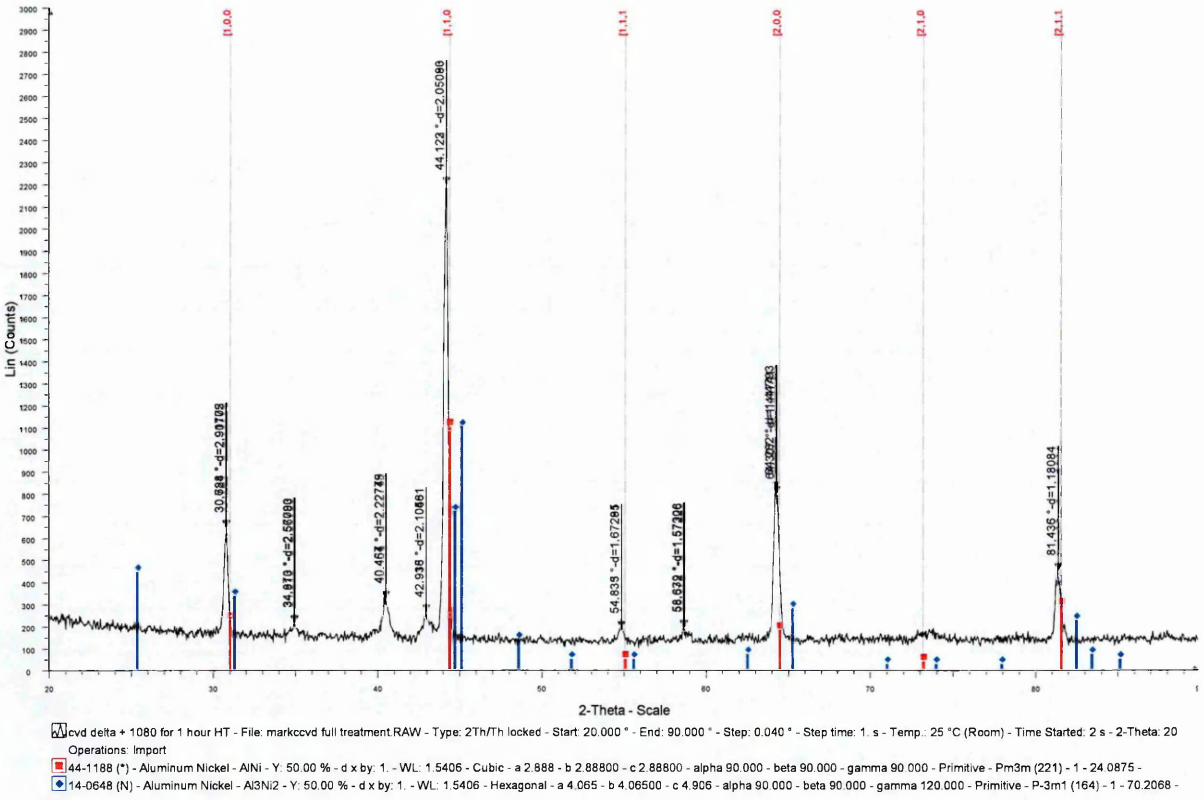

Figure 6-5: XRD Trace of Completed CVD Processed

The red lines from the plot above represent where NiAl would be expected, whereas the blue lines represent Ni_2Al_3, as it can be seen the β-NiAl phase has been produced following this heat treatment.

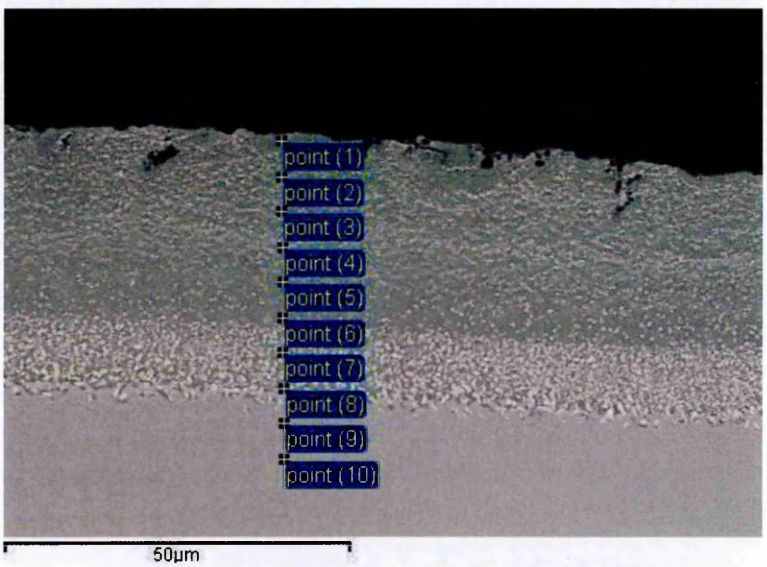

Figure 6-6: Photomicrograph of CVD Produced NiAl

The microstructure of coating is shown in Figure 6-6 with elemental composition shown in Table 6-3 and Figure 6-7. The total thickness of coating is including the interdiffusion zone (IDZ)) is 39.1μm. The IDZ measures 10.3μm thick.

Table 6-3: Elemental Analysis of NiAl Produced by CVD(atomic %)

Spectrum	Al	S	Ti	Cr	Co	Ni	Ta	W	Re
point (1)	44.8		0.3	2.6	6.2	46.0			
point (2)	43.0		0.4	3.6	6.5	44.8		1.6	
point (3)	41.4		0.3	3.8	7.0	46.2		1.5	
point (4)	39.2		0.6	4.6	6.5	47.3		1.7	
point (5)	38.0		0.9	4.3	6.7	50.0			
point (6)	30.4	0.5	1.3	8.8	8.9	46.2		3.9	
point (7)	30.2		1.5	9.1	9.2	46.7		3.3	
point (8)	17.4		1.6	4.9	8.8	64.9		2.4	
point (9)	10.6	0.5	0.9	11.5	12.7	60.0		3.0	0.9
point (10)	13.4		1.3	7.4	9.8	63.7	1.9	2.5	

There are a number of observations present in the above table which are noteworthy. Firstly the aluminium concentration decreases as the depth in the coating increased and seriously reduces once the IDZ is reached. Furthermore, Cr and W concentrations increases as coating thickness increases and are maximal in the IDZ.

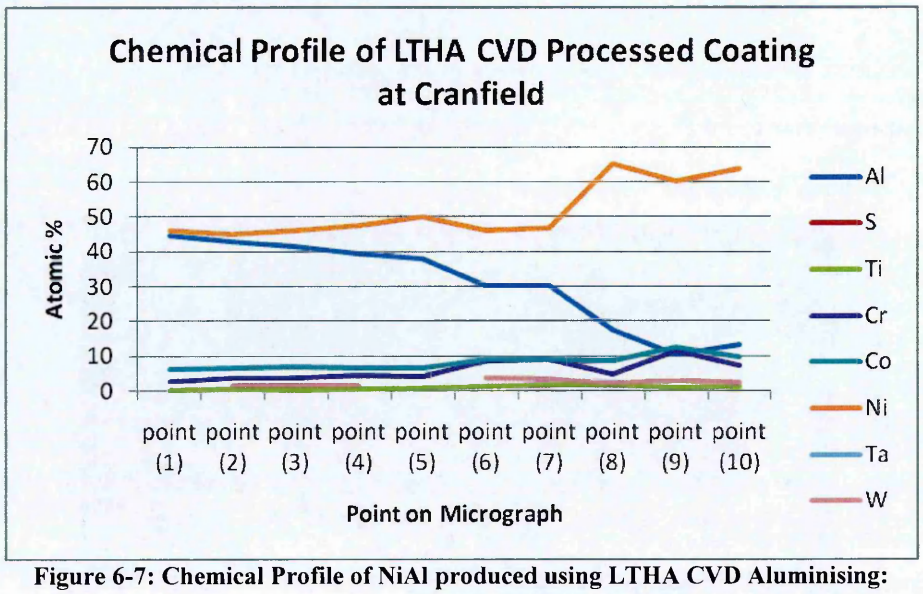

Figure 6-7: Chemical Profile of NiAl produced using LTHA CVD Aluminising:

6.2 Conclusions from the CVD Aluminising Trials at Cranfield

This process has been in use at Cranfield for many years and has been approved for use in aerospace applications. The inward grown aluminium coating forms a β-NiAl throughout the coating (from Table 6-4) up to at least point 5 on the micrograph in Figure 6-6. Although point 6 is slightly above the IDZ there may be interaction between the bulk coating and IDZ due to the 'tear drop' shape arising from the generation of x-rays for chemical analysis.

Table 6-4: Nickel and Aluminium Site Occupancy for CVD LTHA Coating Produced at Cranfield

	Ni	Al
point (1)	53.5	46.5
point (2)	53.2	45.3
point (3)	55.0	43.5
point (4)	56.1	42.2
point (5)	58.9	41.1
point (6)	59.5	36.1
point (7)	60.4	36.3
point (8)	76.2	21.4
point (9)	78.4	17.2

Comparing the two coatings, CVD and ICON based aluminide coatings, it is evident that the aluminium concentration within the ICON coating is consistently higher, more uniform and therefore offers a higher Al reservoir, and thus potentially better for oxidation resistance than in either the HTLA CVD process or the LTHA CVD process.

7 Finite Element Analysis, Differential Scanning Calorimetry and Exothermic Reactions: Understanding the Mechanism of Action for the ICON Process

7.1 Introduction to FEA

Finite element modelling was used to analyse the diffusion of aluminium into the nickel-based superalloy and to verify possible diffusion mechanisms (based on the assumption that this is an inward diffused coating). Diffusion is based on Ficks law which is concerned with the amount of energy (based on a concentration gradient) needed to allow transportation of a substance from an area of high concentration to that of a lower one.

Changes in concentrations can be calculated within a finite element based system by:

Equation 1

$$J_{in} = -D\frac{C_i^t - C_{i-1}^t}{\Delta x} \text{ and}$$

Equation 2

$$J_{out} = -D\frac{C_{i+1}^t - C_i^t}{\Delta x}$$

where: J = diffusion flux (concentration per unit area)

D = Diffusion coefficient

C_i = Concentration in cell i.

Δx = change in length in a single axis

The diffusion coefficient at a given temperature may be calculated using the formula:

Equation 3

$$D_T = Do.e^{(-Q/RT)}$$

Where D_T = Diffusion coefficient at temperature T

Do = Diffusion coefficient or the Arrhenius equation pre-exponent term

Q = Activation Energy

R = Universal gas constant

T = Temperature in Kelvin

Changes in fluxes are given by:

Equation 4

$$\Delta C = C_i^t + (F.(C_{i-1}^t - (2.C_i^t) + C_{t+1}^t))$$

Where :

Equation 5

$$F = \frac{D\Delta t}{\Delta x^2} .$$

and Δt = an increment in time (seconds)

If F is equal to or less that 0.5 then the equation is considered stable in accordance with the Von Neumann stability criterion (i.e. suitable time and distance are chosen).

7.2 The FEA Model

A simple model was created (based on a carburisation model originally proposed by Shipway[179]) where a nickel substrate of infinite thickness was divided into 1 micron thick elements (Figure 7-1). For a more complicated model or for further reading see Crank[180] A further element was added to this, which contained 100% wt. aluminium so diffusion could occur in one direction only. Cell thicknesses were set at 1 micron and time intervals were calculated every minute.

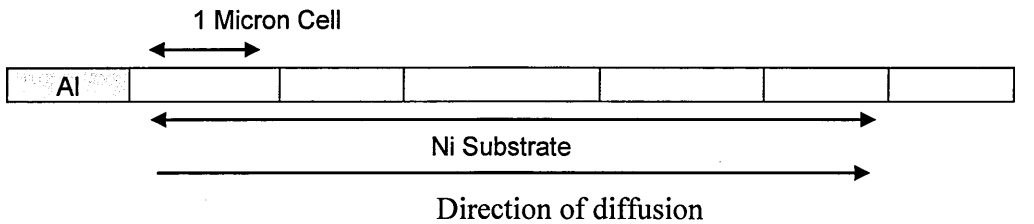

Figure 7-1: Graphic Description of FEA Model used in this Study

Figure 7-2 illustrates the predicted diffusion profile for aluminium diffusing into nickel at the first ICON heat treatment temperature (620°C for 1 hour). This temperature is just below the melting point of aluminium ensuring a solid state diffusion reaction. The FE model suggests little interdiffusion at this temperature with only a 5um deep aluminium profile into the nickel as a result of aluminium diffusion. In practice a $NiAl_3$ surface intermetallic layer was formed at least 40μm thick within 60 minutes of the first heat treatment. Within this study the following parameters were used: D_0=2.9x10^{-12} and Q was 65717 joules.

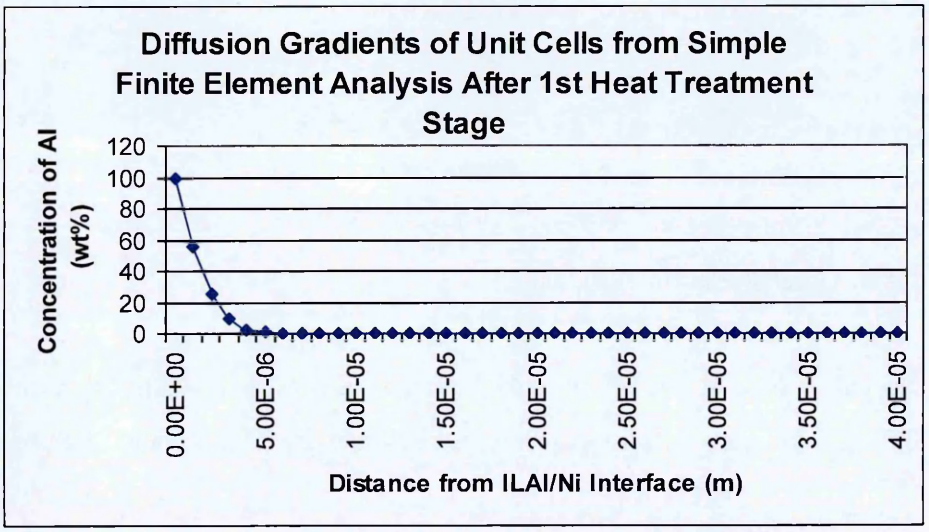

Figure 7-2: Graph of Simple FEA after 1 hour at First Heat Treatment Temperature

The FE model, at this stage in its design, does not take into account the formation of any intermetallics. From the Ni-Al phase diagram (Figure 1-2) one would expect Ni_3Al to form at 13%Al, Ni_5Al_3 to form at 18%Al, NiAl at 25-37% Al, Al_3Ni_2 to form at 44%Al and Al_3Ni to form at 49% Al (all % values are quoted as weight %). When the model is modified to account for intermetallic formation then the resulting diffusion profile forms a Ni_3Al intermetallic surface layer after 6 minutes of heat treatment; as summarised in Table 7-1.

Table 7-1: Predicted Diffusion Profile of ILAl Using ICON Taking into Account the Possibility of Intermetallic Formation

Time (mins)	Diffusion Distance (μm)/Concentration Al (%Wt)					
	0	1 μm	2 μm	3 μm	4 μm	5 μm
0	100	0.00	0.00	0.00E+00	0.00E+00	0.00E+00
1	100	2.49	0.00	0.00E+00	0.00E+00	0.00E+00
2	100	4.86	0.06	0.00E+00	0.00E+00	0.00E+00
3	100	7.11	0.18	1.55E-03	0.00E+00	0.00E+00
4	100	9.25	0.35	5.95E-03	3.85E-05	0.00E+00
5	100	11.29	0.56	1.43E-02	1.85E-04	9.59E-07
6	100	**13.23**	0.82	2.76E-02	5.33E-04	5.52E-06
7	100	13.23	0.82	0.03	0.00	0.00
8	100	13.23	0.82	0.03	0.00	0.00
9	100	13.23	0.82	0.03	0.00	0.00
10	100	13.23	0.82	0.03	0.00	0.00
20	100	13.23	0.82	0.03	0.00	0.00
30	100	13.23	0.82	0.03	0.00	0.00
40	100	13.23	0.82	0.03	0.00	0.00
50	100	13.23	0.82	0.03	0.00	0.00
60	100	13.23	0.82	0.03	0.00	0.00

From this table, one may conclude that once 6 minutes had elapsed and Ni_3Al has formed (probably at only the atomic level), other diffusion processes would essentially stop after the initial heat treatment step (diffusion data from[178]) given the temperature and the time involved. Although it may be argued that a small amount of diffusion will occur due to a diffusion gradient, as the table shows, no change in Al concentration occurs after 6 minutes of running the model (to 2 decimal places). Experimentally, further reaction with aluminium leads ultimately to the formation of $NiAl_3$.

7.2.1 Conclusion from FEA

It appears that this simple modelling does not hold true for the situation shown in reality, and furthermore suggests that improving the complexity of the modelling would not yield significant results as heat evolution, heat capacity and diffusion rates for each intermetallic that may form would be required. Heat treating ILAl for 1 hour at 620°C not only allows the entire Al to react/diffuse (up to 40μm), but the line intermetallic $NiAl_3$ is shown to form. This is problematic for modelling as diffusion coefficients and activation energies have not been calculated for this intermetallic due to its lack of stability. During the second stage of the heat treatment cycle, the $NiAl_3$ is transformed into NiAl. However, the phase diagram shows that before this conversion can take place, the intermetallic Ni_2Al_3 must be first formed if phase equilibria are taken into account.

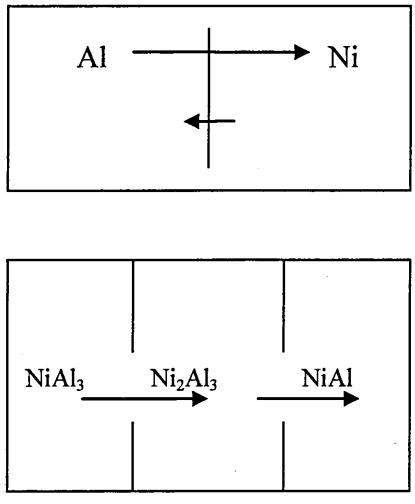

0-620°C
$3Al + Ni = NiAl_3$ at 620°C
Some nickel outward diffusion must occur as FEA predicts that this can not be purely inward diffusion of Al to account for observed coating thickness

620-820°C
$NiAl_3 + Ni = Ni_2Al_3$ (Ni outward diffusion)
$2NiAl_3 - 3Al = Ni_2Al_3$ (Al inward diffusion)
$Ni_2Al_3 + Ni = 3NiAl$ (Ni outward diffusion)
$Ni_2Al_3 - Al = 2NiAl$ (Al inward diffusion)
Or a mixture of the above processes

Figure 7-3: Chemical Equations to Account for Phase Changes Observed

Figure 7-3 depicts possible diffusion mechanisms to account for the formation of NiAl from the first formed $NiAl_3$. It is suggested that some Ni outward formation must occur in addition to the inward Al diffusion (even if at the atomic layer for the formation of the desirable NiAl to occur. As it seems impossible for significant amounts of β-NiAl to form during the ICON process by purely solid state diffusion then other mechanisms must take place to enhance these diffusion processes and provide the necessary reaction driving force.

7.3 Exothermic Reactions: a Chemical Driver for Intermetallic Formation

The FEA data demonstrates that during the ICON heat treatment cycle, coating formation could not only be due to simple solid state diffusion processes. Work done previously by Cranfield[31] has shown that with very thin alternating layers (100-400nm) of Ni, Pt and Al a sufficient amount of chemical energy is released to transform this structure to a (NiPt)Al coating (Carlin manufactured α-NiPtAl coatings and noted that a large exothermic reaction occurring during the heat treatment[31]). To verify that such chemical energy release is possible when reacting electroplated aluminium with a nickel alloy, and therefore provide the energy needed to drive the ICON process, a small sample was prepared for differential scanning calorimetry (DSC).

Initially, samples of ILAl were deposited onto standard CMSX4 samples and then sectioned to fit into the 4mm diameter DSC crucible. As the sample thickness was 3mm and a 40micron thick coating had been applied to the surface the coating/substrate size ratio was not sufficient to get accurate results. Therefore thin sections of commercially pure Ni (Ni 200 alloy) were used as the substrate (100 micron thick). These substrates were then electroplated, sectioned to fit the crucible and tested with the results shown below.

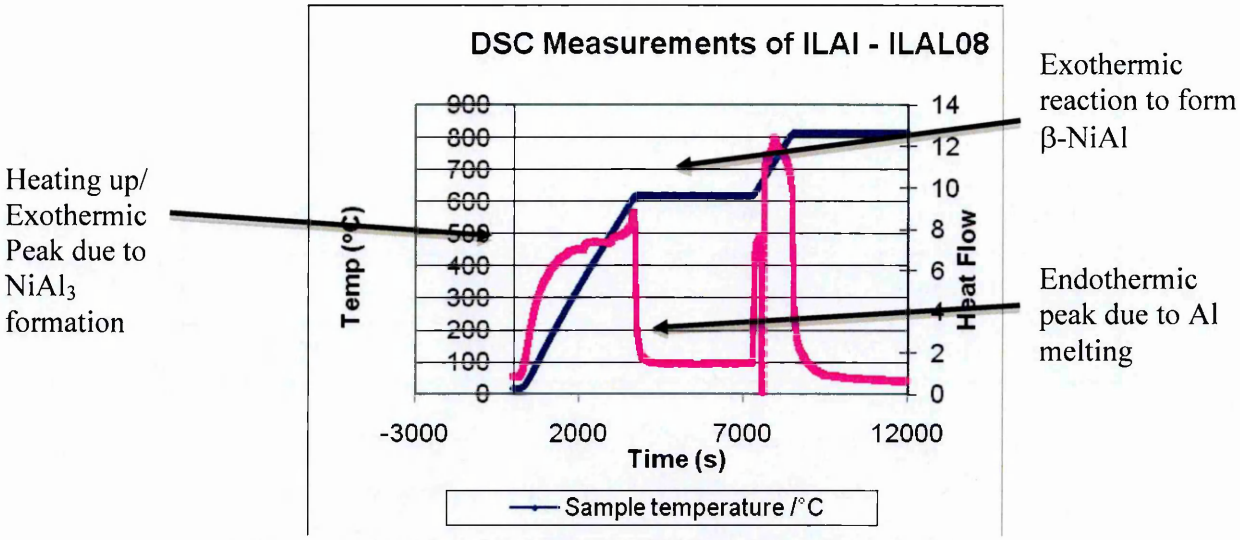

Figure 7-4: DSC Plot of ICON Heat Treatment on ILAI

Figure 7-4 (also in Table 7-2) clearly shows 2 distinct exothermic reaction points which start at approximately 150°C and 670°C respectively.

Using a heat ramp of 10°C per minute and no pauses then the following trace (figure 7-5) also shows two distinct exothermic peaks.

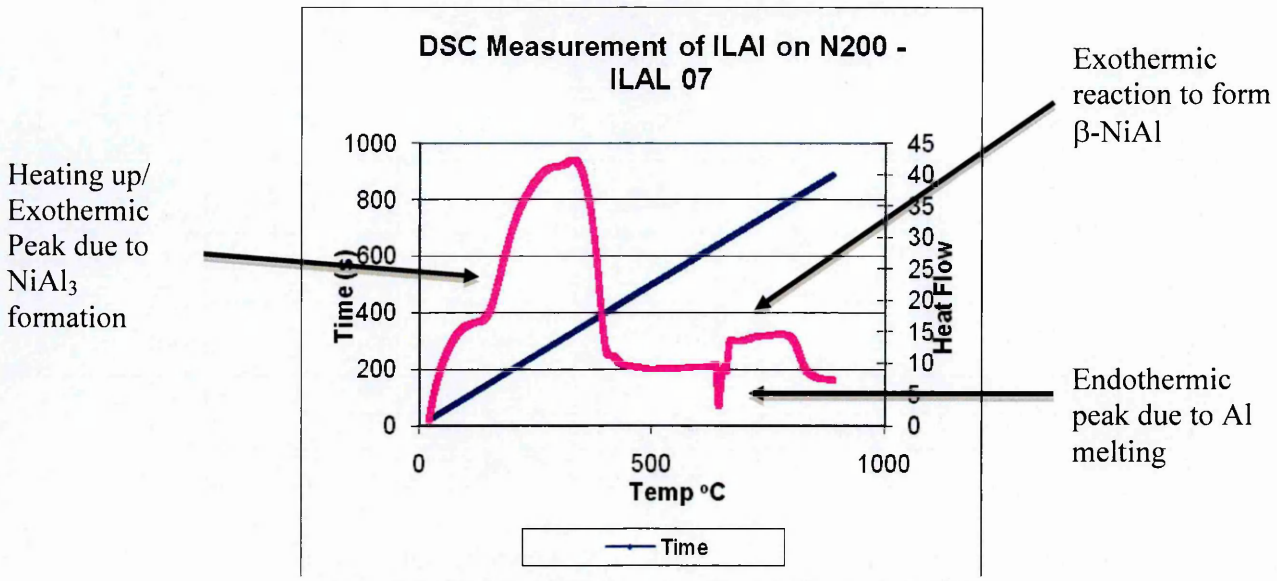

Figure 7-5: DSC Plot of ILAI with a Straight Ramp to 900°C

Table 7-2: Energies of Formation during both ICON and Steady Rate Heat Treatment.

Graph No and Peak	Onset/ Offset °C	Peak °C	Enthalpy (J/g)
ILAl-7a (Figure 7-5)	149.7/ 395.6	332.3	-324.44
ILAl-7b (Figure 7-5)	661.4/ 831.3	787.2	-324.44
ILAl-8a (Figure 7-6)	549.5/ 618.1	612.4	-37.33
ILAl-8b (Figure 7-7)	688.1/ 811.2	738.9	-25.73

Where (a) and (b) represent two exothermic peaks.

Both secondary peaks have similar temperature ranges, however initial peaks are different. It is uncertain why this is the case, but does suggest that some reactions may occur at very low temperatures. The huge difference in enthalpy values cannot be accounted for. However, as there seems to be little reaction during the heat soak, the two values should be theoretically identical, this may be accounted for by sample preparation (more pronounced delamination/cracking reducing the reaction area and therefore reducing exothermic value obtained).

Table 7-3: Onset, Offset and Peak Temperature Values for DSC Plots

Code	Temp.Onset 1 °C	Temp.Offset 1 °C	Temp. Peak 1 °C	Temp.Onset 2 °C	Temp. Offset 2 °C	Temp. Peak 2 °C
ILAl 08	574.5	617.5	612.6	709.7	742.3	722.2
ILAl 06	549.5	618.4	612.4	688.1	811.2	738.9
ILAl 09	401	618	614	655	815	752
ILAl 10	354.6	613.7	613.7	642.5	759.4	665.1
Mean	469.9	616.9	613.2	673.8	781.9	694.6
SD	92.0	1.9	0.7	26.5	31.7	36.7

For Table 7-3 plots ILAl 06, 09 and 10 are not shown but all show similar results to that illustrated in Figure 7-4. The temperatures referred to as '1' in Table 7-3 refer to the initial exothermic reaction (around and before 620°C) and the '2' refer to the 2nd exothermic reaction in the ICON heat treatment. It can be seen though that although the initial onset for the first reaction is quite varied the offset temperature and the peak temperature are both very similar. It is thought that this may be due to sample preparation and possible delamination of the aluminium creating a reduced

coating/substrate interaction zone. The second reaction zones for ILAl 08 and 06 are similar and ILAl 10 and 09 are also similar. However, for this later pairing the exothermic reaction starts before the melting temperature of free aluminium. Note: all graphs show, to various extents, endothermic reactions (not shown in the table) which may be explained by the presence of some free aluminium as the endothermic peaks are around 660°C and aluminium melts at 660.4°C. The lower onset temperatures for reactions (ILAl 09 and 10) may be explained by reviewing the NiAl phase diagram (Figure 1-2) where the eutectic point is, for the NiAl binary system, 639.4°C. Therefore some reactions between the Ni and the Al must have taken place (eutectic point occurs at approximately 5% weight Ni).

7.3.1 Conclusions for DSC

It appears from the figures and the tables within this chapter that the ICON process with steps at 620°C and 820°C are close to, the ideal temperatures at which to heat treat Al on Ni200 to complete the exothermic reactions. It would appear though that no further reactions occur after the 620 and 820°C set points so theoretically the ICON process could be a continuous ramp from 0-820°C and then a quench cool to form β-NiAl. Values of the exothermic reaction energies measured from the plots are less than that expected from the results given in the literature. Aluminium deposition from ionic liquids onto nickel-based superalloys have been demonstrated capable of being heat treated to form β-NiAl intermetallic coatings. This new deposition method is extremely versatile as it can produce intermetallic coatings, whether using heat treatments traditionally applied to CVD processes (both low and high temperature processes) as well as the new ICON process. Traditional routes, using heat treatment regimes akin to that used with the CVD aluminising technique give rise to with a distinct graded composition coating and a large interdiffusion zone.

7.3.2 Conclusions for the ICON Coating

The ICON process offers a promising new heat treatment regime, which operates at temperatures much lower than those used traditionally within the aerospace and industrial gas turbine industry. It has a number of benefits over the traditional heat treatment processes including:

- No over aging or modification of the original substrate which should lead to longer life times for the component.
- No evidence of a grit line. This shows the exothermic nature of the ICON process, with the energy released driving the boundary movement that occurs. This lack of grit line has numerous benefits including maximising coating/substrate interaction and improving bond strength.
- A homogenous composition throughout the coating, which provides improvement over traditionally produced coatings by maximising the available aluminium reservoir for any given coating thickness.

8 TEM Analysis of Second Phase Intermetallic Formation during the ICON Process

8.1 Introduction

As the spot size (the size of the tear drop shape resulting from the electrons penetrating the sample during elemental analysis) used within any SEM is relatively large (approx 3um), and is the case for the SEM at Cranfield it was decided that TEM analysis would improve the resolution and understanding of the overall coating process. Magnifying the planar surface second phase 'line' region and analysing the chemistry using a SFEG SEM shows that there is very little difference between the compositions of the two regions. However, this is probably due to the resolution introduced by spot size of the microscope exceeding the size of the region being studied, thus making it difficult to resolve any differences.

8.1.1 Preparation

TEM sections were prepared using a FIB to mill through the coatings and produce sample which were approximately 1 micron thick (Figure 8-1). The sections were then welded to an omniprobe (Figure 8-2) with Pt and transferred to a copper grid (Figure 8-3) where thinning of the sample continued until a thickness of less than 100nm (Figure 8-4) was achieved (work done at in collaboration with Chalmers Technical University, Gothenburg, Sweden).

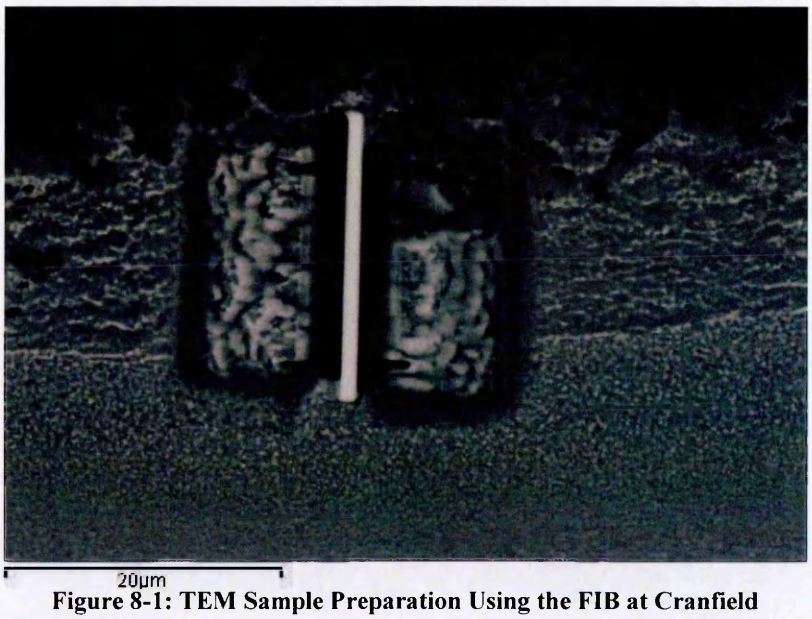

Figure 8-1: TEM Sample Preparation Using the FIB at Cranfield

Figure 8-2: Omiprobe attached to TEM sample

Figure 8-3: TEM Sample after Welding to Sample Holder

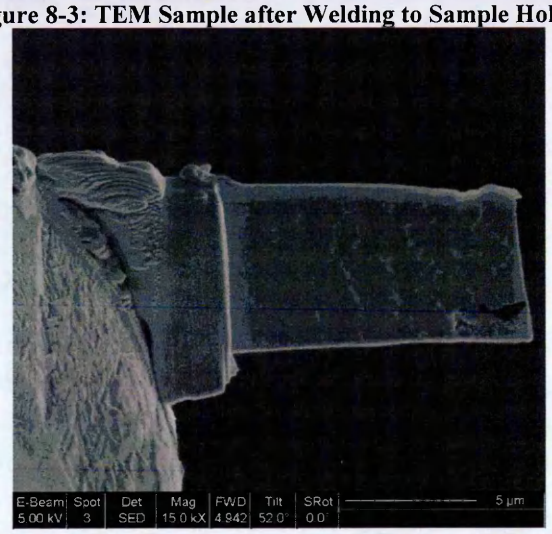

Figure 8-4: TEM Sample after Thinning Attached to Holder and Removal of Omniprobe

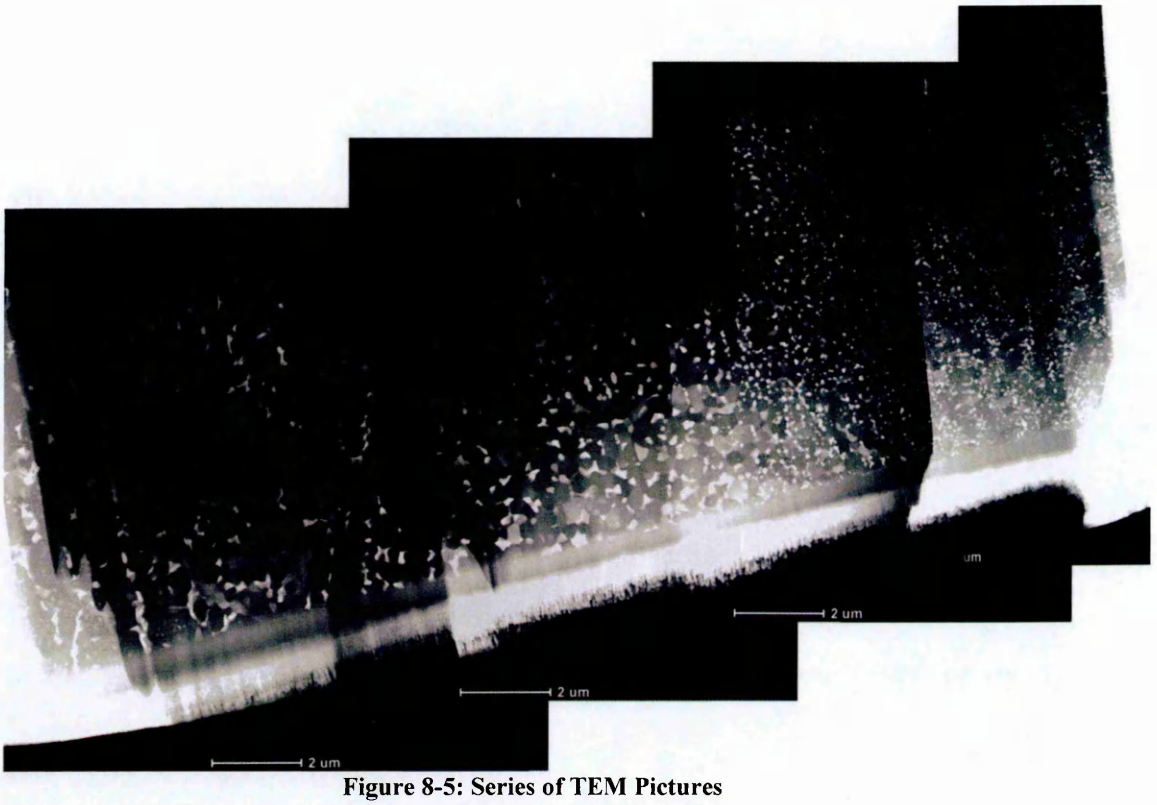

Figure 8-5: Series of TEM Pictures

8.1.2 TEM Images of ICON on CMSX4 (above the line within the 'Secondary phase')

Figure 8-5 shows that after thinning the secondary phases are clearly observed. The micrographs below, (Figure 8-6 and Figure 8-7), show the grain structure formed as a result of the ICON heat treatment for a TEM sample taken above the second phase plane of near continuous precipitates for ICON-based coatings formed on CMSX4 at increasing magnifications. They show that the grains vary in size (from 250nm-2.8μm) and composition, with distinct precipitates present on the grain boundaries. It is thought that the areas of contrast, present within the grains, may actually be contamination introduced as part of the TEM sample preparation.

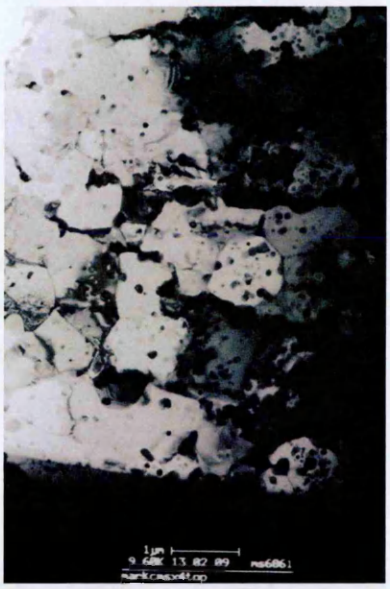

Figure 8-6: TEM Samples of ILAl after ICON Heat Treatment on CMSX4 (above line of Second Phase Particles)

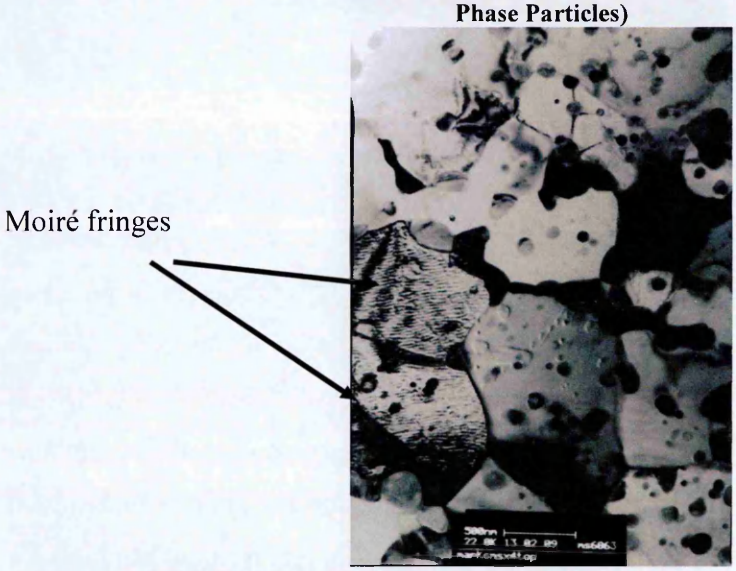

Figure 8-7: TEM Samples of ILAl after ICON Heat Treatment on CMSX4 (above line of Second Phase Particles)

The matrix contains at least 54at.% aluminium with an absence of Ta. The precipitates are rich in Al and Ta but are depleted in Ni (as low as 10at% Ni). Thus, the ICON heat treatment coating is more complex than first envisaged. It has a microstructure that contains β-NiAl grains some 500nm in diameter, that are surrounded by a network of TaAl(Ni) intermetallic precipitates.

Figure 8-8: Magnification of ICON on CMSX4 Sample with Moiré Fringes

Figure 8-8 shows the presence of Moiré fringes where two different grains are overlapping in the Z direction of the photograph but have slightly different orientations.

The observation of Ta in the precipitates at the NiAl boundaries was unexpected. Ta would be expected to show some solubility in NiAl. It can only be therefore assumed that β-NiAl coating containing Ta is less energetically favourable than β-NiAl without at the temperature of processing using the ICON heat treatment and within this reaction system studied. The reasoning for this partitioning into a primary β-NiAl phase and a second phase TaAl(Ni) intermetallic needs to be investigated further.

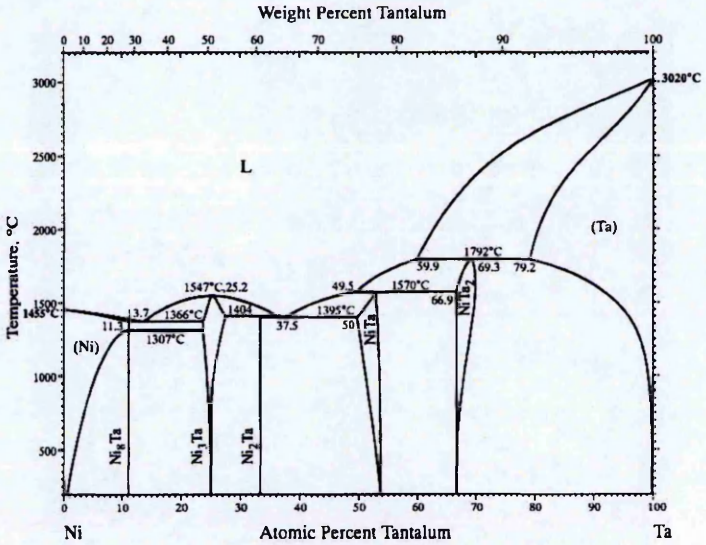

Figure 8-9: Ni/Ta Phase Diagram[177]

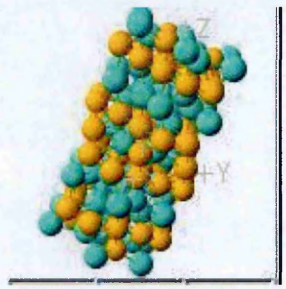

Figure 8-10: Structure of NiTa (Pearson hR13)[172]

Looking at the NiTa phase diagram (Figure 8-9) it can be seen that Ni_xTa_y intermetallics are less likely to form as the majority are line intermetallics at the process temperature used in the ICON heat treatments and therefore must reach a specific stoichiometry before being formed. Out of all the intermetallics possible the NiTa (Figure 8-10) is most likely due to its wider composition range. Similarly, the Ta-Al phase diagram (figure 8-11) shows that most compositions are all line compounds except for Ta_2Al which exists over a wider composition range. All things being equal it is likely that Ta_2Al would form because of ease in achieving the required composition, but this would be further assisted if the formation of AlTa intermetallics were more energetically favourable (Ta_2Al is expected to be more energetically favourable than NiAl due to the higher melting point; Figure 8-11).

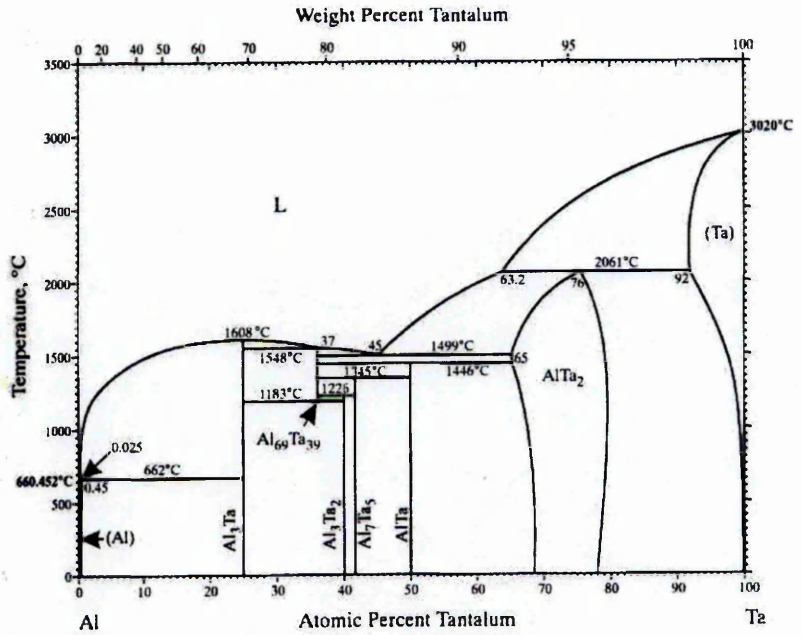

Figure 8-11: Al-Ta Phase Diagram[177]

As it can be seen from the Al-Ta phase diagram as shown in Figure 8-11 most of the Al_xTa_y phases occur at specific compositions existing only as line intermetallics, therefore any deviation in stoichiometry means that these intermetallics will not form. However, assuming that the BCC β-NiAl must form then (AlTa)Ni can well be formed also. The most likely Al:Ti ratio on the Al sublattice would be 1Al:2Ta due to the wide solubility range of Ta_2Al. Alternatively, the first Ta containing intermetallic in equilibrium with the liquid is $TaAl_3$ and this can be easily incorporated into the B2 structure Al sublattice as shown in Figure 8-12.

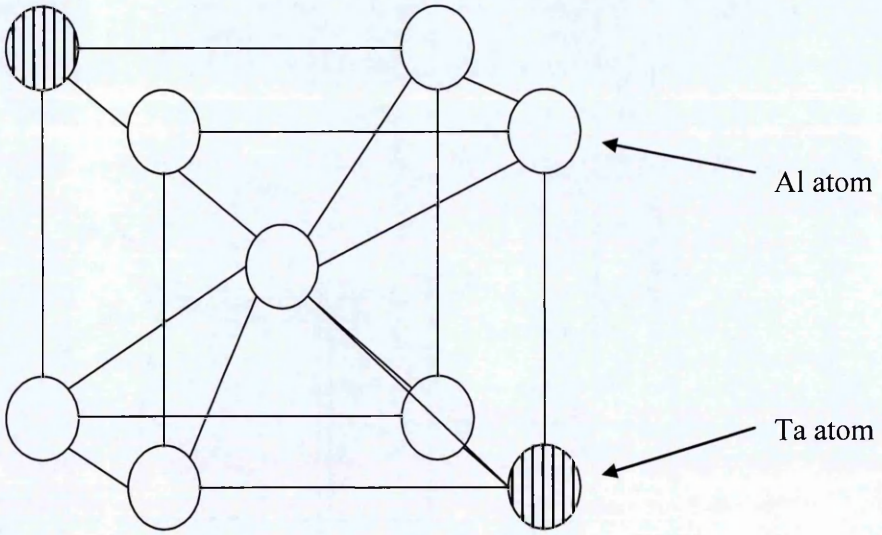

Figure 8-12: Proposed BCC Structure of (AlTa)Ni (Ni central atom)

8.1.3 TEM Images of ICON on GTD111

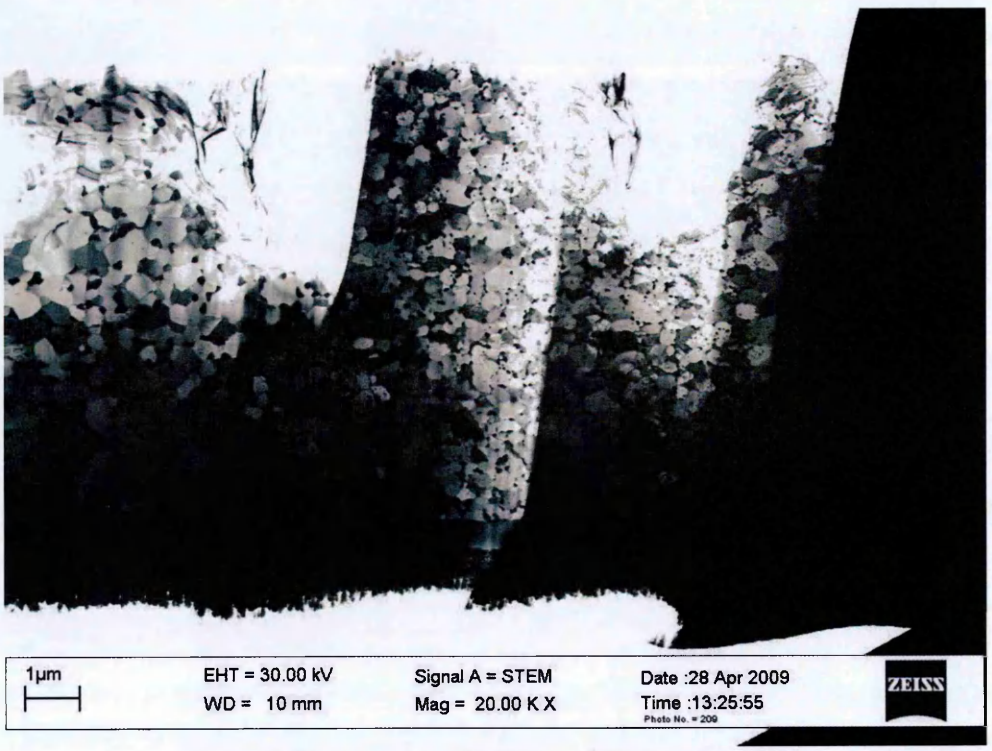

Figure 8-13: Over view of ICON on GTD111 using TEM

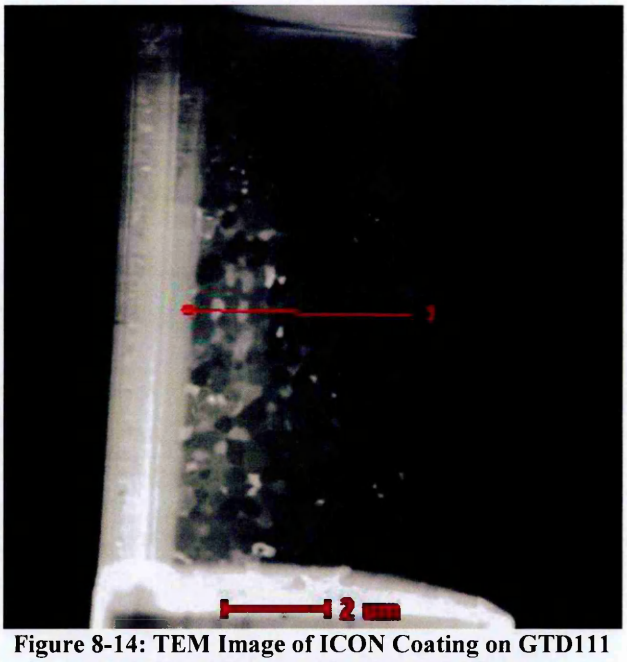

Figure 8-14: TEM Image of ICON Coating on GTD111

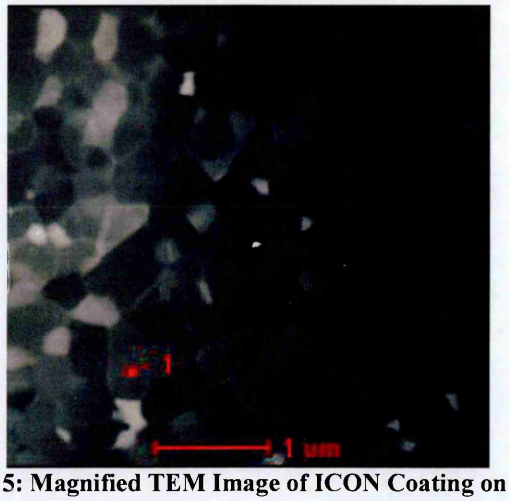

Figure 8-15: Magnified TEM Image of ICON Coating on GTD111

TEM images of the ICON coating are shown in figures 8-13 to 8-15. The TEM of the ICON coating confirms that the coating consist of the β-NiAl phase. However, it is interesting to note that the ICON coating on GTD111 (Figure 8-15) is much cleaner than that of the coating on CMSX4 and the grain size is much smaller (Figure 8-7). It was thought that the reason for the dark circular images on (Figure 8-7) was due to contamination. However, it could be due to multiple nucleation sites, even nucleation within a grain.

8.1.4 Atom Probe Microscopy of ICON on GTD111

By removing a small sample using a FIB it is possible to analyse the sample composition and structure using atomic probe microscopy. This work was done in conjunction with Chalmers University in Sweden.

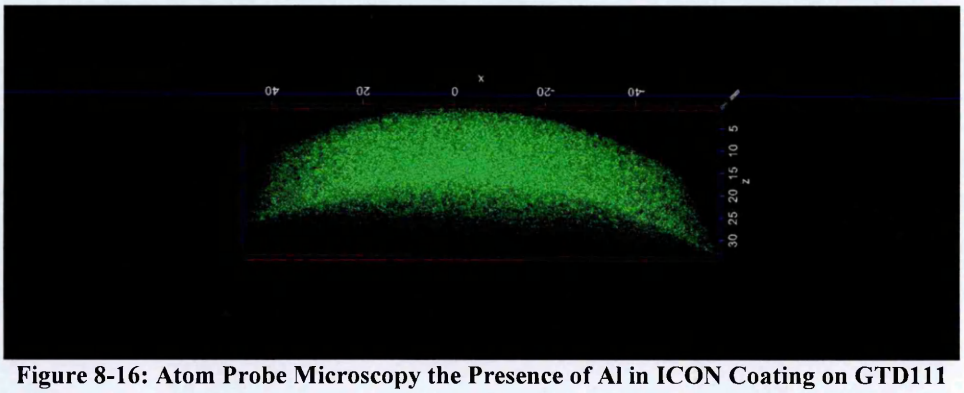

Figure 8-16: Atom Probe Microscopy the Presence of Al in ICON Coating on GTD111

As it can be seen from the figures above and below that both aluminium (Figure 8-16) and nickel (Figure 8-17) are widespread and homogenous throughout the coating. Combining the images of Al and Ni it is possible to show that even at the atomic level, there is no free Ni or Al present within the coating (Figure 8-18).

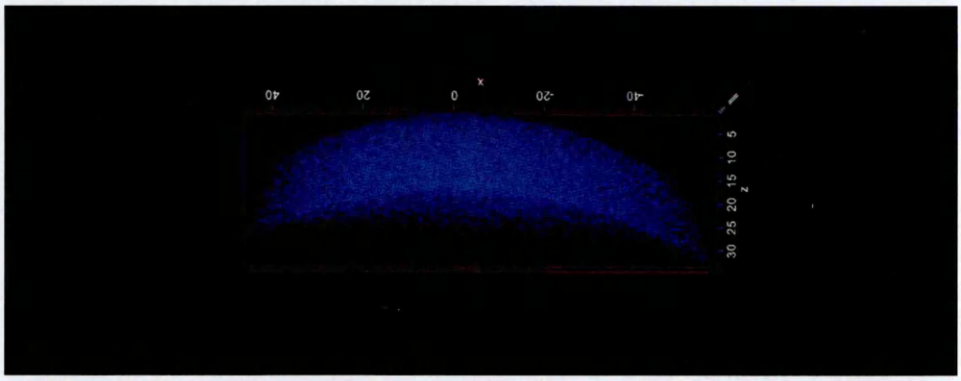

Figure 8-17: Atom Probe Microscopy of Ni within an ICON Coating on GTD111

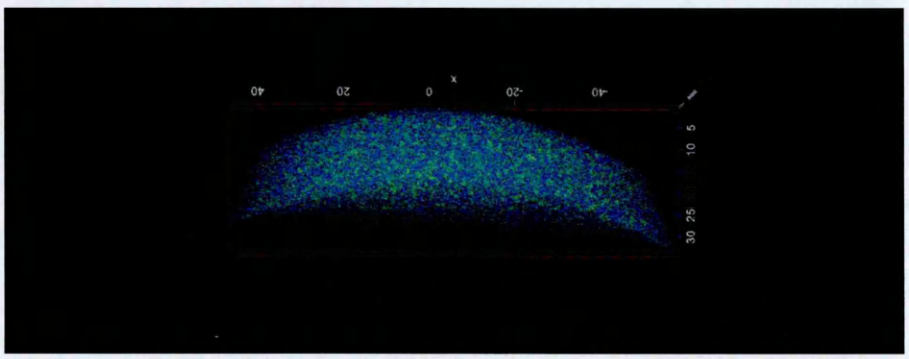

Figure 8-18: Atom Probe Microscopy the Presence of Al (Green) Ni (Blue) in ICON Coating on GTD111

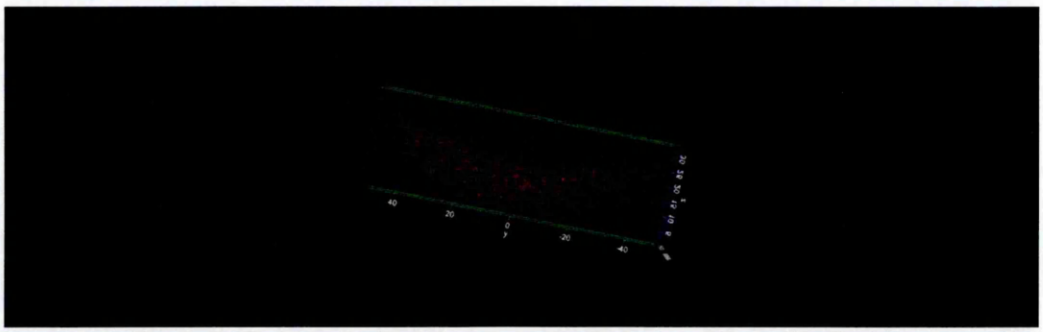

Figure 8-19: Atom Probe Microscopy the Presence of Cu in the Coating

Figure 8-19 shows the presence of a small amount of Cu within the coating: which was unexpected. It is not possible for the Cu to be deposited from the plating process and XRD data showed that no copper was present within the solution or the cathode holders. Furthermore, data produced by Kamavaram[181] showed that an aluminium-coating would have a high purity level regardless of the purity of the cathode. It does not seem possible for the Cu to be an artefact induced by FIB machining. This would therefore suggest that the Cu was a contaminant within the GTD111, but as this is a high temperature alloy and Cu has not been previously found elsewhere within this sample this seems improbable.

9 The ICON Process: A Chemical Energy Enhanced Diffusion Process?

9.1 Introduction

The data within this project has shown that the ICON coatings cannot be formed by pure solid-state diffusion processes themselves. Therefore, other mechanisms must be contributing. The chemical energy released by the various intermetallic reactions, such as those measured with the DSC, can explain the ICON process. The DSC work has shown that there is considerable exothermic energy released within this present system during coating formation; therefore, by reviewing the enthalpy of formation of components which could possible effect the process may give an insight into the process itself.

9.1.1 Enthalpies of Formation

It is clear from the TEM work that many compounds/phases are being formed during the ICON process, for this reason it is worth reviewing the enthalpies of formation of the possible intermetallics formed. Table 9-1 illustrates the enthalpies of formation for various aluminide formations between Ti, V, Cr, Mn, Co, Ni and Cu. It is interesting to note that all these aluminide formations are energetically favourable. However, the nickel aluminides (especially forming the β phase) are extremely exothermic during formation. It should be noted however, that this is purely for binary reactions; some authors have noted the enthalpies of ternary reactions. Huang and Chang[182] measured the thermodynamic properties of NiAlCr and noted that the enthalpies of formation were 36.7, 35.2 and 34.9 for $Ni_{0.72}Al_{0.23}Cr_{0.05}$, $Ni_{0.70}Al_{0.22}Cr_{0.08}$, $Ni_{0.67}Al_{0.21}Cr_{0.12}$ respectively compared to 40.5 kJ/g.atom for Ni_3Al[183]. It should be assumed that to some extent binary, ternary, quaternary etc. reactions will occur during this process.

Table 9-1: Enthalpy of Formation of Selected Aluminides from Literature (kJ/g-atom)

Ti	V	Cr	Mn	Co	Ni	Cu
$Ti_{0.75}Al_{0.25}$ -25.31[184]	$V_{0.6}Al_{0.4}$ -15.04[184]	$Cr_{0.65}Al_{0.35}$ -9.7208[184]	MnAl -43[185]	CoAl -43[185]	$Ni_{0.044}Al_{0.56}$ -58.1[186]	$Cu_{0.777}Al_{0.333}$ -23.4[184]
$Ti_{0.65}Al_{0.35}$ -30.05[184]	$V_{0.5}Al_{0.5}$ -16.80[184]	$Cr_{0.637}Al_{0.363}$ -11.4806[184]	$Mn_{0.50}Al_{0.50}$ -22.04[184]		$Ni_{0.48}Al_{0.52}$ -61.0[186]	$Cu_{0.5}Al_{0.5}$ -18.18[184]
$Ti_{0.55}Al_{0.45}$ -34.99[184]	$V_{0.45}Al_{0.55}$ -20.57[184]	$Cr_{0.57}Al_{0.43}$ -13.5337[184]	$Mn_{0.277}Al_{0.733}$ -21.24[184]		$Ni_{0.495}Al_{0.505}$ -60.7[186]	
$Ti_{0.5}Al_{0.5}$ -36.54[184]	$V_{0.4}Al_{0.6}$ -19.73[184]	$Cr_{0.36}Al_{0.64}$ -15.503[184]	$Mn_{0.20}Al_{0.80}$ -21.7[184]		$Ni_{0.505}Al_{0.495}$ -61.0[186]	
$Ti_{0.45}Al_{0.55}$ -37.50[184]	$V_{0.59}Al_{0.61}$ -20.2[184]	$Cr_{0.3}Al_{0.7}$ -16.0058[184]	$Mn_{0.152}Al_{0.858}$ -12.4[184]		$Ni_{0.55}Al_{0.45}$ -58.4[186]	
$Ti_{0.4}Al_{0.6}$ -38.84[184]	$V_{0.35}Al_{0.65}$ -25.27[184]	$Cr_{0.225}Al_{0.775}$ -16.8019[184]			$Ni_{0.56}Al_{0.44}$ -56.3[186]	
	$V_{0.3}Al_{0.7}$ -25.22[184]	$Cr_{0.115}Al_{0.885}$ -12.5281[184]			$Ni_{0.57}Al_{0.43}$ -53.7[186]	
	$V_{0.25}Al_{0.75}$ -26.86[184]				$Ni_{0.51}Al_{0.39}$ -51.3[186]	
					$NiAl$ =-48[185]	
					$NiAl_3$ = -35[185]	
					$NiAl_3$ = -38[183]	
					$NiAl$ = -60[183]	
					Ni_5Al_3 = -56[183]	
					Ni_3Al = -40.5[183]	

Table 9-2 shows the enthalpies of formation of numerous aluminide intermetallics. However, from the substrates used, only Mo and Nb could be formed based on known alloy additions in the superalloys studied. However, Nb is featured only in IN738 in very low concentrations (approx. 0.75 and 1.8 for IN738 and IN738LC respectively) and may be assumed to have limited affect within the ICON process). The values for the precious metal aluminides Pt, Ru, Rh and Pd aluminides are extremely exothermic (Table 9-2 and Table 9-3). It should be noted that only the exothermic and not endothermic reactions would be stable.

Table 9-2: Enthalpies of Formation of Selected Aluminides from Literature (kJ/g-atom)

Zr	Nb	Mo	Tc	Ru	Rh	Pd
$ZrAl_2$ -20.6[153]	$NbAl_3$ -18.0[153]	Mo_3Al_8 -2.3[153]		RuAl -124.1[154]	RhAl -212.6[154]	PdAl -92 [187]
$ZrAl_3$ -18.0[153]	Nb_3Al 16.0[153]	Mo_3Al 8.1[153]				Pd_2Al -52[153]
$ZrAl_3$ -60[185]						

Table 9-3 shows the enthalpy of reactions of some 5d aluminides (Os and Re are not incorporated within the alloys used within this study). The literature shows that Hf, Ta, Re and Pt are all exothermic and WAl_4 is endothermic (WC would be more likely to be formed as Coltters[188] measured the enthalpy of formation to be -38KJ). It is interesting to note that both Re and Hf (which are only found in CMSX4 compared to the other nickel based alloys used) form aluminides which are exothermic in nature.

Table 9-3: Enthalpies of Selected 5d Aluminides from Literature (kJ/g-atom)

Hf	Ta	W	Re	Os	Ir	Pt
$HfAl_2$ -43.8[152]	$TaAl_3$ -29.9[152]	WAl_4 15.2[152]	Re_2Al -29.6[152]	$OsAl_2$ -44.9[151]	IrAl -185.5[154]	Pt_3Al = -70[189]
$HfAl_3$ -40.6[152]	Ta_2Al -19.9[152]		Re_4Al_{11} -34.5[152]	OsAl -77[154]		Pt_2Al = -80[189]
HfAl -39.9[152]						Pt_5Al_3= -88[189]
						PtAl = -100[189]
						Pt_2Al_3 = -95[189]
						$PtAl_2$ = -84[189]
						Pt_8Al_{21}= -71[189]
						Pt_5Al_{21}= -57[189]
						Pt_3Al = -63.6[152]
						Pt_2Al_3 = -96.5[152]

The above data combined with the SEM analysis shows that ReAl (Table 5-7) has a similar enthalpy of formation as both $NiAl_3$ and Ni_3Al, suggesting that they would both form at the same time thus possibly hindering the transformation from $NiAl_3$ to β-NiAl. Additionally, the formations of Pt aluminides are more energetically favourable reactions than the formation of β-NiAl.

9.2 Carbide Reactions during ICON

One of the unforeseeable facets of this process is the reactions of carbides. As it can be seen below (Figure 9-1 to Figure 9-3) the carbides appear to partially dissociate during the ICON process leaving voids or gas filled bubbles. This, so far, has only been evident on samples of GTD111 where large carbide phases are present. As these carbides also act as Kirkendall markers, they are expected to be very stable and require large amounts of energy to either move them or force the precipitates back into solution.

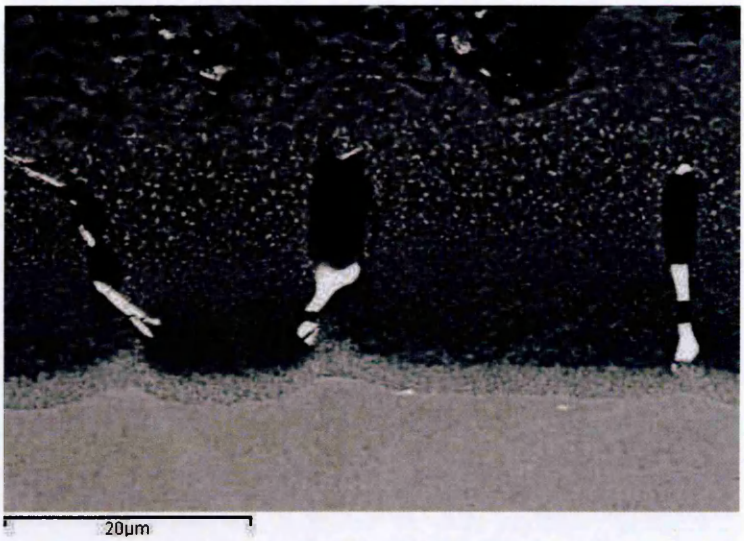

Figure 9-1: Carbides in β-NiAl Coating on GTD111 (BSE Image)

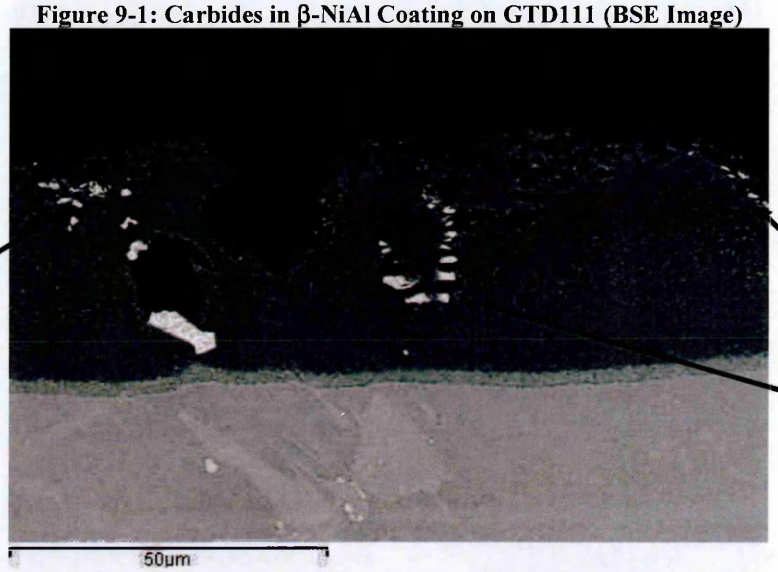

Figure 9-2: Carbides in β-NiAl Coating on GTD111 (BSE Image) (2)

Interestingly, in the above micrographs (Figure 9-1-and Figure 9-2) a number of interesting phenomena are observed:

1. Carbides can be seen again at the outermost section of the coating suggesting that net inward movement of Al occurs during the ICON process.

2. There are two different mechanisms which are acting on the carbide phases; on the left carbide phase (Figure 9-2) the majority of it is now present only as a void whereas the central carbide is interspersed with voids (gas formation) creating a 'zebra' stripe appearance.

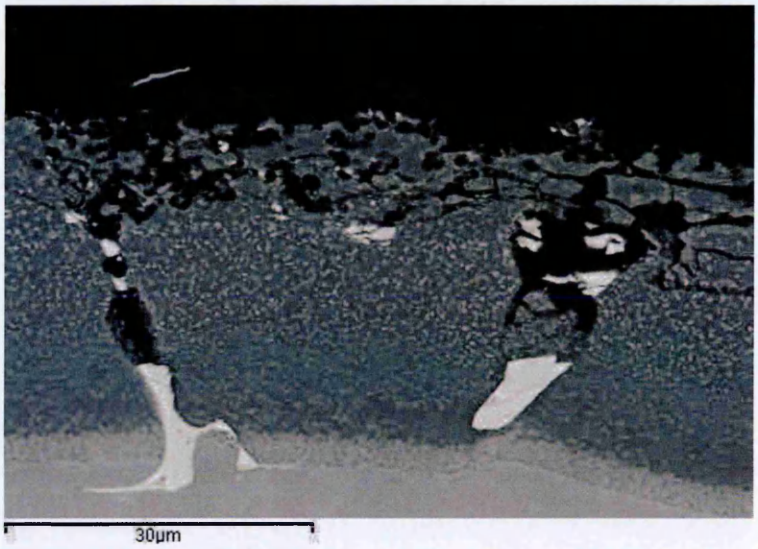

Figure 9-3: Carbides in β-NiAl Coating on GTD111 under BSD (3)

Magnifying the carbide region on the left of the micrograph shown in Figure 9-3 leads to Figure 9-4:

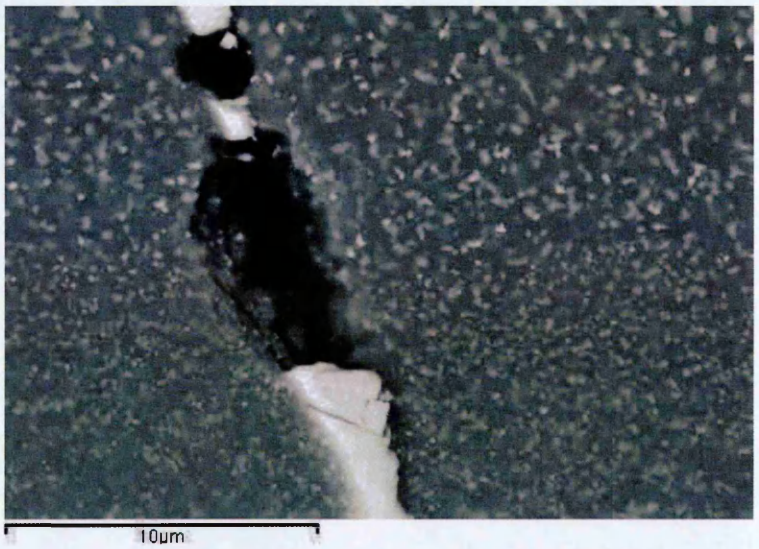

Figure 9-4: Magnified Region of Carbide after ICON Process

Highlighting the regions in Figure 9-4 it was possible to analyse the chemical composition by EDX which leads to Figure 9-5 and Figure 9-6 as well as the results shown in Table 9-4.

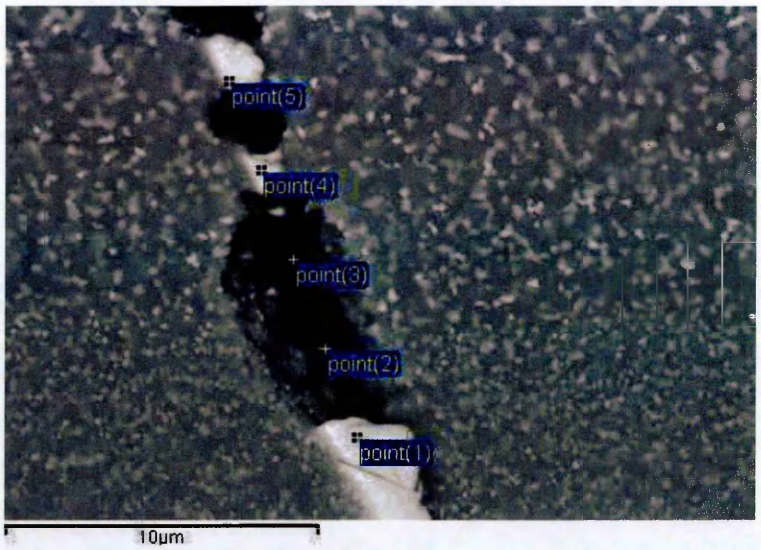

Figure 9-5: Photomicrograph of Carbide Precipitate after ICON Process showing Point of Analysis

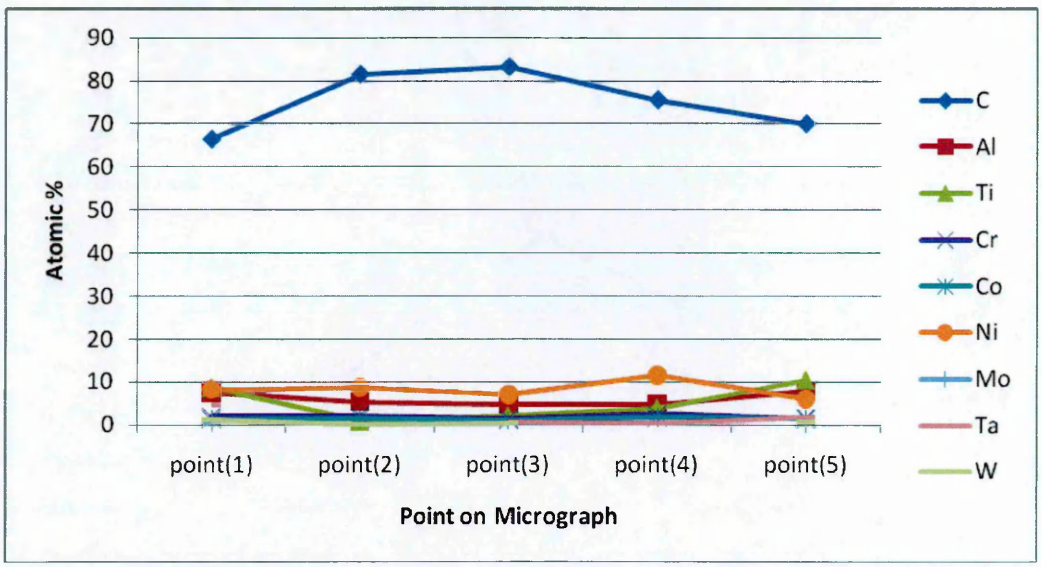

Figure 9-6: Composition Profile of Carbide Precipitate after ICON Process

Table 9-4: Atomic % of Points Highlighted in Figure 9-5

Spectrum	C	Al	Ti	Cr	Co	Ni	Mo	Ta	W
point(1)	66.4	7.4	8.6	2.0	1.3	8.2	0.5	4.5	1.1
point(2)	81.5	5.3	0.9	2.2	1.4	8.7			0.1
point(3)	83.2	4.6	2.0	1.5	1.0	6.9		0.6	0.2
point(4)	75.6	4.6	3.9	2.5	1.8	11.5		0.3	
point(5)	70.1	7.7	10.5	1.6	1.4	6.0	0.3	1.9	0.7

The table above (Table 9-4) shows that the carbide precipitates are complex but predominantly comprise a combination of Ti and Ta carbides. Interestingly, the carbon concentration increases within the void, either suggesting that a carbide particle is beneath or that the surrounding area is carbon rich (tear-drop size (i.e.

volume generating x-rays) is approximately 2um). It should also be noted that point 2 (on the edge of the coating) is much higher in Ni and devoid of any W. Analysing the pore (figure 9-7) gives elemental composition as shown in figure 9-8 and table 9-5.

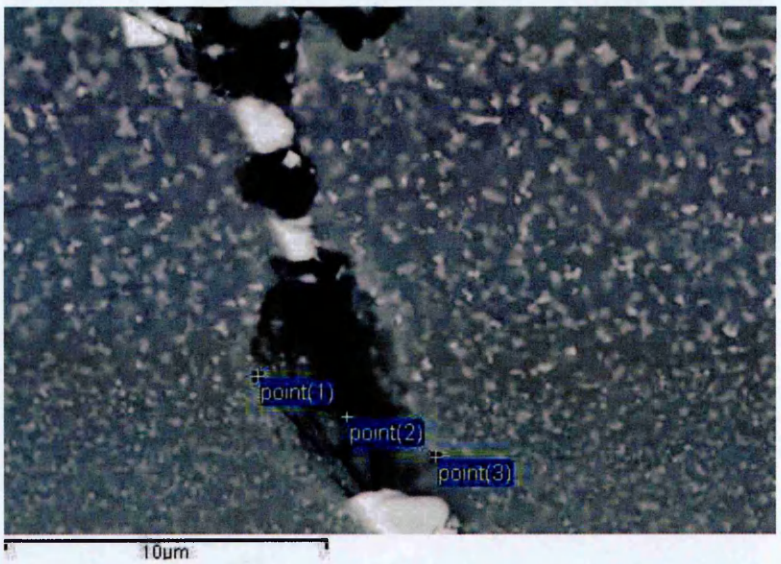

Figure 9-7: Magnified Carbide Precipitate Region with Different Points for Analysis

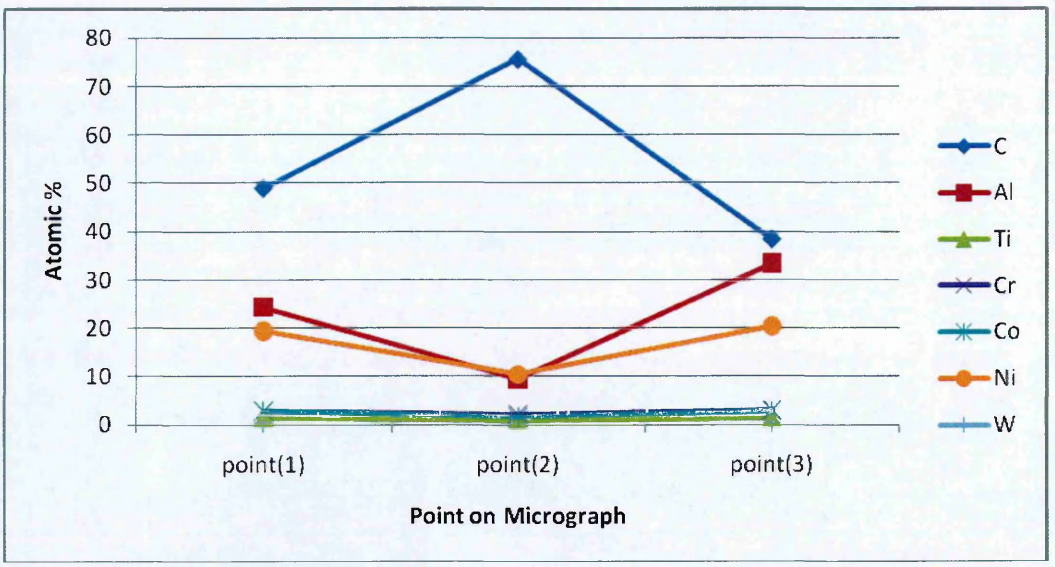

Figure 9-8: Chemical Composition of Points highlighted within Figure 9-7

Table 9-5: Chemical Composition of Points Highlighted in Figure 9-7 (atomic %)

Spectrum	C	Al	Ti	Cr	Co	Ni	W
point(1)	48.9	24.3	1.4	2.8	2.9	19.4	0.4
point(2)	75.6	9.4	0.9	2.2	1.6	10.4	
point(3)	38.3	33.4	1.4	3.1	2.9	20.4	0.3

Table 9-5 shows that within the coating surrounding the void (point 2) there is also an increase in carbon. However, it should be noted that the carbide values are only indicative as carbon is ubiquitous and appears in almost all SEM scans.

The enthalpy of formation of TiC and TaC is -92.9[190] and -38.5[191] kJ/mol respectively, therefore these energies must be reached before any reduction reaction takes place. As the enthalpies of formation of nickel aluminides show (Table 9-1) the value for the formation of TiC is much higher than that for NiAl (approx 60kJ/mol)[58], although it is higher than TaC. However, the value for the formation of $NiAl_3$ (-38kJ/mol[58]) is similar to that of TiC. It is worth noting that if the ICON process is stopped mid way (620°C 1 hour) then the following structure can be viewed (figure 9-9).

Figure 9-9: Micrograph with Carbides Present after 1 hour at 620°C

It is obvious that neither the carbide has melted as the melting point of TaC (3880°C)[192] nor the melting point of TiC can have been met (3170°C)[193] during processing, therefore it must be assumed that local thermodynamics of dissociation/destruction of at least TiC have been met. It is proposed that during the initial ICON phase the TiC rich segments of the complex carbide precipitates are dissolved with some of the carbon entering into solution with the remaining forming CO_2 or CO (both are energetically favourable but under 1000°K the formation of C + O_2 is more likely and this will undergo a reaction even within the confines of a vacuum furnace ($1.98x10^{-68}$atm)). It may be postulated that at a minimum, the free

energy for the formation of β-NiAl is met within the secondary stage of the ICON process; it is therefore possible that sufficient energy could be released to reduce TaC. However, as some carbide precipitates are still present after the ICON process it must be assumed that even if this amount of energy is present, it is only locally on the atomic scale, and only at the surface of the TaC precipitates present.

A possible reaction could be

$$2TaC \Leftrightarrow 2Ta + 2C \Leftrightarrow Ta_2Al + x$$
$$\Delta G = 2(+38) \Leftrightarrow 3(-19.9) \equiv +16.3$$

Therefore the reactant (x) could be anything giving an exothermic reaction of at least 16.3kJ (Ni_xAl_y, CO_2 or $^2/_3Al_4C_3$) for the reaction to occur.

9.2.1 Trapped Grit

This is a positive outcome of the ICON process. Previously, it was said that no entrapped grit is visible at the coating/substrate interface. This would require the local melting of the remaining aluminium coating to permit the grit to effectively 'float' to the free surface. Aluminium inward diffusion would greatly aid this apparent outward motion of any trapped grit.

9.3 Combustion Synthesis/self propagating high temperature synthesis

The cascade reaction mechanism proposed above has been previously described as Combustion Synthesis (CS) or Self Propagating High Temperature Synthesis, which may be defined as:

'The term combustion synthesis (CS) is used to describe exothermic chemical reactions in which the heat generated is utilized to ignite non-reacted portions of the reactants. Starting materials may be pure elements or compounds. Self-propagating high-temperature synthesis (SHS), self-propagating synthesis (SPS) and reaction synthesis (RS) are also terms used to describe the process. Generally, in the CS process, a mixture of reactant powders pressed into a pellet is heated to a critical ignition temperature, Tig, at which exothermic reaction takes place, transforming reactants into products[183].

The CS process was first reported[194] and patented in the USSR in 1971[195] and according to the table below (Table 9-6) it is possible to see that the velocity of the reaction front is very quick, and the combustion temperature itself is also very high. However, Gennari et al.[196] reported that propagation velocities of between 0.3 and 1.4 m/s are possible for NiAl. However, the reported NiAl has a coarse microstructure as shown in Figure 9-10.

Figure 9-10: Coarse Microstructure of NiAl as shown by Gennari et al. [196] (no scale given in original paper)

Table 9-6: Typical Parameters for Combustion Synthesis [197]

Burning velocity	0.1–20 cm/s
Combustion temperature	2300–3800 K
Heating rate	10^3–10^6 K/s
Igniting fluence	10–200 cal/(cm^2 s)
Induction time for ignition	0.2–1.2 s
Ignition temperature	800–1200 K

NiAl has also been produced previously using CS by Yeh et al.[198] where the activation energy needed to synthesis NiAl was calculated to be 128.64kJ/mol. However, although the flame front initiated the reaction, the complete reaction was found to occur after the initial flame front (figure 9-11). It can be seen from the figure below (Figure 9-12) that the presence of TiC promotes reaction speed within NiAl

reactions. This may have implications with the presence of TiC and TaC found in GTD111.

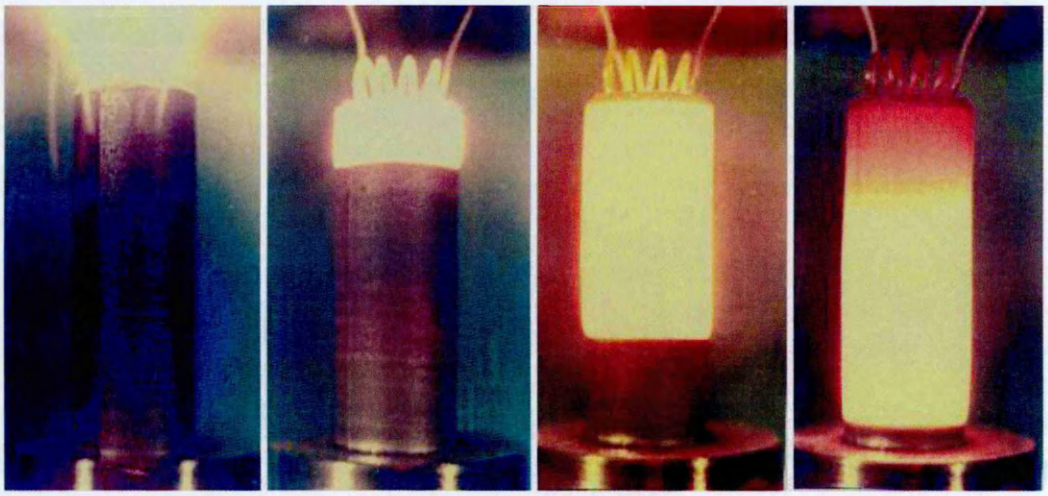

Figure 9-11: Time-lapse Photography of Combustion Synthesis in Action (Ti + B to TiB)[197]

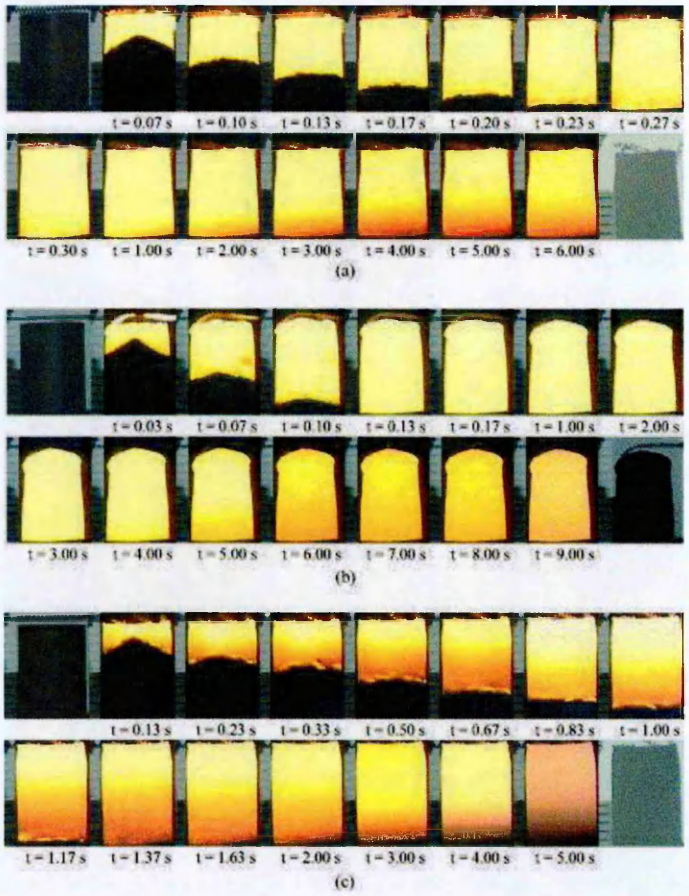

Figure 9-12: Recorded combustion images of SHS processes associated with unpreheated 60% TMD samples composed of (a) 325 mesh Ni and 350 mesh Al, (b) 3–7 μm Ni and 10 μm Al, and (c) 325 mesh Ni, 350 mesh Al, and 18.2 mol.% TiC. [198]

9.3.1 Combustion Synthesis of NiAl

Numerous reviews of CS have been done especially by Feng *et al.* on reaction parameters for CS[199] and classification /modelling[200]. An overall review was conducted by Subrahmanyam and Vijayakumar[201] and a more specific review on nickel aluminides CS was written by Morsi[202]. Morsi has stated that furnace temperatures normally ranged between 550-750°C for 10-15 minutes to produce NiAl, but at temperatures below this reactions are possible. However, a more porous microstructure results. It should be noted that the majority of work done has been conducted with addition of pressure, whereas the ICON process is done without additional isostatic pressure. Furthermore, the majority of CS has been conducted with the use of small pellets of elemental powders or actual melts. The work of Carlin[31] with the use of multiple, very thin layers is closest to combustion synthesis, but Carlin did not propose this as a mechanism for formation, but stated that a 'violent exothermic reaction below the melting point of aluminium' took place. The thin layers of the Carlin coating probably involves CS but on multiple fronts unlike the figures above (Figure 9-12). Furthermore, the measured reaction was -38.2kJ/mol which is below that expected for the formation of β-NiAl. However, Nicholls et al.[30] and Silva[58] were able to produce $PtAl_2$ and NiAl coatings by sputtering and in-situ reaction synthesis. Silva's work used, like Carlin, layers of alternate Ni and Al with an optimum thickness ratio of 1.51:51 (Al:Ni) the author noted that a 9 layer system (9μm thick)was better than 3 or 5 layers but the coating system was very stressed and sometimes suffered from delamination (heat treated at 700°C for 2 hours).

Therefore it is concluded that the ICON process is a form of combustion synthesis, but over much longer time frames and the first that combines a reaction between both a substrate and coating to form a nickel aluminide intermetallic. It is also proposed that this is the first study of combustion synthesis, which involves aluminium deposited from ionic liquids.

9.3.2 Combustion Synthesis within ICON

Some of the literature researching the formation of nickel aluminides have used liquid aluminium; it is proposed that with ICON there is no difference, but that the energy released should be sufficient to melt any remaining aluminium. In the following section a 'cascade reaction' is proposed where an initial reaction leads to others: in

essence controlled CS. The whole mechanism of action of the ICON process including the importance of controlled CS will be discussed further in the following chapter.

10 Diffusion Mechanisms of ICON

10.1 Diffusion within a Liquid Phase

As discussed previously (Figure 4-20) in the presence of water contaminated at high parts per million levels, aluminium deposited from IL forms columnar (Figure 10-1 and to a greater extent Figure 10-3) rather than dense deposits. However, both types of deposits form dense β-NiAl coatings (Figure 10-2, 10-4 and 10-5) when deposited onto suitable substrates. For this to occur there must be some form of liquid phase induced diffusion occurring before the melting point of Al (660°C) as it is known that no free aluminium exists after the initial heat treatment stage.

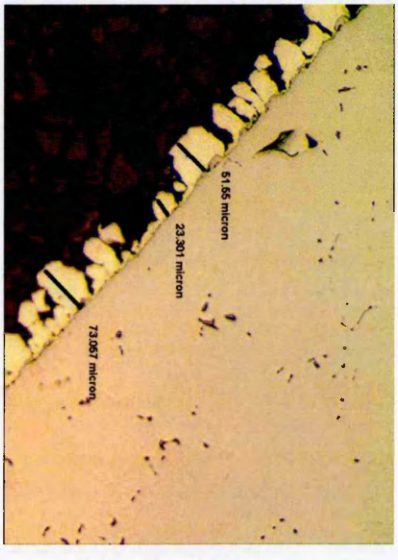

Figure 10-1: ILAl deposited on IN738 in the presence of water

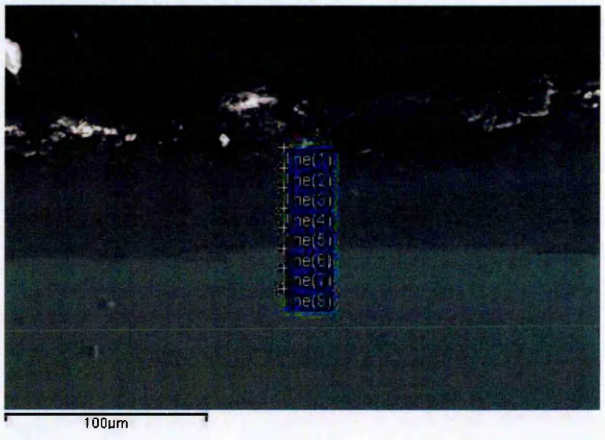

Figure 10-2: ILAl on IN738 after ICON Heat Treatment

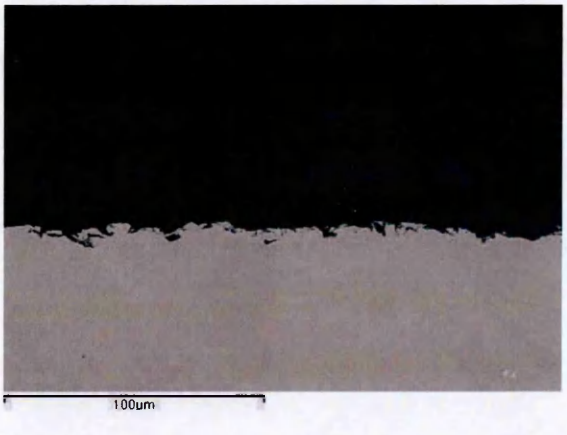

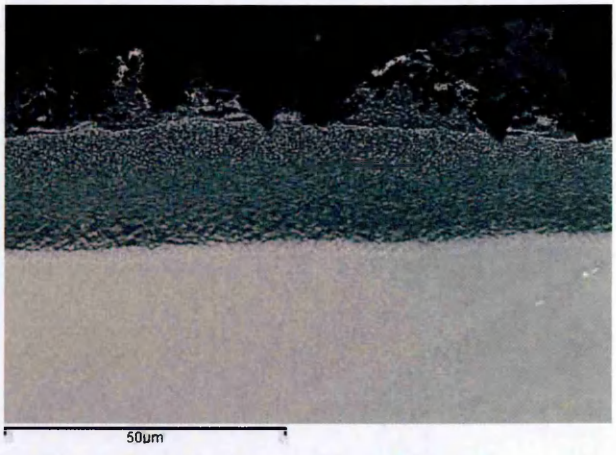

Figure 10-3: Large Columnar Deposits of Al from BMIM on CMSX4 which was later Heat Treated with ICON (Water approx. 100ppm)

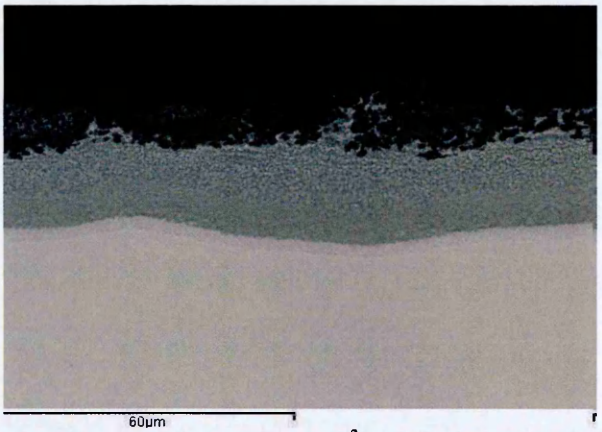

Figure 10-4: ILAl Deposited <2ppm water at 2A/dm^2 and Heat Treated with the ICON Process

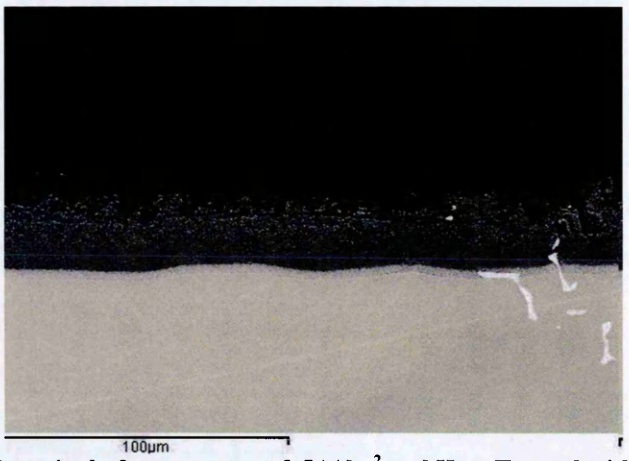

Figure 10-5: ILAl Deposited <2ppm water at 2.5A/dm^2 and Heat Treated with the ICON Process

Additionally, as shown in Table 5-7 with reference to the ICON heat treatment on CMSX4, large elements such as Re were observed to travel relatively large distances, which far exceeds that possible by solid state diffusion mechanisms alone: therefore this migration can only occur within a liquid phase in bulk materials or by surface diffusion or 'short-circuit' diffusion. Further, the relatively small atoms like nickel are more likely to enter into this initial liquid phase than the heavier elements which would lead to a depletion of Ni in the substrate surface and therefore an enrichment of heavier elements (Ta, Re, W etc). This local enrichment has been observed and appears as a lighter region (under BSE detection) or line of secondary phases as shown in Figure 5-24.

Directly comparing the TEM images of Figure 8-7and Figure 8-15, which are for CMSX4 and GTD111 respectively, it is obvious that the latter image shows a grain structure that is much more uniform in size and without the dark circles evident in the

former. The dark circles were thought to be contamination caused during the sample preparation steps. However, the GTD sample underwent the same process steps and is devoid of such 'contamination'. Therefore, it is thought that these areas of contamination provide new nucleation sites occurring on the surface of the newly forming grains themselves and therefore giving rise to variable grain size. It is proposed that during the coating reaction a liquid phase may form. Elements in the liquid are able to migrate freely and nucleation starts by the formation of small islands (step c in Figure 10-6). They are inhibited by either a thermodynamic reaction competing for the element by a near grain and may be engulfed as the other grains enlarge, or this new nucleus has a lower solubility for the element than the surrounding liquid phase and thus forms only a small grain which becomes enveloped by the solidification of this liquid phase upon cooling.

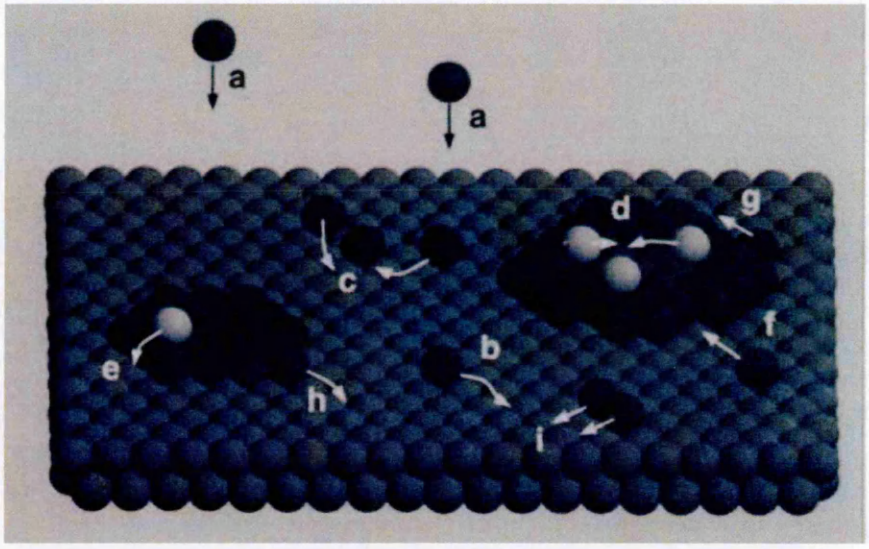

Figure 10-6: Atomistic processes during the growth[203]

Atomistic processes during the growth: a) deposition, b) diffusion on terraces, c) nucleation on islands, d) nucleation on a second-layer island, e) diffusion to a lower terrace, f) attachment to an island, g) diffusion along a step edge, h) detachment from an island, i) diffusion of a dimmer[203] are enhanced by the increased mobility in the liquid phase.

The eutectic point of the Ni/Al Phase diagram (Figure 1-2) is 639.9°C. However, the DSC results show that ILAl 9 and ILAl 10 have onset of reaction at 401 and 354.6°C

respectively (Table 7-3). These exothermic reactions will either promote further reactions and/or the formation of an aluminium/nickel liquid phase. Therefore even though the general temperature is sub 639.9°C (ICON first heat treatment is 620°C), localised temperatures on the atomic scale must exceed the eutectic point. Further, the DSC plots do not show any obvious endothermic reactions. Exothermic peaks suggest large scale melting and that any liquid phase is on the atomic scale.

To move from the $NiAl_3$ to the NiAl phase, one of two routes is possible, either remain in the partial liquidus phase and progress to the beta phase without passing through the Al_3Ni_2 phase (route 1 in Figure 10-7) or straight through the Al_3Ni_2 phase via solid solution diffusion (route 2 in Figure 10-7).

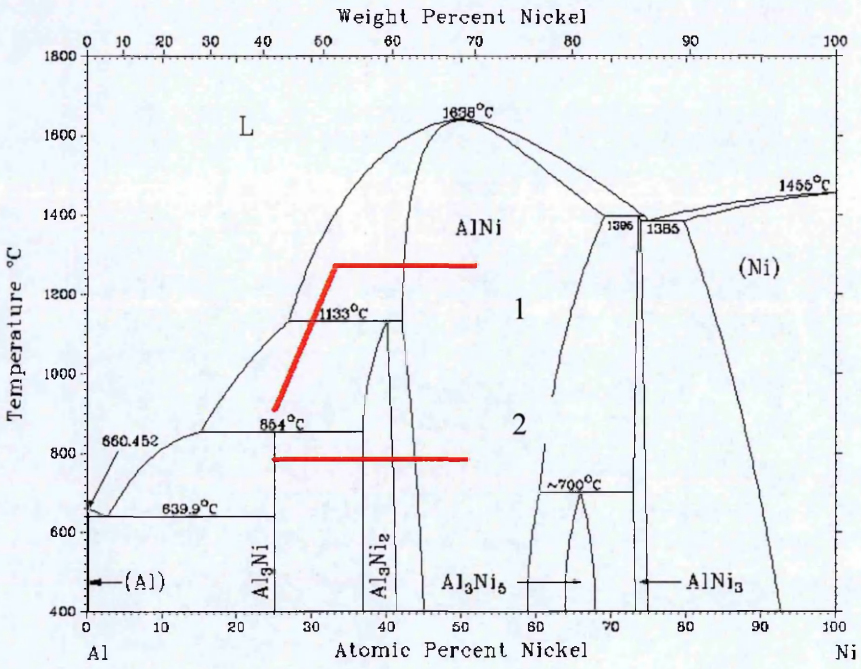

Figure 10-7: NiAl Phase Diagram with Proposed Diffusion Routes

It is thought that the former hypothesis is improbable due to the thermal temperatures needed to exceed the delta phase (Al_3Ni_2) (1133°C).

10.1.1 Understanding the ICON Process: the Influence of the Two Stage Heat Treatment

In an attempt to clarify the mechanism of action for the ICON process on GTD111 the ICON was stopped at three different stages (1 hour at 620°C, 1 hour at 620°C then 740°C for 1 minute and 620°C 1 hour and then 820°C 1 minute) and the

microstructure was analysed using BSE imaging. The first heat treatment was to see if a liquidus phase had been present, the second heat treatment at 740°C was part way through the exothermic reaction range according to the DSC results and finally, the final heat treatment was to see if the ICON process could be improved by reducing the time taken to produce the coatings (improving productionisation) and to what extent it was complete on reaching 820°C.

10.1.2 Heating 620°C for 1 hour

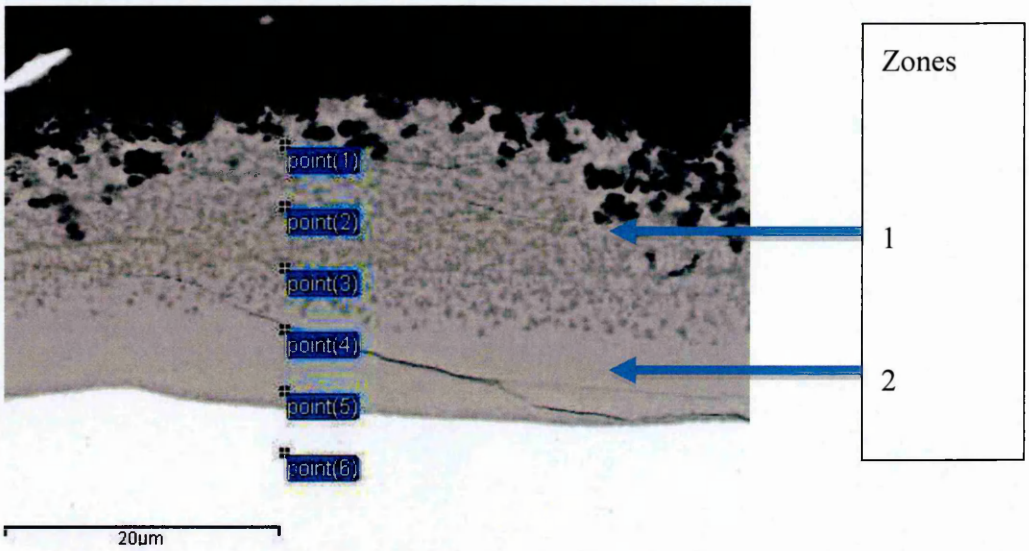

Figure 10-8: Photomicrograph of ILAl Heat Treated at 620°C for 1 hour

Table 10-1: Chemical Composition of Points shown in Figure 10-8 (at %)

Spectrum	Al	Ti	Cr	Co	Ni	Mo	W
point(1)	64.8	0.9	4.1	2.5	27.2		0.5
point(2)	66.9	2.3	6.9	4.0	19.1		0.8
point(3)	66.5	1.6	7.2	3.8	19.9		1.1
point(4)	60.4	1.7	7.4	3.9	25.8		0.8
point(5)	55.6	2.3	6.8	5.0	29.5		0.9
point(6)	5.5	4.2	17.5	10.8	59.1	1.0	1.9

The photomicrograph (Figure 10-8) shows a distinct 2 layer coating structure with a precipitate rich and free zone in the upper and lower halves of the coating respectively (the chemical composition is shown in table 10-1). This was not expected as the XRD data suggests that a homogenous $NiAl_3$ coating would be observed, rather than a coating with distinct phases. Furthermore, there appears to be some undulation in the coating with point 1 shown in the micrograph to be almost halfway between two troughs. Additionally, Figure 9-9 has shown that limited coating is above the

carbides. However, once this reaction is taken to completion the carbides are fully enclosed even if in some cases 'gas-hole' porosity is present.

Table 10-1 shows the chemical composition of the points and table 10-2 shows the atomic fraction of the coating when partition coefficients are assigned. It is possible to see that points 2 and 3(table 10-2) closely correlate to the $NiAl_3$ structure (75% at. Al), but point 4 is almost within the delta phase, whereas point 5 equates to the Ni_2Al_3 phase. The deviation between the XRD traces (shown in 5.2.3) and the microstructures (Figure 10-8) cannot be accounted for, but different specimens were used for the different experiments. However, it should be noted that different thermocouples were used for the two tests and some error within the set point may have occurred.

Table 10-2: Atomic Fraction for Ni type and Al Type Atoms in ILAl Heat Treated on GTD111 at 620°C for 1 hour (%atomic)

	Al	Ni
point(1)	67.7	31.7
point(2)	72.6	26.6
point(3)	71.6	27.2
point(4)	65.9	33.3
point(5)	61.3	37.8
point(6)	18.5	78.7

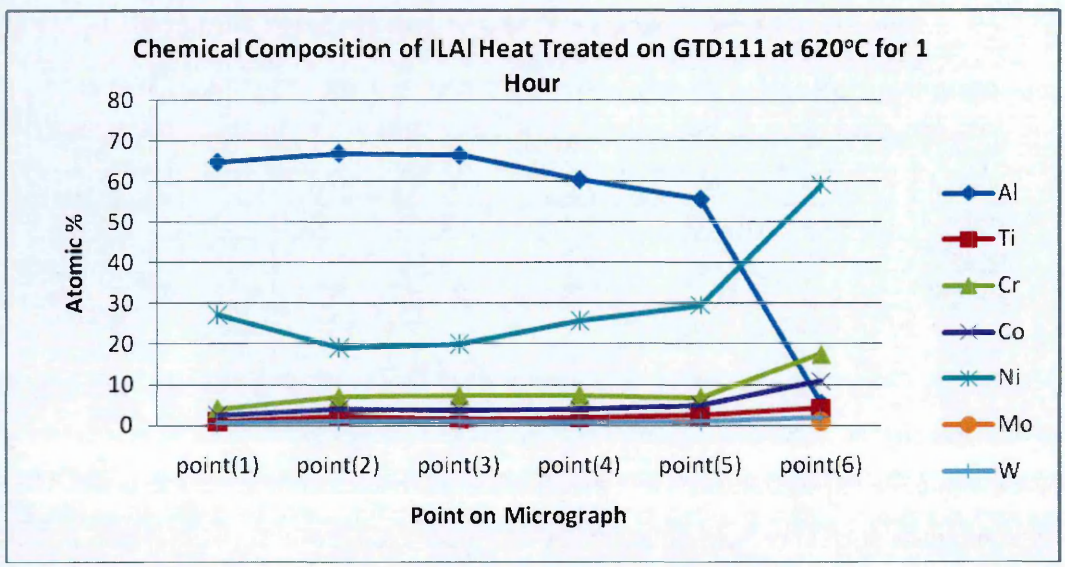

Figure 10-9: Chemical Composition of ILAl Heat Treated at 620°C for 1 hour (points highlighted in Figure 10-8)

The assigning of suitable partition coefficients was undertaken using the formulation of Co, Ni and 0.5Cr being assigned to the Ni sites and Al, Ti and 0.5Cr to the Al sites, however this formulation was designed for the use in site designation for γ/γ' phases. Therefore to see if it is suitable for the $NiAl_3$ intermetallic a review of Cr, Ti, Co aluminides is needed to see if any of these elements can form intermetallics when the Al content reaches 75at%.

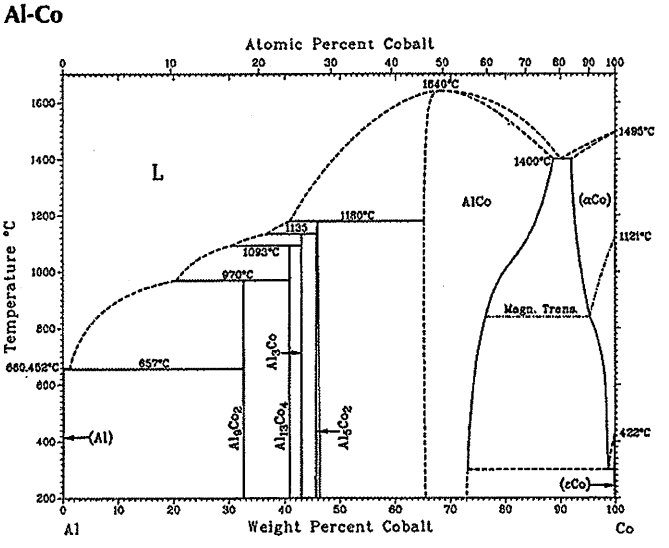

Figure 10-10: Aluminium-Cobalt Phase Diagram[177]

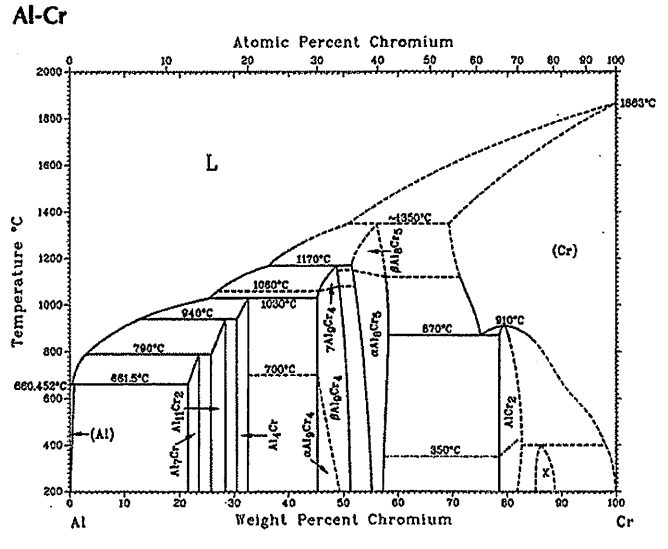

Figure 10-11: Al-Cr Phase Diagram[177]

Al-Ti

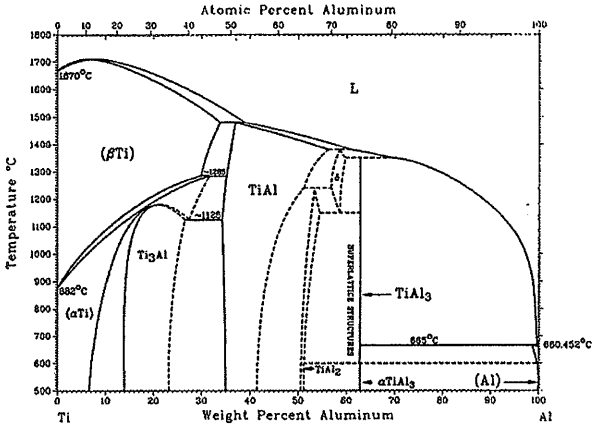

Figure 10-12: Al-Ti Phase Diagram[177]

Co-Ni

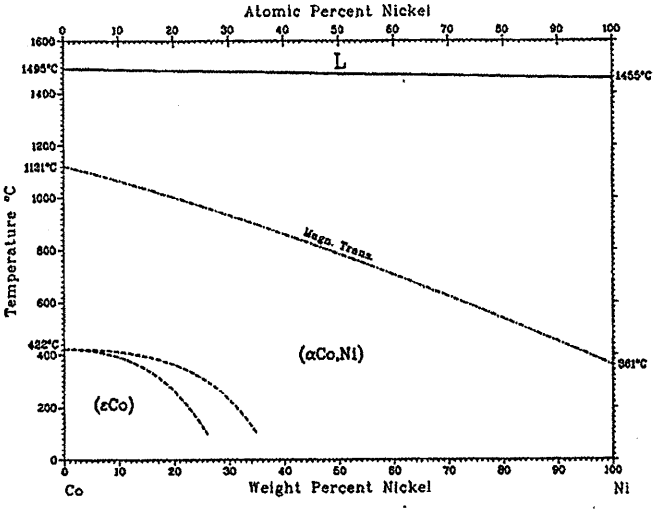

Figure 10-13: Cobalt-Nickel Phase Diagram[177]

Cr-Ni

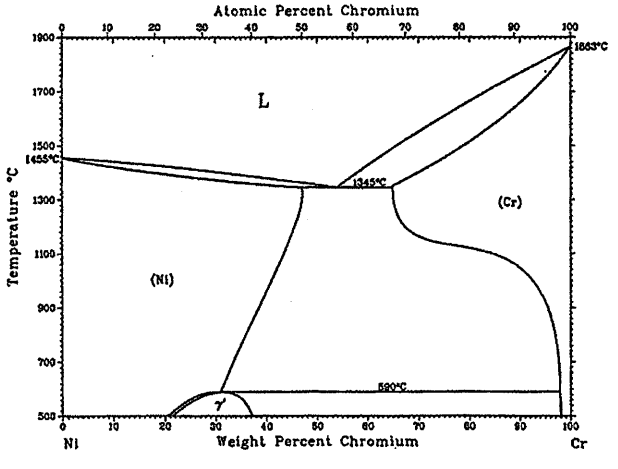

Figure 10-14: Chromium-Nickel Phase Diagram[177]

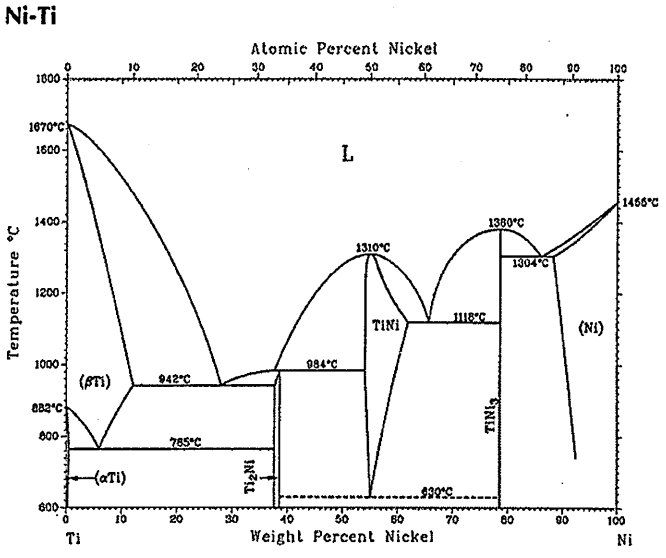

Figure 10-15: Nickel-Titanium Phase Diagram[177]

The phase diagrams (Figure 10-10 to Figure 10-15) suggest that the previous lattice assigning parameters are correct even when looking at Ni levels of only 25at% as no other intermetallics form at 75at% Al. Furthermore, other elements assigned to nickel lattices remain true at only 25at%. However, theorising that Cr is thermodynamically more stable at these ratios on the Al sites rather than being halved between the two, the lattice parameters change to that shown in Table 10-3.

Table 10-3: Modified Ni and Al Fractions of ILAl Heat Treated for 1 hour at 620°C

	Al	Ni
point(1)	69.8	29.7
point(2)	76.1	23.1
point(3)	75.2	23.7
point(4)	69.6	29.6
point(5)	64.7	34.4
point(6)	27.2	70.0

Averaging the Al and Ni sites between points 1 and 4 with the modified partition coefficients (Cr completely sitting on Al sites) then the values of 72.65 and 26.45 at% are found for Al and Ni sites respectively – almost $NiAl_3$ stoichiometry. Additionally, it would be expected that XRD (figure 5.2.3) penetration through the coating would be a maximum of 15um – suggesting that a bi-phasic coating may still be evident as seen before, but at least the outermost 15um of coating consists of the $NiAl_3$ coating.

10.1.3 ILAL Heat Treated at 620°C for 1 hour and 740°C for 1 min

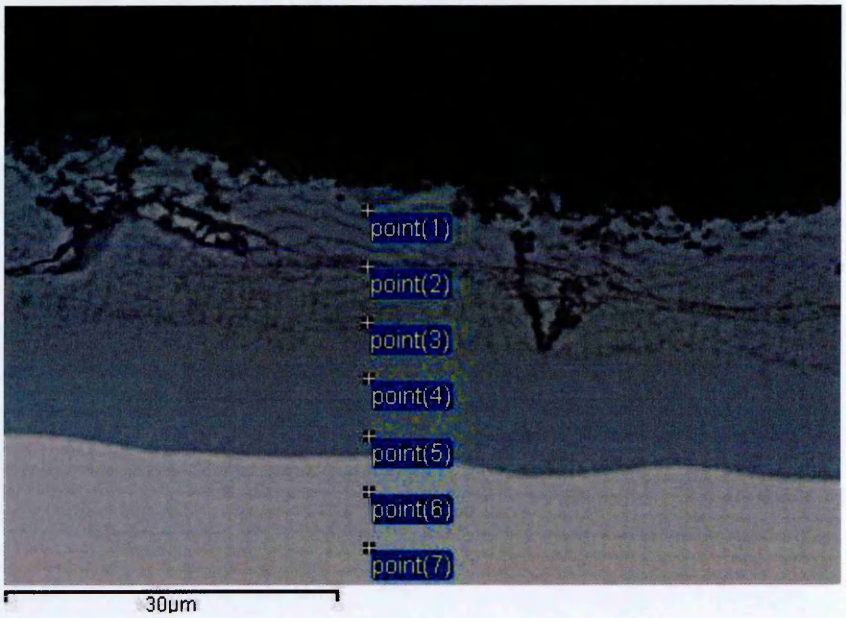

Figure 10-16: Photomicrograph of Part Processed ICON Coating (620°C 1 hour and 740°C 1 min)

It can be seen from the photomicrograph illustrated in Figure 10-16 that there are clearly two distinct phases occurring within the coating with the upper portion being in transition with numerous striations and voids observed. From Table 10-4 and figure 10-17 it can be seen that an increase in Ni content is seen at point 1, whereas points 2-4 have higher aluminium content and slightly elevated Cr content. It should be noted that all the points equate to the delta phase as observed in the NiAl phase diagram (the, aluminium content is very homogenous throughout the coating which is akin to a typical ICON coating. Additionally this is a very stressed coating with numerous cracks appearing throughout the upper segment of the coating.

Table 10-4: Elemental Composition of Part ICON Coating as shown in Figure 10-16

Spectrum	Al	Ti	Cr	Co	Ni	Mo	Ta	W
point(1)	58.3	2.0	2.1	2.4	35.2			
point(2)	63.4	4.6	3.1	2.3	26.5			
point(3)	64.3	2.7	7.0	3.5	22.1			0.4
point(4)	61.2	2.8	5.7	3.8	26.1			0.4
point(5)	57.8	2.9	8.2	3.9	26.4			0.6
point(6)	4.5	4.8	20.7	12.0	55.4	1.3		1.3
point(7)	8.6	9.1	8.6	7.0	63.7	0.8	1.3	1.0

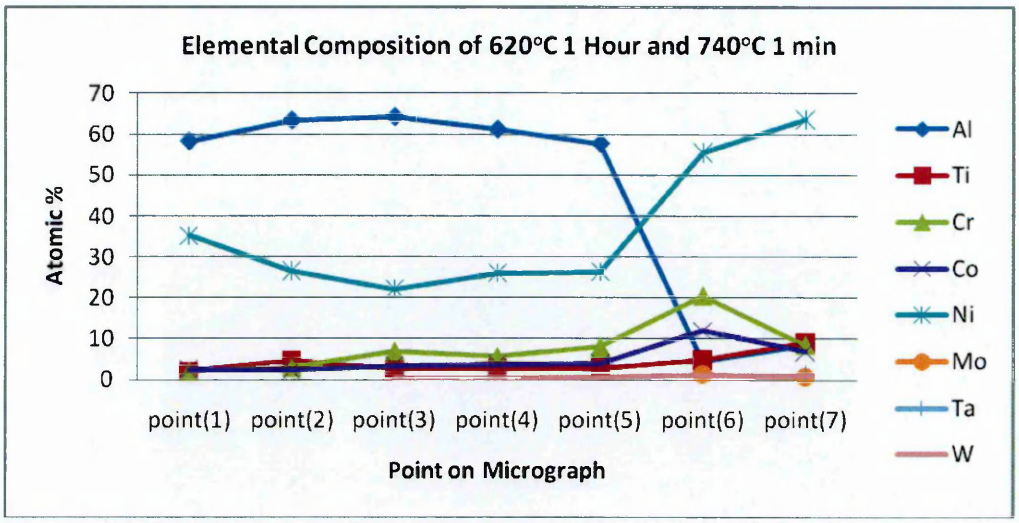

Figure 10-17: Elemental Composition of Part ICON Processed Coating of Points Highlighted in Figure 10-16

10.1.4 ILAl Heat Treated on GTD111 for 620°C for 1 hour and 820°C for 1 Minute

Figure 10-18 shows a BSE image of heat treated ILAl after 1 hour at 620°C and 1 minute at 820°C. Figure 10-19 is the same coating but magnified.

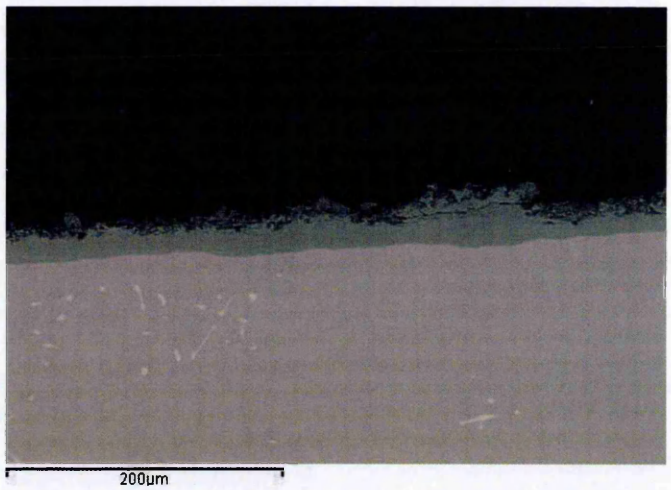

Figure 10-18: Heat Treated ILAl on GTD111 after 1 hour at 620°C and 1 min at 820°C (imaged with BSE)

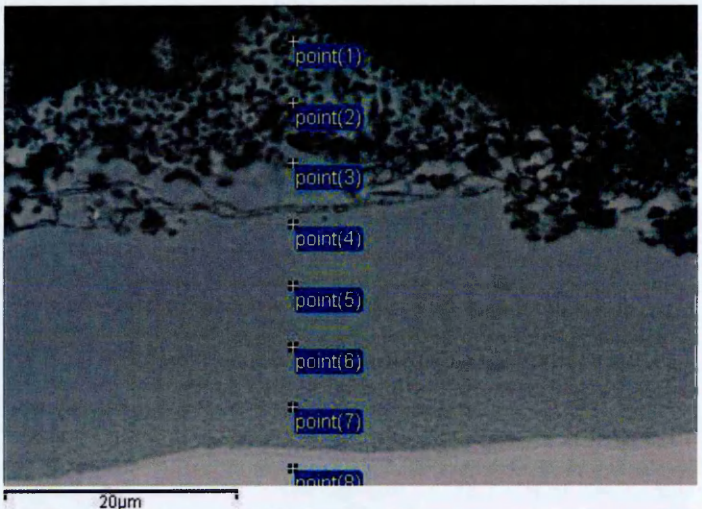

Figure 10-19: Heat Treated ILAl on GTD111 after 1 hour at 620°C and 1 min at 820°C (imaged with BSE - 2)

Point 1 and 2 as shown in Figure 10-19 are found in very porous sections of the coating. Furthermore, between points 3 and 4, a crack can be seen which appears to signal the interface between the main body and porous sections of the coating. Furthermore, the coating as seen in Figure 10-18 (composition shown in table 10-5 and figure 10-20) is not as homogenous as coatings produced with the complete ICON heat treatment regime.

Table 10-5: Chemical Composition of Points Highlighted in Figure 10-19(atomic %)

Spectrum	Al	Ti	Cr	Co	Ni	Ta	W
point(1)	55.1			2.5	42.4		
point(2)	60.0		0.5	3.1	36.4		
point(3)	56.4	6.7	4.3	3.4	28.6	0.7	
point(4)	61.3	2.2	6.6	4.1	25.0		0.8
point(5)	60.8	2.8	9.7	4.0	21.6		1.1
point(6)	58.4	2.0	7.2	4.6	27.0		0.7
point(7)	57.3	2.3	6.4	4.3	29.0		0.7
point(8)	51.9	2.3	7.2	4.8	32.9		0.8

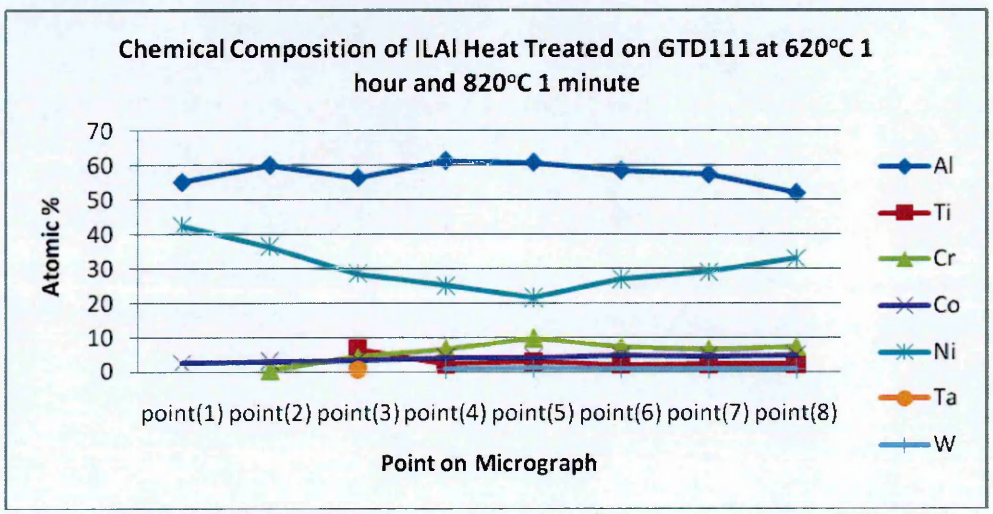

Figure 10-20: Chemical Composition of ILAl Heat garnered from Table 10-5

10.2 Proposed Mechanism for the ICON process

A sample of ILAl is deposited onto substrates such as GTD111, Ni200, IN738, N75 etc. and placed into a vacuum furnace. Very little interaction occurs between the coating and substrate until a temperature of 354-480°C has been attained (DSC data as described in 10.1 as well as data from Carlin[31]). At this temperature there is an initiation reaction between the Ni and Al at the coating/substrate interface with three nickel atoms reacting with a single Al atom forming Ni_3Al. This Ni_3Al is probably only atomic layers thick but acts as a diffusion barrier preventing any further diffusion of Al but permitting Ni to diffuse through into the Al coating from the substrate. As Ni is diffusing out (aided by the exothermic Ni_3Al reaction (-40.5kJ/g-atom)) there is a prevalence of Al atoms and therefore, agreeing with the NiAl phase diagram, Ni_5Al_3 followed by a layer β-NiAl, a layer of Ni_2Al_3 and the final $NiAl_3$ layer is formed (all are exothermic reactions and therefore create a positive feedback reaction). The liquid phase around the grain boundaries promotes movement of Ni and other heavier elements outwards during the initial heat treatment stage (0-620°C for one hour). These boundary regions must increase in temperature, above 639°C.

As it can be seen in Figure 9-9 there is considerable inward movement of the Al into the substrate and therefore an inward mechanism must be present also.

Continuing on to the final rest temperature of 820°C the reaction temperatures start at approximately 670°C where the $NiAl_3$ reacts with a further Ni atom to form Ni_2Al_3 which is also exothermic, however, once again liquid diffusion must occur therefore, once one new grain of Ni_2Al_3 has been formed this leads to self propagation of more Ni_2Al_3 forming. The 'free 'Al' (tainted with some Ni) from the above reaction allows a further liquid phase to form allowing diffusion along greater distances and permitting more Ni from the substrate to migrate into the coating. Finally, Ni_2Al_3 reacts with a further Ni to form the very exothermic NiAl and once again forming a self propagating reaction. Again, like the 1hour soak at 620°C, the soak at 820°C de-stresses the coating, and according to Figure 10-19 possibly maintains some fluidity whereby the coating smoothes out and becomes less undulating. However, at any given time multiple phases are being produced, liquid diffusion is occurring and due

to the exothermic energy release propagating further reactions: therefore the process is almost in a constant state of flux.

10.3 Formation of the Initial Intermetallic Layers

It is thought that the initial intermetallic to be formed is Ni_3Al. However, this inhibits Al diffusion, therefore it is proposed that a small amount of Ni diffusion occurs (atomic level) to allow increased levels of Al to diffuse into the substrate.

The β-NiAl is a BCC crystalline structure as shown below (Figure 10-21):

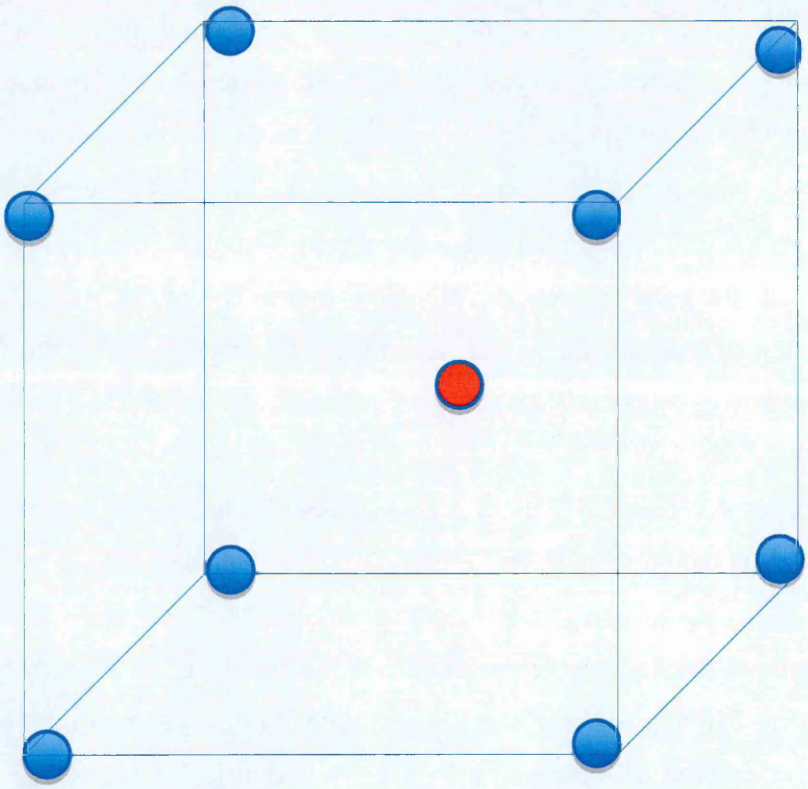

Figure 10-21: BCC Nature of B-NiAl (Aluminium is the red atom)

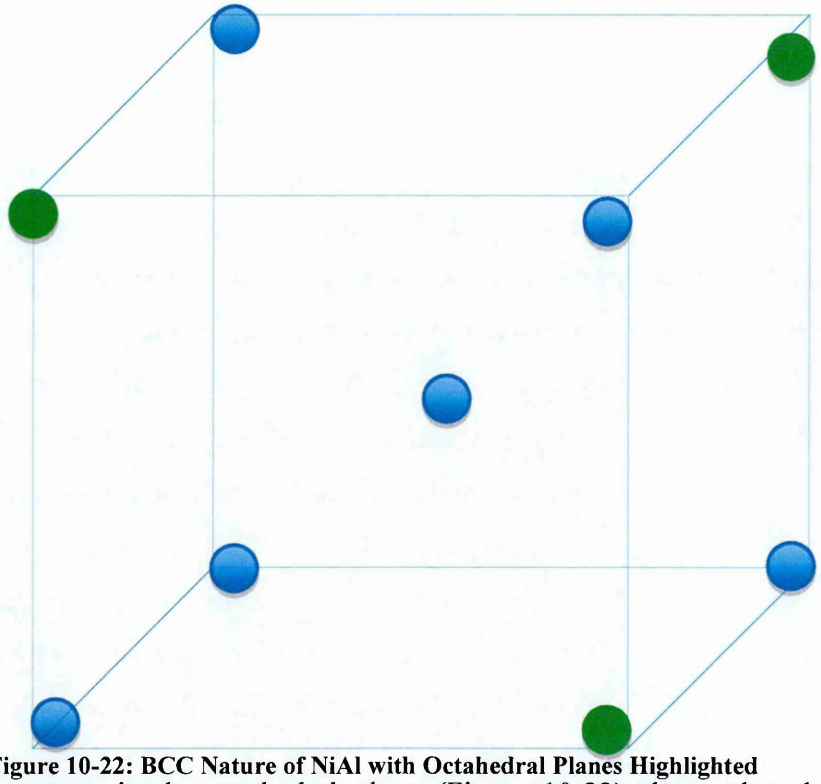

Figure 10-22: BCC Nature of NiAl with Octahedral Planes Highlighted

Taking the atoms in the octahedral plane (Figure 10-22) shows that the atomic layering is in a hcp stacking arrangement with planes of Ni atoms interspersed with Al atoms, furthermore collating this with Figure 10-23 shows that diffusion can occur at the atomic level.

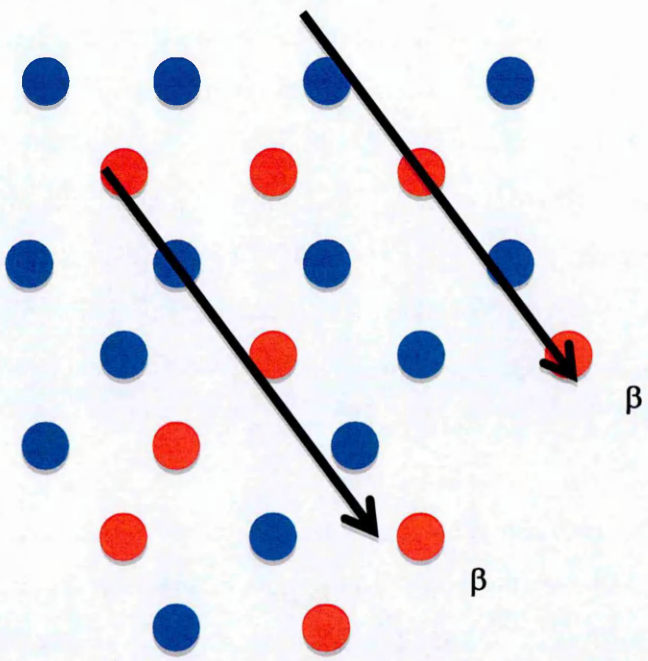

Structure	Plane
β	<110>
β	<110>
β	<110>
γ'	<110>
γ'	<111>
γ'	<111>
γ'	<111>

Figure 10-23: Atomic Arrangement of Phases to Account for Ni and Al Diffusion (Ni bue and Al Red)

Figure 10-23 illustrates in a simplified way how the structural alignment can influence the diffusion flux (octahedral planes of β-NiAl (hcp) on top of octahedral planes of γ'Ni_3Al (hcp)). The atomic alignment shows that both outward diffusion of nickel is possible for the lower temperature heat treatment profile and for possible aluminium inward diffusion when high Al containing aluminides form. Therefore it appears hypothetically possible for the initial $NiAl_3$ to be formed due to outward diffusion of Ni and reaction with the Al coating due to solid state diffusion enhanced by the chemical drivers, previously discussed, with the formation of the different aluminide intermetallics. The 2nd stage of ICON is at 820°C and therefore according to the Ni/Al phase diagram, Ni_5Al_3 will not form and thus β-NiAl will form directly adjacent to γ'-Ni_3Al. The removal of the Ni_5Al_3 atomic plane does not interfere with the atomic diffusion mechanism. It is postulated that by increasing the temperature the thermodynamics essentially allow the unstable line intermetallic $NiAl_3$ to transport and transform Al to Ni_2Al_3 and β-NiAl. This is not a net influx however as Ni_3Al is a diffusion barrier to Al and a mechanism must be in place to allow influx of Al and produce an inward diffused coating. Therefore, using the atomic model as proposed in Figure 10-23 aluminium and nickel can be transported readily to reach the Ni_3Al/β-NiAl or Ni_3Al/Ni_5Al_3 interface where it could react with the Ni_3Al to form more aluminium rich intermetallics, which in turn create a layer of Ni_3Al atoms beneath and thus creating an inward cascade reaction into the substrate. Inward Al diffusion is transported via solid state and short circuit diffusion (enhanced by chemical drivers) forming possibly a transient liquid phase (clusters of aluminium atoms in a liquid phase) can occur via grain boundary pathways. It should be also noted that although the atoms are layered in the above figure (Figure 10-23) in rows of β and γ' aluminide that diagonal planes show alternating atoms of Ni and Al (β). Thus diffusion can also theoretically occur in a similar manner to β-NiAl where in Ni rich aluminides Ni sits on the aluminium sites and vacancies occur in aluminium rich β-NiAl allowing easier diffusion through the two phases.

In addition to this the diffusion between β-NiAl and Ni_3Al is improved by the fact that the substitution of 2 Ni atoms for aluminium atoms and a distortion in the lattice could change the BCC nature of β-NiAl to the FCC Ni_3Al as shown in simpler form in Figure 10-24 and Figure 10-25.

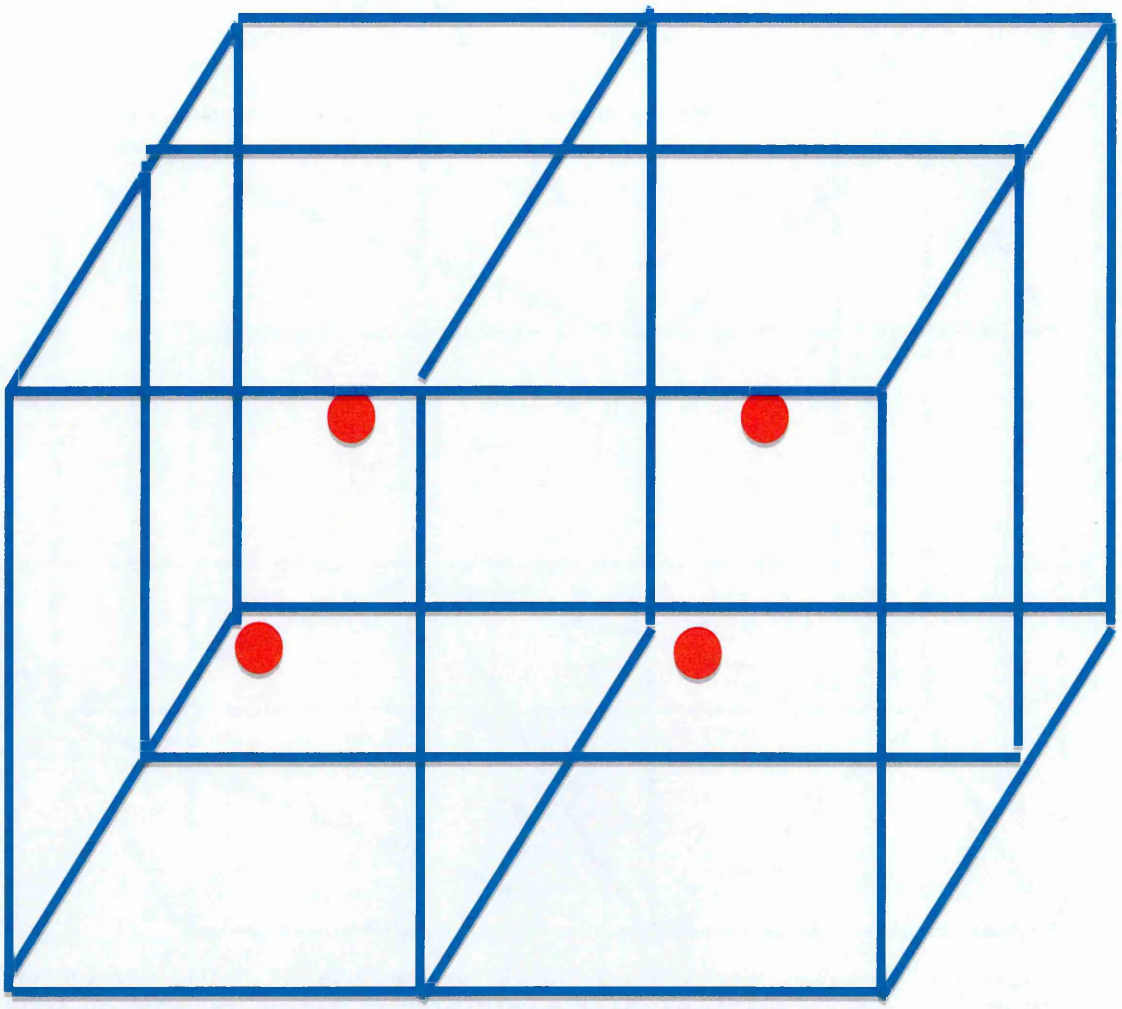

Figure 10-24: Simple Schematic of 4 Strucures of BCC NiAl (bonding to the red Ni atom removed for ease of understanding – the Intersections of the Blue Lines Represent where a Al atom would be)

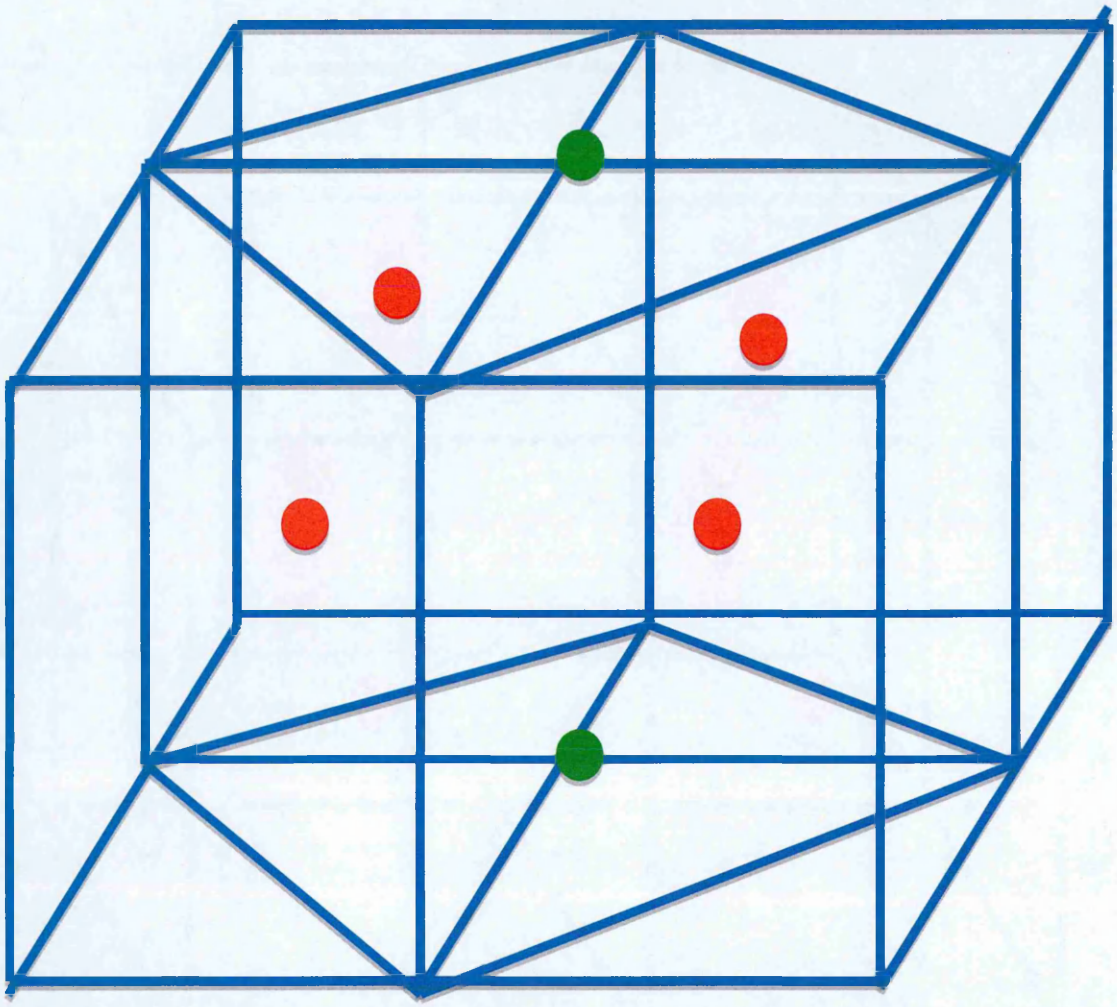

Figure 10-25: Simplified FCC Structure of Ni_3Al Tranformed from BCC NiAl (Red constititutes Ni atoms, Green constitutes Al atoms substituted for Ni atoms, Intersections of Blue lines represent Al atoms)

Ni atoms for Al atoms it is possible to change from the BCC NiAl to the Ni_3Al FCC structure. This enhances the prospect of aluminium diffusing into the substrate and hence increasing the coating thickness. It may also be a reason to account for the small interdiffusion zone as Ni and Al are diffusing out and into the substrate but at a rate that such larger tramp elements remain in solution.

In the presence of Re the reaction is almost the same as above. However, it is thought that the Re competes with Ni to form aluminide intermetallics, therefore inhibiting a cascade reaction. There is still sufficient energy present to form some transient liquid phase at boundaries. However, with the current temperatures and time frames there is insufficient energy to permit the formation of β-NiAl by exothermic reaction at such low temperatures. Possibly modifying the ICON process to 'soak' during the reaction

temperatures could induce β-NiAl. It is thought that when a single crystal of NiAl is formed a cascade reaction will result creating an entire super-lattice of NiAl due to the exothermic energy released.

10.4 Proposed Mechanism of Formation for CVD-type Heat Treatment Parameters

Although the ICON process is a proposed new low temperature heat treatment technique, it does suggest that depositing an Al overlay coating and using CVD type parameters that a similar mechanism of reaction should be involved. The main differences between the ICON and CVD process routes (apart from the temperature) are the heating rates which are 10°C/min and 20°C/min for ICON and CVD respectively. To date, no DSC work has been conducted on the heating of ILAl on a nickel alloy up to 1100°C. Therefore, the straight-line plot shown in Figure 7-5 resembles the closest work done. The work in Figure 7-5 shows that up to 900°C exothermic reactions as shown exist within the ICON process. Therefore, it is probable that by 800°C only Ni_2Al_3 is formed (on the presumption that Re retards β-NiAl formation in CMSX4, therefore, artificially retarding the reaction synthesis would lead to similar phase formations). However, this can only be proven by subsequent work by sectioning a sample undergoing 20°C/min ramp rate at various stages. Although Ni_2Al_3 is formed, it can be assumed from Figure 5-1 that the CVD parameters result in an inward grown aluminide coating, therefore the Ni_2Al_3 coating would agree with the LTHA work of Goward and Boone which then needs further processing to formulate NiAl. The heat treatment from 800°C to 1120°C transforms the coating to the desirable NiAl.

10.5 Conclusion to Diffusion Mechanisms

The outward movement of large elements (Re, W etc.) from the substrate into the coating and the removal of columnar deposits suggest that to some extent diffusion within a liquid phase occurs. According to the Ni/Al phase diagram between the $NiAl_3$ and Ni_2Al_3 phases there is a large liquid/solid region when the temperature exceeds 854°C. Therefore, localised temperatures have to increase by only 35°C during the ICON heat treatment to form a small liquidus phase (at grain boundaries) which may be feasible considering the amount of free chemical energy present during Ni_xAl_y intermetallic formation.

11 Heat Treatment and its Effect on the Coating's Oxidation Behaviour

11.1 Comparison of Various Heat Treatments:

Heat treatments used by our industrial partners were used as standards within this project even though different parameters are typically used at Cranfield University for their CVD type coatings. Therefore, to compare these heat treatments GTD111 was coated with 40 microns of ILAl applied prior to heat treatment and two different heat treatments were used: 1) 1120°C for 2 hours (NP Conditions and 2) 1030°C for 5hours (Cranfield Conditions).

11.2 NP Heat Treatments Parameters

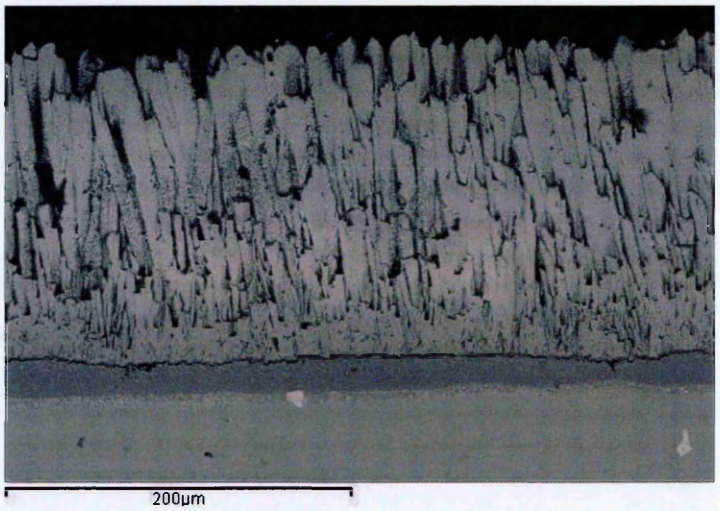

Figure 11-1: Heat Treatment of NiAl Bond Coat System using NP Parameters

Figure 11-1 is the typical microstructure of an ILAl produced coating when heated with NP parameters. It has been described in more detail in 5.2.1 but in essence it produces a β-NiAl coating very similar to a commercial CVD coating.

11.3 Cranfield CVD Heat Treatment Parameters

These parameters are used typically on CMSX4 and normally produce microstructures similar to those shown in Figure 11-1. The following microstructures were produced using the standard Cranfield University parameters (Figure 11-2 to Figure 11-4).

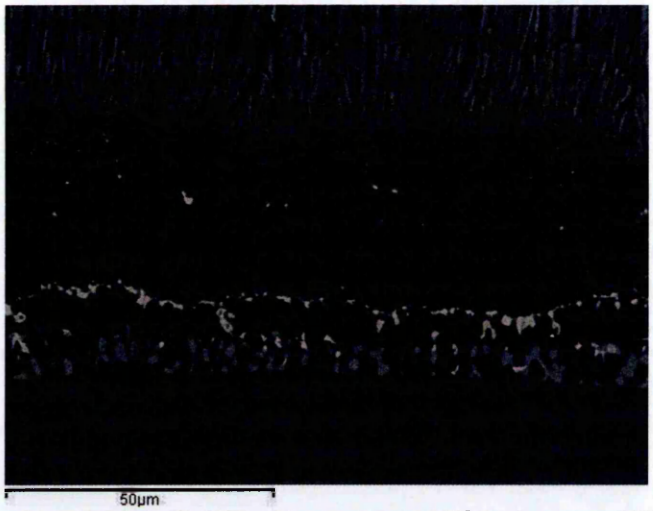

Figure 11-2: HTLA: ILAl Heat-treated for 1030°C 5 hours on GTD111

Figure 11-3: – LTHA: ILAl Heat-Treated at 860oC for 6 hours followed by 1100°C 1 for 1 hour on GTD111 (1)

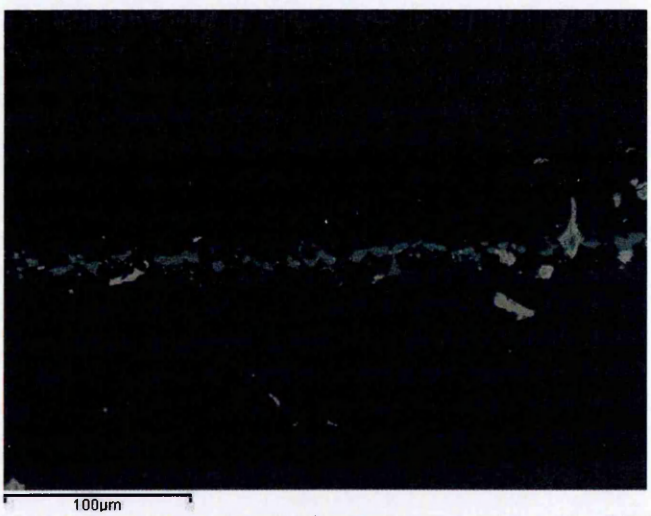

Figure 11-4: LTHA- ILAl Heat-Treated at 860°C for 6 hours followed by 1100°C 1 for 1 hour on GTD111 (2)

The typical heat treatments used at Cranfield both for HTLA and LTHA aluminising appear not to be appropriate for ILAl. The microstructures appear to be over diffused and show early onset of bond coat breakdown through the formation of short circuit paths extended from the secondary reaction zones (depletion of Ni and accumulation of tramp elements). All of the work done previously with CVD aluminising has been conducted on CMSX4, rather than GTD111. Therefore it shows that standard heat treatments are very dependent on the substrates used in a similar way to that observed for the ICON process.

11.4 Cyclic Furnace Testing

To evaluate the effectiveness of the coatings produced from electroplated aluminium, cyclic oxidation was chosen as the most suitable testing method. Cyclic oxidation was primarily conducted on β-NiAl coatings formed from ionic plated aluminium using conventional CVD heat treatment cycles. These tests were undertaken with the IL-NiAl bond coats to an EBPVD TBC. Limited oxidation testing of the ICON process has been undertaken as, for both GTD111 and CMSX4, some further process optimisation may be required. This is due to the formation of the 'induced porosity' of the ICON process on GTD111 and the formation of multiphase coatings using the ICON process on CMSX4. Complete testing of this ICON coating is planned when coatings on other substrates such as IN738LC or other nickel alloys which have low carbon content and are devoid of Re are produced and evaluated. This falls outside this current thesis.

Therefore, two different trials were initiated: ILAl heat treated as per commercial CVD process routes on GTD111 and CMSX4.

11.4.1 Cyclic Oxidation on GTD111

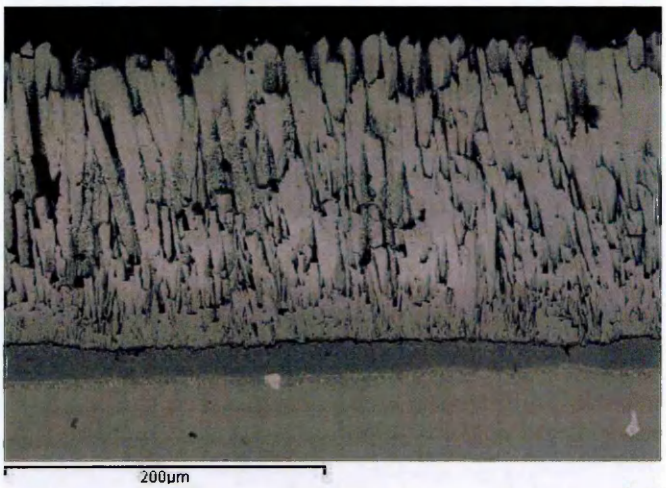

Figure 11-5: Photomicrograph of ILAl on GTD111 Overcoated with an EB-PVD TBC Prior to Cyclic Oxidation (1)

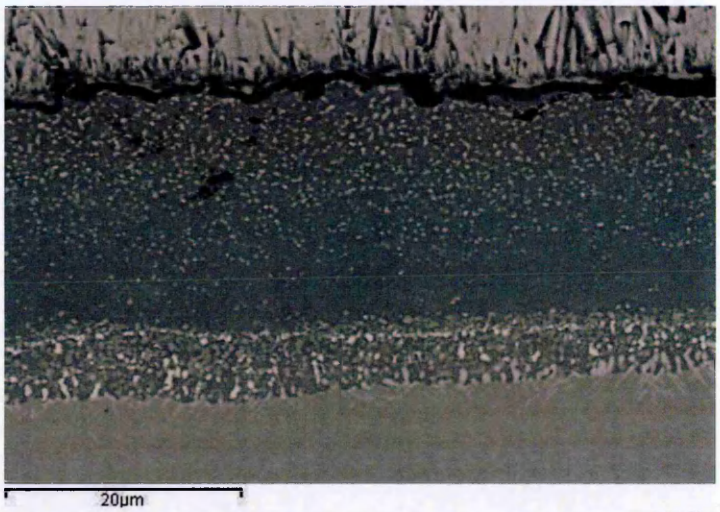

Figure 11-6: Photomicrograph of ILAl on GTD111 Overcoated with an EB-PVD TBC Prior to Cyclic Oxidation (2)

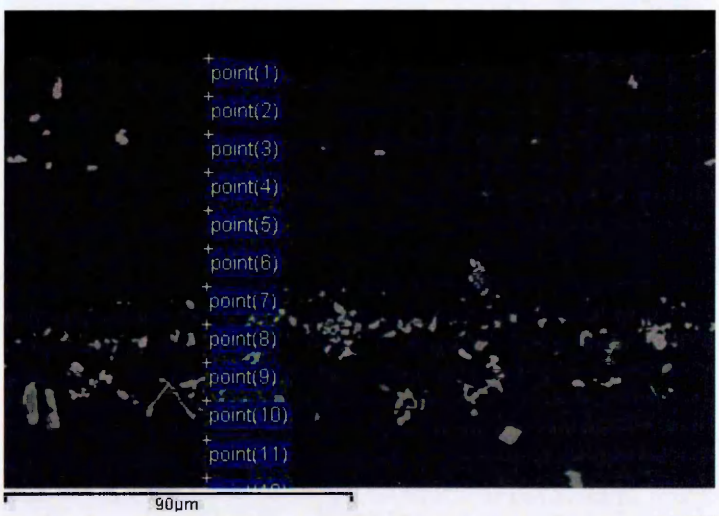

Figure 11-7: Photomicrograph of ILAl on GTD111 after Cyclic Oxidation at 1100°C for 169 hours (A14).

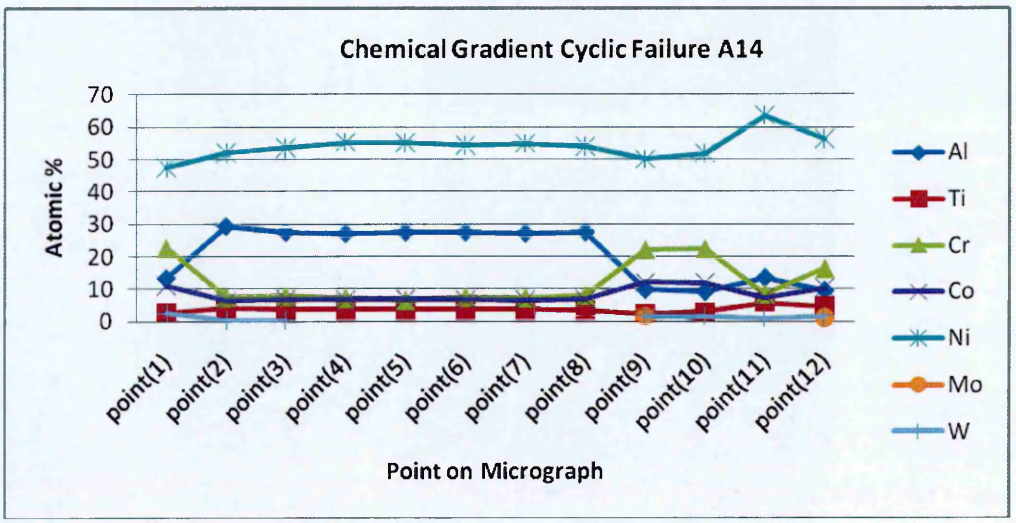

Figure 11-8: Chemical Gradient of Oxidised Sample (A14)

Table 11-1: Elemental Composition Based on Points shown in Figure 11-7

Spectrum	Al	Ti	Cr	Co	Ni	Mo	W
point(1)	13.3	2.9	22.7	11.0	47.5		2.6
point(2)	29.3	4.1	7.6	6.3	52.2		0.5
point(3)	27.5	3.8	7.9	6.8	53.6		0.4
point(4)	27.1	3.7	7.3	6.7	55.3		
point(5)	27.4	3.9	6.6	7.0	55.1		
point(6)	27.5	3.7	7.6	6.8	54.5		
point(7)	27.1	4.0	7.4	6.7	54.9		
point(8)	27.5	3.6	8.1	6.7	54.1		
point(9)	9.8	2.5	22.2	12.0	50.0	1.7	1.7
point(10)	9.1	2.9	22.4	12.0	51.8		1.8
point(11)	13.5	5.9	8.6	7.4	63.6		1.0
point(12)	9.6	4.7	16.3	10.3	56.3	1.2	1.7

The photomicrographs shown in Figure 11-5 and Figure 11-6 show how the overall coatings looked prior to cyclic oxidation, with the columnar structure of the ceramic evident in Figure 11-5 and the magnified bondcoat shown in Figure 11-6. Figure 11-7 and graph (figure 11-8) as well as Table 11-1 show that during oxidation (1100°C for 226 hours) the composition of the coating changes from β-NiAl to γ' (Ni_3Al) agreeing with numerous authors' observations including Angenete[42], Smialek[204], Li[26] and Pint[22] confirming that the Al diffused towards the TGO/bond coat interface to act as the Al reservoir for formation of the protective oxide film and also into the substrate. It should be noted that failure lifetime was associated with spallation of TBC from the bond coat (minimum requirement 20%). The delamination was observed to initiate at the bond coat/TGO interface. Furthermore, the data from Table 11-1 shows that point 1 is Cr rich, however, it would be expected that this region is Al rich (due to

formation of the Al_2O_3 TGO). However, at failure, the Al_2O_3 part of the TGO may well have adhered to the detached TBC revealing a NiCrAl spinel region beneath.

11.4.2 Cyclic Oxidation on CMSX4 at 1100°C

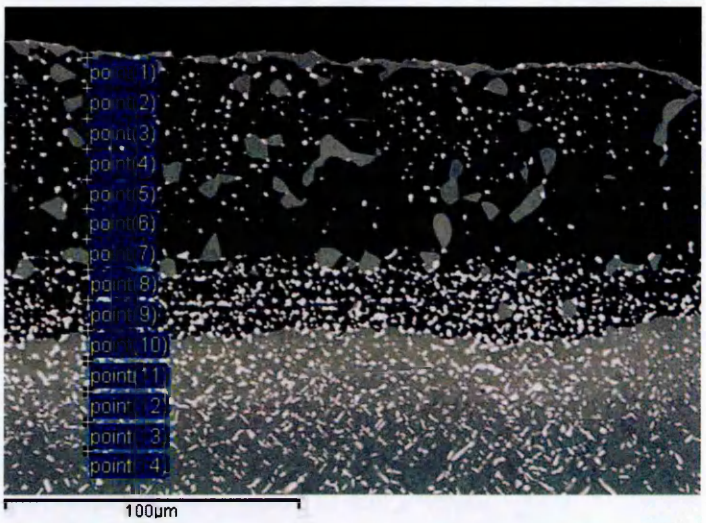

Figure 11-9: ILAl Heat Treated on CMSX4 after Cyclic Oxidation at 1100°C (254 cycles)

Table 11-2: Elemental Composition of ILAl Heat Treated on CMSX4 after Cyclic Oxidation

Spectrum	Al	Ti	Cr	Co	Ni	Mo	Ta	W	Re
point(1)	17.2	1.5	3.5	8.9	63.6		4.0	1.4	
point(2)	31.6	0.7	5.1	7.4	55.2				
point(3)	31.9	0.6	5.1	7.3	54.7			0.4	
point(4)	17.9	1.4	3.4	8.8	63.8		3.5	1.3	
point(5)	31.0	0.7	5.3	7.3	55.2			0.6	
point(6)	31.3	0.7	5.3	7.4	54.9		0.4		
point(7)	31.6	0.7	5.2	7.3	54.8			0.5	
point(8)	27.0	0.6	7.5	8.6	51.7		0.7	2.9	1.1
point(9)	30.4	0.7	6.0	7.7	54.4			0.7	
point(10)	15.8	0.5	14.0	12.8	40.6			11.3	5.0
point(11)	10.8	1.2	7.7	11.0	54.4	1.0	3.2	7.6	3.2
point(12)	16.3	1.6	3.3	8.8	64.3		4.1	1.5	
point(13)	12.6	1.6	7.1	10.6	56.6	0.6	2.6	5.6	2.7
point(14)	13.3	1.2	8.5	10.7	55.6	0.9	2.1	5.0	2.8

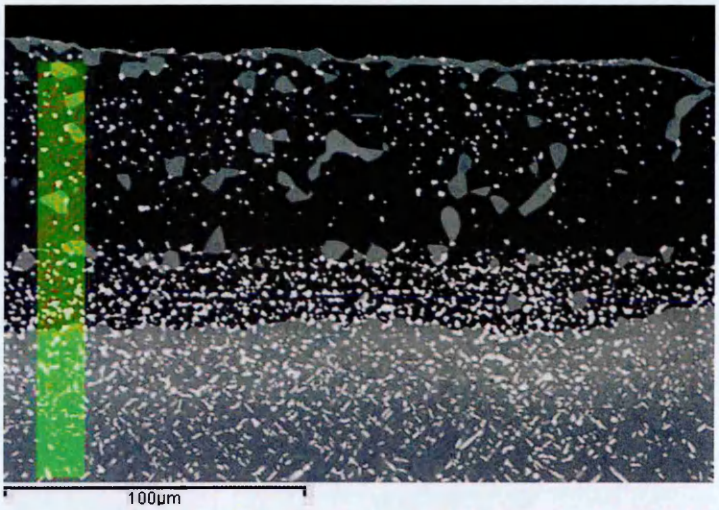

Figure 11-10: Elemental Map of ILAL on CMSX4 after Oxidation at 1100°C for 254 cycles (red = Al, Ni = green)

Figure 11-9 and Table 11-2 show the microstructure and elemental composition of the sample after thermal cycling at 1100°C for 254 cycles. Figure 11-10 shows an elemental map of an oxidised ILAl coating on CMSX4 after 190 hours at 1100°C. Green represents Ni and red equates to where pure Al would be located, therefore it can be seen that the substrate has a bright green colour (as to be expected) but the coating has a green/yellow tinge indicating that Ni is alloying with some Al, but which is Ni rich. This agrees with the EDX data showing that Ni_3Al results after this exposure, and also shows that no free aluminium is evident within the coating.

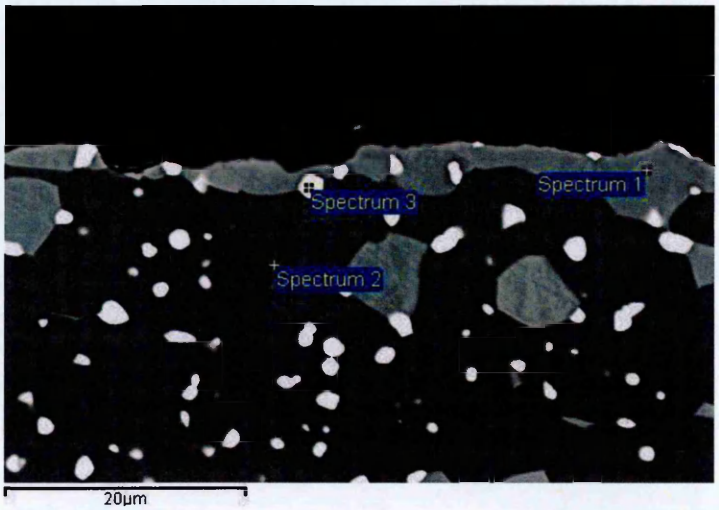

Figure 11-11: Magnified Image of ILAl on CMSX4 after Cyclic Oxidation at 1100°C for 190 hours

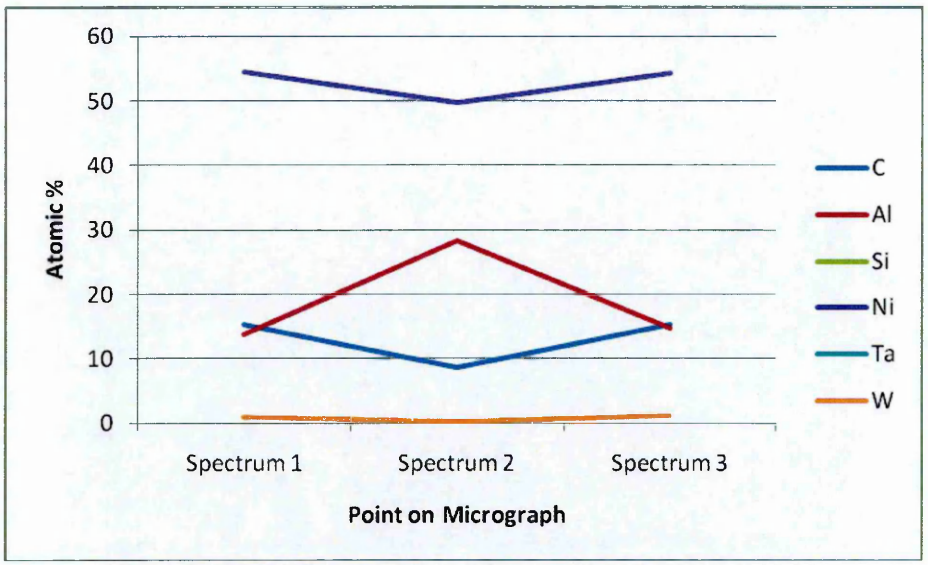

Figure 11-12: Chemical Analysis of Points Shown in Figure 11-11

Table 11-3: Chemical Composition of Points Indicated in Figure 11-11

Spectrum	C	Al	Si	Ni	Ta	W
Spectrum 1	15.4	13.8		54.5	3.3	1.0
Spectrum 2	8.7	28.4	0.7	49.7		0.3
Spectrum 3	15.4	14.8		54.3	2.9	1.1

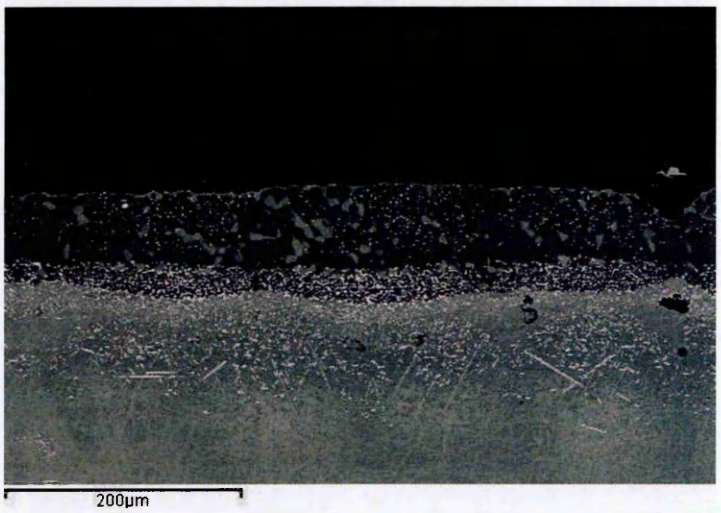

Figure 11-13: ILAl Heat Treated on CMSX4 after Cyclic Oxidation at 1100oC for 345 hours(1)

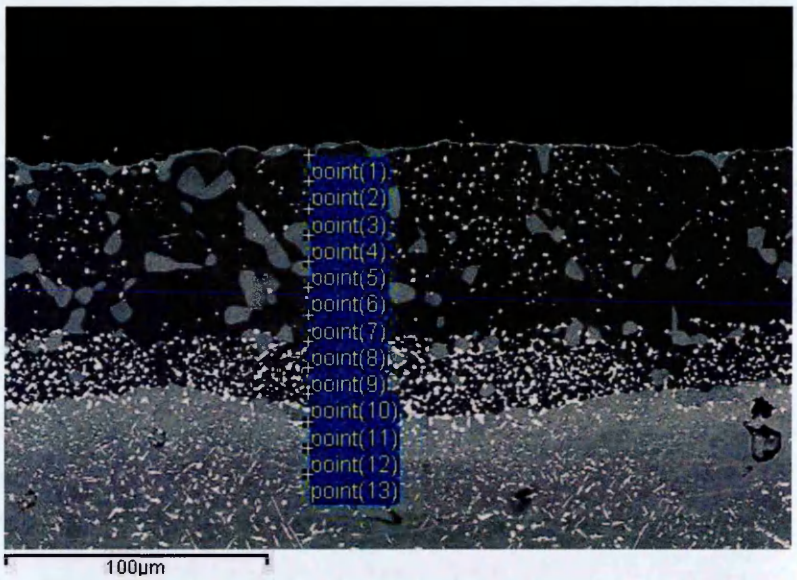

Figure 11-14: Magnified Region from Figure 11-13

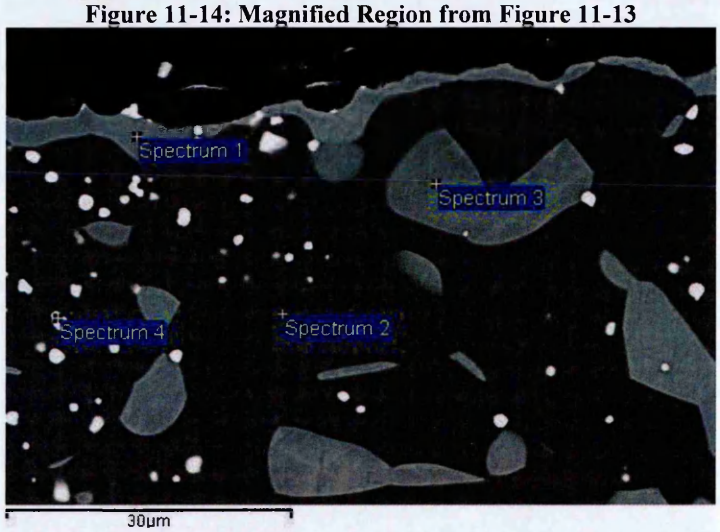

Figure 11-15: Magnified section of Sample shown in Figure 11-13

The microstructures shown in figure 11-11 (elemental composition shown in Table 11-3 and profile in Figure 11-12) Figure 11-13 and Figure 11-15 clearly show that some phase changes in the bond coat have resulted from the cyclic oxidation trials. Figure 11-16 indicates a uniform but depleted aluminium profile in the body of the coating that results from the degradation of the β-NiAl as Al diffuses towards the TBC/bondcoat interface and into the substrate. Therefore, enrichment of aluminium in the area surrounding point 1 is associated with the formation of the protective α-Al_2O_3 scale at the surface of the bondcoat, under the TBC. Further magnification (Figure 11-15) highlights the distinct phases present within the outermost section of the coating as shown in Figure 11-16 below, with the composition at each point given in Figure 11-17. Spectrum 1 and 3 correspond to the formation of Ni_3Al, as a surface layer due to aluminium depletion as a result of forming an alumina protective oxide,

and internal depletion due to the diffusional supply of aluminium to the surface. These two locations could equally well be linked somewhere within this surface region. Spectrum 2 corresponds to depleted β-NiAl.

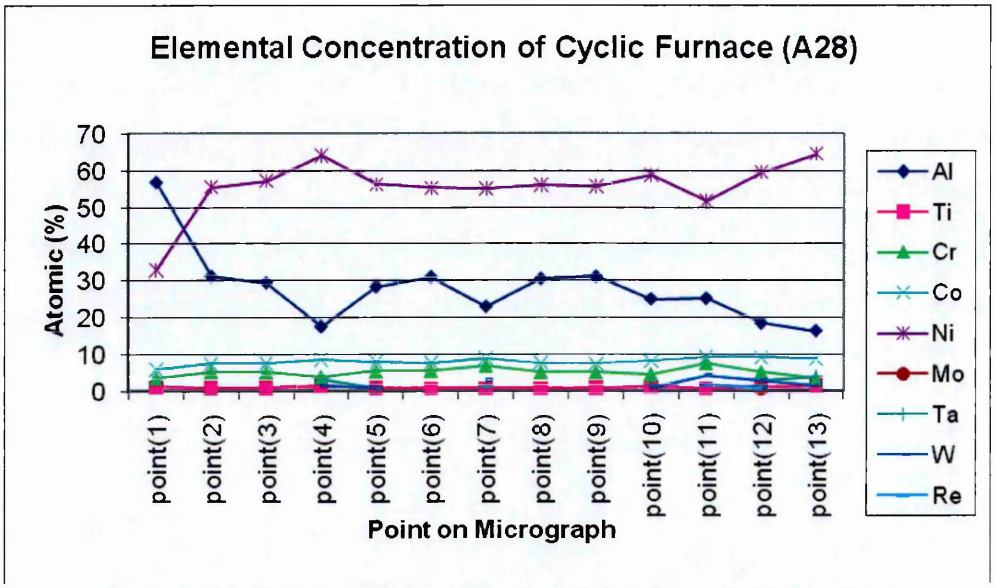

Figure 11-16: Elemental Composition from Points Shown in Figure 11-14

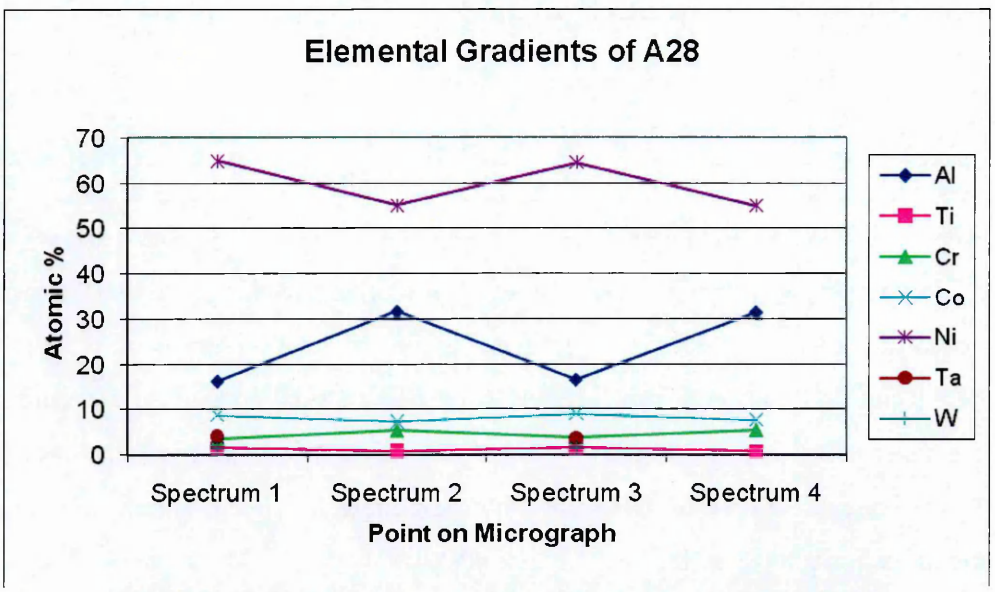

Figure 11-17: Elemental Composition of Points shown in Figure 11-15

It is thought that spectrum 4 does not give an accurate representation of the chemical composition of the bright precipitate phase beneath the spot indicated on the micrograph. The image is compiled using back scattered electrons and therefore the brighter phases of the microstructure should indicate elements with higher atomic weight compared to darker lighter weight atoms. However, the small area size of the bright phase (underneath marker 'Spectrum 4') must be smaller than the actual area

highlighted by the cross-hairs in Figure 11-15 (due to the electrons penetrating the bulk coating) and therefore the area surrounding the bright phase will contribute also. Hence, the composition appears similar to β-NiAl, which is the surrounding matrix phase. The brighter phases must be due to the presence of heavy elements such as W, Ta, and Re which precipitate out under transformation from β-NiAl to γ′ due to the reduced solubility of such refractory elements in γ′. These brighter phases are expected to be refractory metal containing Laves phases. Therefore, it can be concluded that ILAl heat treated on either GTD111 or CMSX4 to form β-NiAl is transformed to Ni_3Al upon high temperature oxidation, plus refractory Laves phases if heavy elements are less soluble in γ'.

11.4.3 Results of Cyclic Oxidation at 1100°C for ILAl Heat Treated using CVD Parameters

Table 11-4: Cyclic Oxidation Values for 40um of ILAl on GTD111 and CMSX4

Substrate	Failure at Cycle No	Average Failure	% TBC Failure
GTD111	134	165	100
GTD111	134		100
GTD111	226		20
CMSX4	254	323	100
CMSX4	460		100
CMSX4	254		100

Cyclic oxidation results are found in Table 11-4. Each cycle equates to approximately 45 minutes 'hot time' therefore average total time at temperature is 123 hours for GTD111 and 242 hours for the CMSX4. It has proved very difficult to compare this data against the literature as little has been published on β-NiAl as a bond coat to a TBC for either GTD111 or CMSX4. However, there has been some work on the cyclic oxidation published for NiPtAl on CMSX4.

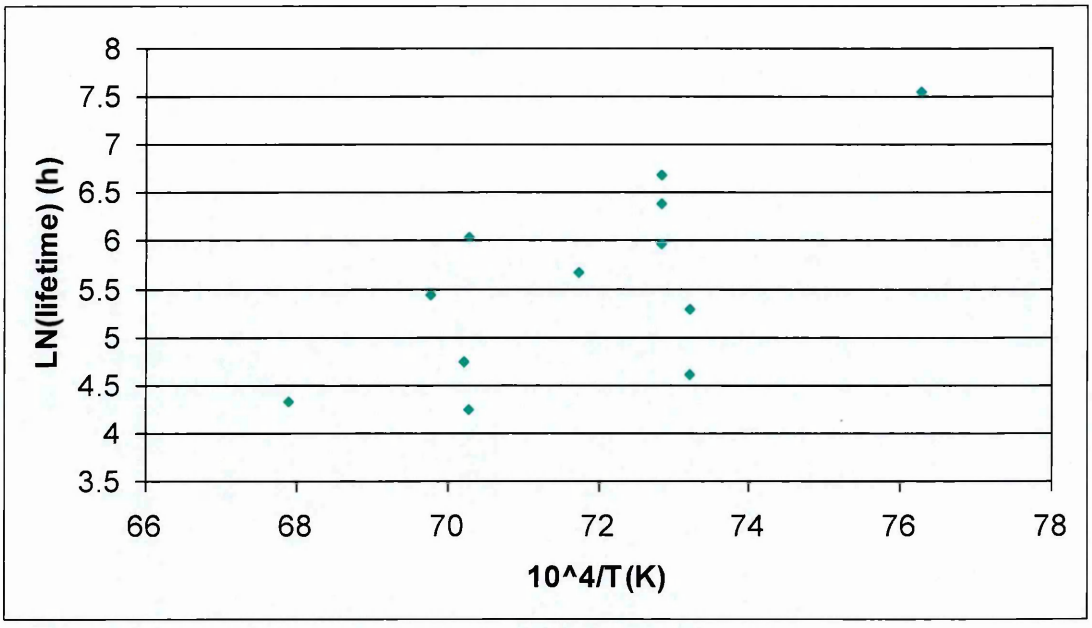

Figure 11-18: Literature Review of NiPtAl Oxidation Rates on CMSX4[161,205]

The biggest problem with this literature data was that the temperature at which the data was obtained was different as the plot in Figure 11-18 shows. Therefore by obtaining an approximate 'best-fit' line through the different points it is possible to correct the data to 1100°C by using the Arrhenius equation and then draw a Weibull plot for 1100°C, through this corrected data:

$$y = mx + b$$

$$m = \frac{y_1 - y_2}{x_1 - x_2}$$

$$\therefore m = \frac{\ln(life_1) - \ln(life_2)}{T_1 - T_2}$$

$$\therefore m(T_1 - T_2) = \ln(life_1) - \ln(life_2)$$

$$\therefore \ln(life_2) = \ln(life_1) - m(T_1 - T_2)$$

Figure 11-19: Equations to Transpose Literature Results to a Reference Temperature of 1100°C

Where $T_1 = 10^4$/Temp from Literature in $^{O}C + 273$, $T_2 = 10^4$/Desired Temperature (1100°C) + 273, $Life_1$ = failure at given temperature in hours

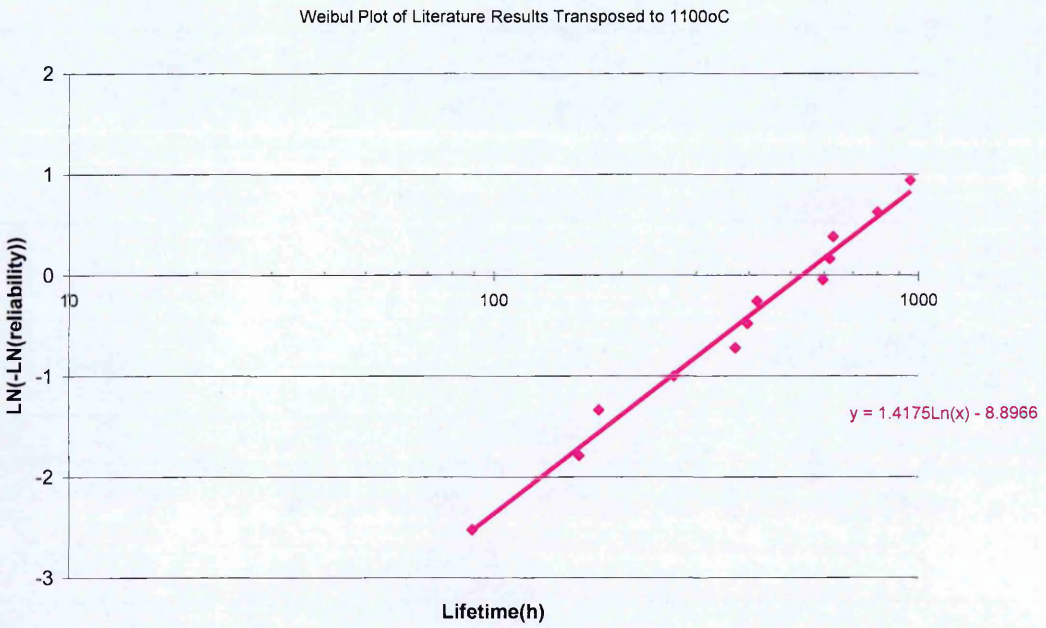

Figure 11-20: Wiebull Plot for Cyclic Oxidation failures at 1100°C from Literature for NiPtAl on CMSX4

Figure 11-20 shows that the characteristic life of NiPtAl (x intercept) based on the equation y=1.4175ln(x)-8.8966) is 532 hours. As Nicholls and Wing have reported that the addition of platinum increases the lifetime of the samples threefold[206], then the approximate characteristic lifetime of NiAl coatings on CMSX4 is expected to be 177 hours. Even if platinum only doubles the lifetime then the characteristic life of β-NiAl would be 266 hours, and this is comparable with the NiAl samples produced using ILAl. This therefore suggests that ILAl to form CVD-type coatings is at least as good as, if not better than that anticipated from the literature for CVD formed β-NiAl coatings. It would be very interesting to see how ICON treated coatings performed and ICON + Pt as well as ILAl with Pt using CVD heat treatment parameters.

12 Industrialisation of Plating Ionic Liquid Aluminium (ILAl)

12.1 Introduction

One of the main aims of this thesis is to see if the process of electroplating from ionic liquids is feasible on a commercial basis. If the process of electroplating from ionic liquids is commercially feasible then it can be assumed that the ICON process and of course other heat treatments are also possible. It has been shown possible to electroplate small buttons (14.5mm diameter x3mm), but transferring this to larger, more complex shapes (especially turbine blades) would allow this whole process to be validated for production on component geometries.

12.2 The Coating of Large Parts and Novel Alloys

As part of the IOLISURF project additional research has been undertaken to electroplate onto welds (both mild steel and Hastalloy X (autogenous and filled welds) and large plates (300mm^2) to form compacted deposits[207]. Furthermore, it has been shown possible to electrodeposit Al onto Al/Li alloys[208] which are thus able to reduce corrosion rates of this type of aircraft structure alloy.

12.3 Electroplating Turbine Blades

One aspect of this technology demonstration was the coating of turbine blades. It is proposed that this technology be an alternative to CVD manufactured diffusion coatings. Therefore, if it was possible to electroplate a complex turbine blade it would demonstrate that this process should be suitable for scaling up to semi-production. A number of scrap blades (buckets) made out of GTD111 were supplied by NP for these initial trials.

It was thought that the best method of obtaining a more uniform coating over a complex shape, eg. a turbine blade, would be best achieved if a conforming anode was constructed by CNC machining. To first demonstrate this technology, a more cost effective method was investigated, that of producing a mould over which the conformal anode could be constructed from aluminium wire. Modelling clay was applied to all aerofoil surfaces of a blade, allowing enough thickness to enable a blade to fit easily between the hollow cathode at a later stage. The clay was then allowed to

set for 24 hours to harden and is shown in Figure 12-1, then aluminium wire and thin sheet was formed around the clay mould to make the conformal anode.

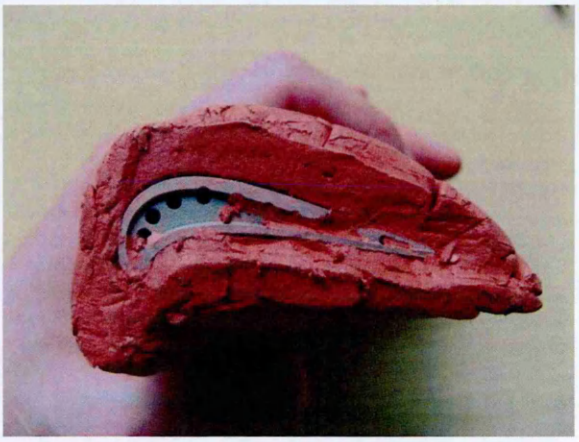

Figure 12-1: Fabrication of a Conforming Anode for Electroplating onto a Turbine Blade

Using this conformal anode, a turbine blade was coated with Al and the coating thickness measured (Figure 12-2). This figure illustrates the distribution in thickness that resulted, varying from 182microns on the leading edge (a region of sharp curvature) to 22 microns on the suction surface near the trailing edge. No coating was found on the trailing edge where the current density would be very large. It should be noted that the red lines drawn on Figure 12-3 represent approximately where the coating starts, so only a minimal area of the blade is left uncoated. Plating aluminium using a conformal anode on aerofoil sections has led to a nodular (columnar) coating morphology. The variation in nodule height (local coating thickness) is most noticeable at places of highest curvature. Curvature is known to affect current distribution, as well as the working distance between the anode and cathode (the blade). Thus the nodular structure reflects this variation in current distribution, especially at the leading and trailing edges.

It is thought that the deployment of robber bars or auxiliary anodes towards the trailing edge could be utilised to reduce the intensity of the electrical field and therefore allow some deposition of coating to occur in this area.

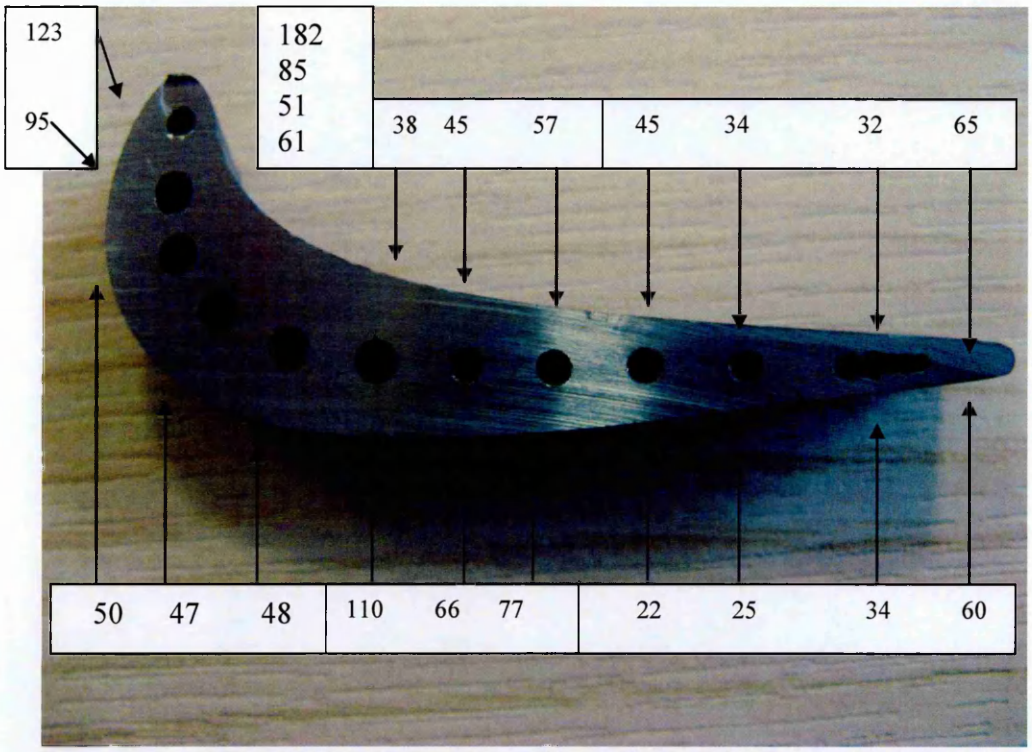

Figure 12-2: Photograph of Plated Turbine Blade with Associated Coating Thickness (um)

Figure 12-3 to Figure 12-7 provide more detailed micrographs of the coating at the various positions around the aerofoil. On all sections an adherent coating was observed, albeit of varying thickness on the leading edge, suction and pressure surfaces.

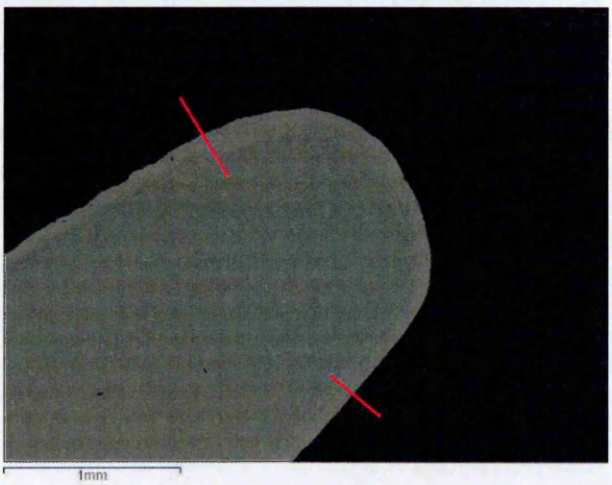

Figure 12-3: Trailing Edge

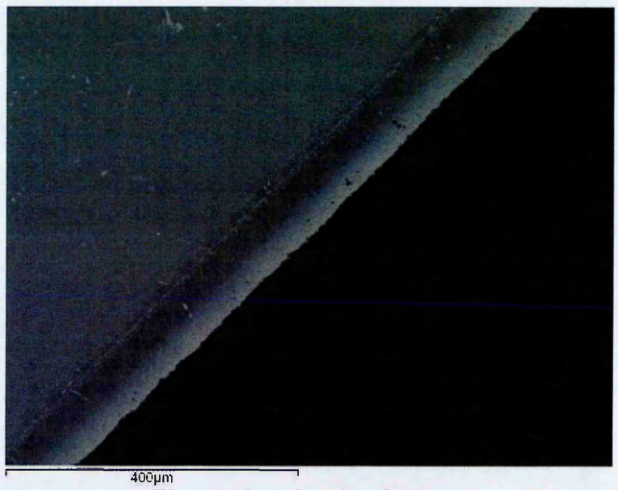

Figure 12-4: Suction Surface

Figure 12-5: Leading Edge

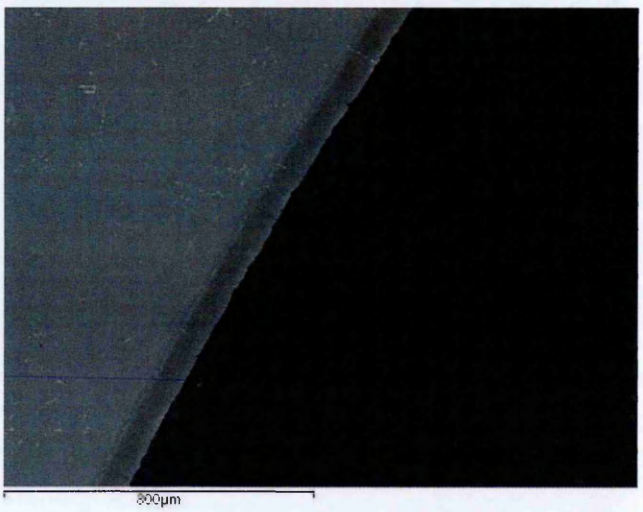

Figure 12-6: Pressure Surface

Figure 12-7: Pressure Surface near the Trailing Edge

By reducing the current density, a much more uniform coating was achieved although this thickness was approximately half of that needed for aerospace applications (40 microns as evident in Figure 12-8). Further trials are needed to optimise the process and create a more uniform, thicker coating. The possible use of auxiliary anodes can be used to locally reduce the deposition rate. However, such columnar deposits are not as detrimental as initially thought, as the 'enhanced diffusion' due to the exothermic reaction process helps remove the columnar boundaries and create a dense coating.

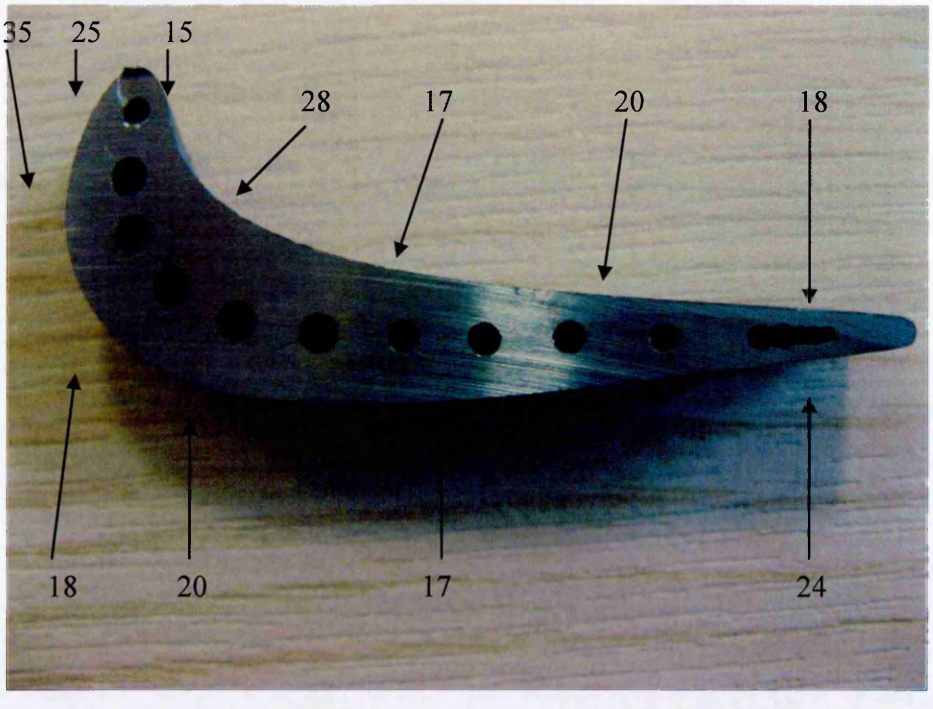

Figure 12-8: Coating Thickness of a GTD111 Turbine Blade with ILAl (thickness in microns)

The columnar nature of the deposits observed on the turbine blades also agree with those results shown in Figure 4-13 to Figure 4-16 where current density was shown to effect the final microstructure. This is consistent with observations of Jianga *et al.*[137] who noted that when using the IL TMPAC (trimethylphenylammonium chloride with $AlCl_3$) and higher densities powdery coatings resulted. Hence it is postulated that a change in nucleation may occur at higher densities because the limit of mass transportation has been met in the IL and there is therefore a depletion of aluminium surrounding the cathode. Jianga states that 'low nuclei densities may represent only the active sites available for nuclei formation and not the number of sites available according to the total of atomic nuclei'.

Having coated the blade with ionic liquid plated aluminium it was found on sectioning that the blades supplied were already aluminised (clearly seen in Figure 12-9 for the trailing edge of a reference blade section). By mounting and sectioning a reference blade, it is possible to analyse the chemical composition and thicknesses used for a CVD deposited aluminised coating within the power generation industry.

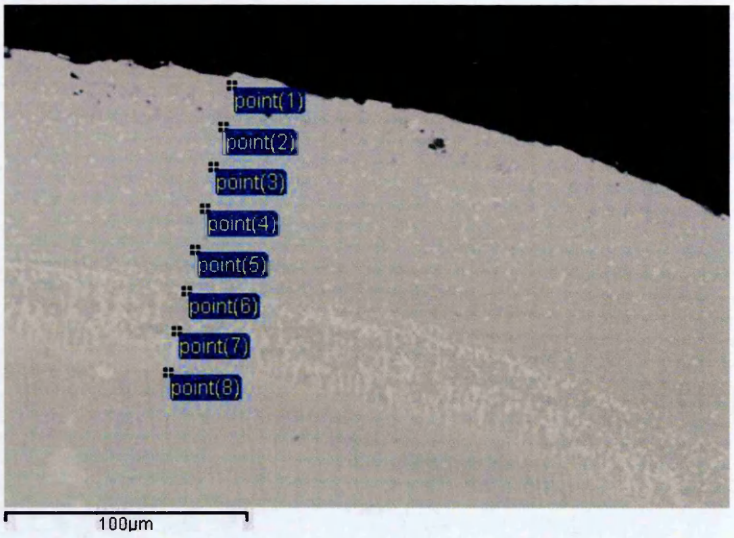

Figure 12-9: Platinum aluminised Coating on the as-received GTD111 Blade - Trailing Edge

Table 12-1: Chemical Analysis of Points Shown in Figure 12-9(%at)

Spectrum	Al	Ti	Cr	Co	Ni	Mo	Ta	W	Pt
point(1)	35.4	2.4	5.0	5.8	47.5				3.9
point(2)	36.0	2.7	4.3	6.1	47.1				3.8
point(3)	34.7	3.0	4.6	6.2	47.8				3.8
point(4)	34.4	3.6	4.8	6.2	47.2				3.8
point(5)	34.6	3.6	5.1	5.9	47.4				3.5
point(6)	19.1	6.0	33.3	5.2	30.3		2.2	1.7	2.3
point(7)	31.3	4.7	8.4	7.0	45.6				3.0
point(8)	8.9	7.0	20.5	10.3	49.1	2.2		2.1	

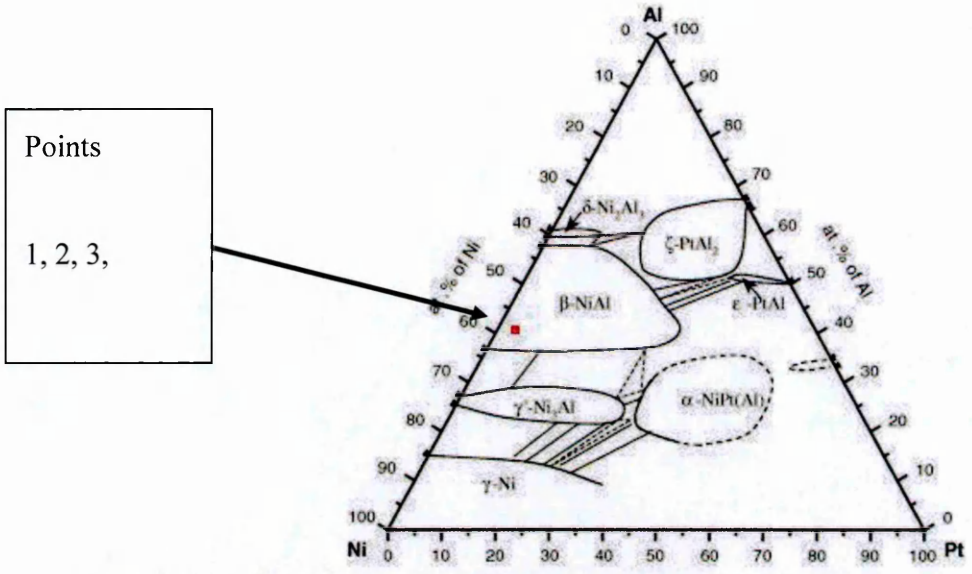

Figure 12-10: NiPtAl Ternary Phase Diagram showing the Composition from Table 12-1

As can be seen from the ternary diagram in Figure 12-10 and Table 12-1, the entire trailing edge coating is extremely homogenous with β-NiAl-phase being measured throughout the coating.

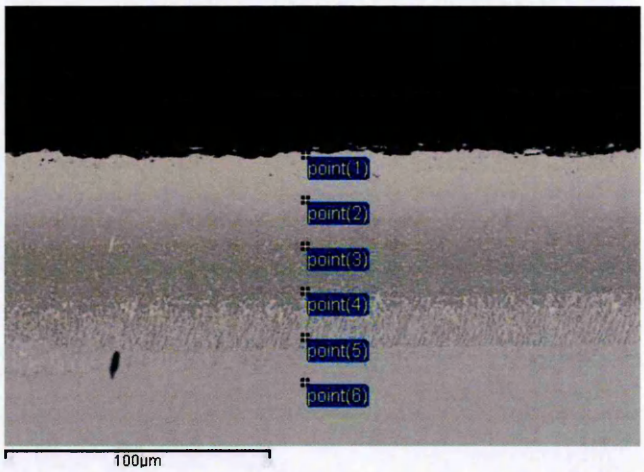

Figure 12-11: As-received Platinum Aluminised Turbine Blade

Table 12-2: Chemical Composition of Platinum Aluminised Blade (pressure side) as-received from NP (at%)

Spectrum	Al	Si	Ti	Cr	Co	Ni	W	Pt
point(1)	42.4			3.4	5.3	39.2		9.6
point(2)	45.2		0.6	2.0	5.4	42.0		4.8
point(3)	42.4		1.7	3.7	6.5	44.9		0.8
point(4)	34.1		4.2	15.7	7.2	38.3	0.5	
point(5)	13.4	1.5	6.6	21.5	7.2	48.0	1.9	
point(6)	7.6	1.6	5.7	19.2	10.3	53.8	1.8	

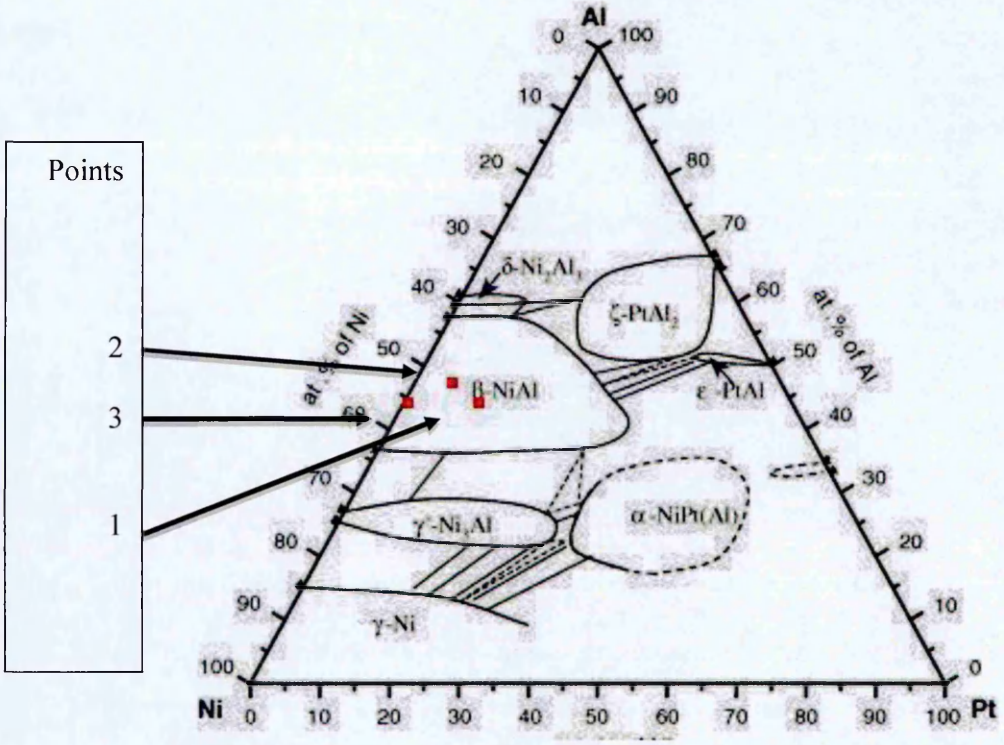

Figure 12-12: Ternary Phase Diagram Depicting Compositions from Table 12-2

Figure 12-12 and Table 12-2 shows that commercial PtNiAl coatings contain the desirable β-phase throughout the diffused coating layer. It should be noted that there is a slight variation in the platinum content of this blade coating compared to the trailing edge. The thicknesses measured were approximately 123 microns for the leading, trailing and suction side, whereas the pressure side measured 100 microns. This is considerably thicker than is used in standard aerospace engines. However, it means now that the thicknesses obtained in Figure 12-2 is almost ideal for that used by NP. To ensure a greater uniformity it would be proposed that the current density is reduced and the plating time extended.

12.4 Gas Use and Industrialisation

The last part investigated of industrialisation was the price of consumables i.e. argon gas. Argon gas is used at Cranfield to minimise the water content presence within the environment chamber. The majority of work done in thesis conducted with high purity (N6.0) Ar which has a purity of 99.9999%. However, 'Pureshield' Ar with a purity of 99.998 was also used successfully in this investigation with a water content below 0.8ppm. One downside of using the lower grade argon was the time to remove water content, which was significantly longer.

Table 12-3: Argon Purity and Cost Comparison

Name	Purity (%)	Cost(£)
High Purity (N6.0)	99.9999	286.77
Research	99.9995	224.74
Zero Grade	99.999	35.79
Pureshield (N4.8)	99.995	14.78

These prices (Figure 12-3) represent the cost for a single 45l bottle of Argon gas. The table above shows that industrially, considerable savings could be made if Pureshield argon was used rather than High Purity argon. Additionally, high purity Al wire (99.9%) has been used for constructing the anodes. Work by Kamavaram[181] has shown that Al from various sources, with varying purities, can be used in conjunction with IL and forms a pure Al coating free from contaminants. Thus, less pure aluminium could be used commercially to deposit ionic liquid processed aluminide coatings.

12.5 Conclusions of Industrialisation

Taking into account the whole of this thesis there are a number of results which suggest how this method could be productionised:

- The ability to form desirable β-NiAl coatings from ionic liquid plated aluminium
- Complex parts (blades) and large components can be plated
- The possibility of increasing the current density but with some sacrifice in deposit efficiency
- That IL can be reused after removal of any oxygen and addition of aluminium chloride salt
- Cheaper inert gas provides a workable alternative to deposit Al coatings
- ILAl can be anodised, therefore it should be possible to easily create hard dense and decorative coatings (Appendix: Anodising ILAl page 201)

Comparing the heat treating of ILAl to the standard CVD process heat treatments, it has been shown:

- Lower temperature heat treatments are possible
- No need for a separate retort

- Proven to be able to form β-NiAl within the preheating stage of an EBPVD coater – no need for a separate heat treatment step

One further point, related to environment and cost issues during processing:

- A multiple use system (CVD powders are single use) and as only Al_2Cl_7 is depleted it should be theoretically possible to be recycled and reused

13 Conclusions

- Aluminium can be plated on to nickel-based superalloys using ionic liquids and then heat treated to form a nickel aluminide coating.
- ILAl can be heat treated with a new novel low temperature regime, or with traditional heat treating parameters to form β-NiAl coatings.
- The ICON process is a new, novel process which utilises temperatures above and below the melting point of aluminium to form the β-NiAl coating – its mechanism of action is complex and involves the interaction of diffusion processes and exothermic reaction synthesis:
    - Finite element analysis has demonstrated that the ICON process does not form β-NiAl coatings as a result of simple diffusion kinetics.
    - Initial reactions occur at the atomic level with Ni_3Al forming and initiating an exothermic reaction
    - The formation of Ni_3Al initially prevents Al diffusing into the nickel substrate, enabling Ni to diffuse outward into the aluminium coating
    - The Ni diffusing through reacts with the Al to form atomic layers of Al_3Ni_5, NiAl, Ni_2Al_3 and finally $NiAl_3$ – the first stage of the ICON process. The formation of $NiAl_3$ is another exothermic reaction driver enabling more reactions to occur with nickel moving outward and Al moving inwards.
    - Heating to 820°C results in further exothermic reactions promoting transformation to Ni_2Al_3 then to NiAl
    - The transition from Ni + 3Al to $NiAl_3$ and $NiAl_3$ to Ni_2Al_3 and NiAl involves some transient liquid phase formation and diffusion within the liquid phase enhances elemental transport.
- Heat treating using standard CVD derived parameters produces interesting results. Using HTLA thermal process routes produces coatings that look appear like LTHA, CVD deposited coatings. The mechanism of action is similar to that of ICON but requires solid-state diffusion to produce the final β-NiAl coating
- Using aluminium, deposition from ionic liquids provide an alternative method of producing bond coats that are at least comparable to traditional CVD

techniques but is considered to be a much cheaper manufacturing route, because:

  - Ionic liquids are reusable rather than the one-use CVD packs
  - No need for a CVD retort
  - Theoretically it is possible use any grade of aluminium for the anode
  - Conventional rather than high purity Ar or N_2 gas can be used as long as water content is below 5ppm

- It is feasible to deposit aluminium from ionic liquids within a production environment.
  - The ability to electroplate turbine blades and large components has been demonstrated
  - It is possible to anodise electroplated components
- It is possible to form β-NiPtAl coatings once Pt is enriched with the surface of the nickel superalloy and then electroplated with aluminium and heat treated using the ICON process.
- Platinum plating from the 5Q salt is very difficult; the P salt is a proven, reproducible method and should be used in future.
- The ICON heat treatment process offers a number of advantages:
  - Low temperature intermetallic coating formation – therefore no need for a recovery heat treatment process.
  - Smaller IDZ therefore greater Al reservoirs.
  - More homogenous coatings – little concentration gradient through the coating.
  - No visible grit line – greater mechanical bond strength.
- Cyclic oxidising ILAl, heat treated with CVD type parameters, gives similar results to traditionally made CVD aluminide coatings and may even offer longer lifetimes.

14 Summary of PhD

Goal from Thesis Aims	Achieved	Comments
Deposit Pt from '5Q' salt	Yes	Reproducibility of deposit was difficult to control
Improved performance of '5Q' Pt salt over deposits made with the P salt for bond coat applications	No	Reproducibility of deposit was difficult to control
Deposit Al from ionic liquids	Yes	Able to deposit from both BMIM and EMIM but limited to current density employed
Deposit Al on an industrial scale	Yes	Able to deposit onto turbine blades and uses more cost effective gasses for the inert atmosphere
Heat treat deposited Al to form a novel bond coat	Yes	Possible to form desirable bond coat chemistry with 2 different heat treatment regimes
Comparative to traditionally produced CVD bond coats	Yes	Using a CVD type heat treatment regime it was possible to recreate CVD 'like' coating chemistry
Able to form bond coats on an industrial scale	No	Reference blades supplied were already aluminised. Theoretically possible though
Able to use a low temperature heat treatment regime to form desirable coatings	Yes	Produces coatings with a higher Al reservoir than traditional coatings

15 Future Work:

The work conducted within this thesis has highlighted a number of possible areas that could be researched further to either improve understanding of the process or to improve coating performance. They can be classified into 4 different categories: 1) Electroplating, 2) Heat treatment regimes, 3) Modelling and 4) Cyclic oxidation. Each are expanded upon within the chapter.

15.1 Electroplating:

15.1.1 Aluminium from Room Stable Ionic Liquids

The largest hindrance to industrialisation of electroplating from ionic liquids is the reaction of the liquid to atmosphere. This has been highlighted within this report due to the effect of water on aluminium deposits. Air- and water-stable ionic liquids for the deposition of aluminium would improve industrialisation, allow larger parts to be manufactured more easily, increase throughput and reduce the overall cost. It has been reported previously that this should be possible, but when it was replicated by INSTM as part of the IOLISURF project it could not be achieved.

15.1.2 Forming New and Novel Aluminides

It has been shown within this thesis that it is possible to form nickel aluminides by the deposition of Al on Ni-based superalloys. Titanium aluminides are desirable within the aerospace industry but are traditionally very hard to form by CVD due to the tenacious oxide formed. It is believed that by preparing the titanium within the environmental chamber and then depositing Al that it should be possible to promote the formation of Ti_xAl_y intermetallics.

15.1.3 Depositing other Metals from Ionic Liquids

Ti is an interesting metal within the aerospace industry. If it was possible to repair Ti alloy defects by electroplating, then it would save scrapping Ti blades, which have defects in them. Additionally Mg cannot be plated from aqueous solutions, and could be a new novel coating or repair material to be plated. Cr is an interesting element to note, as Cr plating is used throughout industry. It is believed that IL Cr has never been

used previously to 'chromise' a surface; therefore further work on this would be of interest and offer an alternative perspective than the current CVD process route.

15.1.4 Addition of Other Elements

NiAl coatings have been shown to have improved oxidation with the addition of oxygen active elements such as Zr and Hf. It could be possible to add small quantities of anhydrous $ZrCl_2$ and/or HfCl to BMIM Al_2Cl_7 to form Al(Zr/Hf) deposits which when heat treated to form more oxygen protective β-NiAl coating.

15.1.5 Platinum P salt

Depositing platinum using the P salt. This has been used within aerospace for a number of years and would appear to be simpler and more reproducible than that of the Q salt. It could therefore be possible to create NiPtAl coatings, solely via electroplating, once electrodeposition of aluminium from ionic liquids is industrialised.

15.1.6 Thin Layer Reaction Synthesis

It can be seen throughout the literature and within this thesis that the formation of most aluminides is generally exothermic in nature. It was shown within 9.1.1 that RhAl was extremely exothermic is nature (202KJ/mol). It may be possible to use this layer to initiate formation of β-NiAl at even lower temperatures or even eliminate/hinder the formation of rhenium aluminides in Re containing superalloys.

15.2 Heat Treatment Regimes

15.2.1 Greater understanding of the ICON process

The mechanism of action of this process is still only a hypothesis. It is recommended that the process is stopped at 50°C intervals between 450 – 800°C all for 1 minute then sectioned and analysed under the SEM and/or the TEM to fully elucidate the mechanism. It is envisaged that the TEM would be the most helpful as the images produced provide much more detail together with crystallographic information, but the time needed to prepare and analyse samples may limit the number of systems that can be studied.

15.2.2 Greater understanding of Heat Treating using CVD Derived Parameters

Like the ICON process, the heat treatment should be stopped during processing to analyse the diffusion mechanisms, when processing at the more elevated heat treatment temperatures, used in conventional CVD aluminide processing.

15.2.3 Modification of ICON for Re Containing Alloys

It appears that Re interferes with the ICON processes. It can be seen from the DSC plot that exothermic reactions occur over a range of temperatures. Therefore, if the temperature ramp rate within the furnace through the reaction temperatures was to reduce from 10°C/min to either 5°C/min or 2°C/min it may be possible to increase the energy created within the process and therefore induce and drive β-NiAl formation, even when adverse reactions limit the extent of β-NiAl formation.

15.3 Modelling

15.3.1 Modelling the Influence of an Anodising Treatment on TBC Spallation

It has been shown within this work that it is possible to anodize both ILAl and β-NiAl coatings from ionic liquids (Anodising ILAl page 201). Numerous authors have noted that, when the TGO exceeds 6-7um, spallation of the TBC normally results. Therefore it is proposed to model this phenomenon with the oxide layer first formed by anodizing the bondcoat and comparing oxide growth rates with those conventionally produced.

15.4 Cyclic Oxidation

15.4.1 Cyclic Oxidation

The accepted method for testing of bond coats is via cyclic oxidation. As this is a completely new method of manufacturing then evidently considerable cyclic oxidation work will be needed to validate the process over arrange of anticipated service temperatures. The largest problem is the effect of Re on the process itself and therefore this prevents direct comparisons to the CVD type of coating. Comparisons of the ICON process against ILAl heat treated with CVD type parameters and reference CVD coatings on alloys such as IN738 would provide further insight. If the ICON process can be modified to work on Re containing alloys then it allows the

process to be used on the proposed third and fourth generation superalloys which would increase the potential market applications greatly.

15.5 Heat Treating Non-Electroplated Aluminium Deposits

To the end of this study, aluminium was deposited via argon-shrouded plasma spraying at atmospheric pressure to approximately 40 microns thickness. The deposits were then heat treated with either CVD derived parameters (after NP) or the ICON heat treatment. The micrographs in (Appendix: Heat Treating Other Al Deposits page 202) show that both heat treatments could be an alternative method of forming NiAl coatings – but further work would be needed to explore this new methodology.

16 References

1. Sims, C.T. (1972), *The Superalloys*, John Willey & Sons, USA.
2. Erickson. G. (inventor) Cannon-Muskegon, (Nov 22, 1994), *Single Crystal Nickel-Based Superalloy*. 5366695.
3. Nicholls, J.R. (2000), 'Designing Oxidation-Resistant Coatings', *Journal of Materials,* Vol. 52, No. 1, pp. 28-35.
4. Goward, G.W. (1988), 'Progress in Coatings for Gas Turbine Engines', *Surface and Coatings Technology,* Vol. 108-109, pp. 79-79.
5. Chen, J.H. and Little, J.A. (1997), 'Degradation of the Platinum Aluminide Coating on CMSX4 at 1100°C', *Surface and Coatings Technology* , Vol. 92, pp. 69-77.
6. Krishna, G.R. , Das, D.K., Singh, V. and Joshi, S.V. (1998), 'Role of Pt Content in the Microstructural Development and Oxidation Performance of Pt–Aluminide Coatings Produced Using a High-Activity Aluminizing Process', *Materials Science and Engineering,* Vol. A251, pp. 40-47.
7. IOLISURF available at: http://www.iolisurf.com/ (accessed 2007).
8. Westbrook, J.H. and Fleischer, R.L. (2000), Intermetallic Compounds, Volume 2 - Basic Mechanical Properties and Lattice Defects of Intermetallic Compounds, John Wiley & Sons,
9. Jianga, T., Chollier Brymb, M.J., Dubéb, G., Lasiaa, A. and Brisarda, G.M. (2006), 'Electrodeposition of Aluminium From Ionic Liquids: Part I—Electrodeposition and Surface Morphology of Aluminium From Aluminium Chloride (AlCl3)–1-Ethyl-3-Methylimidazolium Chloride ([EMIm]Cl) Ionic Liquids', *Surface and Coatings Technology,* Vol. 201, No. 1-2, pp. 1-9.
10. Sims, C.T., Stoloff, N.S. and Hagel, W.C. (1987), *Superalloys*, John Wiley and Sons,
11. Hiller,.D. Defect Energies and Deformation Mechanisms of Single Crystal Superalloys PhD Thesis, Cambridge University. 1984.
12. Sims, C.T. (1972), *Superalloys II*, John Wiley & Sons, USA.
13. Kobayshi, T. , Koizumi, Y., Yokoawa, T., Osawa, M., Harada, H. and Maruko, T. (2005), 'Development of 4th Generation SC Superalloys Without Re', *Nippon Kinzoku Gakkaishi* , Vol. 69, No. 2, pp. 272-275.
14. Threadgill, P. *Intermetallics. Nickel Aluminide Coatings Source: Materials World, Vol. 3, 1995, pp. 187-88,* available at: http://www.azom.com/details.asp?ArticleID=186 (accessed 24/10/05).
15. Okamoto, H. and (ed) (2000), 'NiAl Phase Diagram', in Okamoto, H. *Phase Diagrams for Binary Alloys : Desk Handbook* (2nd edition), ASM International, London, pp. 681-682 .
16. Pichoir, R. (1978), 'Aluminide Coatings on Nickel or Cobalt-Base Superalloys', in D. Coutsouradis *High Temperature Alloys for Gas Turbines*, Applied Science, London,
17. Brumm, M.W., Grabke, H.J. and Wagemann, B. (1994), 'The Oxidation of NiAl-III. Internal and Intergranular Oxidation', *Corrosion Science,* Vol. 36, No. 1, pp. 37-53.

18. Brumm, M.W. and Grabke, H.J. (1992), 'The Oxidation Behaviour of NiAl-I. Phase Transformations in the Alumina Scale During Oxidation of NiAl and NiAl-Cr Alloys', *Corrosion Science,* Vol. 33, No. 11, pp. 1677-1690.

19. Mu, N., Liua, J., Byeona, J.N., Sohna, Y.H. and Navab, Y.L. (2004), 'Long-Term Oxidation and Phase Transformations in Aluminized CMSX-4 Superalloys', *Surface and Coatings Technology,* Vol. 188-189, pp. 27-34.

20. He, J.L., Yua, C.H., Leyland, Wilson, A.D. and Matthews, A. (2002), 'A Comparative Study of the Cyclic Thermal Oxidation of PVD Nickel Aluminide Coatings', *Surface and Coatings Technology,* Vol. 155, No. 1, pp. 67-69.

21. Prescott, R. and Graham, M.J. (1992), 'The Formation of Aluminium Oxide Scales on High-Temperature Alloys', *Oxidation of Metals,* Vol. 38, No. 3-4, pp. 233-254.

22. Pint, B.A. (2004), 'The Role of Chemical Composition on the Oxidation Performance of Aluminide Coatings', *Surface and Coatings Technology,* Vol. 188-189, pp. 71-78.

23. Gleeson, B., Wang, W., Hayashi, D. and Sordelet, D. (2004), 'Effects of Platinum on the Interdiffusion and Oxidation Behaviour of NiAl Based Alloys', *Material Science Forum*, Vol. 461-464, pp. 213-222.

24. Haynes, J.A. , Pint, B.A., Zhang, Y. and Wright, I.G. (2007), 'Temperature Effects on the Cyclic Oxidation Behavior of Beta-NiAl, Beta-NiPtAl and Gamma-Gamma Prime NiPtAl Coatings on Various Superalloys Comparison of the Cyclic Oxidation', *Surface & Coatings Technology (2007),* Vol. 202, No. 4-7, pp. 730-734.

25. Haynes, J.A. , Zhang, Y., Cooley, K.M., Walker, L., Reeves, K.S. and Pint, B.A. (2004), 'High-Temperature Diffusion Barriers for Protective Coatings', *Surface and Coatings Technology,* Vol. 188-189, pp. 153-157.

26. Li, M.J., Sun, X.F., Guan, H.R., Jiang, X.X. and Hu, Z.Q. (2004), 'The Degradation of (Ni,Pd) Al Coatings on Superalloy IN738 During Isothermal Oxidation', *Surface and Coatings Technology,* Vol. 185, No. 2-3, pp. 172-177.

27. Hamadi, S., Bacos, M.P., Poulain, M., Zanna, S., Seyeux, A., Maurice, V. and Marcus, P. (2009), 'Oxidation of a Zr-Doped NiAl Bondcoat Thermochemically Deposited on a Nickel-Based Superalloy', *Materials at High Temperatures,* Vol. 26, No. 2, pp. 195-198.

28. Veal, B.W., Paulikas, A.P., Gleeson, B. and Hou, P.Y. (2007), 'Creep in Alpha-Al2O3 Thermally Grown on NiAl and NiAlPt Alloys', *Surface and Coatings Technology*, Vol. 202, pp. 608-612.

29. Saint-Ramond, B., Carlin, M., Silva, M. and Nicholls, J.R. (2004), 'Low Mass Bondcoats for Robust Thermal Barrier Coatings', *Materials Science Forum,* Vol. 461-464, pp. 265-267.

30. Nicholls, J.R., Winstone, M.R., Deakin, M.J., and Kerry, S. (1996), 'A Platinum Aluminide Coating Diffusion Barrier for the Oxidation Protection of Titanium and Titanium Intermetallic Coatings', Annheim, California, The Minerals, Metals and Materials Society, pp. 199-208.

31. Carlin, M. Design, Manufacture and High Temperature Behaviour of A-Phase Bondcoat for Thermal Barrier Coating. PhD Thesis 2007. Cranfield University.

32. Nicholls, J.R., Long, K.A. and Simms, N.J. (2010), 'Diffusion Coatings', *Shreir Corrosion - Prepublication*

33. Van Aller, T. (inventor) General Electric, (1915), USA. US Patent 1155974.

34. Nichols, E.S., Buger, J.A. and Hanink, D.K. (1965), *Mechanical Engineering,* pp. 52-56.

35. Seelig, R.P. and Steuber, R.J. (1978), 'High Temperature Resitant Coatings for Superalloys', *High Temperature-High Pressure,* Vol. 10, pp. 207-213.

36. Goward, G.W. and Boone, D.H. (1971), ' Mechanisms of Formation of Diffusion Aluminide Coatings on Nickel-Base Superalloys ', *Journal of the Oxidation of Metals,* Vol. 3, pp. 475-495.

37. Nicholls, J.R. (1995), 'High Temperature Coating' Lecture Notes'' Chalmers Technical University, Sweden',.

38. Janssen, M.M.P. and Rieck, G.D. (1967), 'Reaction Diffusion and Kirkendall Effect in the Nickel Aluminide System', *Trans. of the Metallurgical Society of AIME,* Vol. 239, pp. 13721385.

39. Levine, S.R. and Caves, R.M. (1974), 'Thermodynamics and Kinetics of Pack Aluminide Coating Formation on IN-100', *J. Electrochem. Soc.,* Vol. 121, No. 8, pp. 1051-1064.

40. Angenete, J. and Stiller, K. (2002), 'Comparison of Inward and Outward Grown Pt Modified Aluminide Diffusion Coatings on a Ni Based Single Crystal Superalloy', *Surface and Coatings Technology,* Vol. 150, pp. 107-118.

41. Das, D.K., Singh, V. and Joshi, S.V. (2000), 'The Cyclic Oxidation Performance of Aluminide and Pt-Aluminide Coatings on Cast Ni-Based Superalloy CM-247', *The Journal of Minerals, Metals & Materials Society,* Vol. 52, No. 1, available at http://www.tms.org/pubs/journals/JOM/0001/Das/Das-0001.html. (accessed 2010)

42. Angenete, J. , Stiller, K. and Bakchinova. E (2004), 'Microstructural and Microchemical Development of Simple and Pt-Modified Aluminide Diffusion Coatings During Long Term Oxidation at 1050 °C', *Surface and Coatings Technology,* Vol. 176, pp. 272-283.

43. Purvis, A.L. and Warnes, B.M. (2001), 'The Effects of Platinum Concentration on the Oxidation Resistance of Superalloys Coated With Single-Phase platinum Aluminide', *Surface and Coatings Technology* , Vol. 146-147, pp. 1-6.

44. Smith, J.S. and Boone, D.H.(1990) 'Platinum Modified Aluminides-Present Day Status ', Proceedings from *Gas Turbine and Aeroengine Congress and Exposition,* Brussels, Belgium,

45. Meier, G.H. and Pettit, F.S. (1989), 'High-Temperature Corrosion of Alumina-Forming Coatings for Superalloys', *Surface and Coatings Technology,* Vol. 39-40, No. 1, pp. 1-17.

46. Cocking, J.L., Johnston, G.R. and Richards, P.G. (1985), 'Protecting Gas Turbine Components'. *Platinum Metals Review,* Vol. 29, No. 1, pp. 17-26.

47. Tawancy, H.M. and Abbas, N.M. (1991), 'Role of Platinum in Aluminide Coatings', *Surface and Coatings Technology,* Vol. 49, No. 1-3, pp. 1-7.

48. Tawancy, H.M., Sridhar, N., Abbas, N.M. and Rickerby, D. (1995), 'Comparative Thermal Stability Characteristics and Isothermal Oxidation Behavior of an Aluminized and a Pt-

Aluminized Ni-Base Superalloy', *Scripta Metallurgica Et Materialia,* Vol. 33, No. 9, pp. 1431-1438.

49. Monceau, D., Crabos, F., Malie, A. and PieraggiI, B. (2001), 'Effects of Bond-Coat Preoxidation and Surface Finish on Isothermal and Cyclic Oxidation, High Temperature Corrosion and Thermal Shock Resistance of TBC Systems', *Materials Science Forum* , Vol. 369-372, pp. 607-614.
50. Vialus, N. and Monceau, D. (2006), 'Effect of Pt and Al Content on the Long-Term,High Temperature Oxidation Behavior and Interdiffusion of a Pt-Modified Aluminide Coating Deposited on Ni-Base Superalloys', *Surface and Coatings Technology,* Vol. 201, pp. 3846-3851.
51. Felten, E.J. and Pettit, F.S. (1976), 'Development, Growth, and Adhesion of Al_2O_3 on Platinum-Aluminium Alloys', *Oxidation of Metals,* Vol. 10, No. 3, pp. 189-223.
52. Fountain, J.G., Golightly, F.A., Stott, F.H. and Wood, G.C. (1976), 'The Influence of Platinum on the Maintenance of Alpha-Al_2O_3 As a Protective Scale', *Journal of Oxidation of Metals,* Vol. 10, No. 5, pp. 341-345.
53. Hou, P.Y. and McCarty, K.F. (2006), 'Surface and Interface Segregation in B-NiAl With and Without Pt Addition', *Scripta Materialia,* Vol. 54, No. 5, pp. 937-941.
54. Zhang, Y., Haynes, J.A., Lee, W.Y., Wright, I.G., Pint, B.A., Cooley, K.M. and Liaw, P.K. (2001), ' Effects of Pt Incorporation on the Isothermal Oxidation Behavior of Chemical Vapor Deposition Aluminide Coatings', *Metallurgical and Materials Transactions A,* Vol. 32, No. 7, pp. 1727-1741.
55. Jiang, C., Sordelet, D.J. and Gleeson, B. (2006), 'Effects of Pt on the Elastic Properties of B2 NiAl: A Combined First-Principles and Experimental Study', *Acta Materialia,* Vol. 54, pp. 2361-2369.
56. Wing, R.G. and McGill, I.R. (1981), 'The Protection of Gas Turbine Blades', *Platinum Metals Review,* Vol. 25, No. 3, pp. 94-105.
57. Mevrel, R., Duret, C. and Pichoir, R. (1986), 'Pack Cementation Process', *Materials Science and Technology,* Vol. 2, pp. 201-206.
58. Silva, M. (2005). Manufacture and Characterisiation of Ni-Al Intermetallic Coatings by Exothermic Reaction Synthesis. MSc Thesis Cranfield University.
59. Fisher, G. A. (1998) The Optimisation of Bondcoat Oxides for Improved Thermal Barrier Coating Adhesion. PhD Thesis. Cranfield University.
60. Ellingham, H.J.T. (1944), 'Reducibility of Oxides and Sulphides in Metallurgical Processes', *Journal of the Society of Chemical Industry, Transactionas and Communications,* Vol. 63, pp. 125-133.
61. TMS *Ellingham Diagram,* available at: http://www.tms.org/pubs/journals/JOM/0911/fig3.jpg (accessed 2009).
62. Smialek J.L. and Meier, G. (1987), 'High Temperature Oxidation', in Simms, C. T. et al. *In Superalloys II High Temperature Materials for Aerospace and Industrial Power.*, Wiley, Weineim,

63. Grabke, H.J. and Schulze, M. (1999), 'Oxidation of NiAl and FeAl', *Intermetallics,* Vol. 7, No. 10, pp. 1153-1158.

64. Grabke, H. J. Oxidation of Aluminides. (1997) Proceedings for the 4th International Symposium on the High Temperature Corrosion and Protection of Materials. 1, 149-167. Trans Tech Publications.

65. Angenete, J. , Stiller, K. and Langer, V. (2003), 'Oxidation of Simple and Pt Modified Aluminide Diffusion Coatings on Ni Based Superalloys 1. Oxide Scale Microstructure.', *Oxidation of Metals,* Vol. 60, No. 1-2, pp. 47-82.

66. Shanker, S. and Seigle, L.L. (1978), ' Interdiffusion and Intrinsic Diffusion in the NiAl (Delta) Phase of the Al-Ni System.', *Metallurgical and Materials Transactions A,* Vol. 9, No. 10, pp. 1467-1476.

67. Kim, H.J. and Walter, M.E. (2003), 'Characterization of the Degraded Microstructures of a Platinum Aluminide Coating', *Materials Science and Engineering,* Vol. A3560, pp. 7-17.

68. Spitsberg, I. and More, K. (2006), 'Effect of Thermally Grown Oxide (TGO) Microstructure on the Durability of TBCs With PtNiAl Diffusion Bond Coats', *Materials Science and Engineering: A,* Vol. 417, No. 1-2, pp. 322-333.

69. Hou, P.Y. and Tolpygo, V.K. (in press), 'Examination of the Platinum Effect on the Oxidation Behavior of Nickel-Aluminide Coatings', *Surface and Coatings Technology,*

70. Chen, M.W., Glynn, M.L., Ott, R.T., Hufnagel, T.C. and Hemker, K.J. (2003), 'Characterization and Modeling of a Martensitic Transformation in a Platinum Modified Diffusion Aluminide Bond Coat for Thermal Barrier Coatings', *Acta Materialia,* Vol. 51, No. 14, pp. 4279-4294.

71. Zhang, Y., Haynes, J.A., Pint, B.A., Wright, I.G. and Lee, W.Y. (2003), 'Martensitic Transformation in CVD NiAl and (Ni,Pt)Al Bond Coatings ', *Surface and Coatings Technology,* Vol. 163-164, pp. 19-24.

72. Klc, P. and Pelachová, T. (1997), 'Ni–Al Intermetallic Alloy at the Thermocycling Conditions', *Czechoslovak Journal of Physics,* Vol. 47, No. 7, pp. 739-745.

73. Sordelet, D.J., Besser, M.F., Ott, R.T., Zimmerman, B.J., Porter, W.D. and Gleeson, B. (2007), 'Isothermal Nature of Martensitic Formation in Pt-Modified Ni-Al Alloys', *Acta Materialia,* Vol. 55, pp. 2433-2441.

74. Bellis, M. *The History of Electroplating,* (availible at ttp://inventors.about.com/od/estartinventions/a/Electroplating.htm (accessed 2006).

75. Nagy, Z. *Electroplating,* available at: http://electrochem.cwru.edu/ed/ency cl/art- e01-electroplat.htm (accessed 2006).

76. Graham, A.K (1968), *Electroplating Engineering Handbook*, 2nd Edition. Reinhold Press, New York. ISBN: 69-9723

77. Gabe, D.R. (1978), Principles of Metal Surface Treatment and Protection , Pergamon Press, UK.

78. Clark, J. (2002), *The Electrochemical Series,* http://www.chemguide.co.uk/physical/redoxeqia/ ecs.html (accessed 2006).

79. Pfanhauser. W (1949), in ' *Galvanotechnik'*, Akademishce Vanlagsgesellschaft, Lepzig, pp. 870.(in German)
80. Bottger. R (1878), Platinum Plating *.J. Franklin Inst.*,Vol 106..No 5. pp. 348.
81. McMillian, W.G. and Cooper, W. (1910), 'A Treatise on Electro Metallurgy ', Charles Griffin and Co, London, pp. 239.
82. Grube, G.B.D. (1931), The Electrochemical Behaviour of Platinum in HCl Solutions. *Z. Elektrochem,* Vol. 37, pp. 307.
83. Atkinson, R.H. (1959), 'Electrodeposition of Platinum From Chloroplatnic Acid ', *Trans. Inst. Metal Finish,* Vol. 37, pp. 7-16.
84. Keitel, W. Zschiegne, H.E.(1931), *Trans. Electrochem. Soc,* Vol. 59, pp. 273.
85. Lacroix, R.B.CH. (inventor) (1967), France. Patent no: 1356333.
86. G. Hänsel and H. Resch, "Untersuchungen über die Einwirkung von Aminen, Aminosäuren, Sulfonsäuren und Polyacrylsäureamid auf die Elektrokristallisation des Kupfers aus schwefelsauren Elektrolyten," Metalloberfläche, 21 (1967), pp. 268–272.
87. Hopkin, N.Wilson, L.F. (1960), Bright Platinum Plating. *Platinum Metals Review* , Vol. 4, No. 2, pp. 56.-58
88. Powel, A.R.S.A.W. (inventor) (1931), Britain. Patent 363569.
89. Baumgartner, M.E. (1988), 'The Electrodeposition of Platinum and Platinum Alloys', *Platinum Metals Review,* Vol. 32, No. 4, pp. 188-197.
90. Le Penven, R., Levason, W. and Pletcher, D. (1992), 'Studies of Platinum Electroplating Baths Part I: The Chemistry of a Platinum Tetrammine Bath', *Journal of Applied Electrochemistry,* Vol. 22, No. 5, pp. 415.
91. Basirun1, W.J., Pletcher, D. and Saraby-Reintjes, A. (1996), 'Studies of Platinum Electroplating Baths Part IV: Deposits on Copper From Q Bath', *Journal Applied Electrochemistry,* Vol. 26, No. 8, pp. 873-880.
92. Wassercheild, P. and Welton, T.e. (2003), *Ionic Liquids in Synthesis* , Wiley-vch,
93. Oster, E.. (inventor) General Electric Co, (1969), US. Patent 3,423,228.
94. Wilkes, J.S. (2002), 'A Short History of Ionic Liquids—From Molten Salts to Neoteric Solvents', *Green Chem.,* Vol. 4, pp. 73-80.
95. Holbrey, J.R. and Seddon, K.R. (1999), 'Ionic Liquids', *Clean Products and Processes,* Vol. 1, pp. 223-236.
96. Barisci, J.N., Wallacea, G.G., MacFarlaneb, D.R. and Baughman, R.H. (2004), 'Investigation of Ionic Liquids As Electrolytes for Carbon Nanotube Electrodes', *Electrochemistry Communications,* Vol. 6, No. 1, pp. 22-27.
97. Endres, F. (2002), 'Review: Ionic Liquids: Solvents for the Electrodeposition of Metals and Semiconductors', *J. ChemPhysChem,* Vol. 3, pp. 144-154.
98. Marsh, K.N., Boxall, R. and Lichtenthaler, R. (2004), 'Room Temperature Ionic Liquids and Their Mixtures - A Review', *Fluid Phase Equilibria,* Vol. 219, pp. 93-98.

99. Carda-Broch, S., Berthod, A. and Armstrong. D.W. (2003), ' Solvent Properties of the 1-Butyl-3-Methylimidazolium Hexafluorophosphate Ionic Liquid', *Journal of Analytical and Bioanalytical Chemistry,* Vol. 375, No. 2, pp. 191-199.

100. Walden, P.B. (1994) Ueber die Molekulargrösse und elektrische Leitfähigkeit einiger geschmolzenen salze, *Acad. Imper. Sci,* Vol 8. Iss 405-422

101. Hussey, C. L Advances in Molten Salt Chemistry. 5, 185-230. 83 . Amsterdam, Elsevier. Mamantov, G. and Mammatov, C. B.

102. Boon, J.A., Leviskey, A., Pflug, L. and Wilkes, J.S. (1986), 'Friedel-Crafts Reactions in Ambient-Temperature Molten Salts', *J. Organic Chemistry,* Vol. 51, pp. 480-483.

103. Endres, F. and Zein El Abedin, S. (2006), 'Air and Water Stable Ionic Liquids in Physical Chemistry', *Phys. Chem. Chem. Phys,* Vol. 8, pp. 2101-2116.

104. Zein El Abedin1, S., Moustafa1, E.M., Hempelmann, R., Natter, H. and Endres, F. (2005), 'Additive Free Electrodeposition of Nanocrystalline Aluminium in a Water and Air Stable Ionic Liquid', *Electrochemistry Communications,* Vol. 7, No. 11, pp. 1111-1116.

105. Hurley, F.H. and Wier, T.P. (1951), 'The Electrodeposition of Aluminium From Nonaqueous Solutions at Room Temperature', *Journal Electrochemistry Society,* Vol. 98, pp. 203-206.

106. Seddon, K.R., Stark, A. and Torres, M. (2000), 'Influence of Chloride, Water, and Organic Solvents on the Physical Properties of Ionic Liquids', *Pure and Applied Chemistry,* Vol. 72, No. 12, pp. 2275-2287.

107. Schröder, U., Wadhawan, J., Compton, R.J., Marken, F. , Suarez, P.A.Z., Consorti, C.S., De Souza, R.F. and Dupont, J. (2000), 'Water-Induced Accelerated Ion Diffusion: Voltammetric Studies in 1-Methyl-3-[2,6-(S)-Dimethylocten-2-Yl]Imidazolium Tetrafluoroborate, 1-Butyl-3-Methylimidazolium Tetrafluoroborate and Hexafluorophosphate Ionic Liquids', *New Journal of Chemistry,* Vol. 24, pp. 1009-1015.

108. Abbott, A. and McKenzie, K. (2006) Application of ionic liquids to the electrodeposition of metals. *Phys. Chem. Chem. Phys.* **8**, 4265-4279.(Abstract)

109. Hussey, C.L. (1988), 'Room Temperature Haloaluminate Ionic Liquids. Novel Solvents for Transition Metal Solution Chemistry', *Pure and Applied Chemistry,* Vol. 60, No. 12, pp. 1763-1772.

110. Karylian *[BMIM} Model,* available at: http://www.karylian.de/images/bmim_pf6.jpg (accessed 2009).

111. Galinski1, M., Lewandowski1, A. and Stepniak1, I. (2006), 'Ionic Liquids As Electrolytes', *Electrochimica Acta,* Vol. 51, pp. 5567-5580.

112. Bonhôte, P., Dias, A.P., Papageorgiou, N., Kalyanasundaram, K. and Grätzel, M. (1996), 'Hydrophobic, Highly Conductive Ambient-Temperature Molten Salts', *Journal Inorganic Chemistry,* Vol. 35, No. 5, pp. 1168-1178.

113. Earle, M.J., Esperança, J.M.S.S., Gilea1, M.A., Lopes, J.N.C., Rebelo, L.P.N., Magee, J.W.N., Seddon, K.R. and Widegren, J.A. (2006), 'The Distillation and Volatility of Ionic Liquids', *Nature,* Vol. 439, pp. 831-834.

114. Nishida, T. , Tashiro, Y. and Yamamoto, M. (2003), 'Physical and Electrochemical Properties of 1-Alkyl-3-Methylimidazolium Tetrafluoroborate for Electrolytes', *Journal of Fluorine Chemistry,* Vol. 120, No. 2, pp. 135-141.

115. McFarlane, D.R., Sun, J., Golding, J., Meakin, P. and Forsyth, M. (2000), 'High Conductivity Molten Salts Based on the Imide Ion', *Electrochimica Acta,* Vol. 45, No. 8, pp. 1271-1278.

116. Sun, J., Forsyth, M. and MacFarlane, D.R. (1998), 'Room-Temperature Molten Salts Based on the Quaternary Ammonium Ion', *Journal of Physical Chemistry B,* Vol. 102, No. 44, pp. 8858-8864.

117. Fuller, J., Carlin, R.T., De Long, H.C. and Haworth, D. (1994), 'Structure of 1-Ethyl-3-Methylimidazolium Hexafluorophosphate: Model for Room Temperature Molten Salts', *Journal of Chemistry Society, Chemistry Communications,* Iss 3.pp. 299-301.

118. Owens, G.S. and Abu-Omar, M.M. (2002), 'Comparative Kinetic Investigations in Ionic Liquids Using the MTO/Peroxide System', *Journal of Molecular Catalysis A: Chemical,* Vol. 187, No. 2, pp. 215-225.

119. Yu Liu, J.S. and Wen Sun, I. (1997), 'Electrochemical Study of the Properties of Indium in Room Temperature Chloroaluminate Molten Salts', *J. Electrochem. Soc.,* Vol. 144, No. 1, pp. 140-145.

120. Gi-Shong Jeng, E. and Wen Sun, I. (1997), 'Electrochemistry of Tellurium(IV) in the Basic Aluminum Chloride-1-Methyl-3-Ethylimidazolium Chloride Room Temperature Molten Salt', *J. Electrochem. Soc,* Vol. 144, No. 7, pp. 2369-2374.

121. Bandoa, Y., Katayama, Y. and Miuraa, T. (2007), 'Electrodeposition of Palladium in a Hydrophobic 1-n-Butyl-1-Methylpyrrolidinium Bis(Trifluoromethylsulfonyl)Imide Room-Temperature Ionic Liquid', *Electrochimica Acta,* Vol. 53, No. 1, pp. 87-91.

122. Zein El Abedin, S., Welz-Biermann, U. and Endres, F. (2005), 'A Study on the Electrodeposition of Tantalum on NiTi Alloy in an Ionic Liquid and Corrosion Behaviour of the Coated Alloy', *Electrochemistry Communications,* Vol. 7, No. 9, pp. 941-946.

123. Chen, P. and Hussey, C.L. (2004), 'Electrodeposition of Caesium at Mercury Electrodes in the Tri-1-Butylmethylammonium Bis((Trifluoromethyl)Sulfonyl)Imide Room-Temperature Ionic Liquid', *Electrochimica Acta,* Vol. 49, No. 28, pp. 5125-5139.

124. Liua, Q.X., Zein El Abedinl, S. and Endres, F. (2006), 'Electroplating of Mild Steel by Aluminium in a First Generation Ionic Liquid: A Green Alternative to Commercial Al-Plating in Organic Solvents', *Surface and Coatings Technology,* Vol. 201, No. 3-4, pp. 1352-1356.

125. Caporali, S., Fossati, A., Lavacchi, A., Ilaria, P., Tolstogouzov, A. and Bardi, U. (2008), 'Aluminium Electroplated From Ionic Liquids As Protective Coatings Against Steel Corrosion', *Corr. Sci. 50,* Vol. 50, pp. 434-439.

126. Zhao, Y. and VanderNoot, T.J. (1997), 'Electrodeposition of Aluminium From Room Temperature AlCl3-TMPAC Molten Salts', *Electrochimica Acta. Volume 42, Issue 11, 1997, Pages 1639-1643*

127. Carlin, R.T., Crawford, W. and Bersch, M. (1992), 'Nucleation and Morphology Studies of Aluminum Deposited From an Ambient-Temperature Chloroaluminate Molten Salt', *J. Electrochem. Soc,* Vol. 139, No. 10, pp. 2720-2727.

128. Tierney, B.J., Pitner, W.R., Mitchell, J.A. and Hussey, C.L. (1998), 'Electrodepostion of Copper and Copper-Aluminium Alloys From a Room Temperature Chloroaluminate Salt', *J. Electrochem. Soc.,* Vol. 145, No. 9, pp. 3110-3116.

129. Bomparola, R., Caporali, S., Lavacchi, A. and Bardi U. (2007), 'Silver Electrodeposition From Air and Water-Stable Ionic Liquid; an Environmentally Friendly Alternative to Cyanide Baths', *Surface & Coatings Technology,* Vol. 201, pp. 9485-9490.

130. Ping He, P. , Liu, H., Li, Z. and Li, J. (2005) Electrodeposition of Platinum in Room-Temperature Ionic Liquids and Electrocatalytic Effect on Electro-oxidation of Methanol. *Journal of the Electrochemical Society* **152**, E146-E153(Abstract)

131. Mitchell, J.A., Pitner, W.R., Hussey, C.L. and Stafford, G.R. (1996), 'Electrodeposition of Cobalt and Cobalt-Aluminum Alloys From a Room Temperature Chloroaluminate Molten Salt', *J. Electrochem. Soc.,* Vol. 143, No. 22, pp. 3448-3455.

132. Pitner, W.R. and Hussey, C.L. (1997), 'Electrodeposition of Zinc From the Lewis Acidic Aluminum Chloride-1-Methyl-3-Ethylimidazolium Chloride Room Temperature Molten Salt', *J. Electrochem. Soc,* Vol. 144, No. 9, pp. 3095-3103.

133. Gray, E.G., Kohl, P.A. and Winnick, J. (1995), 'Stability of Sodium Electrodeposited From a Room Temperature Chloroaluminate Molten Salt', *J. Electrochem. Soc.,* Vol. 142, No. 11, pp. 3636-3642.

134. Chen, P.U., Lin, Y.F. and Wen Sun, I. (1999), 'Electrochemistry of Gallium in the Lewis Acidic Aluminum Chloride-1-Methyl-3-Ethylimidazolium Chloride Room-Temperature Molten Salt', *J. Electrochem. Soc.,* Vol. 146, No. 9, pp. 3290-3294.

135. Murase, K., Kurosaki, R., Katase, T., Sugimura, H., Hirato, T. and Awakura, Y. (2007), 'Electrochemical Alloying of Copper Substrate With Tin Using Ionic Liquid As an Electrolyte at Medium-Low Temperatures', *J. Electrochem. Soc.,* Vol. 154, No. 11, pp. D612-D616.

136. Welton, T. (1999), 'Room-Temperature Ionic Liquids. Solvents for Synthesis and Catalysis', *Chem Rev.,* Vol. 99, No. 8, pp. 2071-2084.

137. Jianga, T., Chollier Brymb, M.J., Dubéb, G., Lasiaa, A. and Brisarda, G.M. (2006), 'Electrodeposition of Aluminium From Ionic Liquids: Part II - Studies on the Electrodeposition of Aluminum From Aluminum Chloride (AlCl3) - Trimethylphenylammonium Chloride (TMPAC) Ionic Liquids', *Surface and Coatings Technology,* Vol. 201, No. 1-2, pp. 10-18.

138. Caporali, S. (2008), 'Presentation given at IOLISURF Meeting 2008',

139. Pitner, W.R., Hussey, C.L. and Stafford, G.R. (1996), 'Electrodeposition of Nickel-Aluminum Alloys From the Aluminum Chloride-1-Methyl-3-Ethylimidazolium Chloride Room Temperature Molten Salt', *J. Electrochem. Soc., Volume 143, Issue 1, Pp. 130-138 (January 1996),* Vol. 143, No. 1, pp. 130-138.

140. Pitner, W.R. and Hussey, C.L. (1996), 'Electrodeposition of Nickel-Aluminium Alloys From the Aluminium Chloride-1-Methyl-3-Ethylimidazolium Chloride Room Temperature Molten Salt', *J. Electrochem Soc.*, Vol. 143, No. 1, pp. 130-138.

141. Moffat, T.P. (1994), 'Electrodeposition of Ni1–XAlx in a Chloroaluminate Melt', *J. Electrochem. Soc.*, Vol. 141, No. 11, pp. 3059-3079.

142. Ali, M.R., Nishikata, A. and Tsuru, T. (1997), 'Electrodeposition of Co---Al Alloys of Different Composition From the AlCl3---BPC---CoCl2 Room Temperature Molten Salt', *Electrochimica Acta,* Vol. 42, No. 12, pp. 1819-1828.

143. Moffat. T.P (1994), 'Electrodeposition of Al-Cr Metallic Glass', *J. Electrochem. Soc,* Vol. 141, No. 9, pp. L115-117.

144, Ali, M.R., Atsushi Nishikata, A. and Tsuru, T. (1997), 'Electrodeposition of Aluminum-Chromium Alloys From AlCl3-BPC Melt and Its Corrosion and High Temperature Oxidation Behaviors', *Electrochimica Acta,* Vol. 42, No. 15, pp. 2347-2354.

145. Abbott, A.P., Earldey, C.A., Farely, N.R.S., Griffith, G.A. and Pratt, A. (2001), ' Electrodeposition of Aluminium and Aluminium/Platinum Alloys From $AlCl_3$/Benzyltrimethylammonium Chloride Room Temperature Ionic Liquids', *Journal of Applied Electrochemistry*, Vol. 31, pp. 1345-1350.

146. Carlin, R.T., De Long, H.C., Fuller, J. and Trulove, P.C. (1998), 'Microelectrode Evaluation of Transition Metal-Aluminum Alloy Electrodepositions in Chloroaluminate Ionic Liquids', *J. Electrochem. Soc.*, Vol. 145, No. 5, pp. 1598-1607.

147. Hurley, F.H. and WIer, T.P. (1951) The Electrodeposition of Aluminum from Nonaqueous Solutions at Room Temperature. *J. Electrochem. Soc.* **98**, 207-212.(Abstract)

148. Capuanol, G.A., Ducasse, R. and Davenport, W.G. (2004) Electrodeposition of aluminium-copper alloys from alkyl benzene electrolytes. *Journal of Applied Electrochemistry* **9**, 7-13.(Abstract)

149. Alumiplate PLC *Alumiplate*, available at: http://www.alumiplate.com/ (accessed 2009).

150. Grgur, B.N. , Popov, K.I. and Djokic, S.S. (2002), *Fundamental Aspects of Electrometallurgy*, Plenum, NY, USA.

151. Meschel, S.V. and Kleppa, O.J. (1998), 'Standard Enthalpies of Formation of Some 5d Transition Metal Sillides by High-Temperature Direct Synthesis Calorimetry', *Journal of Alloys and Compounds,* Vol. 280, No. 1-2, pp. 231-239.

152. Meschel, S.V. and Kleppa, O.J. (1993), 'Standard Enthalpies of Formation of 5d Aluminides by High-Temperature Direct Synthesis Calorimetry', *Journal of Alloys and Compounds,* Vol. 197, pp. 75-81.

153. Meschel, S.V. and Kleppa, O.J. (1993), 'Standard Enthalpies of Formation of 4d Aluminides by Direct Synthesis Calorimetry', *Journal of Alloys and Compounds,* Vol. 191, pp. 111-116.

154. Jung, W.G. and Kleppa, O.J. (1992), ' Standard Molar Enthalpies of Formation of MeAl (Me = Ru, Rh, Os, Ir)', *Metallurgical and Materials Transactions B,* Vol. 23, No. 1, pp. 53-56.

155. Miedem, A.R. (1973), 'The Elctronegativity Parameter for Transition Metals: Heat of Formation and Charge Transfer in Alloys', *Journal of the Less-Common Metals,* Vol. 32, pp. 117-136.

156. Goncalves, A.P. and Almeida, M. (1996), 'Extended Miedema Model: Predicting the Formation Enthalpies of Intermetallic Phases With More Than Two Elements', *Physica B,* Vol. 228, pp. 289-294.

157. Brundel, C. , Evans, C.A. and Wilson, S. (1992), *Encyclopedia of Materials Characterization*, Butterworth-Heinemann, New York.

158. University of Iowa, U. *Picture Comparing Optical, SEM and TEM Microscopes,* available at: http://www.uiowa.edu/~cemrf/methodology/tem/TEM1.gif (accessed 2009).

159. US Geographical Society *Picture of XRD Technique,* available at: http://pubs.usgs.gov/of/2001/of01-041/htmldocs/images/beam.jpg (accessed 2009).

160. Crystal Site *Picture of Miller Indices,* available at: http://www.crystal.unito.it/mssc2006_cd/tutorials/surfaces/image006.gif (accessed 2009).

161. Craig, M., Chirivi, L., Long, K., Robinson, M., and Nicholls, J.R.'Coatings for Use at High Temperature', *International Conference on Metallurgical Coatings and Thin Films,* San Diego, Ca, USA,

162. Smith, J.(2009) Email sent to M. Craig regarding Platinum Plating. Presentation at the San Deigo Conference

163. Basirun, W.J. and Pletcher, D. (1998), ' Studies of Platinum Electroplating Baths Part VI: Influence of Some Experimental Parameters on Deposit Quality', *Journal of Applied Electrochemistry,* Vol. 28, pp. 167-172.

164. Sahami, S. and Osteryoung, R.A. (1983), 'Voltammetric Determination of Water in an Aluminum Chloride-N-n -Butylpyridinium Chloride Ionic Liquid', *Anal Chem,* Vol. 55, pp. 1970-1973.

165. Kuznetsova, L.A. (2002), 'Microdistribution of Electrolytic Nickel Deposits and Their Surface Topography: Effect of Hydrogen', *Russian Journal of Electrochemistry, Vol. 38, No. 10, 2002, Pp. 1132–1140.*
Original Russian Text Copyright © 2002 by Kuznetsova., Vol. 38, No. 10, pp. 1132-1140 (Translated from Elektrokhimiya, *Vol. 38, No. 10, 2002, pp. 1253–1261.*).

166. Zawodzinski, A.T., Carlin, R.T. and Osteryoung, R.A. (1987), 'Removal of Protons From Ambient-Temperature Chloroaluminate Ionic Liquids', *Anal. Chem.* Vol. 59, pp. 2639-2640.

167. Hanke, C.G. and Lynden-Bell, R.M. (2003), 'A Simulation Study of Water-Dialkylimidazolium Ionic Liquid Mixtures', *J. Phys. Chem. B,* Vol. 107, No. 39, pp. 10873-10878.

168. Eskner, M. and Sandström, R. (2003), 'Measurement of the Ductile-to-Brittle Transition Temperature in a Nickel Aluminide Coating by a Miniaturised Disc Bending Test Technique', *Surface and Coatings Technology,* Vol. 165, No. 1, pp. 71-80.

169. Wang, Y., Liu, Z.K. and Chen, L.Q. (2004), 'Thermodynamic Properties of Al, Ni, NiAl, and Ni3Al From First-Principles Calculations', *Acta Materialia,* Vol. 52, No. 9, pp. 2665-2671.

170. Darolia, R. (2000), 'Ductility and Fracture Toughness Issues Related to Implementation of NiAl for Gas Turbine Applications', *Intermetallics,* Vol. 8, No. 9-11, pp. 1321-1327.

171. D. Vogel, D., Newman, L., Deb, P. and Boone, D.H. (1987), 'Effect of Coating on the Mechanical Properties of the Substrate, Particularly in High and Low-Cycle Fatigue, and Corrosion-Fatigue Ductile-to-Brittle Transition Temperature Behavior of Platinum-Modified Coatings', *Materials Science and Engineering,* Vol. 88, pp. 227-231.

172. United Department of Defence *Phase Structures,* available at: http://cst-www.nrl.navy.mil/lattice/ (accessed 2009).

173. Narita, T., Thosin, K.Z., Fengqun, L., Hayashi, S., Murakami, H., Gleeson, B. and Young, D. 'Development of Re-Based Diffusion Barrier Coatings on Nickel Based Superalloys', *Materials and Corrosion,* Vol. 56, No. 12, 929-929

174. 'Cavaletti, E. Naveos, S. Mercier, S. Josso, P. Bacos, M.P and Monceau, D (2009).'Ni–W diffusion: Its influence on the oxidation behaviour of a NiPtAl coated fourth Generation Nickel-based Superalloys. *Surface and Coatings Technology,* Vol. 204, No. 6-7, pp. 761-765.

175. Hayashi, S. , Ford, S.I., Young, D.J., Sordelet, D.J., Besser, M.F. and Gleeson, B. (2005), 'Alpha NiPt(Al) and Phase Equilibria in the Ni-Al-Pt System at 1150°C', *Acta Materialia* , Vol. 53, pp. 3319-3328.

176. Jiang, C., Besser, M.F., Sordelet, D.J. and Gleeson, B. (2005), 'A Combined First-Principles and Experimental Study of the Lattice Site Preference of Pt in B2 NiAl', *Acta Materialia* , Vol. 55, pp. 2101-2109.

177. Okamoto (2000), *Desk Handbook: Phase Diagrams for Binary Alloys*, ASM International, United States.

178. Fujiwaraa, K. and Horita, Z. (2002), 'Measurement of Intrinsic Diffusion Coefficients of Al and Ni in Ni3Al Using Ni/NiAl Diffusion Couples', *Acta Materialia,* Vol. 50, No. 6, pp. 1571-1579.

179. Shipway, S. (2005), 'Modelling Methods for Finite Element Analysis', Lecture Notes *Nottingham University,*

180. Crank, J. (1975), *Mathematics of Diffusion*, Oxfrod University Press, Oxford.

181. Kamavaram, V., Mantha, D. and Reddy, R.G. (2005), 'Recycling of Aluminum Metal Matrix Composite Using Ionic Liquids:: Effect of Process Variables on Current Efficiency and Deposit Characteristics', *Electrochimica Acta,* Vol. 50, No. 16-17, pp. 3286-3289.

182. Huang, W. and Chang, Y.A. (1999), 'Thermodynamic Properties of the Ni–Al–Cr System', *Intermetallics,* Vol. 7, No. 8, pp. 863-874.

183. Kunrath, O., Reimanis, I.E. and Moor, J.J. (2001), 'Combustion Synthesis of TiC–Cr3C2 Composites', *Journal of Alloys and Compounds,* Vol. 329, No. 1-1, pp. 131-135.

184. Kubaschewski, O. and Heymer, G. (1960), 'Heats of Formation of Transition-Metal Aluminides ', *Trans. Faraday Soc.,* pp. 473-478.

185. Abhika, N.C., Vivek, R., Udhayabanua, V. and Murty, B. (2008), 'Influence of Heat of Formation of B2/L12 Intermetallic Compounds on the Milling Energy for Their Formation During Mechanical Alloying', *Journal of Alloys and Compounds,* Vol. 465, No. 1-2, pp. 106-112.

186. Nash, P. and Kleppa, O. (2001) Composition dependence of the enthalpies of formation of NiAl. *Journal of Alloys and Compounds* **321**, 228-231.(Abstract)

187. Huang, T.S. and Pang, J.G. (1997), 'Thermal Stability of the Pd-Al Alloy Schottky Contacts to N-GaAs', *Materials Science and Engineering B,* Vol. 49, No. 2, pp. 144-151.

188. Coltters, R.G. and Belton, G.R. (1983), ' High Temperature Thermodynamic Properties of the Tungsten Carbide WC Determined Using a Galvanic Cell Technique', *Journal Metallurgical and Materials Transactions A,* Vol. 14, No. 9, pp. 1915-1919.

189. Pretorius, R., Theron, C., Vantomme, A. and Mayer, J. (1999), 'Compound Phase Formation in Thin Film Structures', *Critical Reviews in Solid State and Material Sciences,* Vol. 24, No. 1, pp. 1-62.

190. Meschel, S.V. and Kleppa, O.J. (1997), 'Standard Enthalpies of Formation of Some 3d Transition Metal Carbides by High Temperature Reaction Calorimetry', *Journal of Alloys and Compounds,* Vol. 257, No. 1-2, pp. 227-233.

191. Humphrey, G.L. (1954), 'Heats of Formation of Tantalum, Niobium and Zirconium Oxides, and Tantalum Carbide', *J. Am. Chem. Soc.,* Vol. 76, No. 4, pp. 978-980.

192. Wikipedia *Tantalum Carbide,* available at: http://en.wikipedia.org/wiki/Tantalum_carbide

193. Reade Advanced Materials *Titanium Carbide Powder,* available at: http://www.reade.com/Products/Carbides/titanium_carbide.html (accessed 2006).

194. Merzhanov, A.J. and Borovinskaya, I.P. (1972), 'Self-Propagated High-Temperature Synthesis of Refractory Inorganic Compounds', *Doklady Akademii Nauk SSSR,* Vol. 204, No. N2, pp. 366-369.

195. Merzhanov. A.G et al (inventor) USSR. 'Self-propogating high temperature synthesis' Patent no 255221.

196. Gennari, S. ,Anselmi-Tamburini, U., Maglia, F. and Spinolo, G.A.M.Z. (2006), 'Simulation Study of Wave Propagation Instabilities for the Combustion Synthesis of Transition Metals Aluminides', *J. Phys. Chem. B* , Vol. 110, pp. 7144-7152.

197. Merzhanov. A.G and Sytschev. A.E available at: http://www.ism.ac.ru/handbook/shsf.htm (accessed 2009).

198. Yeh, C.L., Su, S.H. and Chang, H.Y. (2005), 'Effects of TiC Addition on Combustion Synthesis of NiAl in SHS Mode', *Journal of Alloys and Compounds,* Vol. 398, No. 1-2, pp. 85-93.

199. Moore, J.M. and Feng, H.J. (1995), 'Combustion Synthesis of Advanced Materials: Part I. Reaction Parameters', *Progress in Materials Science,* Vol. 39, No. 4-5, pp. 243-273.

200. Moore, J.M. and Feng, H.J. (1995), 'Combustion Synthesis of Advanced Materials: Part II. Classification, Applications and Modelling', *Progress in Materials Science,* Vol. 39, No. 4-5, pp. 275-316.

201. Subrahmanyam, J. and Vijayakumar, M. (1992), 'Review: Self-Propagating High-Temperature Synthesis ', *Journal of Materials Science,* Vol. 27, pp. 6249-6273.

202. Morsi. K. (2001), 'Review: Reaction Synthesis Processing of Ni–Al Intermetallic Materials', *Materials Science and Engineering A,* Vol. 299, No. 1-2, pp. 1-15.

203. Palisaitis, J., Vasiliauskas, R. and Ferro, G. (2008), 'Epitaxial Growth of Thin Films', *Lecture Notes at Linkoping University, Sweden,* pp. 1-16.

204. Smialek, J. and Lowell, C.E. (1974), 'Effects of Diffusion on Aluminum Depletion and Degradation of NiAI Coatings', *Journal Electrochemical Society. Vol 121 P800.* Vol. 121, pp. 800-805.

205. Chirivi, L. (2010), *Optimisation and Oxidation of CN91-Type Platinum Aluminide Coatings* (unpublished PhD thesis), Cranfield University,

206. Nicholls, J. R. and Wing, R. (2002), 'Advanced Coating Systems for Utility Gas Turbines', in Materials for Advanced Power Engineering ((Part 1 edition), Forschungzcentrum, Julich, Germany, pp. 57-71.

207. Bardi, U. et al. (2009), *IOLISURF Final Report*, European Union: Confidential

208. Bardi, U., Caporali, S., Craig, M., Giogetti, A. and Nicholls, J.R. (2009) Electrodeposition of aluminium film on P90 Li–Al alloy as protective coating against corrosion. *Surface and Coatings Technology* **203**, 1373-1378

17 Appendix: Anodising ILAl

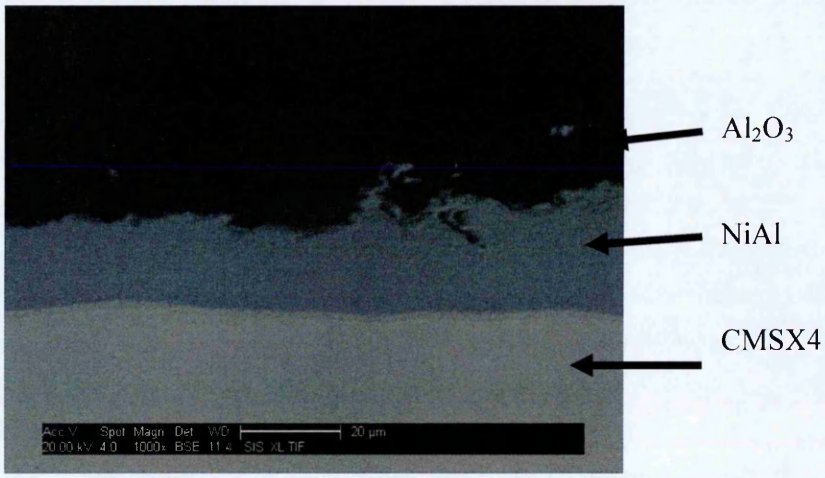

It is believed that this is the first instance of ILAl being anodised (12V in a sulphuric acid anodising solution) to form an alumina layer. Both Cabro and Galvanica which are also industrial partners of the IOLISURF group are interested in putting this process into production. It should be noted that during this project ILAl which had undergone the ICON process to form β-NiAl was also anodised.

18 Appendix: Heat Treating Other Al Deposits

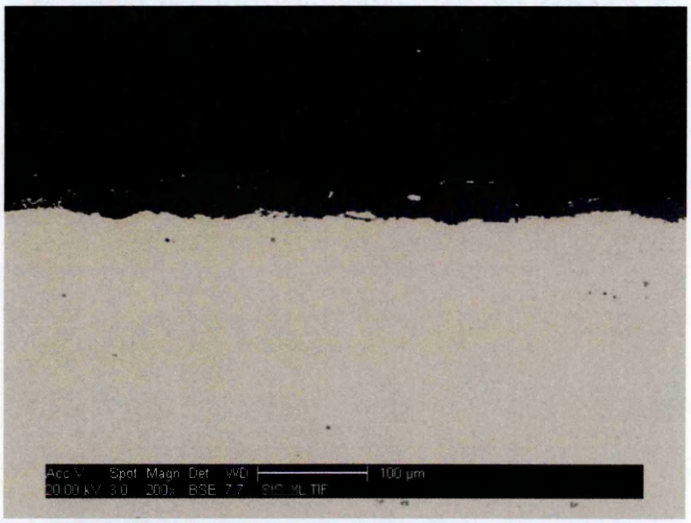

Figure 18-1: Plasma sprayed Aluminium (as received)

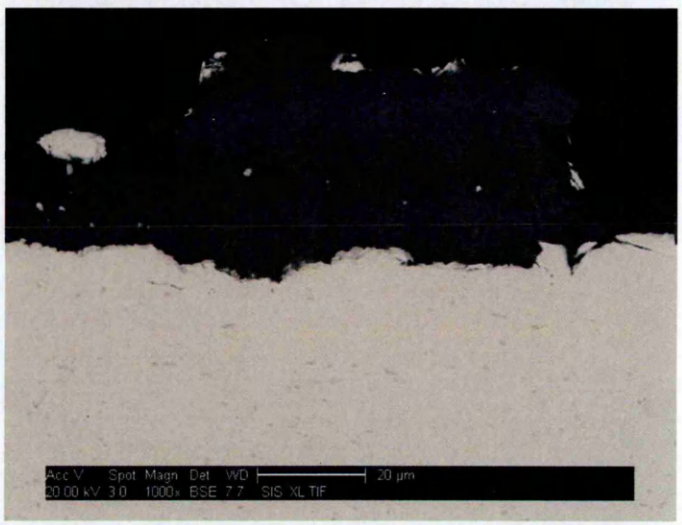

Figure 18-2: Magnified Plasma Sprayed Aluminium

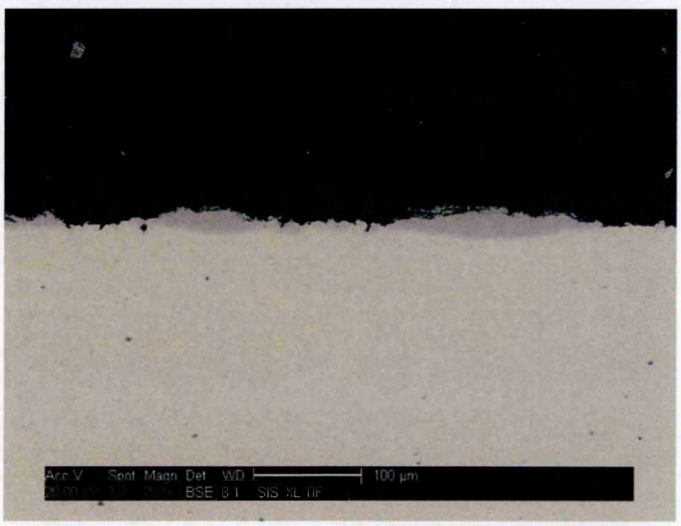

Figure 18-3: Plasma Sprayed Aluminium after ICON

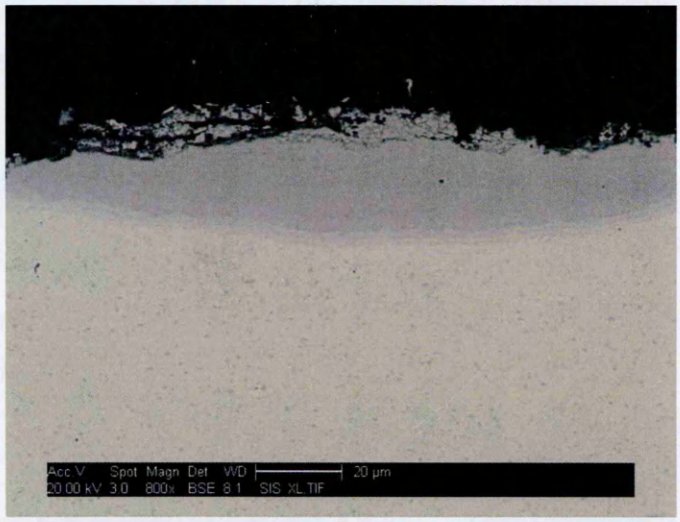

Figure 18-4: Magnified Plasma Sprayed Aluminium after ICON

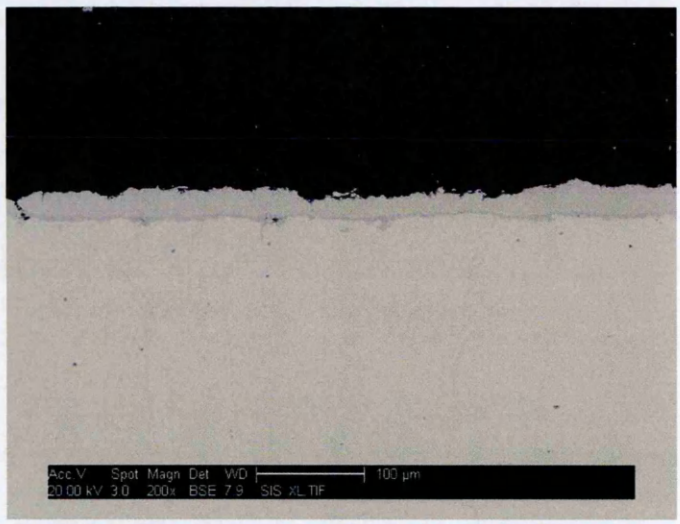

Figure 18-5: Plasma Sprayed Aluminium after NP Parameters